UNIVERSITAT ROVIRA I VIRGILI

CONTINUOUS HYDROGENATION OF CARBON DIOXIDE TO FORMATES AND FORMIC ACID OVER HETEROGENEOUS CATALYSTS

Juan José Corral Pérez

UNIVERSITAT ROVIRA i VIRGILI

Continuous hydrogenation of carbon dioxide to formates and formic acid over heterogeneous catalysts

JUAN JOSÉ CORRAL PÉREZ

DOCTORAL THESIS
2019

DOCTORAL THESIS

CONTINUOUS HYDROGENATION OF CARBON DIOXIDE TO FORMATES AND FORMIC ACID OVER HETEROGENEOUS CATALYSTS

JUAN JOSÉ CORRAL PÉREZ

Supervised by:

Prof. Dr. Atsushi Urakawa

ICIQ-URV

Institut Català d'Investigació Química

UNIVERSITAT ROVIRA i VIRGILI

Tarragona

2019

UNIVERSITAT ROVIRA I VIRGILI
CONTINUOUS HYDROGENATION OF CARBON DIOXIDE TO FORMATES AND FORMIC ACID OVER HETEROGENEOUS CATALYSTS
Juan José Corral Pérez

Prof. Dr. Atsushi Urakawa

Group Leader

Institute of Chemical Research of Catalonia (ICIQ)

The Barcelona Institute of Science and Technology

Av. Països Catalans 16

43007 Tarragona, Spain

CERTIFIES THAT:

The present study, entitled "Continuous hydrogenation of carbon dioxide to formates and formic acid over heterogeneous catalysts", presented by Juan José Corral Pérez for the award of the degree of Doctor, has been carried out under my supervision at the Institute of Chemical Research of Catalonia (ICIQ), and that it fulfils all the requirements to obtain the Degree of Doctor in Chemical Science and Technology.

Tarragona, 1st of June, 2019

Doctoral Thesis Supervisor

浦川 篤

Prof. Dr. Atsushi Urakawa

Acknowledgements

First, I would like to thank my thesis supervisor, Prof. Atsushi Urakawa, for giving me the opportunity to join the Sinergia project in his research group. Thanks to him, I have grown personally and professionally since the PhD adventure started. His support, passion and optimism helped me to face any challenge that came my way. I will never forget our long talks in the car (with flamenco music), airport and synchrotron night shift. I feel very fortunate to have worked with him. ありがとう

I would like to express my sincere gratitude to Prof. Christophe Copéret. My stay in his research group at ETH Zürich has marked a turning point in my career. I am extremely grateful for all the scientific discussions with him. Never shall I forget his amazing dinners and wines, I am still impressed with his cooking skills. Merci beaucoup pour tout !

I would also like to thank all the members of the Sinergia team and collaborators: Prof. Philipp Rudolf von Rohr, Prof. Christophe Copéret, Prof. Joost VandeVondele, Prof. Anton Kokalj, Prof. Aleix Comas-Vives, Prof. Atsushi Urakawa, Dr. Atul Bansode, Dr. C. S. Praveen, Dr. Helena Reymond and Dr. Hung-Kun. It has been a pleasure to work with each one of them. Besides the great results from this fruitful collaboration, this team work has been one of my best experiences.

I would like to express my thanks to all the ICIQ staff. Special thanks to Georgiana, Dolores, José Luis, Xavier, Marc and Jesús, when there is any problem, they are always willing to help. I also thank Aurora for the great administrative support and good moments at ICIQ.

I would like to express my deepest appreciation to all my colleagues from ETH Zürich and ICIQ. I cannot name them all because I would need several pages. From Copéret's group, I have nothing but words of thanks for Andrea, Christopher, Ilia, Lucas, Aleix, Hung-Kun, David, Erwin, Behnaz, Tigran, Wei-Chih, Kim and Patrick. From Urakawa's group, Atul, Dragos, Jordi, Marta, Silvia, Andrea, Lingjun, Sergio, Rohit, Amelia, Andrea, Shunsaku, Shintaro, Takuya, Donato, Yi, Murli, Rui, Joan, Nat and Sorin, I cannot thank them enough for all the good memories in the lab.

Special thanks to Dr. Atul Bansode, I have learnt a lot from him, and he has always supported me. I will never forget our Sinergia trips (even the day we almost missed our flight) and synchrotron shifts. Thanks for everything and our long discussions during the coffee break. अमर रहोस!

Dragos, no tengo palabras suficientes de agradecimiento para ti. Nada más llegar al laboratorio, me ayudaste con todo y me hiciste sentir uno más dentro del grupo. Has sido un apoyo fundamental durante estos años, incluso desde la distancia. Y lo mismo con Dana, aunque no estuviera en el laboratorio, es como si fuera una más de la familia, siempre con una sonrisa y dispuesta a ayudar. ¡Muchísimas gracias! Silvia, cómo olvidar el día que te fui a recoger a la estación de AVE para hacer la entrevista. Desde ese momento, sé que he podido contar contigo para todo. Sin ti, el laboratorio perdió alegría y música de gran calidad. ¡Mil gracias!

Marta i Jordi, sempre estaré agraït pel vostre suport durant aquest anys. Gràcies a vosaltres, ha existit una gran família dins del laboratori. Hem viscuts grans moments junts que mai oblidaré. Jordi, el teu optimisme i bon rotllo han estat essencials al dia a dia. Marta, les nostres xerrades científiques i filosòfiques han marcat un abans i un després, sempre has estat disponible quan he necessitat qualsevol cosa. Moltíssimes gràcies!

También me gustaría agradecer a mis compañeros de Abengoa, especialmente a Verónica Carcelén. Verónica, mi paso por Abengoa fue todo un placer gracias a ti, me enseñaste muchas cosas y eres el ejemplo de una verdadera líder. Durante estos años de tesis, siempre has estado dispuesta a escuchar y ayudar. Espero que en un futuro podamos volver a trabajar juntos. ¡Muchas gracias!

Tampoco me puedo olvidar de mis amigos de la universidad: Anna, Sandra, Samanta, Bárbara, David y Javi. Cada uno de nosotros hemos cogido caminos distintos, no obstante, siempre han estado ahí y su apoyo ha sido esencial. ¡Muchas gracias, chicos!

També he d'agrair als meus amics d'El Vendrell, portem junts des de l'escola i sempre m'han recolzat incondicionalment, amb ells tot és més fàcil. Estefania, Ainhoa, Dani, Esther, Anna, Marta, Teresa i Carles, moltíssimes gràcies per tot! Sense vosaltres, aquests anys haurien estat molt més durs.

Quisiera agradecer a Antonio todo su apoyo incondicional durante estos años. No ha sido fácil con la distancia, pero siempre me ha animado a continuar y a desconectar de la rutina. ¡Muchas gracias por todo y espero que nuestros caminos sigan cruzados!

Por último, darle las gracias a mi familia. Sin mis padres y mi hermano, hubiera sido imposible llegar a escribir esta tesis. Su amor y apoyo incondicionales han permitido que me encuentre escribiendo estas palabras. ¡Muchísimas gracias!

Table of Contents

XIII

1

Introduction and overview

Chapter 1

1.1 The current energy situation

Throughout the course of history, energy has been pivotal in both human and economic developments. Energy drives everything and is part of everyday life. For the very first time, mankind made use of energy by burning wood (biomass) to make fire for cooking and heating. Later, the water and the windmills allowed humans to meet their increasing needs arising from agriculture and farming. It was not until the Industrial Revolution, during the 18th century, when the transition towards the era of fossil fuels began.[1] Currently, according to the report presented by the International Energy Agency (IEA) in 2016,[2] fossil fuels (oil, coal and natural gas) provide 81.1% of the world total primary energy, i.e. the total amount of energy produced directly from natural resources and that the world has at its disposal (**Figure 1.1**). Back in 1973, fossil fuels accounted for 86.7% of the world total primary energy. Hence, after all these years, the global energy supply still relies heavily on finite fossil fuels, which have been formed over millions of years by the remains of dead plants and animals.
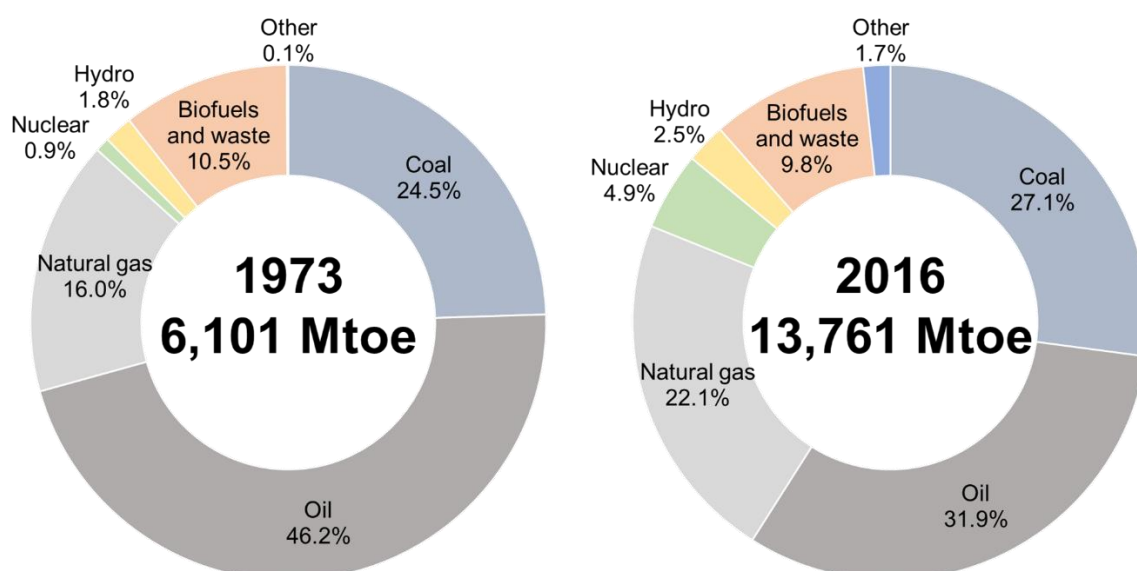
Figure 1.1. World total primary energy supply (TPES) by fuel in 1973 and 2016. World includes international aviation and international marine bunkers. Peat and oil shale are aggregated with coal. Geothermal, solar, wind, tide/wave/ocean and heat are included in other. Energy expressed in millions of tonnes of oil equivalent (1 Mtoe = 4.1868×10^{16} J). Source: International Energy Agency (IEA) – Key world energy statistics from 2018.

The primary energy harvested from nature cannot be directly used by consumers, it must be transformed into a usable form such as electricity, heat and fuels. Electricity, for instance, is generated from the conversion of primary energy sources such as coal, natural gas, uranium (nuclear), hydropower, wind, solar and geothermal. Another example is the crude oil, that must be turned into gasoline, kerosene or diesel so that it can be employed in an engine. As shown in the world total final energy consumption (**Figure 1.2**), the energy mix is still dominated by

UNIVERSITAT ROVIRA I VIRGILI
CONTINUOUS HYDROGENATION OF CARBON DIOXIDE TO FORMATES AND FORMIC ACID OVER HETEROGENEOUS CATALYSTS
Juan José Corral Pérez

Introduction and overview

fossil fuels and most importantly, the consumption has doubled since 1973. The *International Energy Outlook 2017* projects 28% increase in world energy consumption by 2040.[3] It is no wonder that the world energy demand and consumption is increasing due to the economic and population growths. According to an United Nations report, the world's population is projected to reach 8.6 billion inhabitants in 2030, and to increase further to 9.8 billion in 2050.[4] Therefore, the current energy model may be unable to cope with the increasing living standards and the future energy demands.
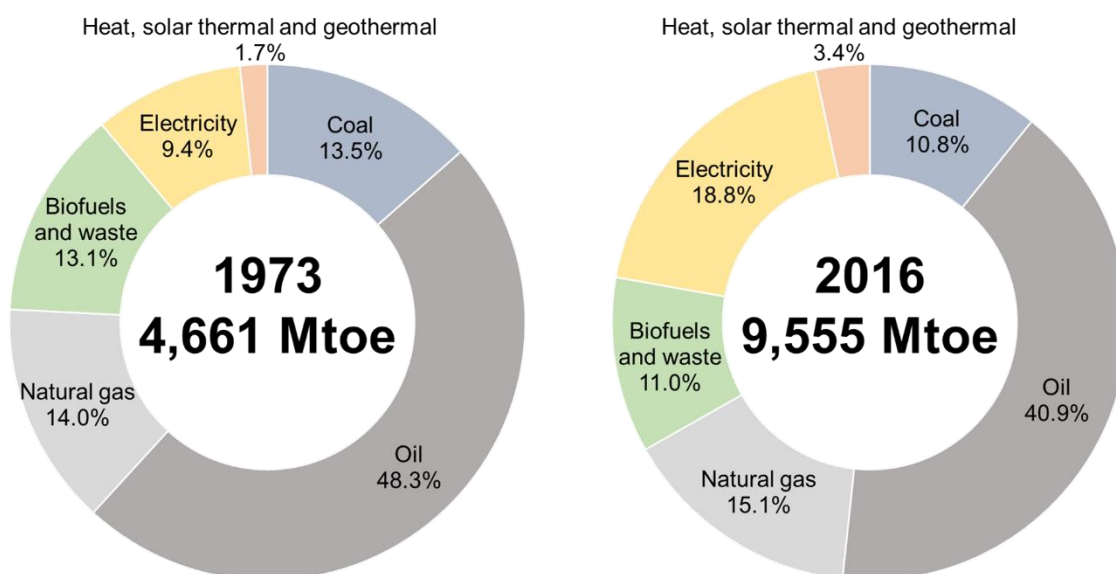
Figure 1.2. World total final consumption (TFC) by fuel in 1973 and 2016. World includes international aviation and international marine bunkers. Peat and oil shale are aggregated with coal. Data for biofuels and waste final consumption have been estimated for a number of countries. Energy expressed in millions of tonnes of oil equivalent (1 Mtoe = 4.1868×10^{16} J). Source: International Energy Agency (IEA) – Key world energy statistics from 2018.

Based on these figures, it is imperative to move towards a more sustainable energy model and change the current one, which is linear and mostly based on the extraction of fossil fuels as depicted in **Figure 1.3**. The continued use of such fuels and the obligatory need of burning them to extract their contained energy has brought two main consequences. On the one hand, the proven reserves of fossil fuels are progressively decreasing and leading to depletion. Unfortunately, it will take centuries for those reserves to be replenished. On the other hand, the combustion of fossil fuels emits carbon dioxide (CO_2) to the atmosphere, thus contributing to the global warming and its environmental consequences.

Chapter 1
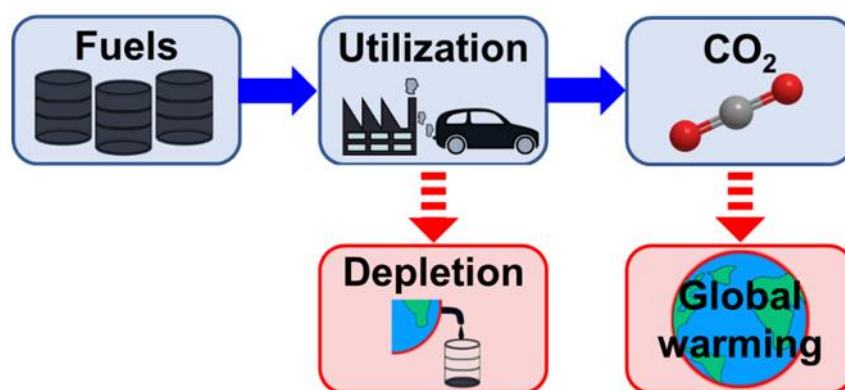
Figure 1.3. Linear energy model based on fossil fuels and its consequences.

It is worth mentioning that most of the global CO_2 emissions are caused by the use of fossil fuel rather than deforestation, agriculture and degradation of soils.[5] Global energy-related CO_2 rose by 1.4% in 2017, an increase of 460 Mt (million tons), reaching a historic high of 32.5 Gt (gigatons).[6] Not unexpectedly, the levels of CO_2 in the atmosphere have been steadily rising over the years reaching record levels slightly above 400 ppm (parts per million).[7] This fact cannot be overlooked because CO_2 is a greenhouse gas (GHG), i.e. it absorbs and emits thermal radiation leading to a planetary warming impact (**Figure 1.4**). During the last 136 years, seventeen of the eighteen warmest years have occurred since 2001.[8] The increase in the average global temperature on Earth has serious impacts, including extreme weather events (floods, droughts, storms, and heatwaves) and sea-level rise, which can suppose a risk for human and natural systems.[9]
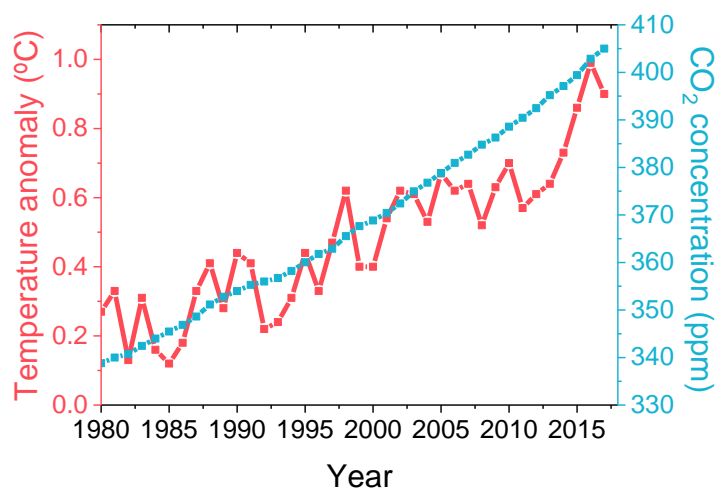
Figure 1.4. Change in global surface temperature and global annual mean concentration of CO_2. Source: NASA's Goddard Institute for Space Studies (GISS) and National Oceanic and Atmospheric Administration/Earth System Research Laboratory (NOAA/ESRL).

There are several ways of combating the current climate change and its imminent environmental threats. One simple approach would be reducing the energy consumption and

UNIVERSITAT ROVIRA I VIRGILI
CONTINUOUS HYDROGENATION OF CARBON DIOXIDE TO FORMATES AND FORMIC ACID OVER HETEROGENEOUS CATALYSTS
Juan José Corral Pérez

Introduction and overview

consequent emissions by taking public transport, increasing energy efficiency at home, increasing the lifetime of products, recycling, etc. All these actions can be done effortlessly provided that individual awareness of the global warming is raised. A huge impact on CO_2 mitigation would be achieved by a global shift toward renewable energy sources such as solar, wind, biomass, hydropower and geothermal. That is why deployment of these virtually inexhaustible energies has been growing rapidly in the last few years. Nevertheless, they contributed only around 14% of global primary energy supply in 2016 (**Figure 1.1**). Hence, it can be envisaged that there is still a long way to go before the share of renewable energies increases in the energy mix. Different factors such as government policies, cost of renewable energy technologies, and price of fossil fuels will play key role in this required energy transition to reduce CO_2 emissions.[10] Meanwhile, carbon capture and utilization can be a decisive strategy in CO_2 mitigation as discussed in the following section.

1.2   Closing the carbon cycle

Nature is wise. The CO_2 emissions from nature such as ocean, vegetation, soil and animals, can be approximately balanced by its natural uptake in ocean and land.[11] However, the increasing release of CO_2 by burning fossil fuels has thrown this carbon cycle out of balance, thus disrupting the climate.[11] In view of the challenges triggered by climate change mitigation, closing the carbon cycle by capturing anthropogenic CO_2 (produced by human activities) and transforming it into chemicals such as fuels is gaining interest in the scientific and industrial communities (**Figure 1.5**). In the first place, the development and implementation of CO_2 capture technologies will be determinant in the subsequent valorisation of CO_2 as an abundant chemical feedstock. There exist commercially available methods to separate this greenhouse gas coming from localised points where combustion takes place, mainly during electricity generation and industrial processes. Nonetheless, these methods are still costly and researchers are facing the challenge of developing much more efficient technologies at competitive prices.[12-13] It is noteworthy that power plants and industries only accounted for 60% of global CO_2 emissions in 2016.[14] In other words, there is still a vast amount of CO_2 that is not emitted by a stationary source, where abovementioned technologies can be implemented. Therefore, considering the impact of mobile sources of CO_2 such as automobiles and aircrafts, capturing CO_2 directly from air would be highly required. Thanks to recent research based on chemical looping, the costs of commercialising the latter technology have been cut down.[15]

Chapter 1
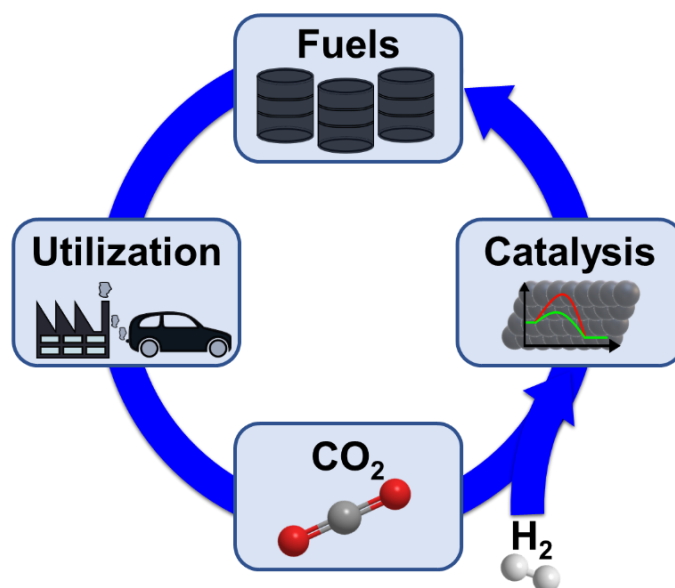
Figure 1.5. Circular energy model to close the carbon cycle.

Once CO_2 is captured and stored, its subsequent conversion to valuable chemicals is not easy at all. It must be recalled that CO_2 is a thermodynamically stable molecule with the standard formation enthalpy of $-393.5 \, kJ \, mol^{-1}$. Hence, its activation requires to overcome such energy at the expense of high temperatures, high pressures, electricity, light, and/or active reactants such as H_2 provided that a catalyst is present. Catalysis offers promising sites to activate this highly stable molecule thus reducing the required energy so that the reaction take place more quickly.[16] The catalyst can be in the same phase as the reactants, i.e. homogenous catalyst, or in a different phase, i.e. heterogeneous catalyst. Homogeneous catalysts offer more advantages than heterogeneous counterparts in terms of reactivity, heat transfer, diffusivity, well-defined active sites and mechanism understanding. Nevertheless, the separation, recovery and recycling of homogeneous catalysts is arduous and costly, hampering their use in large-scale processes in industry. Alternatively, heterogeneous catalysts offers great advantages to transform a large amount of CO_2 into chemicals with increased space-time-yield and benefits from process intensification associated with continuous operation, more facile product/catalyst separation, and catalyst regeneration, thus taking a step forward to close the carbon cycle by valorising CO_2.[17]

1.3   Hydrogenation of carbon dioxide to chemicals

As mentioned above, the activation of CO_2 molecule is possible by using a catalyst and an active reactant such as hydrogen,[18] methanol[19] or epoxides[20]. Among them, H_2 has attracted great interest because it can be sustainably produced via electrolysis of water[21] provided that the electricity is generated from renewable sources such as solar, wind and hydropower. As shown in **Figure 1.6,** CO_2 hydrogenation can lead to the formation of various valuable

UNIVERSITAT ROVIRA I VIRGILI
CONTINUOUS HYDROGENATION OF CARBON DIOXIDE TO FORMATES AND FORMIC ACID OVER HETEROGENEOUS CATALYSTS
Juan José Corral Pérez

Introduction and overview

chemicals such as higher alcohols,[22] methane (CH_4),[23] carbon monoxide (CO),[24] higher hydrocarbons,[25] methanol (CH_3OH),[26] dimethyl ether (CH_3OCH_3),[27] methyl formate[28] and formic acid (HCOOH).[29] All these chemicals can be employed as both a feedstock chemical and a fuel. Interestingly, some of them such as methane,[30] methanol[31] and formic acid[32] can even be used in fuel cells, which convert chemical energy directly into electricity in a very efficient manner. Furthermore, methanol and formic acid can provide a decisive solution in a future hydrogen economy.
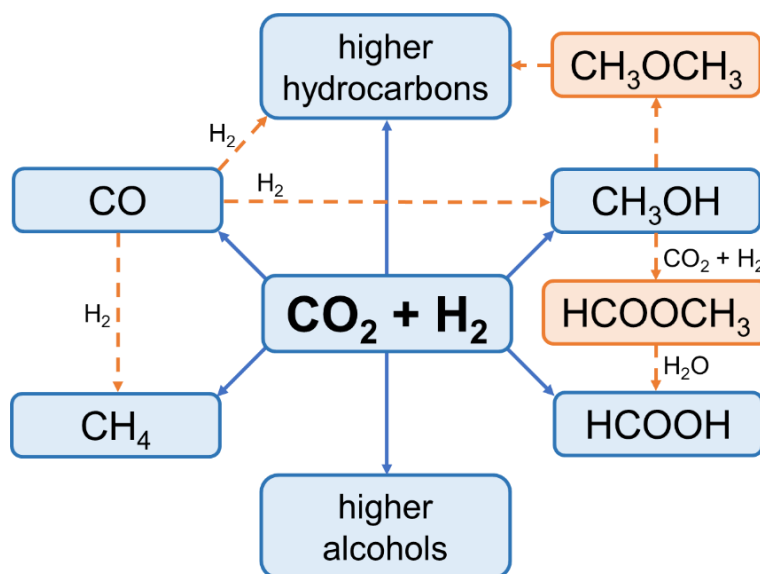
Figure 1.6. CO_2 hydrogenation to chemicals.

Hydrogen is believed to play a key role as an energy carrier, i.e. a substance that contains energy that can be converted to a usable form such as heat or electricity. The use of hydrogen would mark a milestone in combating climate change since water is the only oxidation product when combusted. Nevertheless, its storage and delivery system suppose one of the bigger challenges in the hydrogen economy.[33] Currently, hydrogen storage is based on gaseous-pressurized (> 200 bar) or liquid (-252 °C) hydrogen tanks with major drawbacks such as low hydrogen storage density, safety issues and energy penalty associated with its compression or liquefaction. An alternative is the utilisation of materials based on chemisorption or physisorption of hydrogen. Unfortunately, these intensively studied materials, mainly metallic and complex hybrids, still present significant drawbacks (lack of reversibility, low storage capacity, requirement of high temperatures or pressures) that limit their use as energy carriers for the time being.[34] This is where methanol and formic acid come in, they are promising carrier materials for hydrogen due to their remarkably volumetric density of hydrogen and liquid state at ambient temperature, thereby enhancing its storage, transport and distribution.[35-36] Methanol is composed of two hydrogen atoms more than formic acid. Therefore, methanol has a higher hydrogen storage capacity. However, one equivalent of hydrogen is lost when

Chapter 1

water is formed in the methanol synthesis via CO_2 hydrogenation (Reaction 1.1).[36] This implies a decrease in the atom economy, that is, all the reactant atoms are not found in the desired product.

$$CO_2 + 3H_2 \rightleftarrows CH_3OH + H_2O \qquad (1.1)$$

This is not the case for formic acid, one equivalent of CO_2 reacts with one equivalent of hydrogen to yield one equivalent of formic acid (**Figure 1.7**). This ideal atom economy is the reason why formic acid is preferred over methanol as a hydrogen carrier obtained from CO_2. Ideally, hydrogen should be provided through the decomposition of formic acid via dehydrogenation reaction while the release of CO_2 as a side-product should not suppose any problem, since CO_2 may be captured and hydrogenated to formic acid thus closing the cycle (**Figure 1.7**).[36-37] For both reactions, suitable and efficient catalysts are required. While there exist a vast literature on homogeneous catalysts for these two reactions,[38] [39-40] only a few reports on the direct CO_2 hydrogenation to form formic acid over heterogeneous catalysts can be found.[41-43] This is most likely due to the challenging thermodynamics of such gas-phase reaction, which is strongly endergonic (unfavourable under standard pressure and temperature conditions due to a positive change in Gibbs free energy). Since heterogeneous catalysts have a major potential for large-scale operation (*vide supra*), the aim of this work is to develop such catalytic materials and processes to increase the viability and feasibility of the formic acid synthesis via CO_2 hydrogenation.
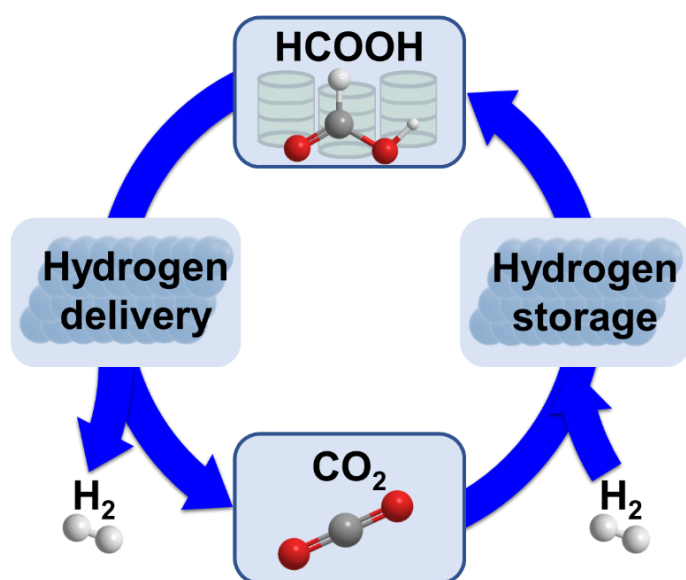
Figure 1.7. The formic acid – carbon dioxide cycle.

UNIVERSITAT ROVIRA I VIRGILI
CONTINUOUS HYDROGENATION OF CARBON DIOXIDE TO FORMATES AND FORMIC ACID OVER HETEROGENEOUS CATALYSTS
Juan José Corral Pérez

Introduction and overview

1.4 Formic acid

1.4.1 Properties and uses

Formic acid, methanoic acid in IUPAC nomenclature, is a colourless and corrosive liquid with a pungent odour. It was first obtained by dry distillation from ants (*formica* in latin), which gave the name to this compound. It is miscible with water and many polar solvents, and partially miscible with hydrocarbons.[44] The most important properties of formic acid are summarised in **Table 1.1**. Interestingly, gaseous formic acid does not behave as an ideal gas due to its hydrogen-bonded dimers (**Figure 1.8**).[45] Despite the relative stability of formic acid at room temperature, in concentrations near 100% it is particularly unstable. Moreover, it can be thermally decomposed via dehydration (Reaction 1.2) or dehydrogenation (Reaction 1.3) reactions.[46] This should not be a problem because most applications require diluted formic acid and the concentration of 85% is the most demanded.[47]

$$HCOOH \rightarrow CO + H_2O \tag{1.2}$$

$$HCOOH \rightarrow CO_2 + H_2 \tag{1.3}$$

Table 1.1. Some chemical and physical properties of formic acid.[48]

Appearance	clear liquid	Boiling point (ºC)	100.8
Molecular formula	CH_2O_2	Flash point (ºC)	69
Molecular weight	46.025 g/mol	Density (at 20 ºC)	1.220 g/cm^3
Melting point (ºC)	8.3	Solubility in H$_2$O	miscible
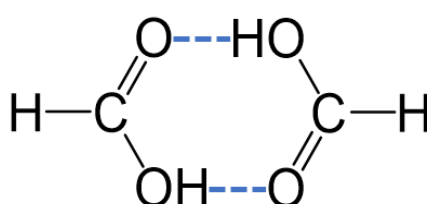
Figure 1.8. Cyclic dimer of formic acid (dashed lines represent hydrogen bonds).

Besides the potential of formic acid as a chemical energy carrier, its largest application is in silage and animal feed preservation, followed by leather and tanning. These applications accounted for nearly 49% of world consumption in 2016. Other uses of formic acid include textile dyeing and finishing, formate salts, pharmaceuticals/food chemicals, rubber chemicals, catalysts, and plasticizers. Although the current world market was amply supplied in 2016, additional world capacity is expected in the upcoming years in order to meet a strong demand growth, which is closely related to rising population and meat consumption.[47]

Chapter 1

1.4.2 Production

Industrially, formic acid can be produced by four different processes: acidolysis of formate salts, oxidation of hydrocarbons, hydrolysis of formamide, and methyl formate hydrolysis. The first one is the oldest industrial process carried out with mineral acids such as sulfuric and phosphoric acid. The main inconvenient of this reaction is the generation of salts such as sulfates and phosphates as by-products. For a long time, formic acid was also obtained as a by-product of the oxidation of hydrocarbons to produce acetic acid. Nowadays, acetic acid is produced via carbonylation of methanol without the formation of formic acid. The hydrolysis of formamide to yield formic acid played an important role in Europe. However, this route poses problems such as consumption of ammonia and sulfuric acid, as well as production of ammonium sulfate. Due to the economic and environmental downsides of these three processes, the hydrolysis of methyl formate without undesirable by-products was commercially developed.[44, 49] Further details on methyl formate will be given in **Section 1.5**.

Currently, most of the installed capacity for formic acid production is based on methyl formate hydrolysis (Reaction 1.4).[44] This reaction is autocatalytic, that is, the reaction product (formic acid) is itself the catalyst for the hydrolysis. Even so, in some processes a strongly acidic ion-exchange resin can be employed as a catalyst.[50] Unfortunately, formic acid is acid enough to catalyse the back-esterification of the reaction products to methyl formate. Therefore, separating the unreacted methyl formate without back-esterification is quite challenging. Nonetheless, the main problem lies in the fact that the hydrolysis is a reversible reaction with a relatively unfavourable equilibrium. In order to overcome such restriction, there exist two main options, as described below.

The first one consists on using a large excess of one of the reactants, i.e. higher than stoichiometric ratio, to drive the equilibrium forward. In the Kemira-Leonard process, an excess of methyl formate is employed and formic acid is dehydrated by distillation, concentrations up to 98 wt% of formic acid are obtained by connecting a second dehydration column.[51] Alternatively, in the BASF process, hydrolysis is carried out with an excess of water. This approach has an energy penalty associated with the removal of the excess water from formic acid. It should be recalled that simple distillation cannot provide concentrations of formic acid in water higher than the azeotropic composition. Hence, it is usually required to make use of pressure-swing distillation (two columns operating at two different pressures) or entraining agents such as ethers, esters and ketones. Due to the high energy consumption of these processes, extractive distillation by means of a basic extractant is a good alternative.[52] For instance, BASF is separating the water via liquid–liquid extraction with a secondary amide and the extract is distilled to obtain formic acid (90-98 wt%).[53] Another approach developed by

UNIVERSITAT ROVIRA I VIRGILI
CONTINUOUS HYDROGENATION OF CARBON DIOXIDE TO FORMATES AND FORMIC ACID OVER HETEROGENEOUS CATALYSTS
Juan José Corral Pérez

Introduction and overview

BASF to overcome such unfavourable equilibrium is to use an additive, such as a tertiary amine. This additive forms an adduct with formic acid (Reaction 1.5), thus decreasing the amount of free formic acid in the solution so that the equilibrium is shifted towards the products.[54] Subsequently, formic acid can be distilled from the base without decomposition.[55]

$$HCOOCH_3 + H_2O \rightleftarrows HCOOH + CH_3OH \tag{1.4}$$

$$HCOOH + NR_3 \rightleftarrows HCOOH \cdot NR_3 \tag{1.5}$$
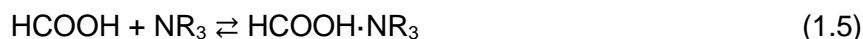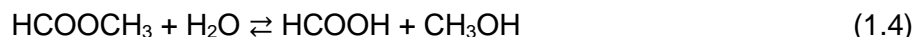
1.4.3 Hydrogenation of carbon dioxide

In addition to methyl formate hydrolysis, formic acid can also be produced from CO_2 and hydrogen. CO_2 hydrogenation to formic acid (Reaction 1.6) is not only a key strategy for CO_2 mitigation and H_2 economy, but also supposes an important advantage in industry due to the absence of water in the product recovery. In the 1980s, BP chemicals first introduced this technology and BASF has developed it (Reaction 1.7).[56-57] In this reaction, an homogeneous catalyst based on Ru is required together with a tertiary amine such as trihexylamine ($[CH_3(CH_2)_5]_3N$), and an alcohol such as methanol at 50-70 ºC and 100-120 bar. The formic acid–amine complex is thermally dissociated at 150-185 °C (Reaction 1.8). Besides Ru, other transition metal complexes based on Ir, Rh, Pd, Ni, Fe, Ti, and Mo have also been reported with excellent activities.[38] The main disadvantage of this process is the recovery and recycling of expensive and soluble catalysts. This is further confirmed by a study that evaluates the technological and economic feasibility of such approach. According to the study, the plant is technically feasible but it is not economically sustainable.[58] A solution to decrease the operating costs would be the use of heterogeneous catalysts, only then may CO_2 hydrogenation to formic acid inch closer to commercial viability.
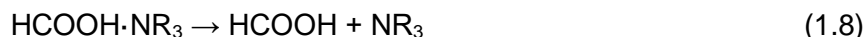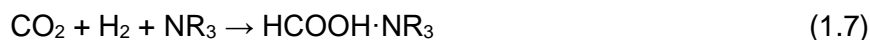
$$CO_2 + H_2 \rightarrow HCOOH \tag{1.6}$$

$$CO_2 + H_2 + NR_3 \rightarrow HCOOH \cdot NR_3 \tag{1.7}$$

$$HCOOH \cdot NR_3 \rightarrow HCOOH + NR_3 \tag{1.8}$$

The greatest hindrance to the development of heterogeneous catalysts arises from serious thermodynamic limitations of this reaction. It must not be forgotten that the conversion of gaseous carbon dioxide and hydrogen into liquid formic acid is strongly endergonic due to the unfavourable entropic contribution ($\Delta G^0_{298K} = 32.9$ kJ mol^{-1}). Note that in all the reports that make use of homogeneous catalysts, the solvent allows the reaction to become exergonic (favourable under standard pressure and temperature conditions due to a negative change in Gibbs free energy), for example when operating in the aqueous phase ($\Delta G^0_{298K} = -4$ kJ

Chapter 1

mol^{-1}).[17] An additional constraint is the thermal decomposition of formic acid over metal surfaces.[35] Notwithstanding these challenges, the use of heterogeneous catalysts is doable because it has been demonstrated that the thermodynamic equilibrium can be disturbed by secondary reaction or molecular interaction. The following is a brief outline of the most relevant findings in this field.

The first attempt to synthesize formates by hydrogenation reaction using a heterogeneous catalyst was reported in 1914. Under relatively mild conditions in the presence of H_2, Pd black was employed as catalyst while alkali/alkaline earth (bi)carbonates as the CO_2 source. [59] Later, in 1935, formamide was synthesized via CO_2 hydrogenation at high pressure (400 bar) over a Raney Ni catalyst. Primary and secondary amines in alcohol as solvent were also added in the reaction mixture.[41] Ru nanoparticles in the presence of an ionic liquid or triethylamine together with water is a more recent example of this reaction catalysed by pure metal catalysts.[60-61] Even though these pure metal catalysts show good activities, the common strategy in heterogeneous catalysis consists of dispersing active metals onto support materials to increase the number of active sites. This has been proven effective by a few studies using Pd, Ru or Au as active metals supported on different materials such as metal oxides, hydrotalcites and activated carbon.[62-65] For instance, Au nanoparticles were supported on metal oxides such as Al_2O_3, TiO_2, ZnO and CeO_2 and the highest catalytic performance was observed for Au/Al_2O_3. Its superior activity was attributed to Au nanoparticles together with the basic sites of Al_2O_3.[64] Nonetheless, the roles of metal and support in the reaction were not clearly revealed. This is by no means a simple task and a few studies that tackle this issue are available. Therefore, some questions common to all heterogeneous catalysts, like the location and nature of active sites, still remain unanswered.

That is one of the reasons why heterogenized molecular catalysts are recently gaining interest. This kind of catalysts is based on the immobilization of molecular metal complexes on a solid support, thus benefiting from the advantages of both homogeneous and heterogeneous catalysis. In other words, they can provide a higher activity, well-defined active sites that allow a better understanding of the relationship between structure and reactivity, and an easier catalyst handling and separation. Since a lot of effort has been deployed to catalyse homogeneously the CO_2 hydrogenation to formic acid/formates employing Ir- and Ru-based complexes, such transition metal complexes with a wide range of ligands have been supported on solid matrices based on SiO_2 and polymers.[66-68] Among these supports, porous organic frameworks (POFs) are attracting increasing attention because they possess abundantly available coordinating sites such as N atoms to stably immobilize molecular complexes.[69-70] Within this category of materials, covalent triazine frameworks (CTFs), which are made upon

UNIVERSITAT ROVIRA I VIRGILI
CONTINUOUS HYDROGENATION OF CARBON DIOXIDE TO FORMATES AND FORMIC ACID OVER HETEROGENEOUS CATALYSTS
Juan José Corral Pérez

Introduction and overview

trimerization of aromatic nitriles, have been recently used to immobilize Ir complexes due to the presence of numerous bipyridylic moieties.[71-72] Although these studies show that these heterogeneous catalysts can be successfully synthesized, their activity in the CO_2 hydrogenation to formic acid only has been tested in the presence of solvents and basic additives under batch conditions, thus not taking advantage of continuous operation (*vide supra*). Furthermore, the stability of these grafted catalysts related to metal leaching as well as the surface species formed during the reaction have not been deeply investigated yet.

In summary, according to the state of the art of the heterogeneous catalysts reported for the synthesis of formic acid/formates via CO_2 hydrogenation, the catalysts can be roughly divided into the following two categories: (un)supported metal catalysts and heterogenized molecular catalysts. The common strategies to overcome the thermodynamic restrictions of this reaction consist of reacting formic acid/formates with primary or secondary amines to yield formamides, or simply neutralization with a weak base such as tertiary amines or alkali/alkaline earth bicarbonates. Both strategies can restrain the industrial development of this process due to the operation costs associated with separation and post-synthetic steps of the additives. To address this concern, the reaction of unstable formic acid from CO_2 and H_2 with methanol to yield methyl formate is an attractive alternative for a base-free process.

1.5 Methyl formate

1.5.1 Properties and uses

Methyl formate, also known as methyl methanoate, is the simplest carboxylate ester. It is a slightly corrosive and volatile liquid soluble in water and most organic solvents.[73] The most significant properties of methyl formate are summarized in **Table 1.2**. Its main application is as intermediate in the large manufacture of formic acid (*vide supra*) and derivatives such as formamide. In fact, methyl formate has been proposed as a potential intermediate in C_1 chemistry.[73] Besides this, in industry it is also used as an agricultural fumigant[74] and a blowing agent for foams.[75]

Table 1.2. Some chemical and physical properties of methyl formate.[48]

Appearance	colourless liquid	Boiling point (ºC)	31.5
Molecular formula	$C_2H_4O_2$	Flash point (ºC)	-19
Molecular weight	60.052 g/mol	Density (at 20 ºC)	0.977 g/cm^3
Melting point (ºC)	-100	Solubility in H_2O (at 20 ºC)	0.30 g/cm^3

Chapter 1

1.5.2 Production

The liquid-phase carbonylation of methanol (Reaction 1.9) in the presence of a strong base to produce methyl formate represents a mainstream technology, which was first introduced by BASF.[76] Typically, this reaction is performed using sodium methoxide ($NaOCH_3$) as catalyst at 80 ºC and 40 bar. The reported methanol conversion is around 30% while the conversion of carbon monoxide is about 95%.[44] This process is common in the first stage of the different licenced Kemira-Leonard and BASF processes for formic acid synthesis via methyl formate hydrolysis. Note that in both processes, the methanol formed during the hydrolysis (Reaction 1.4) is recycled to the carbonylation step (Reaction 1.9). The main drawbacks of methanol carbonylation are associated with the use of an alkaline metal methoxide catalyst. Besides the costs of separating and recycling this catalyst, formation of formate salts as side-products with lower solubility can cause plugging. Furthermore, the catalyst can not only cause equipment corrosion but also lead to operational problems in presence of moisture and CO_2.[76-77] This may be the reason why BASF attempted to decrease the amount of catalyst at expenses of increasing the temperature and pressure (up to 250 bar) for a continuous preparation of methyl formate.[78]

$$CH_3OH + CO \rightarrow HCOOCH_3 \hspace{3cm} (1.9)$$

Despite the reliability of methanol carbonylation to produce methyl formate, methanol dehydrogenation (Reaction 1.10) has attracted great attention because methanol is the only reactant, hydrogen is a useful product and most importantly, the catalyst is heterogeneous. Using a $Cu–Zn–Zr/Al_2O_3$ catalyst, the conversion of methanol is around 59% with 90% of selectivity to methyl formate at 250 °C and atmospheric pressure.[76] Mitsubishi Gas Chemical Co. Ltd. has commercialised this process on a large scale.[79] As depicted in **Figure 1.9**, in addition to the commercial synthetic routes, other approaches have also been explored such as oxidative dehydrogenation of methanol,[80] direct synthesis from syngas,[81] dimerization of formaldehyde[82] and CO_2 hydrogenation in presence of methanol (Reaction 1.11).

$$2CH_3OH \rightarrow HCOOCH_3 + 2H_2 \hspace{3cm} (1.10)$$

$$CO_2 + H_2 + CH_3OH \rightarrow HCOOCH_3 + H_2O \hspace{2cm} (1.11)$$
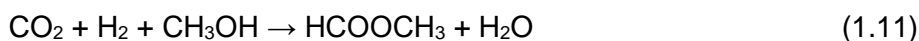
The latter has recently gained interest owing to the increasing pressure to valorise CO_2. The methyl formate production from CO_2 has been demonstrated using both homogeneous[83-85] and heterogeneous catalysts.[28, 64, 86-87] The reported homogeneous catalysts are based on Ru complexes and, as expected, basic additives such as triethylamine are employed in the reaction.[83-85] Due to the abovementioned disadvantages of using homogeneous catalysts,

UNIVERSITAT ROVIRA I VIRGILI
CONTINUOUS HYDROGENATION OF CARBON DIOXIDE TO FORMATES AND FORMIC ACID OVER HETEROGENEOUS CATALYSTS
Juan José Corral Pérez

Introduction and overview

special attention is given to the base-free methyl formate production via CO_2 hydrogenation over heterogenous catalysts in the presence of methanol.[28, 64, 87-88] In spite of scarce academic research on this approach, it may open up new avenues for the continous production of formic acid, as further discussed in the next section.
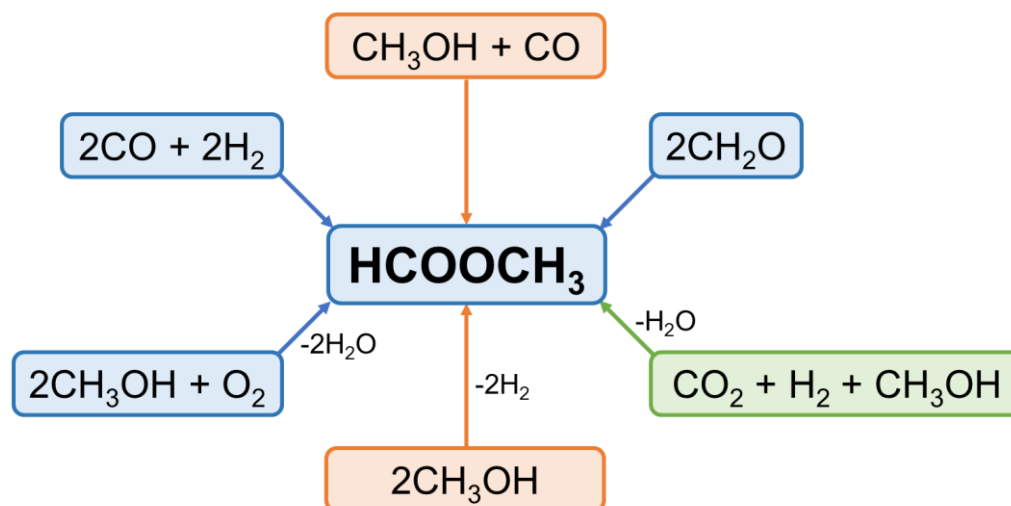
Figure 1.9. Synthetic routes to produce methyl formate.

1.5.3 Methyl formate as an intermediate

After having an overall look at the synthesis routes of formic acid and methyl formate, a new synthetic path to continuously produce formic acid via CO_2 hydrogenation can be proposed. The key relies on including a secondary reaction using methyl formate as intermediate. In fact, this is not new if one further observation regarding the industrial synthesis of formic acid is made. According to the sum of the two involved reactions, i.e. methanol carbonylation and methyl formate hydrolysis, formic acid can be obtained directly from CO and H_2O (Reaction 1.12). Even so, this reaction is not favourable and methyl formate is formed as an intermediate to bypass such thermodynamic hindrance.

$$CH_3OH + CO \rightarrow HCOOCH_3$$
$$HCOOCH_3 + H_2O \rightarrow HCOOH + CH_3OH$$
$$\overline{\qquad\qquad\qquad\qquad\qquad\qquad\qquad\qquad}$$
$$CO + H_2O \rightarrow HCOOH \qquad\qquad (1.12)$$
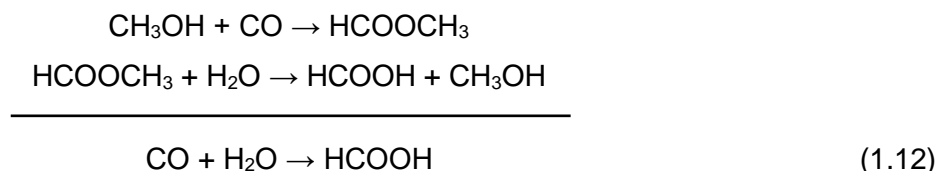
Analogously, the same strategy can be applied to the direct formic acid synthesis over heterogeneous catalysts as summarised in **Figure 1.10**. In the first reactor, CO_2 is hydrogenated to formic acid/formates and methanol prior to their further transformation to methyl formate in the same reactor. While Cu-based catalysts for the methanol synthesis are commercially available, the catalysts for formic acid/formate synthesis prior to its esterification will be evaluated in the present thesis. The first option is to use more conventional catalysts,

Chapter 1

i.e. metal supported on metal oxides, where formate species are generated on the catalyst surface and reacted with methanol to give methyl formate. The second option is to use heterogenized molecular catalysts where molecular structures active in formic acid synthesis are mimicked. The two catalysts for methanol and formic acid/formate syntheses may be physically mixed or spatially and sequentially separated. These reactions will be examined under high pressure conditions because according to Le Châtelier's principle, elevated pressures are expected to positively influence the products formation.[88-89] Methyl formate produced in *Reactor 1* will be hydrolysed in the presence of known catalysts (acidic zeolites and resins) in *Reactor 2* to simultaneously yield formic acid and methanol.
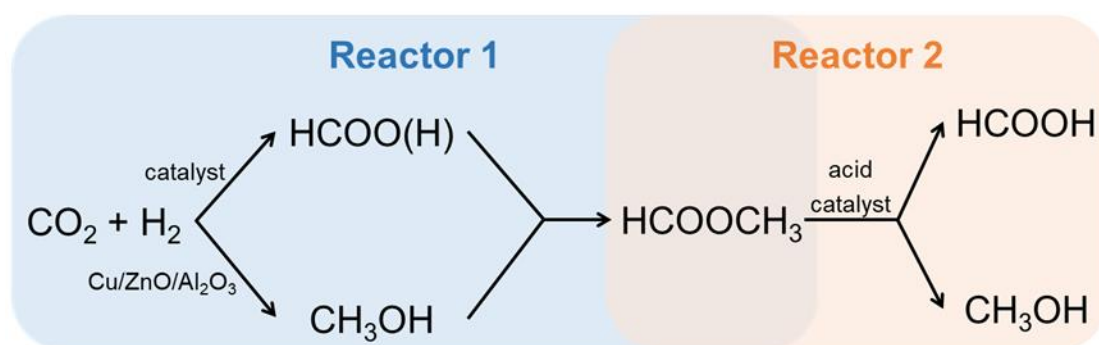
Figure 1.10. The new synthetic approach of formic acid and methanol using two sequentially connected reactors packed with heterogeneous catalysts (water is not shown for brevity).

1.6 Aim and overview of the thesis

The aim of the present thesis is to explore new catalytic materials and processes to continuously form methyl formate via CO_2 hydrogenation, while taking advantage of the high-pressure conditions. Methanol is co-fed into the reactor in order to facilitate methyl formate synthesis, thus reducing the complexity of the catalytic system before switching to *in situ* formation of methanol by inclusion of a commercial Cu-based catalyst. This stepwise approach can lead to a better identification of the critical parameters that are decisive for the reaction performance. The heterogeneous catalysts evaluated include both supported metal and heterogenized molecular ones, which are economically advantageous compared to homogeneous counterparts. *In situ* and *operando* spectroscopic characterization of reaction intermediates over these catalysts, coupled with computational chemistry, is performed to provide key insights into the active sites and reaction mechanisms. This study represents a step forward in including methyl formate as a transient intermediate to circumvent the thermodynamic constraints that hamper the formic acid synthesis from CO_2 and H_2 over heterogeneous catalysts.

Chapter 2 thoroughly describes the materials, methods and systems that have been employed in the present work. Special emphasis is put on the high-pressure micro-reactor

UNIVERSITAT ROVIRA I VIRGILI
CONTINUOUS HYDROGENATION OF CARBON DIOXIDE TO FORMATES AND FORMIC ACID OVER HETEROGENEOUS CATALYSTS
Juan José Corral Pérez

Introduction and overview

setup for the continuous catalytic hydrogenation of CO_2 in the presence of a third liquid reactant such as methanol. The systems for *in situ* and *operando* spectroscopy are also highlighted together with the data treatment procedures.

Chapter 3 deals with the continuous methyl formate synthesis via CO_2 hydrogenation in the presence of methanol over silica-supported metal nanoparticles. Silica is chosen as a neutral support in order to probe the specific reactivity of copper, silver and gold in such reaction. This study highlights the importance of employing combined methodologies (transient *in situ* and *operando* vibrational spectroscopy, and DFT) to uncover fundamental catalytic reaction steps taking place at metal-support interfaces.

Chapter 4 shows the reactivity of γ-Al_2O_3 and ZrO_2 supported silver nanoparticles in comparison to the SiO_2 counterpart. Various process parameters such as temperature, gas hourly space velocity (GHSV) and molar ratio of reactants are evaluated to optimize the hydrogenation of CO_2 to methyl formate. *In situ* and *operando* vibrational spectroscopic studies together with multivariate analysis shed light on the key role of support in supported silver nanoparticles.

Chapter 5 explores the use of a heterogenized iridium complex under continuous operation in the synthesis of methyl formate and formic acid. Surface species formed over this molecular heterogeneous catalyst are first revealed by *in situ* spectroscopic studies. The stability of the catalyst is discussed in terms of iridium coordination before and after the reaction by *ex situ* X-ray absorption spectroscopy (XAS).

Chapter 6 summarises the most remarkable results of the thesis and offers a brief outlook on the catalytic conversion of CO_2 to formic acid.

Chapter 1

Bibliography

1. Bithas, K.; Kalimeris, P., A Brief History of Energy Use in Human Societies. In *Revisiting the Energy-Development Link: Evidence from the 20th Century for Knowledge-based and Developing Economies*, Springer International Publishing: Cham, 2016; pp 5-10.
2. *Key World Energy Statistics*; International Energy Agency: 2018.
3. *International Energy Outlook*; International Energy Agency: 2017.
4. *World Population Prospects*; United Nations: 2017.
5. *Climate Change 2014*; Intergovernmental Panel on Climate Change: 2014.
6. *Global Energy & CO_2 Status Report*; Internation Energy Agency: 2017.
7. Dlugokencky, E.; Tans, P. https://www.esrl.noaa.gov (accessed December 25).
8. https://climate.nasa.gov (accessed December 18).
9. https://earthobservatory.nasa.gov (accessed December 17).
10. *Renewable Energy Sources and Climate Change Mitigation: Special Report of the Intergovernmental Panel on Climate Change*. Cambridge University Press: Cambridge, 2011.
11. https://science.nasa.gov/ (accessed December 21).
12. Lockwood, T., *Enrgy. Proced.* **2017,** *114*, 2658-2670.
13. Koytsoumpa, E. I.; Bergins, C.; Kakaras, E., *J. Supercrit. Fluid.* **2018,** *132*, 3-16.
14. *CO_2 Emissions from Fuel Combustion - Highlights*; Internation Energy Agency: 2018.
15. Keith, D. W.; Holmes, G.; St. Angelo, D.; Heidel, K., *Joule* **2018,** *2* (8), 1573-1594.
16. Álvarez, A.; Borges, M.; Corral-Pérez, J. J.; Olcina, J. G.; Hu, L.; Cornu, D.; Huang, R.; Stoian, D.; Urakawa, A., *Chemphyschem* **2017,** *18* (22), 3135-3141.
17. Álvarez, A.; Bansode, A.; Urakawa, A.; Bavykina, A. V.; Wezendonk, T. A.; Makkee, M.; Gascon, J.; Kapteijn, F., *Chem. Rev.* **2017,** *117* (14), 9804-9838.
18. Wang, W.; Wang, S.; Ma, X.; Gong, J., *Chem. Soc. Rev.* **2011,** *40* (7), 3703-3727.
19. Bansode, A.; Urakawa, A., *ACS Catal.* **2014,** *4* (11), 3877-3880.
20. Klaus, S.; Lehenmeier, M. W.; Anderson, C. E.; Rieger, B., *Coordin. Chem. Rev.* **2011,** *255* (13), 1460-1479.
21. Ursua, A.; Gandia, L. M.; Sanchis, P., *P. IEEE* **2012,** *100* (2), 410-426.
22. Bai, S.; Shao, Q.; Wang, P.; Dai, Q.; Wang, X.; Huang, X., *J. Am. Chem. Soc.* **2017,** *139* (20), 6827-6830.
23. Su, X.; Xu, J.; Liang, B.; Duan, H.; Hou, B.; Huang, Y., *J. Energy Chem.* **2016,** *25* (4), 553-565.
24. Gonçalves, R. V.; Vono, L. L. R.; Wojcieszak, R.; Dias, C. S. B.; Wender, H.; Teixeira-Neto, E.; Rossi, L. M., *Appl. Catal. B-Environ.* **2017,** *209*, 240-246.
25. Li, W.; Wang, H.; Jiang, X.; Zhu, J.; Liu, Z.; Guo, X.; Song, C., *RSC Adv.* **2018,** *8* (14), 7651-7669.
26. Gaikwad, R.; Bansode, A.; Urakawa, A., *J. Catal.* **2016,** *343*, 127-132.
27. Bansode, A.; Urakawa, A., *J. Catal.* **2014,** *309*, 66-70.
28. Yu, K. M. K.; Yeung, C. M. Y.; Tsang, S. C., *J. Am. Chem. Soc.* **2007,** *129* (20), 6360–6361.
29. Weilhard, A.; Qadir, M. I.; Sans, V.; Dupont, J., *ACS Catal.* **2018,** *8* (3), 1628-1634.
30. Murray, E. P.; Tsai, T.; Barnett, S. A., *Nature* **1999,** *400*, 649.
31. Kamarudin, S. K.; Achmad, F.; Daud, W. R. W., *Int. J. Hydrogen Energ.* **2009,** *34* (16), 6902-6916.
32. Aslam, N. M.; Masdar, M. S.; Kamarudin, S. K.; Daud, W. R. W., *APCBEE Proc.* **2012,** *3*, 33-39.
33. Veneri, O., Hydrogen as Future Energy Carrier. In *Hydrogen Fuel Cells for Road Vehicles*, Springer London: London, 2011; pp 33-70.
34. Zhou, L., *Renew. Sust. Eerg. Rev.* **2005,** *9* (4), 395-408.
35. Plass, L.; Bertau, M.; Linicus, M.; Heyde, R.; Weingart, E., Methanol as a Hydrogen and Energy Carrier. In *Methanol: The Basic Chemical and Energy Feedstock of the*

UNIVERSITAT ROVIRA I VIRGILI
CONTINUOUS HYDROGENATION OF CARBON DIOXIDE TO FORMATES AND FORMIC ACID OVER HETEROGENEOUS CATALYSTS
Juan José Corral Pérez

Introduction and overview

Future: Asinger's Vision Today, Bertau, M.; Offermanns, H.; Plass, L.; Schmidt, F.; Wernicke, H.-J., Eds. Springer Berlin Heidelberg: Berlin, Heidelberg, 2014; pp 619-655.

36. Enthaler, S.; von Langermann, J.; Schmidt, T., *Energ. Environ. Sci.* **2010,** *3* (9), 1207-1217.
37. Müller, K.; Brooks, K.; Autrey, T., *Energ. Fuel.* **2017,** *31* (11), 12603-12611.
38. Jessop, P. G.; Joó, F.; Tai, C.-C., *Coordin. Chem. Rev.* **2004,** *248* (21), 2425-2442.
39. Treigerman, Z.; Sasson, Y., *ChemistrySelect* **2017,** *2* (21), 5816-5823.
40. Morris, D. J.; Clarkson, G. J.; Wills, M., *Organometallics* **2009,** *28* (14), 4133-4140.
41. Farlow, M. W.; Adkins, H., *J. Am. Chem. Soc.* **1935,** *57* (11), 2222-2223.
42. Mondelli, C.; Puértolas, B.; Ackermann, M.; Chen, Z.; Pérez-Ramírez, J., *ChemSusChem* **2018,** *11* (17), 2859-2869.
43. Moret, S.; Dyson, P. J.; Laurenczy, G., *Nat. Commun.* **2014,** *5*, 4017.
44. Formic Acid. In *Ullmann's Encyclopedia of Industrial Chemistry*, 2011.
45. Balabin, R. M., *J. Phys. Chem. A* **2009,** *113* (17), 4910-4918.
46. Yasaka, Y.; Yoshida, K.; Wakai, C.; Matubayasi, N.; Nakahara, M., *J. Phys. Chem. A* **2006,** *110* (38), 11082-11090.
47. https://ihsmarkit.com/products/formic-acid-chemical-economics-handbook.html (accessed December 24).
48. https://pubchem.ncbi.nlm.nih.gov (accessed January 7).
49. Jogunola, O.; Salmi, T.; Wärnå, J.; Mikkola, J.-P.; Tirronen, E., *Ind. Eng. Chem. Res.* **2011,** *50* (1), 267-276.
50. Saari, K.; Tirronen, E.; Vuori, A.; Lahtinen, M. Method for preparing formic acid. 1998.
51. Leonard, J. D. Preparation of formic acid by hydrolysis of methyl formate. 1979.
52. Buelow, H.; Hohenschutz, H.; Schmidt, J. E.; Sachsze , W. Purification of formic acid by extractive distillation. 1978.
53. Germann, E. A process for the continuous preparation of methyl formate. 1961.
54. Jogunola, O.; Salmi, T.; Mikkola, J.-P., *J. Mol. Liq.* **2014,** *196*, 334-339.
55. Maria Fries, D.; Mohl, K.-D.; Schäfer, M.; Schneider, D.; Bassler, P.; Rittinger, S.; Teles, J. H. Method for producing formic acid. 2012.
56. Green, M. J.; Lucy, A. R.; Kitson, M.; Smith, S. J. The production of formic acid from a nitrogenous base, carbon dioxide and hydrogen. 1988.
57. Schaub, T.; Paciello, R.; Mohl, K.-D.; Schneider, D.; Schaefer, M.; Rittinger, S. Process for preparing formic acid. 2009.
58. Pérez-Fortes, M.; Schöneberger, J. C.; Boulamanti, A.; Harrison, G.; Tzimas, E., *Int. J. Hydrogen Energ.* **2016,** *41* (37), 16444-16462.
59. Bredig, G.; Carter, S. R., *Ber. Dtsch. Chem. Ges.* **1914,** *47* (1), 541-545.
60. Srivastava, V., *Catal. Lett.* **2014,** *144* (10), 1745-1750.
61. Umegaki, T.; Enomoto, Y.; Kojima, Y., *Catal. Sci. Technol.* **2016,** *6* (2), 409-412.
62. Su, J.; Yang, L.; Lu, M.; Lin, H., *ChemSusChem* **2015,** *8* (5), 813-816.
63. Stalder, C. J.; Chao, S.; Summers, D. P.; Wrighton, M. S., *J. Am. Chem. Soc.* **1983,** *105* (20), 6318-6320.
64. Filonenko, G. A.; Vrijburg, W. L.; Hensen, E. J. M.; Pidko, E. A., *J. Catal.* **2016,** *343*, 97-105.
65. Hao, C.; Wang, S.; Li, M.; Kang, L.; Ma, X., *Catal. Today* **2011,** *160* (1), 184-190.
66. Schmid, L.; Rohr, M.; Baiker, A., *Chem. Commun.* **1999,** (22), 2303-2304.
67. Xu, Z.; McNamara, N. D.; Neumann, G. T.; Schneider, W. F.; Hicks, J. C., *ChemCatChem* **2013,** *5* (7), 1769-1771.
68. McNamara, N. D.; Hicks, J. C., *ChemSusChem* **2014,** *7* (4), 1114-1124.
69. Yang, Z.-Z.; Zhang, H.; Yu, B.; Zhao, Y.; Ji, G.; Liu, Z., *Chem. Commun.* **2015,** *51* (7), 1271-1274.
70. Gunniya Hariyanandam, G.; Hyun, D.; Natarajan, P.; Jung, K.-D.; Yoon, S., *Catal. Today* **2016,** *265*, 52-55.
71. Park, K.; Gunasekar , G. H.; Prakash, N.; Jung, K.-D.; Yoon, S., *ChemSusChem* **2015,** *8* (20), 3410-3413.

Chapter 1

72. Bavykina, A. V.; Rozhko, E.; Goesten, M. G.; Wezendonk, T.; Seoane, B.; Kapteijn, F.; Makkee, M.; Gascon, J., *ChemCatChem* **2016,** *8* (13), 2217-2221.
73. Lee, J. S.; Kim, J. C.; Kim, Y. G., *Appl. Catal.* **1990,** *57* (1), 1-30.
74. Song, C.; Scharf, M. E., *Pestic. Biochem. Phys.* **2008,** *92* (2), 77-82.
75. Modesti, M.; Adriani, V.; Simioni, F., *Polym. Eng. Sci.* **2000,** *40* (9), 2046-2057.
76. Rong, L.; Xu, Z.; Sun, J.; Guo, G., *J. Energy Chem.* **2018,** *27* (1), 238-242.
77. Joerg, K.; Mueller, F.-J.; Irgang, M.; Marosi, L.; Borchert, G. Preparation of methyl formate. 1989.
78. Lippert, F.; Hohn, A.; Dahlhaus, J. Continuous preparation of methyl formate. 1995.
79. Yoneoka, M.; Osugi, M. Process for producing methyl formate. 1976.
80. Kaichev, V. V.; Popova, G. Y.; Chesalov, Y. A.; Saraev, A. A.; Zemlyanov, D. Y.; Beloshapkin, S. A.; Knop-Gericke, A.; Schlögl, R.; Andrushkevich, T. V.; Bukhtiyarov, V. I., *J. Catal.* **2014,** *311* (Supplement C), 59-70.
81. Zhao, H.; Fang, K.; Zhou, J.; Lin, M.; Sun, Y., *Int. J. Hydrogen Energ.* **2016,** *41* (21), 8819-8828.
82. Mueller, L. L.; Griffin, G. L., *J. Catal.* **1987,** *105* (2), 352-358.
83. Jessop, P. G.; Hsiao, Y.; Ikariya, T.; Noyori, R., *J. Chem. Soc., Chem. Commun.* **1995,** (6), 707-708.
84. Krocher, O.; Koppel, R. A.; Baiker, A., *Chem. Commun.* **1997,** (5), 453-454.
85. Yadav, M.; Linehan, J. C.; Karkamkar, A. J.; van der Eide, E.; Heldebrant, D. J., *Inorg. Chem.* **2014,** *53* (18), 9849-9854.
86. Yu, K. M. K.; Tsang, S. C., *Catal. Lett.* **2011,** *141* (2), 259-265.
87. Wu, C. Y.; Zhang, Z. F.; Zhu, Q. G.; Han, H. L.; Yang, Y. Y.; Han, B. X., *Green Chem.* **2015,** *17* (3), 1467-1472.
88. Dietrich, J.; Schindler, S., *Z. Anorg. Allg. Chem.* **2008,** *634* (14), 2487-2494.
89. Gaikwad, R.; Bansode, A.; Urakawa, A., *J. Catal.* **2016,** *343* (Supplement C), 127-132.

UNIVERSITAT ROVIRA I VIRGILI
CONTINUOUS HYDROGENATION OF CARBON DIOXIDE TO FORMATES AND FORMIC ACID OVER HETEROGENEOUS CATALYSTS
Juan José Corral Pérez

Introduction and overview

UNIVERSITAT ROVIRA I VIRGILI
CONTINUOUS HYDROGENATION OF CARBON DIOXIDE TO FORMATES AND FORMIC ACID OVER HETEROGENEOUS CATALYSTS
Juan José Corral Pérez

Chapter 1

2

Materials and methods
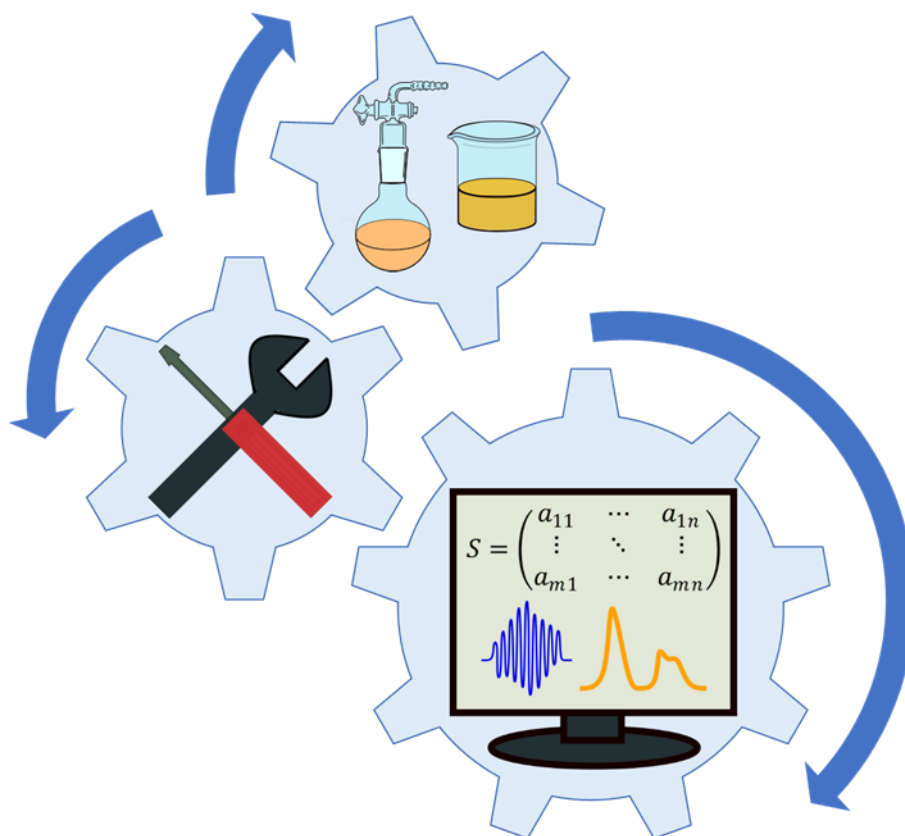
Chapter 2

2.1 Introduction

Catalysis has helped to shape the world we live in. This term was firstly introduced by the Swedish chemist Jöns Jacob Berzelius in 1835 to describe that the rate of a chemical reaction could be accelerated by adding a substance (catalyst) that was not consumed during the process.[1] Since then, catalysis has revolutionized the chemical industry and has opened up new opportunities for making processes more efficient and sustainable. In particular, heterogeneous metal catalysts have been proven advantageous in industrial catalysis such as energy production, chemicals manufacture and materials synthesis among others.[2] The main goal in catalyst design and development is to achieve high activity, selectivity, and stability at low cost.

Generally, heterogeneous catalysis offers great advantages to transform a large amount of reactant(s) with increased space-time-yield and benefits from process intensification associated with continuous operation, more facile product/catalyst separation and catalyst regeneration. The use of micro-reactors under continuous flow conditions makes the heterogeneous catalysts even much more attractive. Micro-reactors are preferred over lab-scale reactors (with inner diameter in the range of sub-inches) since the smaller size of reactor tube offers various advantages. Thanks to the shorter diffusion lengths, mixing efficiency increases and the mass transfer hindrance is reduced. By reducing the reaction volume, the thickness of the reactor wall can be decreased due to the less force exerted on its wall, hence minimizing thermal gradients and heat transfer limitations. Not only characteristics such as mass and heat transport, space-time-yield and reaction selectivity can be improved, but it also enables higher pressure operation and handling dangerous chemicals more safely.[3]

The remaining challenge in heterogeneous catalysis is to understand how a reactant is transformed into a product. Identifying the active sites that directly participate in the catalytic reaction and elucidating its mechanism are pivotal for the rational design of better and new catalysts. Performing spectroscopy over the catalyst material under reaction conditions is a powerful tool for providing answers to this big challenge. To this end, *in situ* spectroscopy has been extensively employed to provide fundamental information about catalytic structure and surface species under reaction or controlled environments. However, such technique cannot establish relationships among catalyst structure, surface intermediates and catalytic performance. That is why *operando* spectroscopy has emerged since 2002, this methodology simultaneously measures the reactivity under reaction or relevant conditions. The field of *operando* spectroscopy has been under intense development to contribute to a better understanding and development of catalytic processes.[4-6]

UNIVERSITAT ROVIRA I VIRGILI
CONTINUOUS HYDROGENATION OF CARBON DIOXIDE TO FORMATES AND FORMIC ACID OVER HETEROGENEOUS CATALYSTS
Juan José Corral Pérez

Materials and methods

This chapter covers all the aspects mentioned above. It establishes the protocols and methods developed during the present thesis for the synthesis of the catalyst materials, the building up of a micro-reactor setup to evaluate their catalytic activity at high pressure under continuous operation, the characterisation *in situ* of the chemical species formed over the catalyst surface as well as deciphering their role in the reaction, and the rigorous analysis of spectroscopic data by means of multivariate spectral analysis.

2.2 Catalyst materials

Since heterogeneous catalysis relies on the chemical species adsorbed on the surface, maximizing the surface-to-volume ratio of the active sites is required not only to decrease cost but also increase performance. For this purpose, metals are usually dispersed onto high surface area supports such as metal oxides. Furthermore, the chemical properties of supports (e.g. acid and basic sites) can influence the catalytic activity and create unique sites with the metallic particles.[7] Among all the methods available for the synthesis of these supported catalysts, impregnation method and surface organometallic approach are employed in the present research work.

2.2.1 Impregnation method

Impregnation is the simplest and most common technique to prepare metal supported catalysts.[8] The preparation of impregnated catalysts consists of mixing a solution that contains a metal salt precursor with a support, followed by drying and subsequent calcination (**Figure 2.1**). While drying removes the excess of solvent, calcination converts the salt form into metal or oxide. If the volume of the metal salt solution is equal to the pore volume of the support, the method is called incipient wetness impregnation. Conversely, wet impregnation refers to an excess of the solution over the pore volume. The advantage of this fast method is that the support can be prepared separately. Furthermore, the metal is well dispersed while there is no loss of material within the support phases. The distribution of the active species on the support can vary depending on the type and concentration of precursor salt, solvent, temperature, type of support and contact time with support.
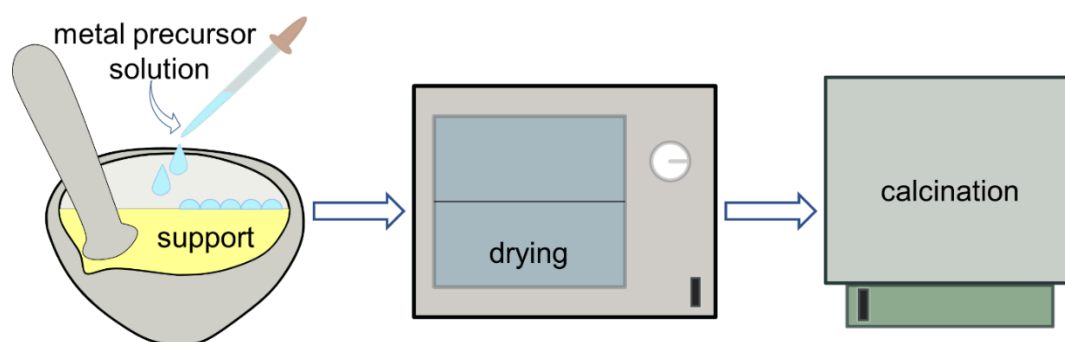
Figure 2.1. Schematic representation of impregnation method.

Chapter 2

Most of the catalysts in this thesis are prepared by the incipient wetness impregnation method using the corresponding precursors dissolved in water. Commercial metal oxides are directly employed as supports. The catalysts were dried overnight in an oven at 100 °C and subsequently calcined in air at 400 °C (the heating ramp rate is kept at 4 °C min^{-1}) for 4 h.

2.2.2 Surface organometallic approach

Surface organometallic chemistry (SOMC) is an approach that allows to synthesize heterogeneous catalysts with well-defined active sites that can be fully characterized. The principle of SOMC is to treat the surface of a support, i.e. metal oxide, as a ligand onto which molecular complexes can be covalently anchored (grafted) via one or more M-O bonds. In the present work, SOMC approach is employed to generate supported metal catalysts rather than single-site catalysts. Within the context of the importance of the interface between the metal and support, this technique allows to prepare catalysts with a narrow size distribution of metal nanoparticles.[9-10]
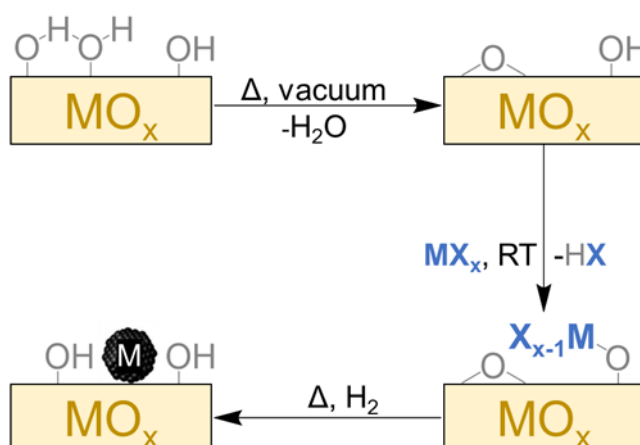
Figure 2.2. Schematic representation of the dehydroxylation of a metal oxide surface and subsequent grafting-reduction sequence.

The process is described as follows (**Figure 2.2**). Since the support surface plays a key role on its reactivity towards reactive inorganic species, all the supports (SiO$_2$, Al$_2$O$_3$ and ZrO$_2$) are carefully pre-treated. Firstly, milli-Q water is added until getting a slurry of the oxide powder. Afterwards, it is dried at ca. 120 °C for several days in an oven to get large agglomerates. The obtained agglomerates are sieved to 250−400 µm particle size. Then, the support (MO$_x$) is placed in a reactor tube (4.5 cm in diameter and ca. 50 cm in length) at 500 °C (60 °C h^{-1}) under synthetic air (60 mL min^{-1}) to remove the organic impurities (calcination), and under vacuum to determine the density of surface hydroxyl groups (dehydroxylation). The reactor is cooled down under high vacuum and the support material is stored under Ar in a solvent-free glove box. Once the support is dehydroxylated, a metal complex with a sufficiently reactive anionic ligand (MX$_x$) is grafted onto it under anhydrous and anaerobic conditions.

UNIVERSITAT ROVIRA I VIRGILI
CONTINUOUS HYDROGENATION OF CARBON DIOXIDE TO FORMATES AND FORMIC ACID OVER HETEROGENEOUS CATALYSTS
Juan José Corral Pérez

Materials and methods
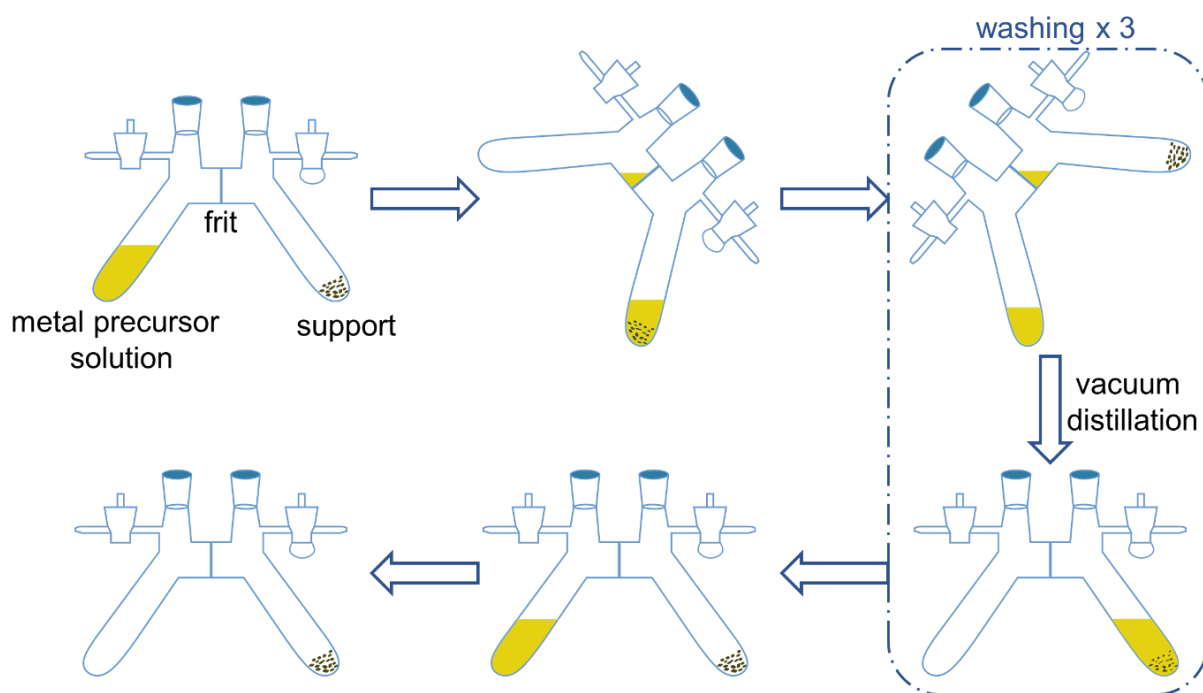
Figure 2.3. Schematic representation of the grafting in a double-Schlenk flask.

In this study, silver mesityl (silver, tetrakis[m-(2,4,6-trimethylphenyl)]tetra-,cyclo (9CI)) is chosen as the organometallic precursor. As shown in **Figure 2.3**, 100 mg of silver mesityl are dissolved in dry pentane (20 mL) in one side of the double-Schlenk while 1.0 g of support is added to the other side under argon. The solution containing the precursor is added to the support through the filter of the double-Schlenk and the resulting suspension is slowly stirred. After 4 hours of reaction at room temperature, the supernatant is filtered into the other arm of the double-Schlenk. In order to remove the unreacted precursor and the product of the grafting reaction, the solvent is transferred back into the other arm of the double-Schlenk via vacuum distillation. The filtrate is then separated from the solid as in the previous step. This washing is repeated 3 times. The grafted support is dried under high vacuum conditions ($\approx 10^{-6}$ mbar) and reduced at 500 °C (100 °C h^{-1}) under H$_2$ atmosphere for 5 h. After reduction, the supported metal catalyst is cooled down to room temperature under H$_2$ before vacuum treatment and storage under argon. The operation is monitored by infrared (IR) spectroscopy at the various stages of the preparation.

2.3 High-pressure CO$_2$ hydrogenation reactor setup

This section describes the design and components of a high-pressure lab scale micro-reactor setup for the continuous catalytic hydrogenation of CO$_2$ in the presence of methanol (CH$_3$OH) up to 300 bar. The analytical system and automated micro-reactor operation are also discussed thoroughly.

Chapter 2

2.3.1 Reactor design and setup

The schematic representation of the high-pressure setup used in this work is depicted in **Figure 2.4**. The reactor setup consists of compression and flow control of the reactants, i.e. H_2, CO_2 and CH_3OH, the reactor and analytical systems, and reactor automation. Each part is described in detail below.

2.3.1.1 Compression and flow control of the reactants

The three different reactants, H_2, CO_2 and CH_3OH, are compressed separately and the ways of controlling the respective flows differ from each other.

The maximum pressure of commercially available hydrogen cylinders is 200 bar. To achieve pressures up to 430 bar, the hydrogen gas cylinder is connected to an air driven hydrogen gas booster (Haskel) using 1/8" SS (stainless steel) tubing (Sandvik) with ID (inner diameter) of 1.75 mm. Two non-return valves (NRV-1 and NRV-2), also called check valves, are connected at the inlet and outlet of gas booster, respectively, to ensure one directional flow. The outlet of gas booster is connected to a H_2 gas reservoir, consisting of three 6-meter coils of 1/4" SS tubing (Sandvik, ID 2.95 mm) connected in series, in order to provide high flow of H_2 when required. A pressure reducing regulator PR-1 (TESCOM) is connected before the reservoir to remove the pressure pulsations caused by the boosting cycles of the gas booster. Two high pressure needle valves (NV-1 and NV-3) are installed at the outlet of the gas booster and between two reservoir coils, respectively, in case high pressure H_2 needs to be released manually due to maintenance tasks or safety reasons. The H_2 reservoir can be isolated from the reactor system if required by means of two high pressure needle valves (NV-2 and NV-4) connected at the inlet and outlet of H_2 reservoir. As shown in **Figure 2.4**, the pressure in H_2 reservoir is measured by pressure indicator PI-2. Due to pressure reducing regulator PR-1, the pressure in H_2 reservoir is ca. 30 bar smaller than the pressure at the outlet of gas booster, which is measured by pressure indicator PI-1. Any overshoot of pressure above 450 bar is avoided by a pressure relief valve (PRV-1) connected in between the H_2 reservoir and mass flow controller (MFC). Filters F-1 (10 µm) and F-2 (2 µm) (VICI, Europe) are connected to ensure the removal of any debris or dust particles that may have a negative effect on the gas booster or MFC. Finally, the flow of hydrogen to the reactor system is controlled by a high-pressure thermal mass flow controller (Bronkhorst, Hi-Tec). A non-return valve (NRV-3) is placed at the outlet of MFC so that neither liquid CO_2 nor methanol can flow back to MFC.

UNIVERSITAT ROVIRA I VIRGILI
CONTINUOUS HYDROGENATION OF CARBON DIOXIDE TO FORMATES AND FORMIC ACID OVER HETEROGENEOUS CATALYSTS
Juan José Corral Pérez

Materials and methods
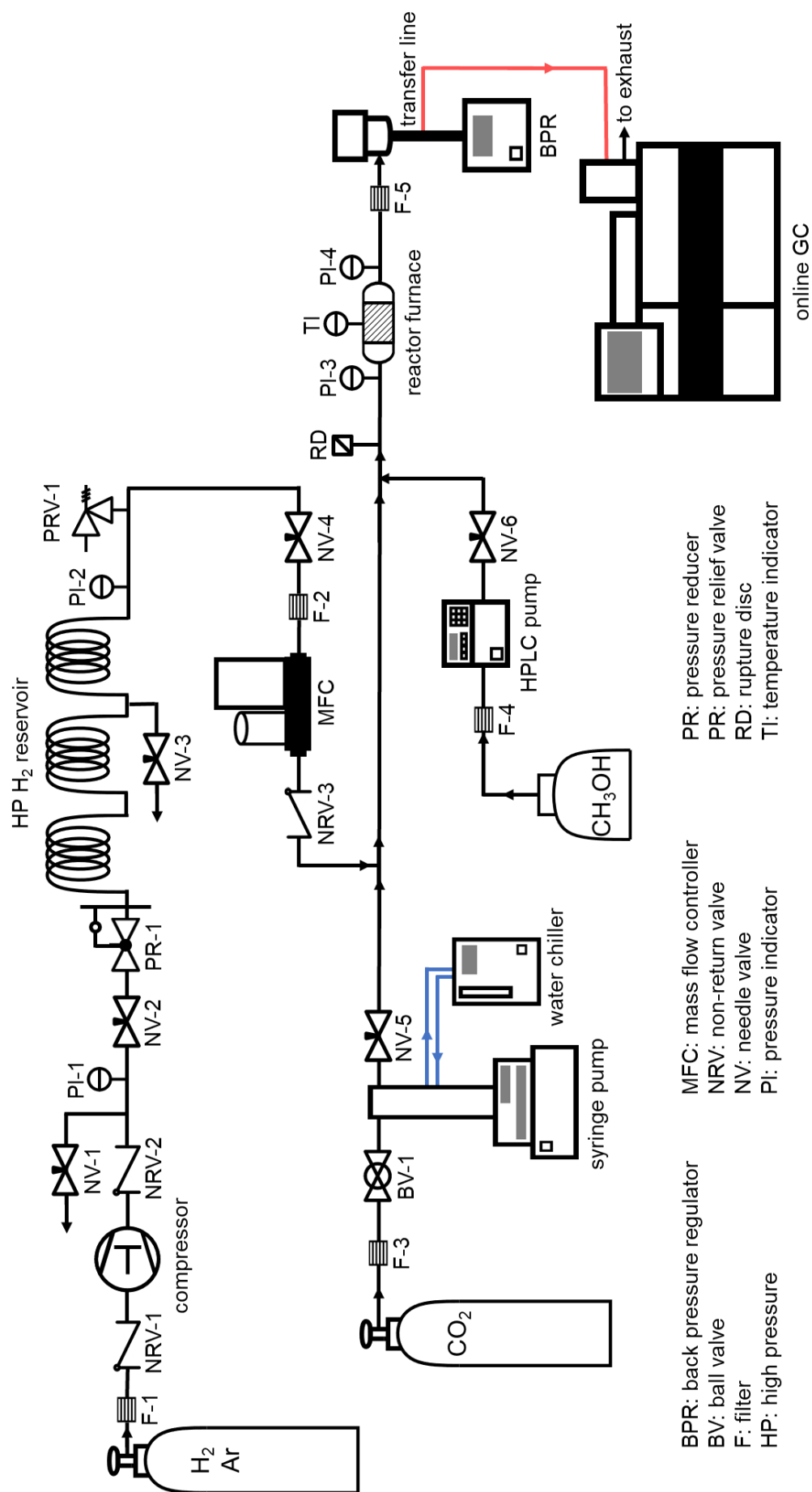
Figure 2.4. Schematic flow diagram of a high-pressure micro-reactor setup.

Chapter 2

A high-pressure syringe pump (Teledyne ISO, 260D) is used to dispense the liquid CO_2. A commercial liquid CO_2 cylinder is connected to the inlet of syringe pump via a high-pressure ball valve BV-1 (HyLok). The barrel of syringe pump integrates a cooling jacket to avoid changes in the density of liquid CO_2 caused by variations in ambient temperature. A constant temperature water circulation bath (Huber) is used to keep the cooling jacket at 20 ºC. The needle valve NV-5 at the outlet of syringe pump allows to pressurize the reactor system gradually.

A glass bottle containing liquid methanol is connected to the inlet of a high pressure HPLC pump (Jasco, PU-2080 Plus) which controls the flow of methanol. The needle valve NV-6 is of great importance to first pressurize methanol before its constant flow to the reactor system, thus avoiding fluctuations in the feeding composition.

2.3.1.2 The reactor system

The reactor system consists of a 1/4" SS tube (Sandvik) with an ID of 2.95 mm and c.a. 20 cm in length, together with a heating system (**Figure 2.5**). Two SS bodies of 15 cm in length covered with ceramic insulation material are part of the heating system. The reactor is completely embedded between the SS bodies thanks to two mortises. Another L-shape mortise was made to place a thermocouple (type K) that touches the reactor. Two resistive cartridge heaters are inserted into the bottom SS body. Both thermocouple and heating cartridge are connected to a PID controller (Watlow, EZ-zone) so that the temperature of the reactor is regulated.
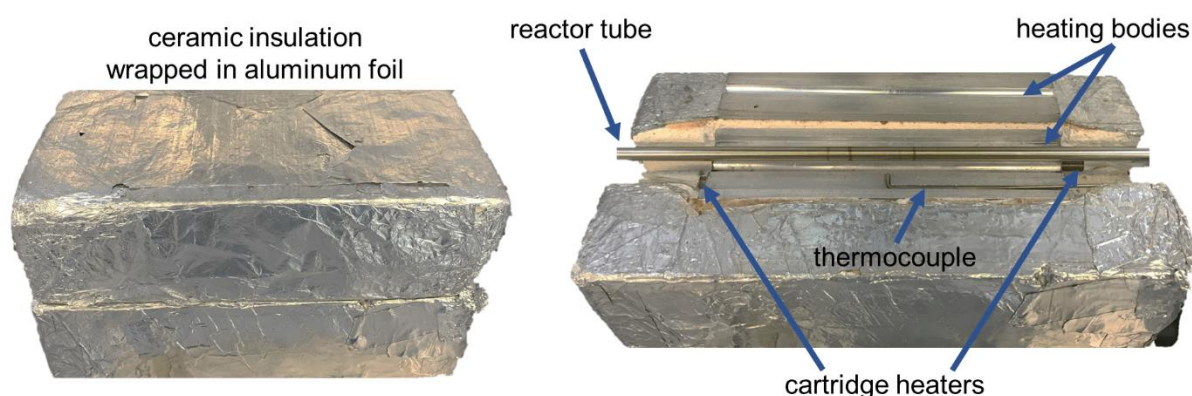
Figure 2.5. The reactor system and its components.

As depicted in **Figure 2.4**, a rupture disc RD-1 is placed at the inlet of the reactor tube for a quick response pressure relief in case of burst pressure. The pressure drop across the catalyst bed placed inside the reactor is measured with two pressure transmitters PI-3 and PI-4 (STW) connected to a digital pressure readout system (HaoYing). The pressure in the reactor system is controlled by a back pressure regulator (Jasco, BP-2080) with low internal

UNIVERSITAT ROVIRA I VIRGILI
CONTINUOUS HYDROGENATION OF CARBON DIOXIDE TO FORMATES AND FORMIC ACID OVER HETEROGENEOUS CATALYSTS
Juan José Corral Pérez

Materials and methods

dead volume. A 0.5 µm filter frit F-5 (Vici) is placed after the reactor to prevent any catalyst particle entering into the back pressure regulator. Any solid particle can scratch the inner needle of the back pressure regulator, thus leading to leaks and operational problems. The product stream from the outlet of back pressure regulator is fed to the online gas chromatograph (GC) through a transfer line heated at 150 ºC. This temperature keeps the products in vapour phase to avoid any difficulty in the analytical system.

2.3.1.3 Analytical system

All the gaseous products are analysed by an online gas chromatograph (Bruker, 456-GC) during the steady state operation of the reaction. The current GC configuration allows to detect all possible product components formed in CO_2 hydrogenation reaction as well as Fischer-Tropsch reaction products. It has two independent parallel detection channels equipped with TCD (Thermal Conductivity Detector) and FID (Flame Ionization Detector) detectors for a fast analysis. Helium is used as carrier gas on both channels. The online injection of sample is possible thanks to different valve combinations integrated with the GC and heated at 150 ºC. Two independent 6-port valves are used for the sample injection on TCD and FID channels respectively. The TCD channel is equipped with Hayesep-Q (1 m x 1/8" x 2 mm) and CP-Molsieve-13X (1.5 m x 1/8" x 2 mm) packed columns connected in series. The first column pre-splits the product mixture into permanent gases (O_2, H_2, N_2, CO, CH_4) and other components such as CO_2, methanol, dimethyl ether and hydrocarbons. Afterwards, the permanent gases are passed via a 6-port valve to the second column where the separation takes place. The FID channel is provided with a fused silica (60 m x 0.53 mm, 5 µm) capillary column to separate compounds such as alcohols, aldehydes and acetates. The column oven is kept at 45 ºC for 3 min to provide a better separation of permanent gases. Subsequently, oven temperature is increased to 175 ºC at two different rates (15 ºC min^{-1} until reaching 150 ºC followed by 20 ºC min^{-1}) and held for 1 min. Hence, the total analysis takes 12.25 min.

The data acquisition and analysis are performed by Galaxie software. An external standard method is employed to quantify the concentration of detected components. Commercial cylinders containing gas mixtures of known composition are used to create the corresponding calibration curves. For liquid samples such as methanol, ethanol and methyl formate, they are evaporated in a 2 L Tedlar bag filled with a specific volume of nitrogen to know the ratio of components in the gaseous mixture.

2.3.1.4 Reactor automation

The reactor automation is implemented using LabVIEW software (National Instruments). The LabVIEW program (**Figure 2.6**) monitors and controls the critical parameters of the high-pressure setup remotely. The flow of the reactants (CO_2, H_2 and CH_3OH) and the temperature
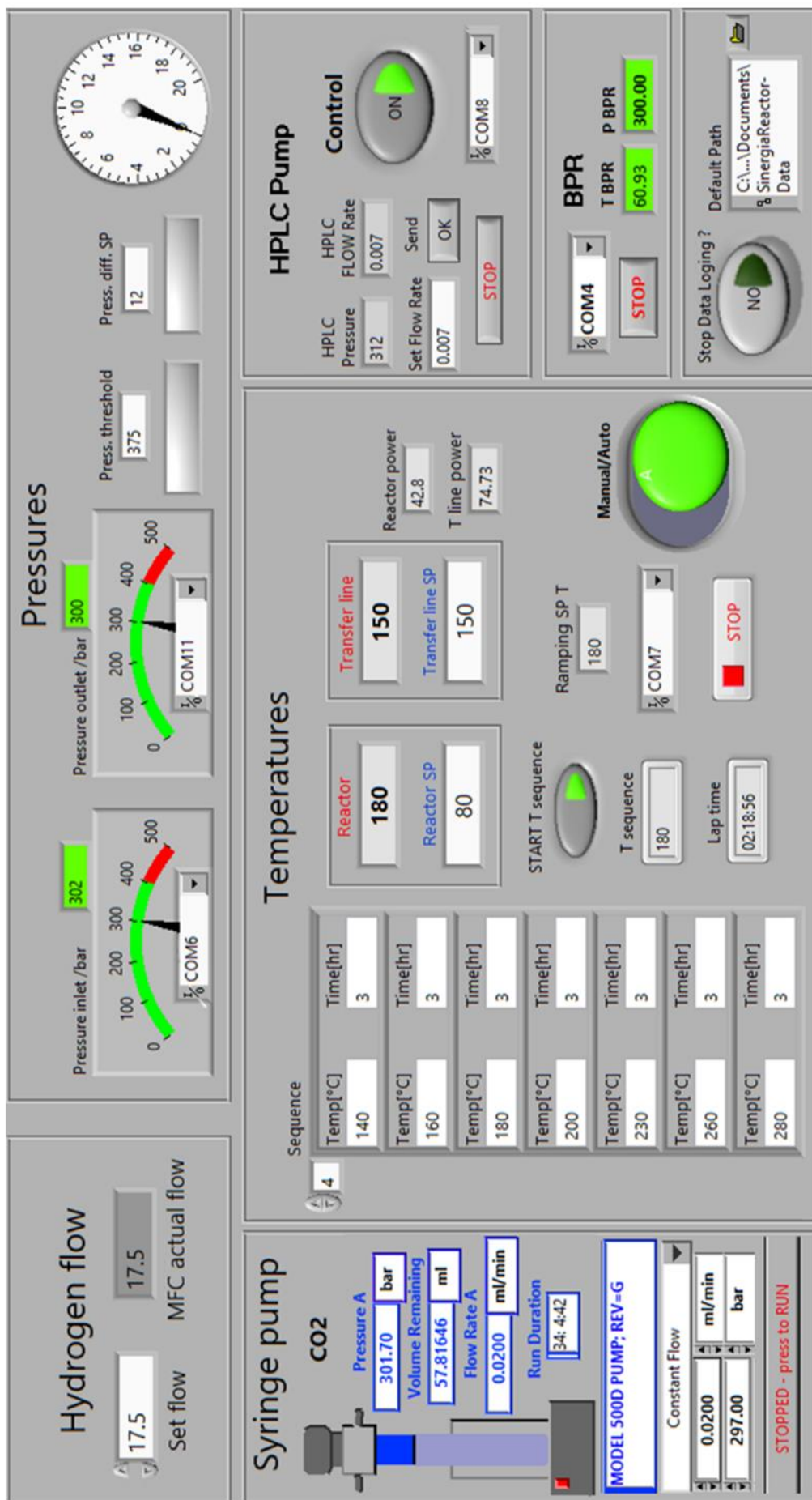
Chapter 2

Figure 2.6. LabVIEW control panel of high-pressure micro-reactor setup.

UNIVERSITAT ROVIRA I VIRGILI
CONTINUOUS HYDROGENATION OF CARBON DIOXIDE TO FORMATES AND FORMIC ACID OVER HETEROGENEOUS CATALYSTS
Juan José Corral Pérez

Materials and methods

of the reactor can be controlled via the developed program. In case of temperature, it can be controlled in manual or auto mode. In auto mode, a temperature sequence is set for a desired amount of time. The time starts counting as soon as the temperature reaches the specified setpoint. Once time is elapsed, the next value in the temperature sequence is sent to the heating controller. The communication between the setup components (syringe pump, mass flow controller, HPLC pump, heating and digital pressure readout systems and back pressure regulator) and the computer is possible by serial port communication. All the instruments are connected to a communication hub using a DB9 RS-232 connector. This hub is connected to the computer via USB 2.0.

In order to increase the safety of the high-pressure plant, all the process values such as pressure, pressure drop across the catalyst bed, reactants flow and temperature are continuously recorded and their deviation from the setpoint value activates an emergency shutdown procedure. Such procedure sets all the reactants flow to zero and turns off the heating system. Furthermore, all the devices have an internal alarm facility that increases the safe operation of the reactor system.

2.3.2 Reactor operation

The catalyst powder is pressed in a pellet die with 10 ton of pressure for 10 minutes. The resulting pellet is subsequently crushed using mortar-pastel and sieved to 100-300 µm particle size. Before loading the sieved catalyst, a small bent piece of hollow tube is inserted from the bottom of reactor tube (**Figure 2.7**). This tube together with a packed bed of quartz wool act as a support for the catalyst inside the reactor tube, thus preventing the catalyst bed from moving by pressure or flow. The catalyst is placed inside the reactor tube, which is tapped to ensure a uniform distribution of catalyst particles. The distance of the catalyst bed is always measured by inserting a needle into the reactor tube before and after the catalyst loading. After the reaction, the catalyst can be easily recovered by emptying the reactor tube.
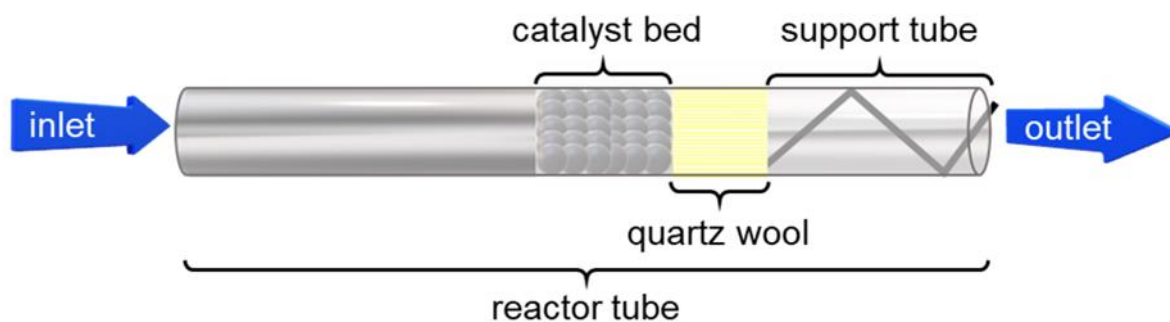

Figure 2.7. Placement of catalyst inside the reactor tube.

Chapter 2

The reactor tube is placed inside the furnace (heating system) and connected to the system by 1/4" compression fittings. Prior to the reaction, the catalyst is reduced in the stream of Ar (10%) and H_2 (90%) at 260 °C for 2 h at atmospheric pressure. The heating ramp rate is kept at 10 ºC min^{-1}. After the reduction, the heating is turned off to cool down the reactor tube under the steady flow of H_2/Ar. Afterwards, the reactor is pressurised with liquid CO_2 up to the reaction pressure by setting the back pressure regulator and running the syringe pump in constant pressure mode. Once the desired pressure is reached, the syringe pump is switched to constant flow mode to establish a steady liquid CO_2 flow through the reactor. Then, methanol is pressurised to slightly above the reaction pressure using a HPLC pump before its constant flow to the reactor system. The outlet flow of the back pressure regulator is measured with a volumetric flow meter to estimate the corresponding gas hourly space velocity (GHSV).

The reactor is kept at 80 ºC to avoid the presence of liquid methanol. The line that connects the reactor outlet with the BPR must be also heated to achieve the stable feed composition (**Figure 2.8**). After reaching a constant feed composition, the reactor is heated at different temperatures, which are automatically controlled by the LabVIEW program. The outlet stream from the back pressure regulator is fed to the online GC to determine the molar concentration of reactants and products during the steady state operation of the reaction. Argon is used as an internal standard for gas chromatography analysis and product selectivity is calculated taking only carbon-containing products into account. All the values are calculated by averaging over several injections after product concentrations are stabilized. At least two different runs are carried out to ensure the tendency and accuracy of the catalytic performance.
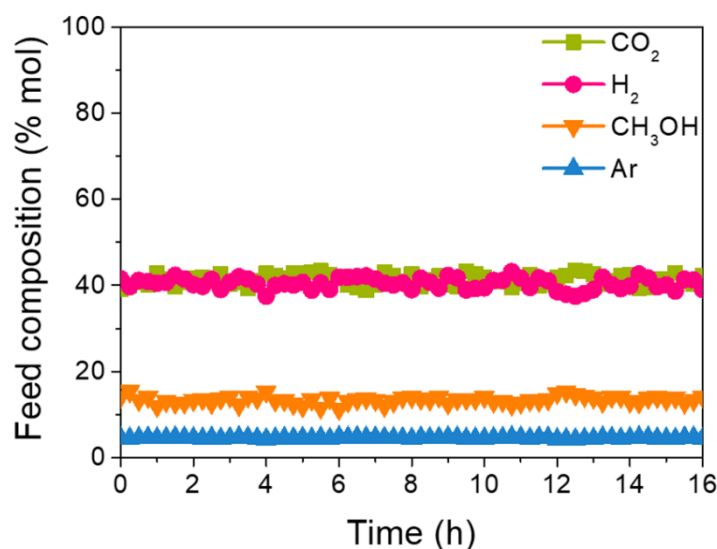
Figure 2.8. Stability of the feed composition along the time.

UNIVERSITAT ROVIRA I VIRGILI
CONTINUOUS HYDROGENATION OF CARBON DIOXIDE TO FORMATES AND FORMIC ACID OVER HETEROGENEOUS CATALYSTS
Juan José Corral Pérez

Materials and methods

2.4 *In situ* and *operando* DRIFTS studies

Infrared spectroscopy is one of the most popular and powerful techniques for the study of heterogeneous catalysts. Since most of the molecular vibrations absorb infrared (IR) radiation at characteristic frequencies, this analytical tool allows the characterization of catalysts and the chemical species formed over their surface. Among the different IR absorption spectroscopic setups, DRIFTS (diffuse reflectance infrared Fourier transform spectroscopy) has gained prominence in heterogeneous catalysis to facilitate the detection of complex surface processes. Unlike other modes, such as transmission, DRIFTS can directly measure powder catalysts, even when they are opaque to IR radiation, without previous sample preparation.[11]

2.4.1 High-pressure DRIFTS cell

In a DRIFTS measurement, the sample is illuminated by the IR beam and the scattered light is collected with appropriate optics. The Praying Mantis (Harrick) accessory offers an efficient diffuse reflection illumination and collection system based on a series of ellipsoidal mirrors (**Figure 2.9**). In order to take advantage of the *in situ* and *operando* measurements (*vide supra*), the development of DRIFTS cells to place the catalyst under reaction conditions, which may involve harsh conditions such as high temperature and pressure, is highly desirable. In this work, a high-pressure reaction cell has been designed and built (**Figure 2.9**).
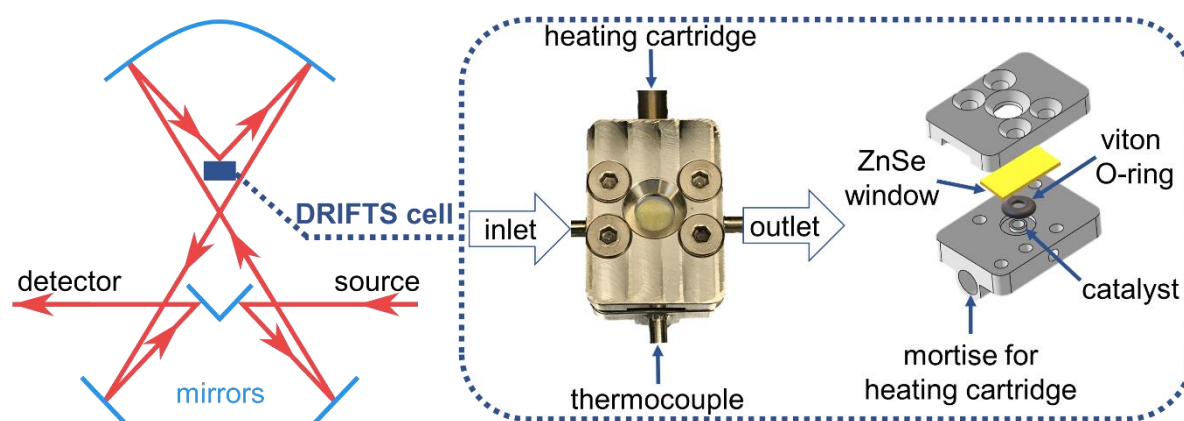
Figure 2.9. Diagram of the optical system in Praying Mantis (Harrick) and high-pressure DRIFTS cell.

The DRIFTS cell consists of two stainless steel elements, the cap and the main body. The latter has three independent channels of 3 mm in diameter (for inlet, outlet and thermocouple) connected with a cylindrical cavity (3 mm in diameter and 3 mm in vertical length), where the catalyst is placed. A thin layer of quartz wool below the catalyst particles is required to avoid clogging in any channel. The temperature in the reaction cell is regulated with a PID controller (Watlow, EZ-zone), which is connected to a thermocouple and heating cartridge. While the thermocouple (type K) is in close contact with the catalyst, the heating cartridge (6.60 mm in
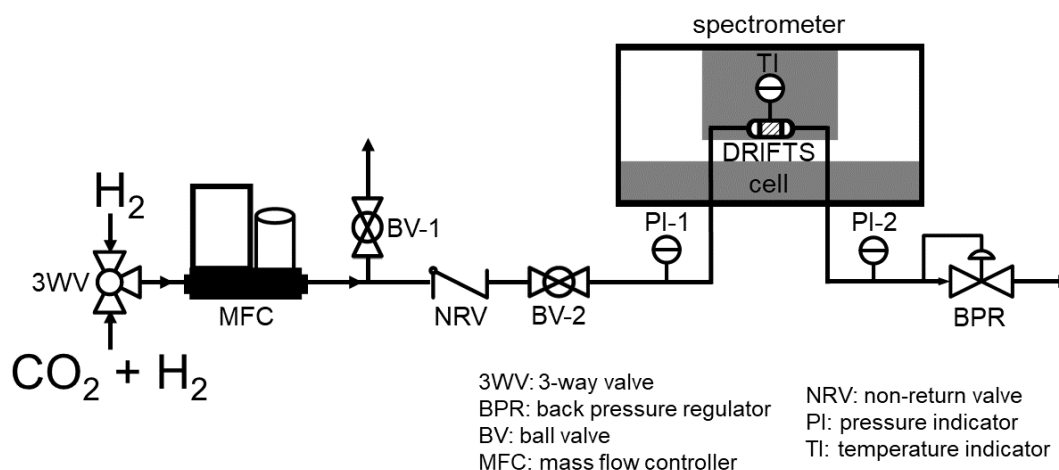
Chapter 2

diameter and 28 mm in length) is introduced into a mortise of the main body. Due to the reduced size of the cell (34 x 24 x 17 mm) and the 1.5 mm of stainless steel that separates the upper part of the heating cartridge from the catalyst cavity, the thermal gradients and heat transfer limitations are minimised.

An O-ring is placed between a flat zinc selenide window (IR transparent, 15 x 19 x 4 mm) and the cell body so that the cell can work under high pressure without leaks, provided that the tap is tightly fixed to the cell by using four screws. The thickness of the ZnSe window, the O-ring and the small catalyst cavity allows working pressures up to 90 bar. The material of the O-ring limits the maximum working temperature, ca. 260 ºC in case of Viton. The two opposite holes located on the main body allows to mount the cell in a Praying Mantis (together a temperature insulation cloth). The key advantage of the developed cell relies on the plug-flow design with minimized gas volume, thereby enhancing the signals from surface species.[12]

2.4.2 Steady state measurement

In a typical steady state measurement, about 10-15 mg of the catalyst in powder form or sieved to the desired particle size is placed in the high-pressure reaction cell, which is mounted in a Praying Mantis (Harrick). The spectra are collected using a Bruker Vertex70v FT-IR spectrometer equipped with a liquid-nitrogen-cooled MCT detector at 4 cm^{-1} resolution. As shown in **Figure 2.10**, The flow of gases is controlled by mass flow controllers (Bronkhorst). Prior to the measurements, the sample is reduced *in situ* at 260 °C in H_2 stream (10 NmL min^{-1} H_2) for 1 h. Subsequently, the system is cooled to a specific temperature in the H_2 stream and then exposed to the reactant mixture (usually CO_2:H_2 = 1:1 molar ratio, total flow 10 NmL min^{-1}) at the desired pressure. The pressure in the cell is regulated by a back-pressure regulator (Bronkhorst or VICI). The spectra are acquired with OPUS software every 24 seconds to follow the reaction, stabilization process of the catalysts as well as the evolution of surface species.

Figure 2.10. Schematic flow diagram of the experimental setup to perform in situ DRIFTS.

UNIVERSITAT ROVIRA I VIRGILI
CONTINUOUS HYDROGENATION OF CARBON DIOXIDE TO FORMATES AND FORMIC ACID OVER HETEROGENEOUS CATALYSTS
Juan José Corral Pérez

Materials and methods

2.4.3 Transient measurement

Although *in situ* DRIFTS under steady state operation can monitor the chemical species formed over the catalyst surface, its main limitation lies on the spectroscopic analysis, which can be complicated by the presence of spectator species.[5, 13] Spectators are not directly involved in the reaction and their spectral bands can interfere with those of active species. **Figure 2.11** represents the typical situation of signals obtained by *in situ* spectroscopy, where the coexistence of spectator and active species together with unavoidable noise leads to an unclear and noisy picture. Ideally, this image should be clearer by increasing the sensitivity. However, the signals of the active species are still interfered with the ones coming from the spectators. Ideally, only the active species should be monitored with high temporal and spatial resolution to get insights into its intrinsic dynamic behaviour.[13]
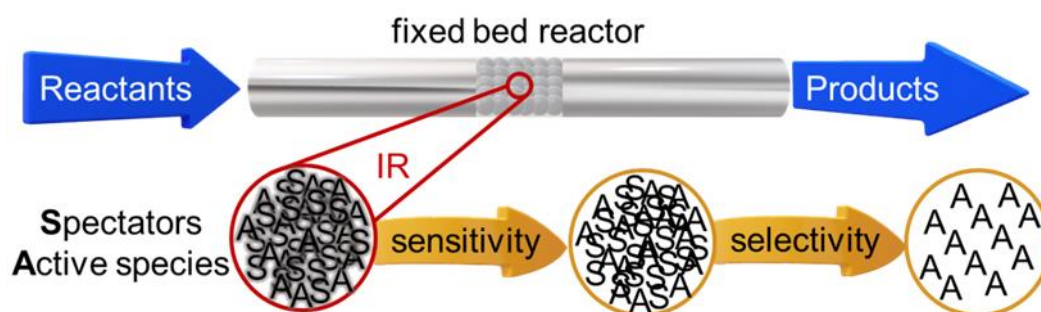
Figure 2.11. Typical situation of signals obtained by *in situ* spectroscopy and how it may be improved by increasing sensitivity and selectivity.

Transient response techniques offer a solution to discern the signals originated from spectators and active species respectively. It consists of utilizing a periodic perturbation (stimulation) of a system by external parameters to influence the concentration or kinetics of the species involved in the chemical reaction. Proper selection of the stimulation such as gas composition, reaction temperature and pressure, is crucial so that the species of interest are selectively observed. As shown in **Figure 2.12**, the response of the active species oscillates largely at the same frequency as that of the stimulation. After some periodic perturbations, the signal reaches a quasi steady-state that can be averaged into one period to improve the signal to noise ratio considerably.[13]

Chapter 2
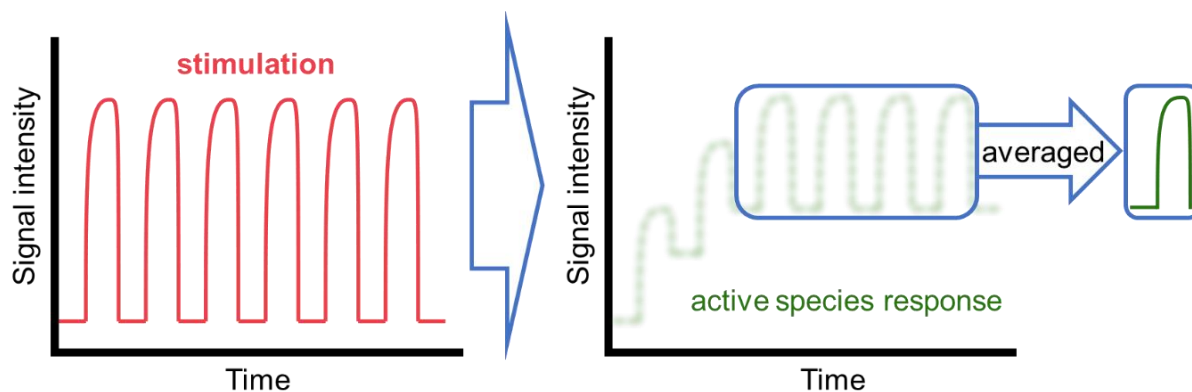
Figure 2.12. Schematic representation of a periodic stimulation that affects the response of an active species. The averaged response highlights the enhance in sensitivity.

In the present thesis, this kind of measurement is performed by means of a switching valve which changes the stream of reactant gases to introduce a periodic concentration perturbation. At least 5 consecutive cycles are performed to average the last 3 ones by using MATLAB, thus improving the sensitivity. The last spectrum of each perturbation cycle is taken as the background to obtain the rest of absorbance spectra. As an example, in the concentration perturbation experiment depicted in **Figure 2.13**, CH_3OH is continuously introduced into the DRIFTS cell by passing argon through a saturator while two different reactants are switched between CO_2:H_2 (1:1 molar ratio) and Ar respectively. The pressure drop across the catalyst bed inside the cell is measured with two pressure indicators placed in the inlet and outlet of the cell (PI-1 and PI-2). In order to conduct experiments at moderate pressure and to avoid a pressure drop due to the gas switching, two back pressure regulators are placed in the outlet of the cell and exhaust line (BPR-1 and BPR-2). In *operando* studies, the products are continuously analysed by mass spectrometry (OmniStar GSD 320 O series, Pfeiffer Vacuum) to follow their corresponding concentration profiles.
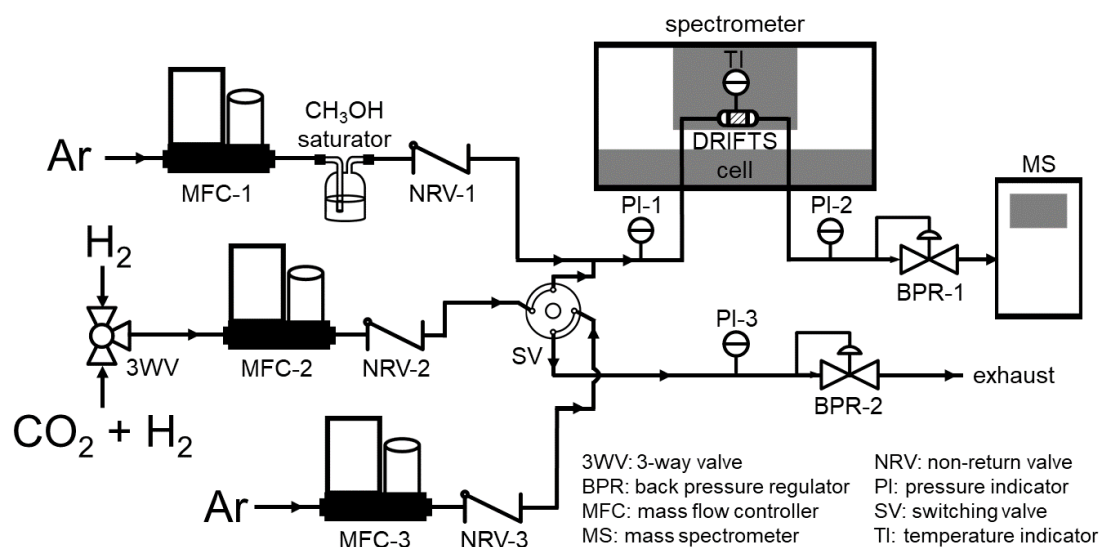
Figure 2.13. Schematic flow diagram of the experimental setup to perform *operando* transient DRIFTS.

UNIVERSITAT ROVIRA I VIRGILI
CONTINUOUS HYDROGENATION OF CARBON DIOXIDE TO FORMATES AND FORMIC ACID OVER HETEROGENEOUS CATALYSTS
Juan José Corral Pérez

Materials and methods

2.5 Multivariate spectral analysis by means of Multivariate Curve Resolution

The transient *in situ* and *operando* techniques can generate overwhelming amounts of data that hinder the proper interpretation of the catalytic systems. Despite the selectivity issue can be tackled with the signal changes introduced by a stimulation, the concentration of active species is typically low and the large spectator signals can still hide the key information. The raw spectroscopic data together with powerful tools such as modulation excitation spectroscopy (MES) and multivariate spectral analysis, allows not only a better data processing but also a selective and sensitive monitoring of the dynamic behaviour of the active species involved in the complex catalytic system.[12-13] Among these tools, multivariate analysis offers a promising approach to the interpretation of spectra when overlapping signals of multiple species coexist on the catalyst surface.

Multivariate spectral analysis is performed by means of multivariate curve resolution (MCR). MCR is a chemometric method used for better data processing and deconvolution of the complex spectra down to individual components based on kinetic resolution. It has become popular due to its ability to deliver the pure response profiles (e.g. spectra, pH profiles, time profiles, elution profiles) of the chemical species of an unresolved mixture when no previous information is available about the nature and composition of these mixtures. This blind-source feature is required when appropriate reference spectra are unavailable. This may be due to the exclusive presence of some catalytically active species under transient *operando* conditions. The following is a brief description of the MCR-ALS (Multivariate Curve Resolution Alternating Least Square) method. More details about the algorithm and MATLAB scripts are reported elsewhere.[14-15]

MCR methods consists of extracting relevant information of the pure components in a mixture system through a bilinear model (Equation 2.1). The experimental data matrix (**D**) is decomposed into the product of matrices **C** (columns) and **S**^{T} (rows). These two matrices correspond to the pure spectra of each component (**S**^{T}) and their corresponding concentration profiles (**C**), respectively. **E** is the matrix of residuals, i.e. the difference between the experimental data (**D**) and the reproduced data (**CS**^{T}). A constrained Alternating Least Squares (ALS) algorithm is used to solve such bilinear model. These constraints enable a better interpretability of the profiles in **C** and **S**^{T}. For instance, the pure spectrum of a chemical species cannot be negative (non-negativity constraint). MCR-ALS is an iterative method that works by optimizing a set of initial estimates of concentration profiles or spectra under the action of constraints until a convergence criterion is achieved. This criterion can be either a

Chapter 2

predefined number of iterations or when the difference in the standard deviation of the residuals between consecutive iterations is lower than a threshold value.[14-15]

$$D = CS^T + E \qquad\qquad (2.1)$$

Applied to a spectroscopic data set obtained during a transient *in situ* or *operando* measurement, each row in the matrix D contains an averaged spectrum at a specific time of the perturbation cycle and each column, the averaged absorbances along the cycle at a specific wavenumber. MCR analysis describes the raw data set as the sum of the signal contributions coming from each of the species that behaves kinetically different. A more graphical example is shown in **Figure 2.14**. If the experiment is carried out under *operando* conditions, relationships between the concentration profiles of products and surface species can be established, thus leading to the most sought-after objective in heterogeneous catalysis field, i.e. the full understanding of the catalytic processes that take place over the catalyst surface.
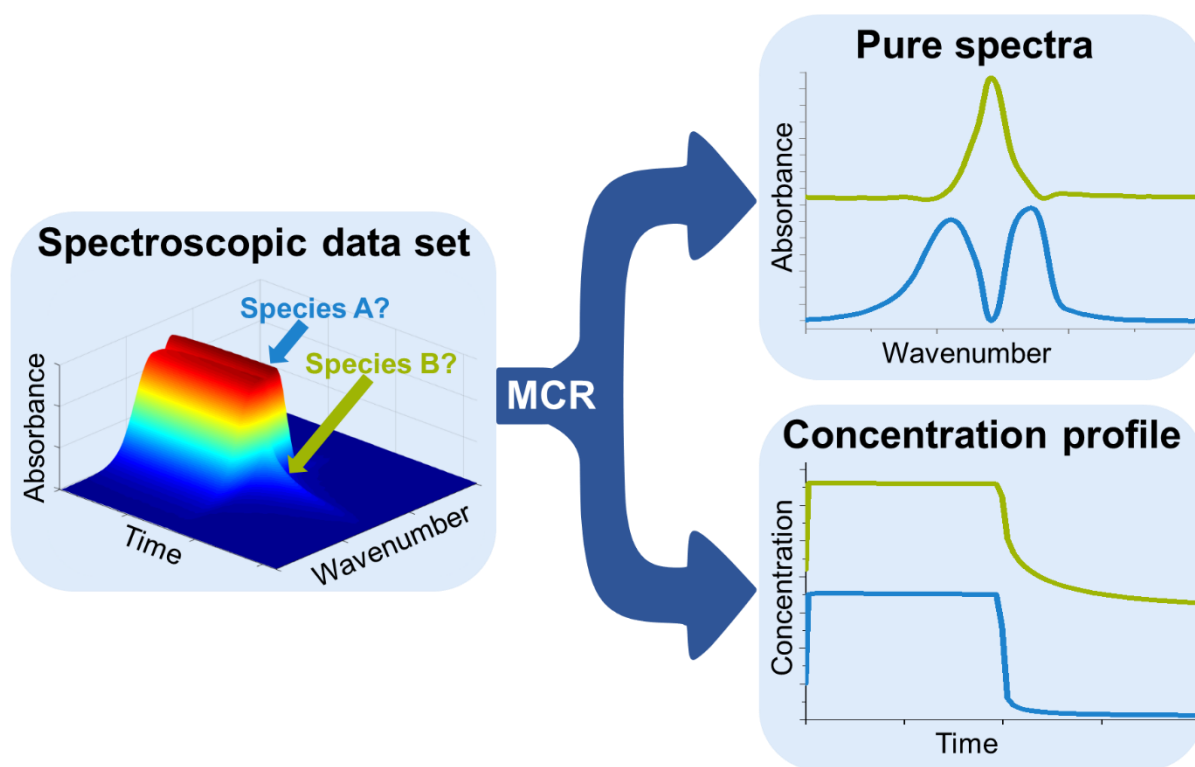
Figure 2.14. Solving the mixture analysis problem in a spectroscopy data set by using multivariate curve resolution (MCR).

UNIVERSITAT ROVIRA I VIRGILI
CONTINUOUS HYDROGENATION OF CARBON DIOXIDE TO FORMATES AND FORMIC ACID OVER HETEROGENEOUS CATALYSTS
Juan José Corral Pérez

Materials and methods

Bibliography

1. Lindström, B.; Pettersson, L. J., *CATTECH* **2003,** *7* (4), 130-138.
2. Ma, Z.; A Zaera, F., Heterogeneous Catalysis by Metals. In *Encyclopedia of Inorganic Chemistry*, 2006.
3. Hessel, V., *Chem. Eng. Technol.* **2009,** *32* (11), 1655-1681.
4. Bañares, M. A., *Catal. Today* **2005,** *100* (1), 71-77.
5. Weckhuysen, B. M., *Phys. Chem. Chem. Phys.* **2003,** *5* (20), 4351-4360.
6. Urakawa, A., *Curr. Opin. Chem. Eng.* **2016,** *12*, 31-36.
7. Boudart, M., *J. Mol. Catal.* **1985,** *30* (1), 27-38.
8. Richardson, J. T., *Principles of Catalyst Development*. Springer US: 1989.
9. Copéret, C.; Comas-Vives, A.; Conley, M. P.; Estes, D. P.; Fedorov, A.; Mougel, V.; Nagae, H.; Núñez-Zarur, F.; Zhizhko, P. A., *Chem. Rev.* **2016,** *116* (2), 323-421.
10. Copéret, C.; Fedorov, A.; Zhizhko, P. A., *Catal. Lett.* **2017,** *147* (9), 2247-2259.
11. Zaera, F., *Chem. Soc. Rev.* **2014,** *43* (22), 7624-7663.
12. Urakawa, A.; Maeda, N.; Baiker, A., *Angew. Chem. Int. Edit.* **2008,** *47* (48), 9256-9259.
13. Urakawa, A.; Bürgi, T.; Baiker, A., *Chem. Eng. Sci.* **2008,** *63* (20), 4902-4909.
14. Jaumot, J.; de Juan, A.; Tauler, R., *Cemometr. Intell. Lab.* **2015,** *140*, 1-12.
15. de Juan, A.; Jaumot, J.; Tauler, R., *Anal. Methods* **2014,** *6* (14), 4964-4976.

UNIVERSITAT ROVIRA I VIRGILI
CONTINUOUS HYDROGENATION OF CARBON DIOXIDE TO FORMATES AND FORMIC ACID OVER HETEROGENEOUS CATALYSTS
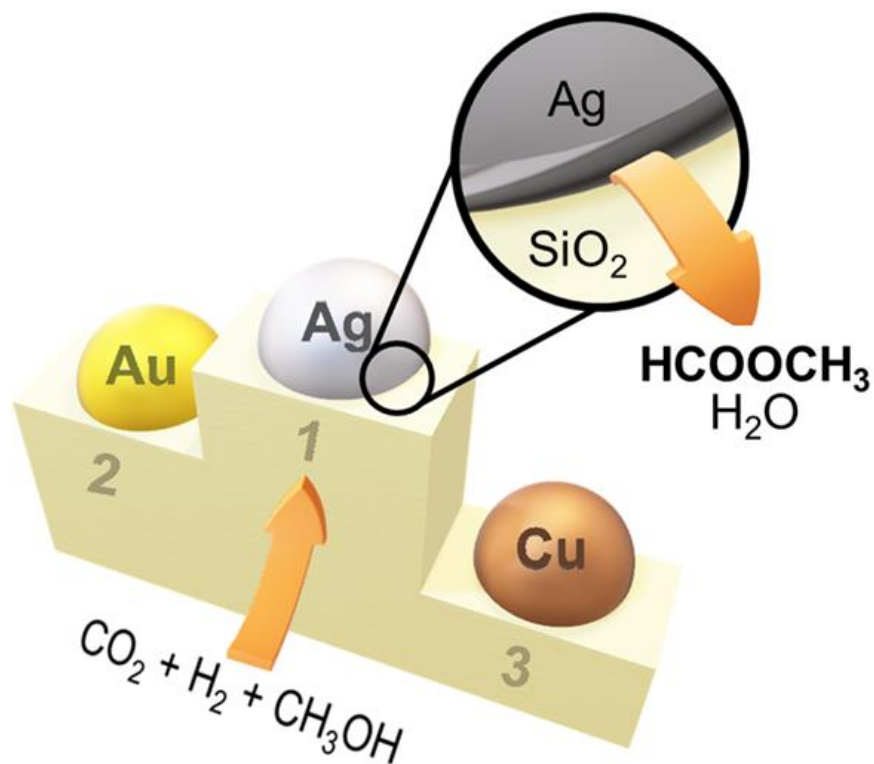Juan José Corral Pérez

Chapter 2

3

Metal effect and mechanistic insights

Decisive role of perimeter sites in silica-supported Ag nanoparticles in selective hydrogenation of CO_2 to methyl formate in the presence of methanol

Chapter 3

3.1 Introduction

Methyl formate (MF) is a building block molecule in C_1 chemistry as well as a possible intermediate to produce chemical energy carriers.[1] This molecule can be used to produce several industrially important chemicals such as acetic acid,[2] ethylene glycol,[3] methanol and formic acid.[4] In particular, both formic acid and methanol can be obtained simultaneously by simple hydrolysis reaction of MF. Commercially, MF is produced by the reaction of carbon monoxide (CO) and methanol[5] or via dehydrogenation of methanol.[6] Other synthesis routes like oxidative dehydrogenation of methanol[7] and dimerization of formaldehyde[8] have also been actively investigated. Among the alternative routes, the synthesis of MF from CO_2 and H_2 has recently attracted attention[9-10] owing to the increasing pressure to valorise CO_2 with the aim to mitigate its notorious impacts on climate change and to reduce our dependency on fossil fuels, provided that H_2 is produced from renewable and intermittent energy sources.[11]

A few approaches have been reported to produce MF from CO_2, for instance, by photocatalytic reduction of CO_2[12-13] and CO_2 hydrogenation in the presence of methanol (Reaction 3.1). The latter was demonstrated using both homogeneous[14-16] and heterogeneous catalysts.[9-10, 17-18] Generally, heterogeneous catalysis offers great advantages to transform a large amount of reactant(s) with increased space-time-yield and benefits from process intensification associated with continuous operation, more facile product/catalyst separation and catalyst regeneration. In fact, an efficient heterogeneous catalyst that promotes such a reaction would be key in developing the continuous synthesis of thermodynamically-unstable formic acid starting from CO_2 and H_2,[19] since MF can serve as an intermediate and methanol can also be produced by CO_2 hydrogenation.[19]

$$CO_2 + H_2 + CH_3OH \rightleftarrows HCOOCH_3 + H_2O \qquad (3.1)$$
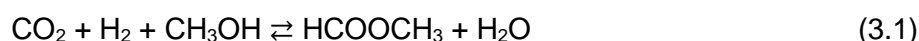
Only Cu and Au supported on metal oxides were reported as heterogeneous catalysts for the CO_2 hydrogenation to MF under batch rather than flow conditions.[9-10, 17-18] Interestingly, Ag has not been investigated so far despite its similarity to Cu in terms of hydrogenation activity.[20-21] Other metals such as Ru, Ni and Pd were reported as promoters to $Cu/ZnO/Al_2O_3$ catalyst positively influencing the yield of MF.[17] Among Au catalysts, the ZrO_2 supported ones show higher activities compared to those supported on CeO_2 and TiO_2; this difference was ascribed to the amphoteric nature of the support, i.e. the acidic and basic sites promoting the adsorption of CO_2 and desorption of formic acid intermediate, respectively.[9] Support effects were also evidenced with Au/Al_2O_3 which provides a two-fold increase in yield by comparison to Au/TiO_2.[10] These studies reveal the importance of appropriate combination of metal and support for improving the catalytic performance in the CO_2 hydrogenation to MF.

However, to date, the roles of metal and support as well as reaction mechanisms including the type of reactive surface species have not been clarified. It has been proposed that MF is formed by a reaction of CH_3OH with either surface formates or formic acid intermediates.[9, 17-18] This was supported by the lack of MF production in the absence of CH_3OH[17] despite the formation of formate species on the catalyst surface as suggested by *ex situ* IR studies.[10, 18] Therefore, it remains a challenge to determine the reactive intermediates and active sites that control the catalytic activity in the MF synthesis under reaction conditions.

In this work, we thus explore the reactivity of silica-supported Ag nanoparticles in comparison to the corresponding Cu and Au systems for continuous MF synthesis from CO_2 and H_2 in the presence of CH_3OH. *In situ* and *operando* vibrational spectroscopic studies together with DFT calculations are performed to identify the reactive intermediate species and verify the location and nature of active sites and the underlying hypothesis of MF synthesis involving the reaction of surface formates.

3.2 Experimental

3.2.1 Materials

Silver nitrate (>99%, Alfa Aesar), copper (II) nitrate trihydrate (>98%, Alfa Aesar), hydrogen tetrachloroaurate (III) hydrate (99.999%, Alfa Aesar), silica (Alfa Aesar) and methanol (>99%, Sigma Aldrich) were used as received. Deionized water was used for catalyst synthesis. Liquid CO_2 (>99.9993%) and 10% Ar in H_2 (>99.999% for Ar or H_2, prior to mixing) were purchased from Abelló Linde.

3.2.2 Catalyst synthesis

All catalysts were prepared by the incipient wetness impregnation method using the corresponding precursors (silver nitrate, copper (II) nitrate trihydrate and hydrogen tetrachloroaurate (III) hydrate) and silica as support. The catalysts were dried overnight in an oven at 100 °C and subsequently calcined in air at 400 °C (the heating ramp rate was kept at 4 °C min^{-1}) for 4 h.

3.2.3 Reaction system

Catalytic tests were performed in a continuous flow fixed-bed microreaction system. Details of the setup and the method of product analysis are described in **Chapter 2, Section 2.3.** In a typical experiment, 300 mg of catalyst (pelletized, crushed and sieved to 100-300 µm particle size) was loaded in a tubular reactor (ID: 2.95 mm, OD: 6.35 mm) and reduced in the stream of Ar (10%) and H2 (90%) at 260 °C for 2 h at atmospheric pressure. After the reduction, the catalyst bed was cooled down to room temperature. Then, the reaction mixture

Chapter 3

(CO$_2$:H$_2$:CH$_3$OH = 4:4:1 molar ratio) was introduced into the reactor at a flow rate of 59 Nml min^{-1}. The pressure in the reactor was regulated by an automatic back-pressure regulator. The data points were collected by an online gas chromatograph during the steady state operation of the reaction at specified temperature (140-280 °C) and pressure (160 and 300 bar). Ar was used as an internal standard for gas chromatography analysis and product selectivity was calculated taking only carbon-containing products into account.

3.2.4 DRIFTS measurements

A custom-made high-pressure reaction cell, with a cylindrical cavity (3 mm in diameter and 3 mm vertical length) to place the catalyst powder, mounted in a Praying Mantis (Harrick) DRIFTS optical system was used. The spectra were collected using a Bruker Vertex70v FT-IR spectrometer equipped with a liquid-nitrogen-cooled MCT detector at 4 cm^{-1} resolution. Details of the setup and method of *in situ/operando* and transient measurements are provided in **Chapter 2, Section 2.4**.

3.2.5 Raman measurements

In situ Raman analysis were performed in the continuous CO$_2$ hydrogenation setup described elsewhere.[22] The setup was complemented with a fibre-launched Raman spectrometer (Renishaw, InVia) equipped with a λ = 532 nm solid state Nd:YAG excitation line (power at full transmission 60 mW, 1800 l mm^{-1} holographic grating, Olympus *x*20 SLW objective). The optical access into the reaction zone was granted by a micro-view cell implemented at the rear end of a tubular reactor (ID = 1 mm). Detailed description of the view-cell is reported elsewhere.[23] The view-cell and reactor were inserted in a thermally isolated heating body letting the top surface of the view-cell partially free for the insertion of the remote probe for Raman analysis.

3.2.6 Multivariate spectral analysis

Multivariate spectral analysis was performed by means of multivariate curve resolution (MCR). MCR is a chemometric method used for better data processing and deconvolution of the complex spectra down to individual components based on kinetic resolution. It delivers the pure response profiles of the chemical species of an unresolved mixture when no previous information is available about the nature and composition of these mixtures. More details of the method and software used are specified in **Chapter 2, Section 2.5**.

3.2.7 DFT calculations

Calculations were performed in the framework of DFT using the generalized gradient approximation of Perdew–Burke–Ernzerhof (PBE)[24] and dispersion correction of Grimme.[25-26]

UNIVERSITAT ROVIRA I VIRGILI
CONTINUOUS HYDROGENATION OF CARBON DIOXIDE TO FORMATES AND FORMIC ACID OVER HETEROGENEOUS CATALYSTS
Juan José Corral Pérez

Metal effect and mechanistic insights

Adsorption, reaction, and vibrational calculations on metal surfaces were performed using the Quantum ESPRESSO package[27] and plane-wave basis set with ultrasoft pseudopotentials.[28] On the other hand, the calculations on SiO_2 surface were performed with the CP2K code[29] using GTH pseudopotentials,[30] plane-waves and Gaussian DZVP basis sets.[31] Further computational details are described in **Appendix A, Section A.1**.

3.3 Results and discussion

3.3.1 Catalytic activity

Catalysts based on Cu, Ag and Au nanoparticles (<11 nm at 1 wt% metal loading; **Appendix A**, **Table A.4**) supported on high surface-area silica (155 m^2 g^{-1}) are prepared by wetness impregnation method. Silica is chosen as a neutral support in order to probe the specific reactivity of the three different metals in the hydrogenation of CO_2 in the presence of methanol at 160 and 300 bar (**Figure 3.1**). At 300 bar, CH_3OH conversion to MF increases significantly at higher temperatures in the order of the Ag > Au > Cu catalysts, while no activity is found for silica in the absence of metal particles (data not shown). For the Ag and Cu catalysts, the MF selectivity remains almost constant at around 100% at all temperatures examined, whereas the formation of carbon monoxide (S_{CO} = 19.7%) is observed at 280 °C and 300 bar with Au/SiO_2.
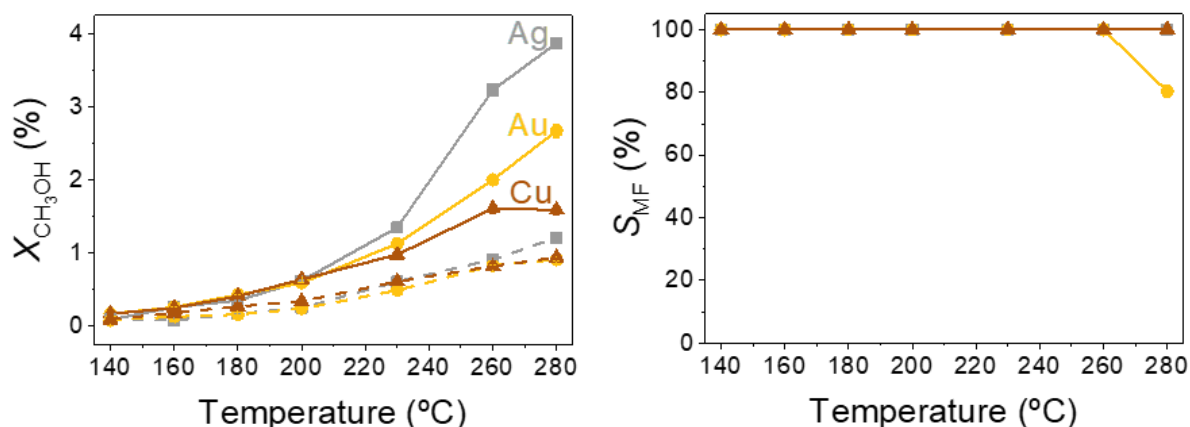
Figure 3.1. Effects of temperature and pressure on CH_3OH conversion (X_{CH_3OH}) and selectivity to MF (S_{MF}) over silica-supported 1 wt% metal catalysts. Reaction conditions: $CO_2:H_2:CH_3OH$ = 4:4:1 (molar ratio), pressure = 160 bar (dashed line) and 300 bar (solid line), GHSV = 9,000 h^{-1}.

Although high MF selectivity (>99.9%) has been reported for Au/ZrO_2 catalyst at lower temperature and pressure (200 °C and 160 bar) under batch operation[9], gold nanoparticles supported on different metal oxides are known to be catalytically active for the water-gas shift reaction and its reverse reaction, i.e. CO_2 hydrogenation to produce CO, favored at higher temperatures.[32] It is worth highlighting that increasing the reaction pressure from 160 to 300

Chapter 3

bar results in a drastic increase in the MF yield. Assuming that MF is formed via the reaction of CH_3OH and surface formates, this result suggests that the formation of reactive formate species is promoted at higher pressure in addition to the kinetic advantages induced by the higher fluid density and the enhanced actual contact time of the reactants with the catalysts, as previously observed for CH_3OH synthesis via CO_2 hydrogenation.[33-34]

3.3.2 Surface species involved in CO_2 hydrogenation

In situ DRIFTS and Raman measurements are performed to gain insights into the surface species formed from CO_2 and H_2 that may be linked to MF formation. As depicted in **Figure 3.2**, similar surface formate species with characteristic bands at 1600, 1688, 2711, 2817 and 2952 cm^{-1} are observed for the three catalysts under the mixture of CO_2 and H_2 (1:1 molar ratio) at 230 °C. In Raman spectra (**Figure 3.2**), the bands at 1330 and 1580 cm^{-1}, also assigned to surface formates,[35] appear after exposing Cu/SiO_2 catalyst to reactant mixture at 200 and 400 bar.
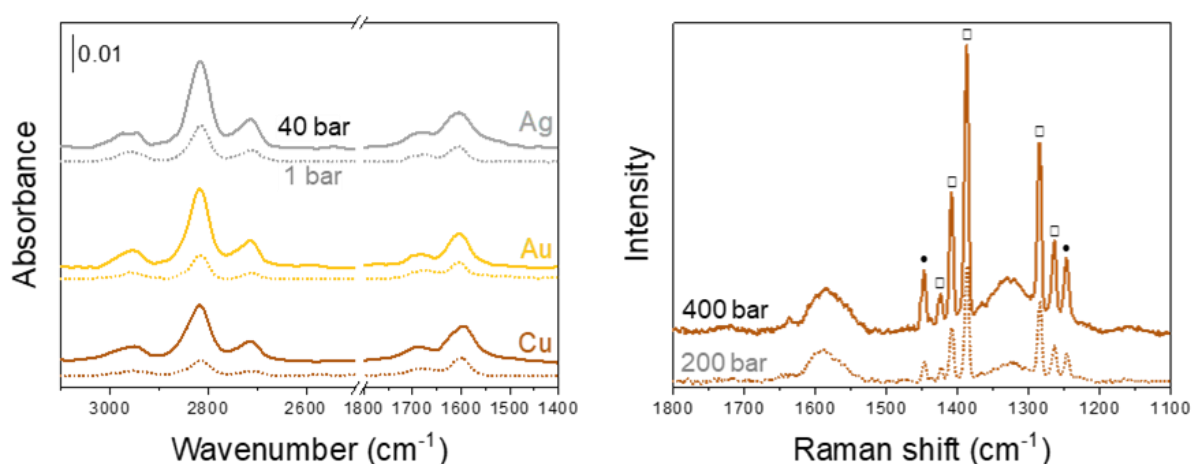
Figure 3.2. *In situ* DRIFT and Raman spectra of supported 1 wt% metal catalysts upon exposure to CO_2:H_2 = 1:1 (molar ratio) at 230 °C. (left) *In situ* DRIFT spectra at pressure = 1 (dashed line) and 40 (solid line) bar. (right) *In situ* Raman spectra of 1 wt% Cu/SiO_2 at pressure = 200 (dashed line) and 400 (solid line) bar. Characteristic bands due to the reactant mixture are shown with symbols: CO_2 (●) and H_2 (□).

Increasing the pressure of CO_2 and H_2 in the DRIFTS and Raman cells up to their respective maximum technical limits results in a drastic increase in the concentration of formate species as confirmed by the increased absorbance of their bands (**Figure 3.2**). This is also consistent with the higher MF yield observed at higher pressure (**Figure 3.1**). Although spectral features are similar for Cu, Ag and Au as expected from DFT calculations (**Appendix A**, **Table A.5**), more pronounced formation of formate species over Ag/SiO_2 compared to Cu/SiO_2 and Au/SiO_2 is evident at higher pressure (**Appendix A**, **Table A.7**). This trend is

UNIVERSITAT ROVIRA I VIRGILI
CONTINUOUS HYDROGENATION OF CARBON DIOXIDE TO FORMATES AND FORMIC ACID OVER HETEROGENEOUS CATALYSTS
Juan José Corral Pérez

Metal effect and mechanistic insights

also consistent with more facile formation of stable κ^2-formate (typically called bidentate formate) over the Ag surface as predicted by DFT calculations, i.e., calculated activation barriers for formate formation are 0.61, 0.71, and 0.97 eV on Ag, Cu, and Au, respectively (**Appendix A**, **Section A.1.1**). Based on the DFT results, we find that the activation energy for the formation of surface formates (HCOO) is simply given by the interplay between weak and strong adsorption bonding of H and HCOO, respectively. The relation between the activation energies (E^*) and the adsorption binding energies of κ^2-HCOO (E_b^{HCOO}) and H (E_b^H) is shown in **Figure 3.3**, while the corresponding activation energy estimator, $E^* \approx 0.6E_b^{HCOO} - E_b^H$, is derived in **Appendix A**, **Section A.1.2**. The lowest energy barrier for formate formation over Ag can be thus attributed to its weak binding to H and sufficiently strong binding to HCOO. Both factors promote this reaction step in a synergistic way, since one reactant is destabilized (H) while the product is stabilized (HCOO). In contrast, Au binds HCOO too weakly, whereas Cu binds H too strongly.
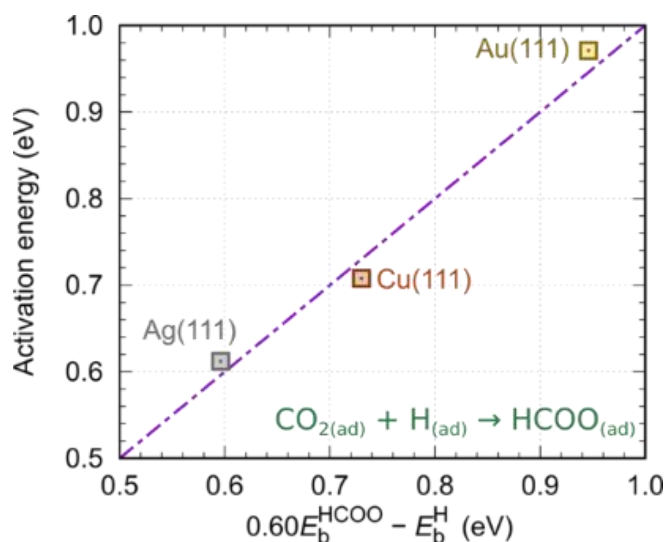
Figure 3.3. Correlation between the PBE-D''/plane-wave calculated[27] and estimated activation energies for the formate formation on Cu(111), Ag(111), and Au(111); PBE-D'' stands for PBE functional[24] with reparametrized D2 dispersion correction of Grimme.[25] The activation energy estimator, $E^* \approx 0.6E_b^{HCOO} - E_b^H$, is derived in **Appendix A**, **Section A.1.2**. E_b^{HCOO} and E_b^H are the adsorption binding energies of bidentate κ^2-HCOO and H, respectively. The RMS error of the estimator is 0.03 eV and the largest error is 0.03 eV.

As indicated by catalytic and *in situ* spectroscopic results, the concentration of surface formate species is directly linked to the MF yield. To gain more information about the nature of the observed surface species (**Figure 3.2**), a transient *in situ* DRIFTS study is performed by passing alternatively the reactant gas (CO_2:H_2 at 1:1 molar ratio) and an inert gas (Ar) over 1 wt% Ag/SiO_2 catalyst at 230 °C (**Figure 3.4a**). Under these conditions, the bands at 2711, 2817 and 2952 cm^{-1} in the ν(C-H) region gradually appear and disappear, apparently in a

Chapter 3

synchronized fashion with the band at 1600 cm^{-1}, confirming their attribution to κ^2-formate species over the Ag surface.[36-38] This assignment is consistent with DFT calculations (**Appendix A**, **Table A.5**) and their identical temporal evolutions of kinetically distinguishable component spectra (i.e. spectra with chemically distinct origins) extracted by a multivariate spectral analysis (**Figure 3.4b** and **4c**, κ^2-HCOO).
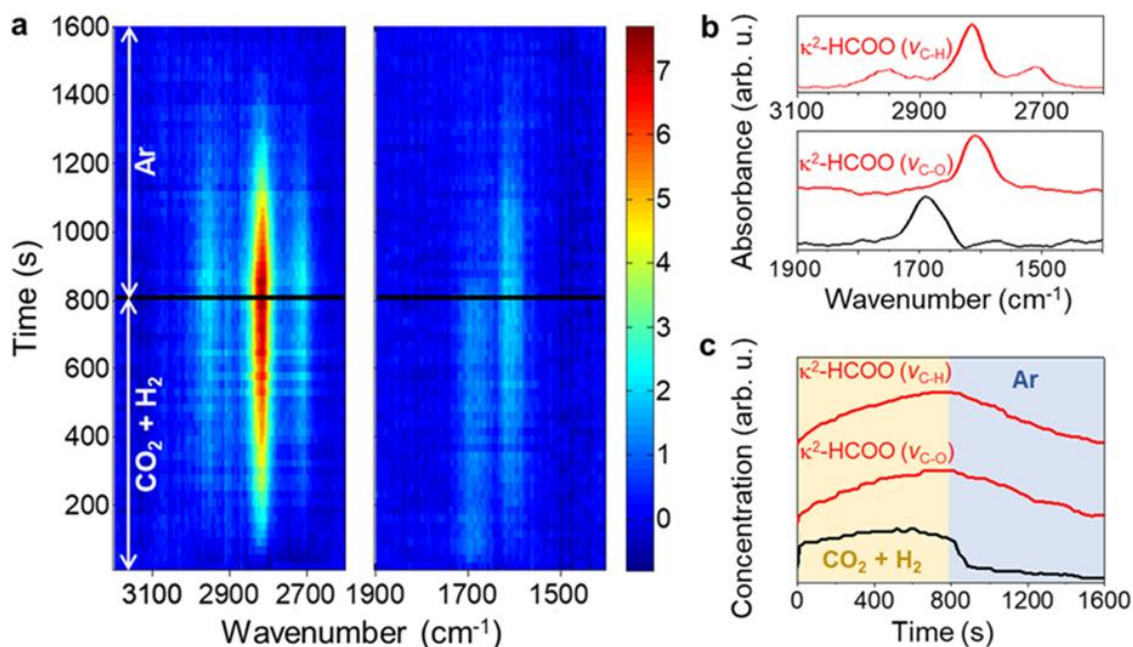
Figure 3.4. Transient DRIFTS study on CO_2 hydrogenation over 1 wt% Ag/SiO$_2$ catalyst. **a**, Time-resolved DRIFT spectra upon exposure to CO_2:H$_2$ = 1:1 molar ratio (the first half period) and then to Ar (the second half period) concentration perturbation experiment at 230 °C and 5 bar. The DRIFT spectra are shown in milli-absorbance unit taking the last spectrum in the Ar atmosphere as background. **b**, Components spectra obtained by MCR analysis applied on the time-resolved DRIFT spectra. **c**, Concentration profiles of the corresponding components spectra obtained by the multivariate spectral analysis.

On the other hand, the chemical origin of the band at 1688 cm^{-1} is more difficult to elucidate. However, the possible candidate species are formates, carbonates, formic acid, and carbonic acid (H$_2$CO$_3$). DFT calculations reveal that monodentate κ^1-formate species are too short lived to be observed by vibrational spectroscopy (**Appendix A**, **Table A.6**) although they display v(C−O) frequency in the same range (**Appendix A**, **Table A.5**). Neither can they be carbonates since their v(C−O) frequency changes significantly depending on the studied metal (**Appendix A**, **Table A.5**). According to DFT calculations, formic acid would be a good candidate, displaying the matching v(C−O) frequency (**Appendix A**, **Table A.5**). However, from the experimental counterpart, the absence of the characteristic band in the v(C−H) region with the identical temporal profile as that at 1688 cm^{-1} speaks against its attribution to formic acid or related species. This makes carbonic acid a sound potential candidate. According to

UNIVERSITAT ROVIRA I VIRGILI
CONTINUOUS HYDROGENATION OF CARBON DIOXIDE TO FORMATES AND FORMIC ACID OVER HETEROGENEOUS CATALYSTS
Juan José Corral Pérez

Metal effect and mechanistic insights

DFT calculations it displays a matching v(C−O) frequency (**Appendix A**, **Table A.5**) and, furthermore, it lacks the C−H bonds thus supporting the absence of the characteristic band in the v(C−H) region.
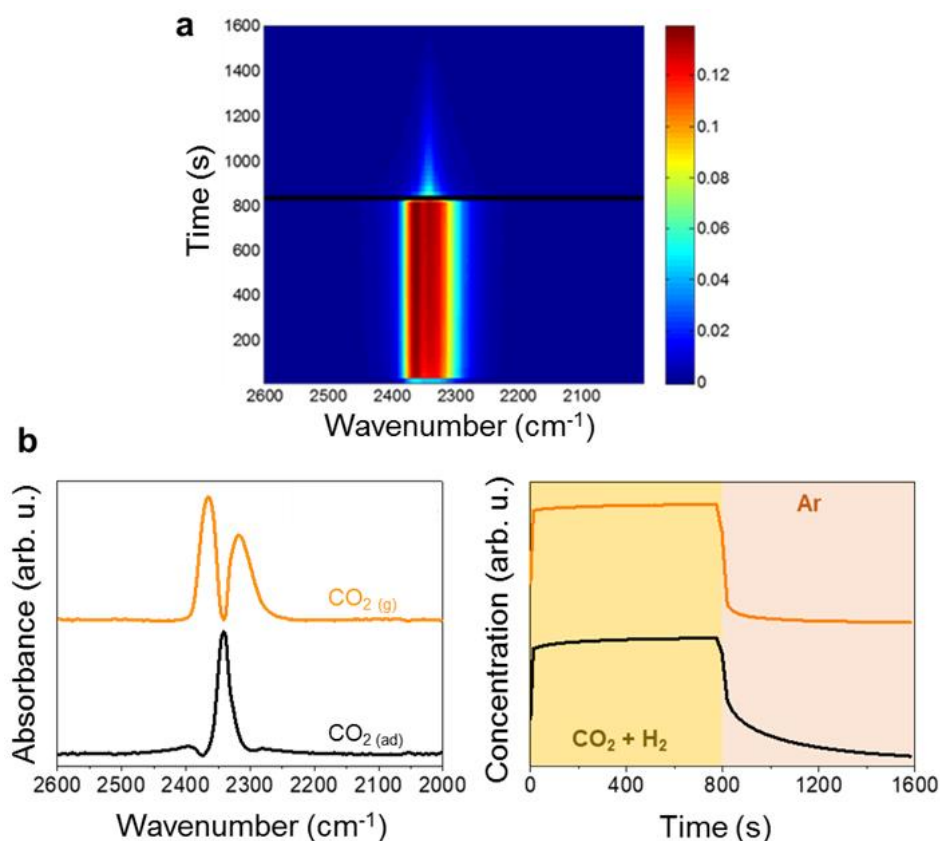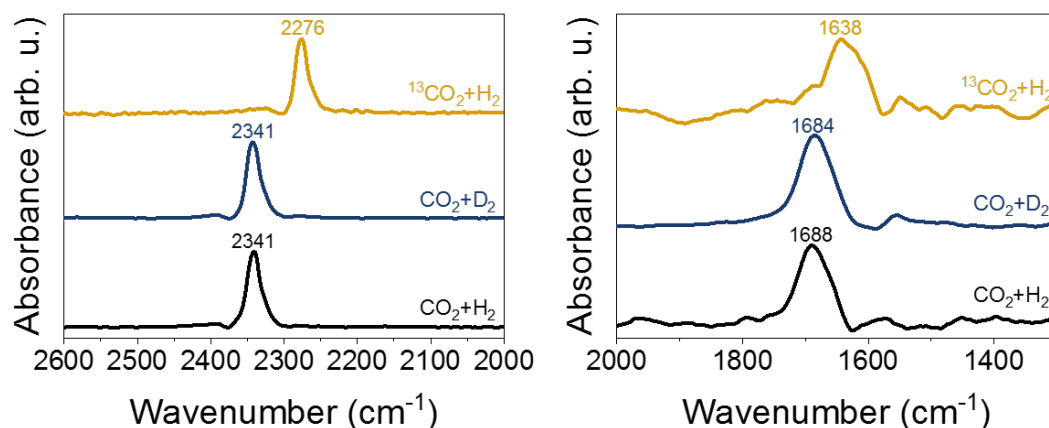

Figure 3.5. a, Time-resolved DRIFT spectra of 1 wt% Ag/SiO$_2$ upon exposure to CO$_2$:H$_2$ = 1:1 molar ratio (the first half period) vs. Ar (the second half period) concentration perturbation experiment at 230 °C and 5 bar. The DRIFT spectra were calculated taking the last spectrum in the Ar atmosphere as background. **b**, (left) Two components spectra, i.e. gaseous CO$_2$ and adsorbed CO$_2$, and (right) the corresponding concentration profiles obtained by MCR analysis applied on the depicted DRIFT spectra.

To corroborate the assignment of 1688 cm^{-1} band, we performed further analysis. A deeper look into the spectral region where a strong signal of gaseous CO$_2$ dominates (**Figure 3.5a**) shows the presence of a band at 2341 cm^{-1}, which overlaps with the bands of gaseous CO$_2$, but is kinetically separable (**Figure 3.5b**). This identification is possible thanks to the disentangling power of the multivariate spectral analysis and the plug-flow design of the DRIFTS cell with minimized gas volume,[39] thereby enhancing signals from surface species. Importantly, the comparison of the concentration profiles of the kinetically pure component spectra clarifies that the band at 1688 cm^{-1} behaves kinetically identical to the band at 2341 cm^{-1} for Ag/SiO$_2$ (**Figure 3.4c and 3.5b**). This observation suggests that the two bands at 1688 and 2341 cm^{-1} originate either from the same surface chemical species or from kinetically indistinguishable species appearing at the same time. Isotopic labelling studies using ^{13}CO$_2$

Chapter 3

and D_2 (**Figure 3.6**) show that both bands are due to the vibration of C−O bonds, with a negligible involvement of hydrogen for the band at 1688 cm^{-1}.

Figure 3.6. DRIFT spectra of adsorbed CO_2 (left) and H_2CO_3 (right) obtained by MCR analysis applied on the time-resolved DRIFT spectra of pure 1 wt% Ag/SiO$_2$ upon exposure to CO_2 + H_2, CO_2 + D_2 and $^{13}CO_2$ + H_2 (the first half period) vs. Ar (the second half period). Concentration perturbation experiment at 230 °C and 5 bar ($^{13}CO_2$ + H_2 at 1 bar).

In literature, the band at 2341 cm^{-1} has been reported and assigned to asymmetric stretching of CO_2 adsorbed on SiO_2 due to its interaction with silanol groups.[40-42] Also, a transient *in situ* DRIFTS study performed by alternatingly passing CO_2 (without H_2) vs. Ar over bare SiO_2 reveals the emergence of the same band at 2341 cm^{-1} under CO_2 (**Appendix A**, **Figure A.9**). The involvement of the OH groups on SiO_2 during the CO_2 sorption process is also evident from the apparent, reversible decrease of the OH bands upon CO_2 admission (**Appendix A**, **Figure A.10**). The different chemical nature of the two kinetically indistinguishable bands is indeed confirmed by their intensity ratio (I_{2341}/I_{1688}), which varies under different reaction conditions (CO_2 vs. Ar and CO_2 + H_2 vs. Ar) over Ag/SiO$_2$ and SiO$_2$, respectively (**Table 3.1**). It is worth noting that the intensity of the band at 1688 cm^{-1} is higher (smaller value of the I_{2341}/I_{1688} ratio) in the presence of H_2, indicating direct/indirect involvement of hydrogen in the formation or stabilization of the surface chemical species corresponding to this band.

Table 3.1. Intensity ratio of the bands at 2341 and 1688 cm^{-1} under different reactant gases. Intensity was calculated by multiplying absorbance by concentration values obtained by MCR analysis applied on the DRIFT spectra of 1 wt% Ag/SiO_2 and SiO_2 catalysts at 230 °C and 5 bar. $CO_2:H_2$ = 1:1 (molar ratio).

Catalyst	Gas flow	$(I_{2341}/I_{1688})\cdot100$
SiO$_2$	CO$_2$ vs. Ar	1.69
	CO$_2$ + H$_2$ vs. Ar	1.36
Ag/SiO$_2$	CO$_2$ vs. Ar	2.06
	CO$_2$ + H$_2$ vs. Ar	1.48

The spectral characteristics indicated that the surface species is possibly carbonic acid. Thus, we evaluated by DFT calculations the formation of carbonic acid on a surface model of highly hydroxylated SiO_2 (**Figure 3.7a**)[43] and found that this species is significantly stabilized by the formation of multiple hydrogen-bonds present on the SiO_2 surface (**Figure 3.7b**). The most favorable structures of adsorbed carbonic acid are those formed through the reaction of CO_2 with adsorbed water rather than with a gaseous water molecule. The reaction Gibbs energy for this structure (**Figure 3.7b**) is slightly endergonic at 230 °C and 5 bar (+0.49 eV), which may explain the necessity for higher pressure to boost its formation and consequently the catalytic activity, provided that this species is involved in the reaction mechanism. Alternatively, defects on SiO_2 surface, which are not taken into account in our surface model, may further stabilize its formation. Hence, all data above and DFT calculations (**Appendix A**, **Section A.1.4**) point to the attribution of the band at 1688 cm^{-1} to carbonic acid adsorbed on highly hydroxylated silica in equilibrium with adsorbed CO_2 and H_2O; note that H_2O is assumed to be present on the silica surface due to its pretreatment.[43] Such species is likely formed in a microporous/defect region of the silica support or at the interface between silica and Ag nanoparticles where such adsorption would be favored.

Curiously, the amount of adsorbed CO_2, indicated by the band at 2341 cm^{-1}, is boosted when Ag is present on the SiO_2 surface (**Appendix A**, **Figure A.11**), probably because Ag-SiO_2 interaction enhances the number of adsorption sites (i.e. hydroxyl groups) at the perimeter of Ag particles on SiO_2.[34] Consequently, a facilitated formation of adsorbed carbonic acid at/near the perimeter sites can be assumed. This implied importance of the perimeter sites is in line with the smaller pressure-dependency of the amount of adsorbed carbonic acid observed at 1688 cm^{-1} compared to that of κ^2-formate on Ag observed at 1600 cm^{-1} (**Figure 3.2**, **Appendix A**, **Figure A.7**). The restricted number of the active sites at the perimeter and their expectedly higher reactivity explain the relatively-constant concentration of the former against pressure variations, while the high pressure-dependency of the latter (**Figure 3.2**)

Chapter 3

indicates varying coverage of surface formates on Ag dynamically responding to the reactant pressure.
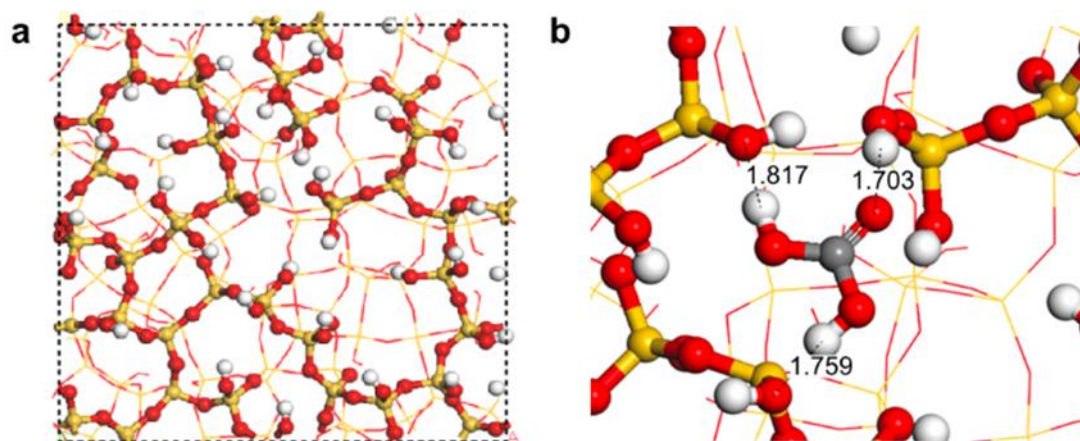
Figure 3.7. a, Top view of the optimized structures of the a, initial SiO_2 surface (7.2 OH nm^{-2}). **b**, Inset of the most stable structure of carbonic acid adsorbed on the SiO_2 surface as obtained from PBE-D3/DZVP calculations. The representative distances, which characterize the hydrogen-bonds of carbonic acid with silanols of the SiO_2 surface are shown in Å.

3.3.3 Mechanistic insights into methyl formate formation

According to the above observations, Ag enhances CO_2 adsorption and carbonic acid formation, possibly rendering the Ag-SiO_2 interface more active for specific catalytic transformations. To better understand the role of active surface species and where the reaction takes place, transient DRIFTS measurements under *operando* conditions (i.e. simultaneous reactivity measurements by mass spectrometry (MS)) are performed. Despite the lower pressure (5 bar) of these experiments due to technical limitations, the reactivity could be evaluated to firmly establish relationships among catalyst structure, surface intermediates and catalytic activity. In the first experiment, Ag/SiO_2 is first pre-exposed to the gas flow of CO_2 + H_2 + CH_3OH (vapor), followed by exposure to CH_3OH and then switched back to CO_2 + H_2 + CH_3OH. The two gas atmospheres are switched repeatedly and periodically. Similar to the identification of surface chemical species (**Figure 3.4**), the IR spectra of "kinetically separable" species and their concentration profiles are obtained by the multivariate spectral analysis of the time-resolved DRIFT spectra, firmly identifying the presence of adsorbed CH_3OH (or methoxy), adsorbed CO_2, κ^2-formates and adsorbed carbonic acid (**Figure 3.8a** and **Appendix A**, **Figure A.13, A.14 and A.15**). No spectral changes are observed when pure silica is used (**Appendix A**, **Figure A.16**), hence the spectral changes observed for Ag/SiO_2 stem from Ag or the Ag-SiO_2 interface.
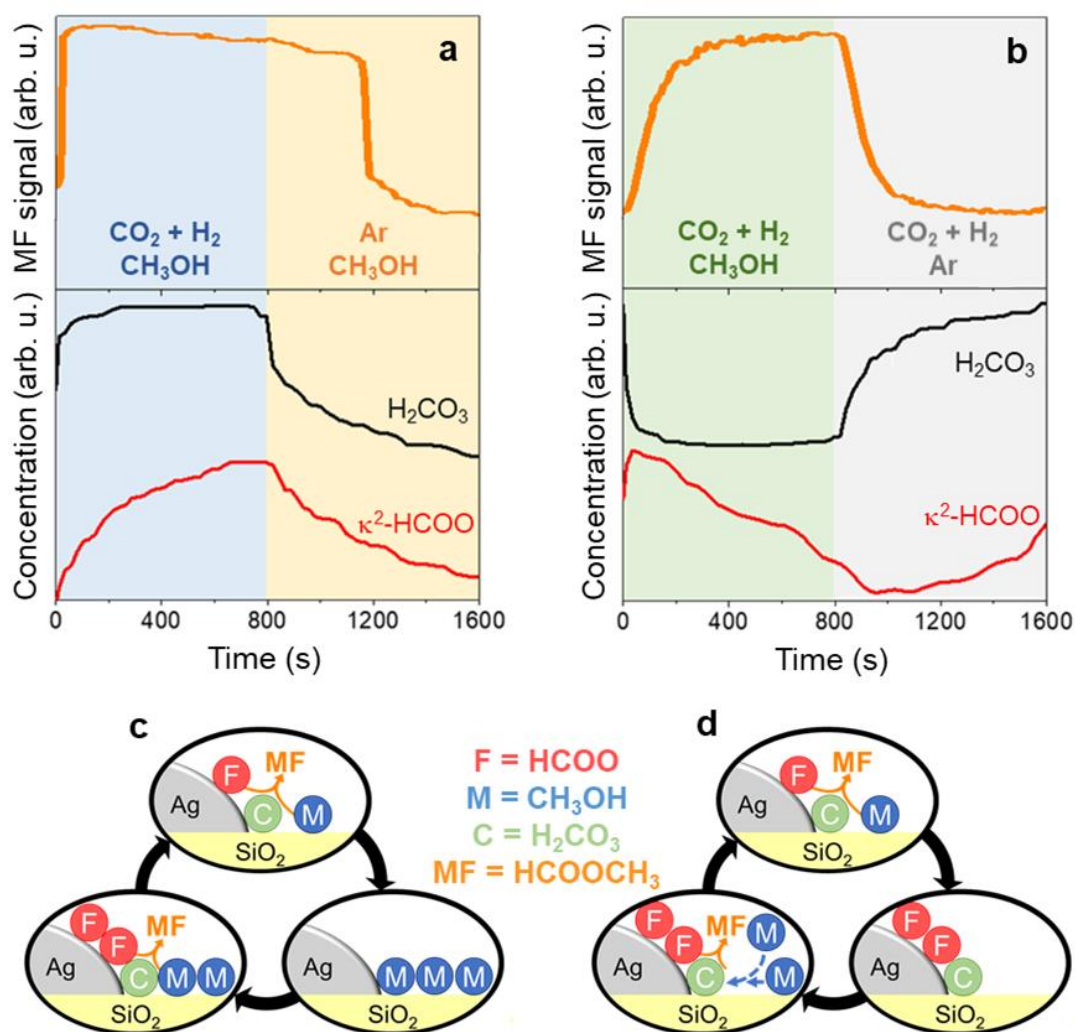
Figure 3.8. *Operando* DRIFTS studies on the esterification of formates with CH_3OH to MF over 1 wt% Ag/SiO_2. **a**, **b**, MS signal of MF (m/z = 60, top graphs) and concentration profiles of adsorbed carbonic acid and κ^2-formates obtained by the multivariate spectral analysis (bottom graphs). The analysis was applied on the time-resolved DRIFT spectra of 1 wt% Ag/SiO_2 upon exposure to **a**, $CO_2 + H_2 + CH_3OH$ (the first half) vs. $Ar + CH_3OH$ (the second half period), and **b,** $CO_2 + H_2 + CH_3OH$ (the first half) vs. $CO_2 + H_2 + Ar$ (the second half period) at 230 °C and 5 bar (total pressure). **c**, **d**, Suggested mechanisms for the formation of MF from CO_2, H_2 and CH_3OH in studies **a** and **b**, respectively

When the atmosphere is changed from CH_3OH to $CO_2 + H_2 + CH_3OH$ (the first half period of **Figure 3.8a**), first a rapidly-increasing and then relatively constant MF production is observed. The MF formation profile upon the gas switching matches well with that of carbonic acid (**Figure 3.8a**) but inversely with that of adsorbed CH_3OH (**Appendix A**, **Figure A.15**). Interestingly, when the reaction mixture is switched to CH_3OH (the second half period), a lasting production of MF is observed until the surface concentrations of κ^2-formate and adsorbed carbonic acid are very low (**Figure 3.8a**). To gain further insights into the mechanism, a second *operando* DRIFTS study is performed by exposing the catalyst to the

Chapter 3

gas flow of CO_2 + H_2 and followed by alternatingly passing the flows of CO_2 + H_2 + CH_3OH and CO_2 + H_2 (**Figure 3.8b** and **Appendix A**, **Figure A.20, A.21 and A.22**). In this case, the rapid and lasting formation of MF detected previously (**Figure 3.8a**) is not observed, and the amount of formed MF changes gradually in response to the switch of the gas atmosphere, specifically to methanol.

Importantly, the MF formation rate is not determined by the concentration of formates on Ag because the concentration profiles of surface formates and gaseous MF are uncorrelated (**Figure 3.8a-b**). The continuing formation of MF after switching from CO_2 + H_2 + CH_3OH to CH_3OH and the sudden ceasing of MF formation only after surface formates on Ag are mostly depleted (**Figure 3.8a**) imply that formates over the Ag surface gradually migrate toward the perimeter sites (spillover) for their further transformation to MF or formates formed at the interface remain there unless methanol reacts, even in the absence of CO_2 and H_2 in the atmosphere. Moreover, we assume that formates first transform into formic acid which then reacts with methanol to yield MF. In the presence of CO_2 and H_2, κ^2-formates formed on Ag via CO_2 hydrogenation are expected to react with the surface H located on Ag to yield formic acid. DFT calculations indeed support this scenario and show that Ag and Au are superior to Cu for formation of formic acid, i.e., the reaction is exothermic on Ag and Au and the activation barrier is low enough for reaction to be facile at 230 °C (**Appendix A**, **Section A.1.3**). This is consistent with the catalytic results (**Figure 3.1**) and literature reports.[9-10] However, this path cannot explain the formation of MF in the absence of CO_2 and H_2 (**Figure 3.8a**). One plausible path is the proton transfer from the carbonic acid to surface formates at the perimeter sites where these surface species are known to be concentrated (*vide supra*). Thus, the spillover of formates on Ag allows retaining a constant amount of reactive formic acid formation at the perimeter sites so that such species react with methanol to yield MF (Reaction 3.2).

$$HCOOH + CH_3OH \rightleftarrows HCOOCH_3 + H_2O \qquad (3.2)$$
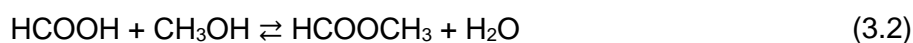
Furthermore, the availability of CH_3OH that can react with formic acid also plays another critical role in the MF formation. CH_3OH can strongly adsorb over SiO_2 (**Appendix A**, **Figure A.17 and A.18**) and thus its availability near the active perimeter sites can lead to immediate formation of MF (**Figure 3.8a**) if CH_3OH is continuously fed (**Figure 3.8c**). On the other hand, when it is discontinuously fed, MF concentration profile follows the expected profile of CH_3OH vapor in the *operando* cell, manifesting that the adsorption and diffusion of CH_3OH on the catalyst surface are rate-limiting due to the strong binding of CH_3OH on SiO_2 under the evaluated transient conditions. The adsorbed CH_3OH can be therefore depleted in the vicinity

UNIVERSITAT ROVIRA I VIRGILI
CONTINUOUS HYDROGENATION OF CARBON DIOXIDE TO FORMATES AND FORMIC ACID OVER HETEROGENEOUS CATALYSTS
Juan José Corral Pérez

Metal effect and mechanistic insights

of Ag through MF formation (**Figure 3.8d**), which is why the adsorption of CH_3OH and its access to the perimeter sites affect critically the MF formation rate.
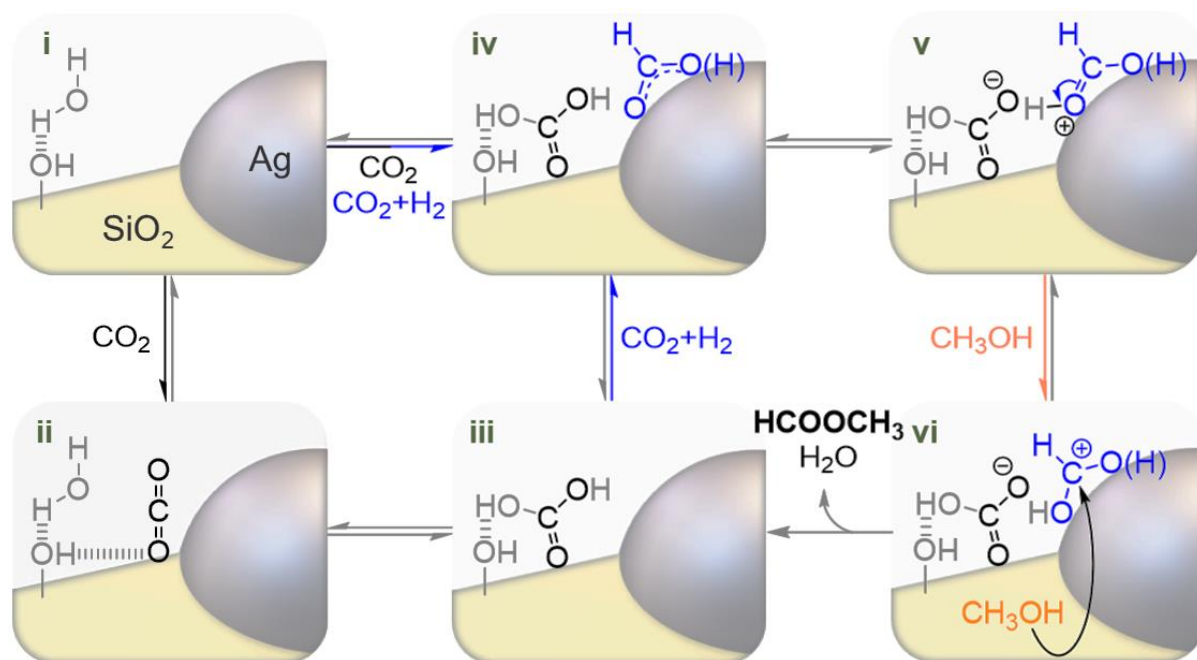
Figure 3.9. A proposed mechanism for the CO_2 hydrogenation to MF in the presence of CH_3OH over Ag/SiO_2. For further description, in particular the meaning of symbol "(H)", see text

On the basis of the *in situ* and *operando* studies described above, a mechanism for the CO_2 hydrogenation to MF in the presence of CH_3OH over Ag/SiO_2 is proposed (**Figure 3.9**, i-vi). CO_2 is adsorbed on SiO_2 due to its interaction with silanol groups (i-ii). Carbonic acid in equilibrium with CO_2 and water adsorbed on SiO_2 near Ag is readily formed (iii, *vide supra*). κ^2-Formates (iv, without H in bracket) are formed from CO_2 and H_2 over the Ag surface and transformed to formic acid either via hydrogenation with surface H (iv, with H in bracket) or via protonation through carbonic acid residing at the perimeter sites (v, without H in bracket). These formate or formic acid (v), that can also be protonated through carbonic acid, is the intermediate yielding MF through its reaction with surface adsorbed CH_3OH (vi) as indicated by the abrupt decrease in the adsorbed CH_3OH concentration **Appendix A**, **Figure A.15**). The close match in the concentration profiles of carbonic acid and MF (**Figure 3.8**) suggests that the esterification reaction between formic acid and methanol is accelerated by the presence of carbonic acid formed near the perimeter sites either through catalyzing formic acid formation or mediating the esterification reaction (**Figure 3.9**). All the results above converge to highlight the importance of the metal-support interface, particularly the perimeter sites, for the catalytic reaction. Also for a related reaction, hydrogenation of CO_2 to methanol, the transformation of the key formate intermediates to CH_3OH[19, 33-34, 44-45] was reported to be favoured at the metal-support interface for a Cu/ZrO_2 catalyst[34, 46] and the current study further affirms the important

Chapter 3

roles of such sites. These mechanistic insights are highly important for the catalyst design since adsorption strength and diffusion rate of CH_3OH, which affect the reaction rate, would be uniquely determined by the nature of support.

3.4 Conclusion

In summary, we uncovered that Ag is particularly active among coinage metals in continuous MF synthesis from CO_2, H_2 and CH_3OH due to its superior activity in the formation of surface formates and subsequent formic acid. Ag displays the lowest activation barrier for the formation of formates, because it binds atomic hydrogen weakly and formates strong enough, whereas Au binds formates too weakly and Cu binds H too strongly. The nature of the surface species formed over the catalyst was unambiguously elucidated by transient *in situ* DRIFTS studies and DFT calculations. The use of transient *operando* vibrational spectroscopy identified Ag-SiO_2 interface as the active site in the formation of MF via the esterification of surface adsorbed methanol with formic acid in the presence of carbonic acid. Such a reaction is proposed to be promoted by carbonic acid in equilibrium with adsorbed CO_2 in interaction with water/hydroxyls on SiO_2, a so-called neutral support. These insights and employed combined methodologies are expected to facilitate rational catalyst design by tuning active metal and support materials for this and other reactions.

UNIVERSITAT ROVIRA I VIRGILI
CONTINUOUS HYDROGENATION OF CARBON DIOXIDE TO FORMATES AND FORMIC ACID OVER HETEROGENEOUS CATALYSTS
Juan José Corral Pérez

Metal effect and mechanistic insights

Bibliography

1. Lee, J. S.; Kim, J. C.; Kim, Y. G., *Appl. Catal.* **1990,** *57* (1), 1-30.
2. Jenner, G.; Nahmed, E. M., *J. Organomet. Chem.* **1991,** *407* (1), 135-142.
3. Celik, F. E.; Lawrence, H.; Bell, A. T., *J. Mol. Catal. A-Chem.* **2008,** *288* (1-2), 87-96.
4. Reymond, H.; Vitas, S.; Vernuccio, S.; von Rohr, P. R., *Ind. Eng. Chem. Res.* **2017,** *56* (6), 1439-1449.
5. Di Girolamo, M.; Lami, M.; Marchionna, M.; Sanfilippo, D.; Andreoni, M.; Galletti, A. M. R.; Sbrana, G., *Catal. Lett.* **1996,** *38* (1), 127-131.
6. Tonner, S. P.; Trimm, D. L.; Wainwright, M. S.; Cant, N. W., *Ind. Eng. Chem. Prod. RD* **1984,** *23* (3), 384-388.
7. Kaichev, V. V.; Popova, G. Y.; Chesalov, Y. A.; Saraev, A. A.; Zemlyanov, D. Y.; Beloshapkin, S. A.; Knop-Gericke, A.; Schlögl, R.; Andrushkevich, T. V.; Bukhtiyarov, V. I., *J. Catal.* **2014,** *311* (Supplement C), 59-70.
8. Mueller, L. L.; Griffin, G. L., *J. Catal.* **1987,** *105* (2), 352-358.
9. Wu, C. Y.; Zhang, Z. F.; Zhu, Q. G.; Han, H. L.; Yang, Y. Y.; Han, B. X., *Green Chem.* **2015,** *17* (3), 1467-1472.
10. Filonenko, G. A.; Vrijburg, W. L.; Hensen, E. J. M.; Pidko, E. A., *J. Catal.* **2016,** *343*, 97-105.
11. Mikkelsen, M.; Jorgensen, M.; Krebs, F. C., *Energy Environ. Sci.* **2010,** *3* (1), 43-81.
12. Chen, J. S.; Xin, F.; Qin, S. Y.; Yin, X. H., *Chem. Eng. J.* **2013,** *230*, 506-512.
13. Qin, S. Y.; Xin, F.; Liu, Y. D.; Yin, X. H.; Ma, W., *J. Colloid Interface Sci.* **2011,** *356* (1), 257-261.
14. Jessop, P. G.; Hsiao, Y.; Ikariya, T.; Noyori, R., *J. Chem. Soc., Chem. Commun.* **1995,** (6), 707-708.
15. Krocher, O.; Koppel, R. A.; Baiker, A., *Chem. Commun.* **1997,** (5), 453-454.
16. Yadav, M.; Linehan, J. C.; Karkamkar, A. J.; van der Eide, E.; Heldebrant, D. J., *Inorg. Chem.* **2014,** *53* (18), 9849-9854.
17. Yu, K. M. K.; Yeung, C. M. Y.; Tsang, S. C., *J. Am. Chem. Soc.* **2007,** *129* (20), 6360–6361.
18. Yu, K. M. K.; Tsang, S. C., *Catal. Lett.* **2011,** *141* (2), 259-265.
19. Álvarez, A.; Bansode, A.; Urakawa, A.; Bavykina, A. V.; Wezendonk, T. A.; Makkee, M.; Gascon, J.; Kapteijn, F., *Chem. Rev.* **2017,** *117* (14), 9804-9838.
20. Oakton, E.; Vile, G.; S. Levine, D.; Zocher, E.; Baudouin, D.; Perez-Ramirez, J.; Coperet, C., *Dalton T.* **2014,** *43* (40), 15138-15142.
21. Vile, G.; Perez-Ramirez, J., *Nanoscale* **2014,** *6* (22), 13476-13482.
22. Tidona, B.; Urakawa, A.; Rudolf von Rohr, P., *Chem. Engin. Process* **2013,** *65* (Supplement C), 53-57.
23. Reymond, H.; von Rohr, P. R., *Rev. Sci. Instrum.* **2017,** *88* (11).
24. Perdew, J. P.; Burke, K.; Ernzerhof, M., *Phys. Rev. Lett.* **1996,** *77* (18), 3865-3868.
25. Grimme, S., *J. Comput. Chem.* **2006,** *27* (15), 1787-1799.
26. Grimme, S.; Antony, J.; Ehrlich, S.; Krieg, H., *J. Chem. Phys.* **2010,** *132* (15), 154104.
27. Giannozzi, P.; Oliviero, A.; Thomas, B.; Oana, B.; Marco Buongiorno, N.; Matteo, C.; Roberto, C.; Carlo, C.; Davide, C.; Matteo, C.; Nicola, C.; Ivan, C.; Andrea Dal, C.; Stefano de, G.; Pietro, D.; Robert, D.; Andrea, F.; Andrea, F.; Guido, F.; Giorgia, F.; Ralph, G.; Uwe, G.; Feliciano, G.; Tommaso, G.; Junteng, J.; Mitsuaki, K.; Hsin-Yu, K.; Anton, K.; Emine, K.; Michele, L.; Margherita, M.; Nicola, M.; Francesco, M.; Ngoc Linh, N.; Huy-Viet, N.; Alberto, O.-d.-l.-R.; Lorenzo, P.; Samuel, P.; Dario, R.; Riccardo, S.; Biswajit, S.; Martin, S.; Ari Paavo, S.; Alexander, S.; Iurii, T.; Timo, T.; Paolo, U.; Nathalie, V.; Xifan, W.; Stefano, B., *J. Phys-Conds. Mat.* **2017,** *29* (46), 465901.
28. Vanderbilt, D., *Phys. Rev. B* **1990,** *41* (11), 7892-7895.
29. Hutter, J.; Iannuzzi, M.; Schiffmann, F.; VandeVondele, J., *Wires. Comput. Mol. Sci.* **2013,** *4* (1), 15-25.
30. Goedecker, S.; Teter, M.; Hutter, J., *Phys. Rev. B* **1996,** *54* (3), 1703-1710.

Chapter 3

31. VandeVondele, J.; Hutter, J., *J. Chem. Phys.* **2007,** *127* (11), 114105.
32. Shekhar, M.; Wang, J.; Lee, W.-S.; Williams, W. D.; Kim, S. M.; Stach, E. A.; Miller, J. T.; Delgass, W. N.; Ribeiro, F. H., *J. Am. Chem. Soc.* **2012,** *134* (10), 4700-4708.
33. Bansode, A.; Tidona, B.; von Rohr, P. R.; Urakawa, A., *Catal. Sci. Technol.* **2013,** *3* (3), 767-778.
34. Larmier, K.; Liao, W.-C.; Tada, S.; Lam, E.; Verel, R.; Bansode, A.; Urakawa, A.; Comas-Vives, A.; Copéret, C., *Angew. Chem. Int. Edit.* **2017,** *56* (9), 2318-2323.
35. Wang, J.; Xu, X.; Deng, J.; Liao, Y.; Hong, B., *Appl. Surf. Sci.* **1997,** *120* (1–2), 99-105.
36. Clarke, D. B.; Bell, A. T., *J. Catal.* **1995,** *154* (2), 314-328.
37. Bando, K. K.; Sayama, K.; Kusama, H.; Okabe, K.; Arakawa, H., *Appl. Catal. A-Gen.* **1997,** *165* (1), 391-409.
38. Fisher, I. A.; Bell, A. T., *J. Catal.* **1998,** *178* (1), 153-173.
39. Urakawa, A.; Maeda, N.; Baiker, A., *Angew. Chem. Int. Edit.* **2008,** *47* (48), 9256-9259.
40. Ueno, A.; Bennett, C. O., *J. Catal.* **1978,** *54* (1), 31-41.
41. Roque-Malherbe, R.; Polanco-Estrella, R.; Marquez-Linares, F., *J. Phys. Chem. C* **2010,** *114* (41), 17773-17787.
42. McCool, B.; Tripp, C. P., *J. Phys. Chem. A* **2005,** *109* (18), 8914-8919.
43. Comas-Vives, A., *Phys. Chem. Chem. Phys.* **2016,** *18* (10), 7475-7482.
44. Bansode, A.; Urakawa, A., *J. Catal.* **2014,** *309* (Supplement C), 66-70.
45. Gaikwad, R.; Bansode, A.; Urakawa, A., *J. Catal.* **2016,** *343* (Supplement C), 127-132.
46. Lam, E.; Larmier, K.; Wolf, P.; Tada, S.; Safonova, O. V.; Copéret, C., *J. Am. Chem. Soc.* **2018,** *140* (33), 10530-10535.

UNIVERSITAT ROVIRA I VIRGILI
CONTINUOUS HYDROGENATION OF CARBON DIOXIDE TO FORMATES AND FORMIC ACID OVER HETEROGENEOUS CATALYSTS
Juan José Corral Pérez

Metal effect and mechanistic insights

UNIVERSITAT ROVIRA I VIRGILI
CONTINUOUS HYDROGENATION OF CARBON DIOXIDE TO FORMATES AND FORMIC ACID OVER HETEROGENEOUS CATALYSTS
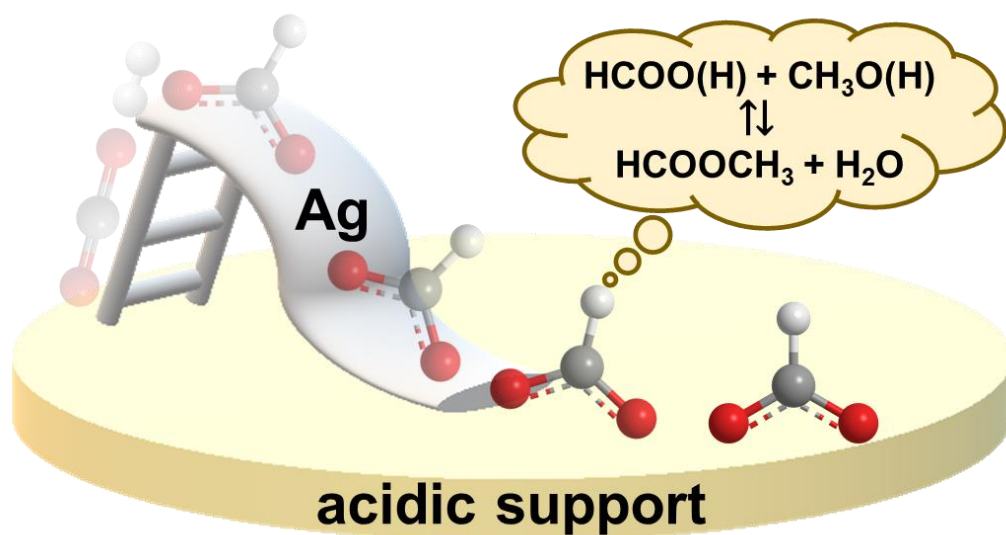Juan José Corral Pérez

Chapter 3

4

Support effect and mechanistic insights

Lewis acidic supports promote the selective carbon dioxide hydrogenation to methyl formate in the presence of methanol over Ag catalysts

Chapter 4

4.1 Introduction

Methyl formate (MF) is an important intermediate in C_1 chemistry[1] as well as a potential intermediate in the continuous synthesis of thermodynamically-unstable formic acid through hydrolysis of MF.[2] In industry, it is also used as a blowing agent for foams[3] and as an agricultural fumigant.[4] The most common commercial route to synthesize MF is the base-catalysed reaction of methanol and carbon monoxide at 80 ºC and 40 bar (Reaction 4.1).[5]

$$CO + CH_3OH \rightleftarrows HCOOCH_3 \tag{4.1}$$

Although high MF selectivity is achieved in this process, methanol conversion is only about 30% and the use of sodium methoxide as a catalyst presents some disadvantages such as equipment corrosion, the need of high purity reactants, and low process efficiency due to difficulty in separating the product and the catalyst, an intrinsic problem for most homogeneous production processes.[5] Therefore, synthesizing MF via heterogeneous catalytic continuous process would be highly desirable. Metal-based heterogeneous catalysts have been proven active in alternative synthetic routes of MF such as methanol dehydrogenation[6-7], oxidative dehydrogenation of methanol[8-9] and carbon dioxide (CO_2) hydrogenation in the presence of methanol (Reaction 4.2).[10-12]

$$CO_2 + H_2 + CH_3OH \rightleftarrows HCOOCH_3 + H_2O \tag{4.2}$$
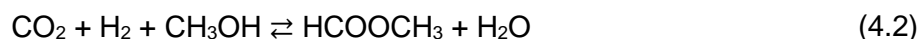
Of them, the last route is particularly appealing because it valorizes CO_2 in the context of climate change mitigation.[13] However, efficient catalysts and processes are required to convert highly stable CO_2 to MF;[14] a reaction that still suffers from low catalytic activities. Methanol conversion up to 5% has been achieved by gold nanoparticles supported on ZrO_2 at 160 bar under batch operation (maximum turnover frequency (TOF) of 534 h^{-1}).[10] In our recent work, we demonstrated that SiO_2-supported Ag nanoparticles outperform Cu and Au counterparts in the continuous selective catalytic hydrogenation of CO_2 to methyl formate in the presence of methanol.[15] A detailed mechanistic study showed that adsorbed methanol reacts with formate species or formic acid, initially formed over Ag sites, at the perimeter sites of Ag on SiO_2 to yield MF.[15] Since even SiO_2, generally considered as a neutral and catalytically innocent support, plays key roles in the reaction, it is anticipated that the reaction performance and mechanism can be influenced by the nature of the support material. Indeed, materials such as Al_2O_3 and ZrO_2 with strong acido-basic properties[16-17] can activate CO_2 and methanol, and they may potentially stabilise reaction intermediates promoting MF formation.[18-19] In fact, support effect for this reaction has been discussed, albeit not investigated in details, for supported gold nanoparticles.[10, 20]

UNIVERSITAT ROVIRA I VIRGILI
CONTINUOUS HYDROGENATION OF CARBON DIOXIDE TO FORMATES AND FORMIC ACID OVER HETEROGENEOUS CATALYSTS
Juan José Corral Pérez

Support effect and mechanistic insights

Therefore, we reason that investigating alternative supports could help improving MF yield. Towards this goal, Ag nanoparticles are supported on selected metal oxide materials via wetness impregnation method and evaluated in the MF synthesis. In order to compare the various supports without additional interference of metallic particle size, we have also used Surface Organometallic Chemistry (SOMC) to prepare supported Ag nanoparticles with a narrow particle size distribution and similar size on various supports.[21] Process parameters such as temperature, gas hourly space velocity (GHSV) and molar ratio of reactants are studied to achieve the highest MF yield and to gather information on reaction mechanisms. Finally, transient *in situ* and *operando* diffuse reflectance infrared Fourier transform spectroscopy (DRIFTS) studies in combination with multivariate spectral analysis[15, 22-23] are performed to elucidate the origin of support effects in relation to the formation of reactive intermediate species, their dynamics and the location of active surface species in MF synthesis.

4.1 Experimental

4.1.1 Materials

Silver nitrate (>99%, Alfa Aesar) and methanol (>99%, Sigma Aldrich) were used as received. Commercial supports (SiO_2, ZrO_2 and Al_2O_3) were partially dehydroxylated at 500 °C (see **Chapter 2, Section 2.2.2**). Pentane was purified over two solvent purification alumina columns (MBraun) and degassed prior to use. H_2 for catalyst preparation was purified over activated R3-11 BASF catalyst and activated 4 Å molecular sieves. Silver mesityl was synthesized as reported in literature and stored in an argon filled glovebox.[24] Deionized water was used for catalyst synthesis. Liquid CO_2 (>99.9993%) and 10% Ar in H_2 (>99.999% for Ar or H_2, prior to mixing) were purchased from Abelló Linde.

4.1.2 Materials characterisation

Fourier transform infrared (FTIR) measurements of the catalysts prepared via the SOMC approach were performed on a Bruker Alpha spectrometer inside a glovebox under Ar atmosphere. The powder samples were pressed into a thin disk using a 7 mm die set. Typically, 24 scans were collected for each spectrum at a resolution of 4 cm^{-1}. Background spectra were collected under Ar atmosphere.

The metal content was quantified by inductively coupled plasma optical emission spectrometry (ICP-OES) or energy-dispersive X-ray spectroscopy (EDX).

Chapter 4

Transmission Electron Microscopy (TEM) images were recorded on a JEOL 1011 while scanning transmission electron microscopy images were recorded on an aberration-corrected Hitachi HD2700CS microscope with a high angle annular dark field detector (HAADF STEM).

Brunauer-Emmett-Teller (BET) surface area was determined by N_2 physisorption experiments using Quantachrome Instruments, AUTOSORB iQ. Prior to the measurements, the material (100 mg) was outgassed at 150 °C and 4 mbar to clean the sample surface and pores.

4.1.3 Reaction system

Catalytic tests were performed in a continuous flow fixed-bed microreaction system. Details of the setup and the method of product analysis are described in **Chapter 2, Section 2.3**. In a typical experiment, 150-1000 mg of catalyst (pelletized, crushed and sieved to 100-300 μm particle size) was loaded in a tubular reactor (ID: 2.95 mm, OD: 6.35 mm) and reduced in the stream of Ar (10%) and H2 (90%) at 260 °C for 2 h at atmospheric pressure. After the reduction, the catalyst bed was cooled down to room temperature. Then, the reaction mixture (CO_2:H_2:CH_3OH = 4:4:1 molar ratio) was introduced into the reactor at a specific flow rate. The pressure in the reactor was regulated by an automatic back-pressure regulator. The data points were collected by an online gas chromatograph during the steady state operation of the reaction at specified temperature (120-260 °C) and pressure (300 bar). Ar was used as an internal standard for gas chromatography analysis and product selectivity was calculated taking only carbon-containing products into account.

4.1.4 DRIFTS measurements

A custom-made high-pressure reaction cell, with a cylindrical cavity (3 mm in diameter and 3 mm vertical length) to place the catalyst powder, mounted in a Praying Mantis (Harrick) DRIFTS optical system was used. The spectra were collected using a Bruker Vertex70v FT-IR spectrometer equipped with a liquid-nitrogen-cooled MCT detector at 4 cm^{-1} resolution. Details of the setup and method of *in situ*/*operando* and transient measurements are provided in **Chapter 2, Section 2.4**

### 4.1.5 Multivariate spectral analysis

Multivariate spectral analysis was performed by means of multivariate curve resolution (MCR). MCR is a chemometric method used for better data processing and deconvolution of the complex spectra down to individual components based on kinetic resolution. It delivers the pure response profiles of the chemical species of an unresolved mixture when no previous

UNIVERSITAT ROVIRA I VIRGILI
CONTINUOUS HYDROGENATION OF CARBON DIOXIDE TO FORMATES AND FORMIC ACID OVER HETEROGENEOUS CATALYSTS
Juan José Corral Pérez

Support effect and mechanistic insights

information is available about the nature and composition of these mixtures. More details of the method and software used are specified in **Chapter 2, Section 2.5**.

4.2 Results and discussion

4.2.1 Catalyst synthesis and catalytic performance

Preliminary screening of selected support materials (ZrO_2, γ-Al_2O_3, CeO_2, pumice as well as SiO_2, **Appendix B**, **Table B.1**) was carried out using Ag as the active metal for MF synthesis from CO_2 and H_2 in the presence of CH_3OH. These catalysts are synthesized via incipient wetness impregnation using silver nitrate as precursor and subsequently calcined in air at 400 °C for 4 h. The nominal silver loading is kept constant at 1 wt% (actual Ag loading is 1-2 wt% according to EDX, **Appendix B**, **Table B.2**). These Ag catalysts are evaluated in the continuous MF synthesis at high pressure (300 bar) because of the beneficial effect of pressure on reaction performance.[15] At low temperatures, all Ag catalysts with the various supports exhibit full selectivity to MF at our detection limit, and importantly those supported on ZrO_2 and γ-Al_2O_3, that are known Lewis acidic supports, display superior catalytic activity (**Figure 4.1**).
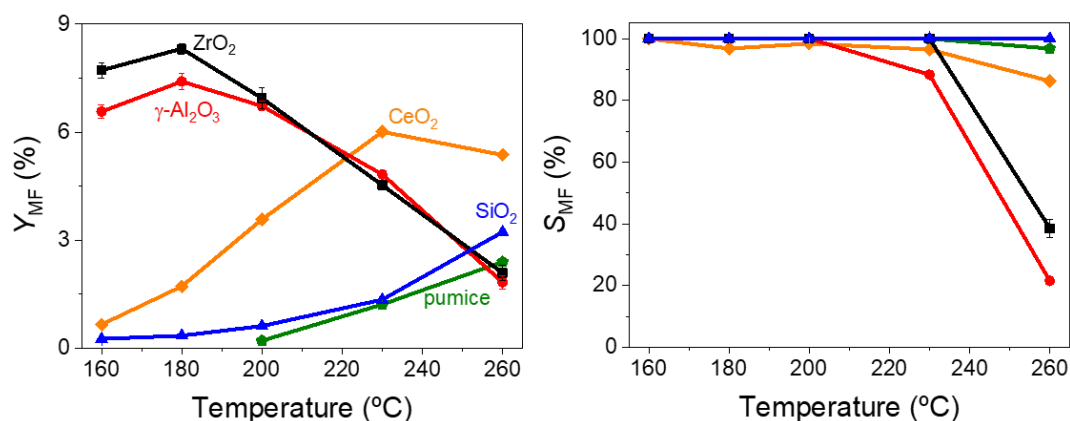

Figure 4.1. Effects of temperature on methanol-based MF yield (Y_{MF}) and selectivity to MF (S_{MF}) over pumice- (green), silica- (blue), ceria- (orange), γ-alumina- (red) and zirconia- (black) supported Ag catalysts prepared via the impregnation method. Reaction conditions: CO_2:H_2:CH_3OH = 4:4:1 (molar ratio), 300 bar, GHSV = 9000 h^{-1}.

Besides the clear influence of the type of support used for the Ag catalysts on MF yield, the Ag particle size may also affect the catalytic performance. In order to discern if the superior MF yield arises from the support or Ag particle size, comparative Ag catalysts supported on ZrO_2, γ-Al_2O_3 and SiO_2 are synthesized via the SOMC approach.[21, 25-28] While Ag/ZrO_2 and Ag/γ-Al_2O_3 are chosen because of their high activity (vide supra), Ag/SiO_2 is used as a benchmark because of its previously reported activity in this particular reaction.[15] Thanks to

Chapter 4

SOMC, narrowly dispersed Ag nanoparticles of similar sizes (2.6 ± 0.6 nm) are obtained on all supports by grafting silver mesityl on the surface hydroxyl groups of the respective support (partially dehydroxylated at 500 ºC), followed by reduction under H_2 at 500 °C for 5 h (**Figure 4.2**).
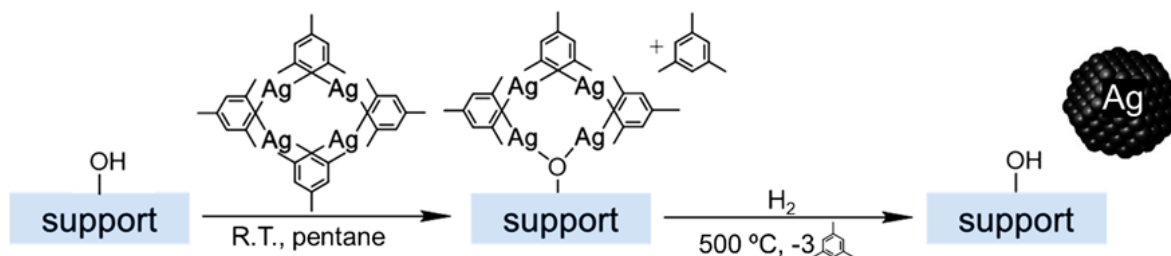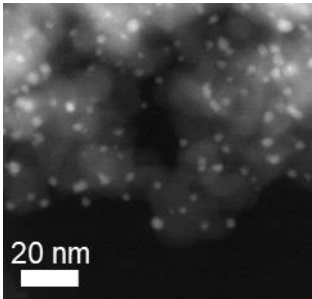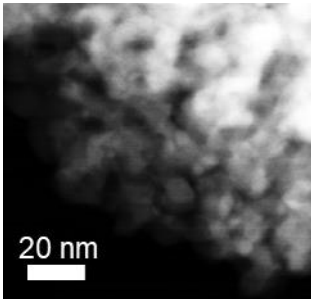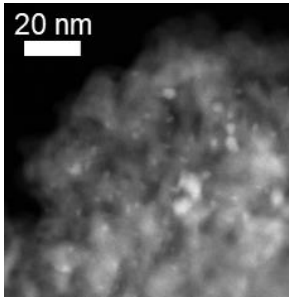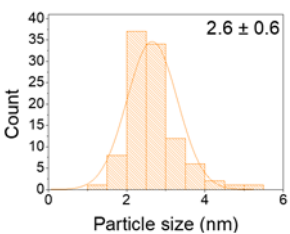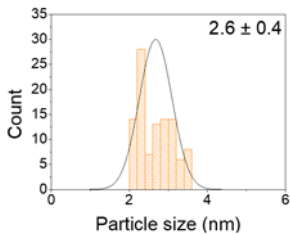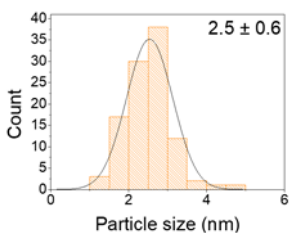

Figure 4.2. Schematic representation of the grafting-reduction sequence for supported Ag nanoparticles catalysts prepared via the SOMC approach.

The operation is monitored by infrared spectroscopy at the various stages of the preparation. **Figure 4.3** shows the IR spectrum of SiO_2, ZrO_2, γ-Al_2O_3 (black) that mainly displays v(OH) stretching frequencies from OH groups. After grafting (red), C-H stretching bands from silver mesityl appear in the 2700–3100 cm^{-1} region while the intensity of the OH bands strongly decreased or were only slightly perturbed. This confirms the grafting of the molecular precursor by chemical reaction with the surface OH groups according to **Figure 4.2**. Upon reduction (blue), the v(CH) bands disappear while the v(OH) band reappear as an indication that the organic ligands are removed. The formation of Ag particle with virtually identical size (**Table 4.1**) for the three catalysts allows interrogating the support effects on the hydrogenation of CO_2 in the presence of methanol.
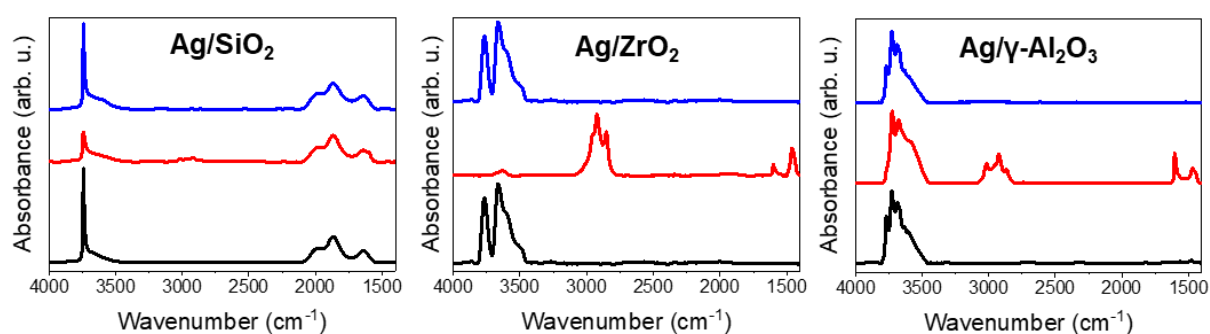

Figure 4.3. FTIR spectra of silica-, zirconia- and γ-alumina-supported silver catalysts prepared via the surface organometallic chemistry (SOMC) approach during preparation: (black) support calcined at 500 ºC, (red) silver mesityl grafted on the support, (blue) after reduction under H_2 at 500 °C for 5 hours.

UNIVERSITAT ROVIRA I VIRGILI
CONTINUOUS HYDROGENATION OF CARBON DIOXIDE TO FORMATES AND FORMIC ACID OVER HETEROGENEOUS CATALYSTS
Juan José Corral Pérez

Support effect and mechanistic insights

Table 4.1. HAADF-STEM images, metal loading (determined by ICP) and BET surface area of silica-, zirconia- and γ-alumina-supported silver catalysts prepared via the surface organometallic chemistry (SOMC) approach.

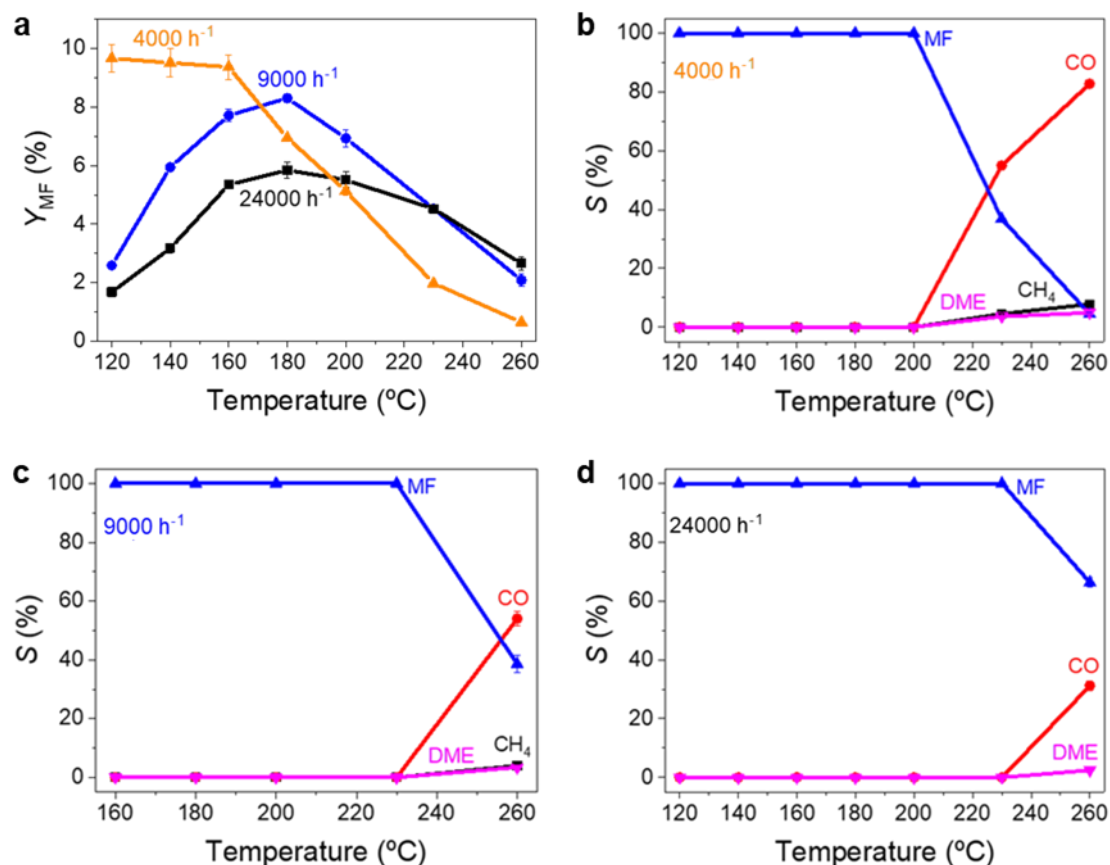|	SiO$_2$	ZrO$_2$	γ-Al$_2$O$_3$
Ag (wt%)	1.2	1.8	2.0
Ag size (nm)	2.6 ± 0.6	2.6 ± 0.4	2.5 ± 0.6
S$_{BET}$ (m^2/g)	159	99	140

The supported Ag catalysts prepared via SOMC (**Figure 4.4**, dashed line) are evaluated in the CO$_2$ hydrogenation to MF in the presence of methanol and compared to the counterparts prepared via impregnation (**Figure 4.4**, solid line) by means of weight time yield of MF (WTY_{MF}) and selectivity to MF (S_{MF}). As depicted in **Figure 4.4**, there are no significant differences between the catalytic activities of the materials prepared by the two different methods for the same type of support material. γ-Al$_2$O$_3$ and ZrO$_2$ supported Ag catalysts show similar catalytic trends. Both support materials facilitate MF formation at lower temperatures when compared to SiO$_2$. MF is exclusively formed over Ag/SiO$_2$ in the whole evaluated temperature range (**Figure 4.4**)[15] while DME and CO are the predominant products for Ag/Al$_2$O$_3$ and Ag/ZrO$_2$, respectively, at higher temperatures (**Figure 4.5c, Appendix B**, **Figure B.1 and B.2**). Note that in the absence of Ag nanoparticles over γ-Al$_2$O$_3$ and ZrO$_2$, only DME is observed as product at temperatures higher than 200 ºC (**Appendix B**, **Figure B.3**). Hence, silver nanoparticles promote the formation of MF and CO, but effects of its particle size are not evidently observed, thus highlighting the dominant effects of support material on the MF synthesis. This is also indicated by the formation of side-products since the selectivity to MF is strongly affected by the nature of support material at high temperatures.

Chapter 4
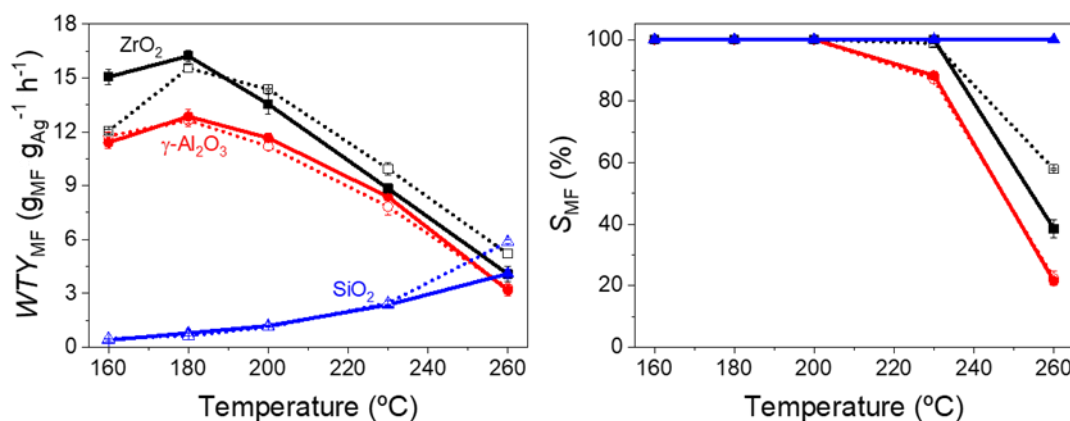
Figure 4.4. Effects of reaction temperature on weight time yield of MF (WTY_{MF}) and selectivity to MF (S_{MF}) over silica- (blue), γ-alumina- (red) and zirconia- (black) supported Ag catalysts prepared via the impregnation method (solid line) and the SOMC approach (dashed line). Reaction conditions: CO_2:H_2:CH_3OH = 4:4:1 (molar ratio), 300 bar, GHSV = 9000 h^{-1}.

A more detailed study regarding the effect of the gas hourly space velocity (GHSV) over the most reactive catalyst, i.e. Ag/ZrO_2 prepared by the impregnation method, is performed in a wider range of reaction temperatures to gather information on what is limiting the MF formation rate. **Figure 4.5a** shows that upon increasing GHSV from 9000 to 24000 h^{-1}, i.e. decreasing the residence time of the reactants in the catalytic reactor, MF yield (methanol conversion basis) drops with the similar reactivity trend with the maximum at 180 °C. On the other hand, MF yield increases drastically at 4000 h^{-1} in the lower temperature range (120-160 ºC), reaching close to 10% MF yield and without showing a maximum MF yield in the temperature range examined. It is interesting to note that the MF yield drops more rapidly towards higher temperatures at 4000 h^{-1} in comparison to the higher GHSV cases (**Figure 4.5**). This drop in MF yield is obviously related to the amount of CO formed, which is more pronounced at lower GHSV (**Figure 4.5b**). A closer look into MF yield (**Figure 4.5a**) upon increasing reaction temperatures shows that the onset temperature of CO formation (**Figure 4.5b-c**) and the maximum temperature where MF yield drops are highly related. These results imply that the reaction is kinetically more limited at the higher GHSV due to the short residence time. The observed correlation between the MF drop and CO formation suggests that CO is formed through the decomposition of MF possibly over the acidic sites,[29-30] although we cannot fully exclude the possibility of reverse water-gas shift reaction through a surface intermediate for CO formation since this reaction is favoured at higher temperatures.[31]

UNIVERSITAT ROVIRA I VIRGILI
CONTINUOUS HYDROGENATION OF CARBON DIOXIDE TO FORMATES AND FORMIC ACID OVER HETEROGENEOUS CATALYSTS
Juan José Corral Pérez

Support effect and mechanistic insights

Figure 4.5. a, Effects of GHSV on MF yield (Y_{MF}) and selectivity (S) to MF, DME, CO and CH$_4$ at **b**, 4000, **c**, 9000 and **d**, 24000 h^{-1} over zirconia-supported Ag catalyst prepared via the impregnation method. Reaction conditions: $CO_2:H_2:CH_3OH = 4:4:1$ (molar ratio) and 300 bar.

There is a small temperature window where MF yield drops upon increasing reaction temperatures while only MF is observed (e.g. 160-200 ºC at 4000 h^{-1}, **Figure 4.5a-b**). This drop is more pronounced at lower GHSV and hence at longer reaction time in the catalytic reactor. These observations indicate that prior to CO formation, MF decomposition to CO_2, H_2 and methanol may become prominent at longer residence time. This as well as the higher MF yield at lower GHSV and temperatures (**Figure 4.5a**) imply that the MF formation is kinetically controlled through a delicate balance between its formation and decomposition. Furthermore, while DME is observed at elevated temperatures when CO is also present (**Figure 4.5b-c**), DME is likely formed through dehydration of methanol over the acidic sites of the support because Ag/A$_2$O$_3$ (**Appendix B**, **Figure B.2**) shows high DME selectivity and Al$_2$O$_3$ is a well-known active catalyst for methanol dehydration.[13]

With the implication of MF formation being kinetically limited, attempts are made to increase MF yield by varying the molar ratios of the reactants at low GHSV (4000 h^{-1}) over Ag/ZrO$_2$ prepared by the impregnation method (**Figure 4.6**). When the partial pressure of CO_2 and H_2 is roughly halved by increasing the methanol concentration ($CO_2:H_2:CH_3OH = 2:2:1$ molar

Chapter 4

ratio), MF yield drops (**Figure 4.6**). In sharp contrast, when the partial pressure of CO_2 and H_2 is drastically increased (CO_2:H_2:CH_3OH = 30:30:1 molar ratio), the MF yield increases to values up to 22%. The practically identical WTYs at 4:4:1 and 2:2:1 molar ratios indicate that at constant GHSV, hence residence time, the conversion rates of methanol per unit time do not change significantly. However, WTY drops greatly at 30:30:1 molar ratio. This is a clear indication that at this ratio, the amount of methanol on the catalyst surface is rate-limiting due to lower methanol partial pressure and/or abundant coverage of formates/formic acid on the catalyst surface, thus highlighting how critical the formation of formate species or methanol adsorption is for this reaction. Under this limiting condition, higher portion of methanol can be reacted compared to CO_2 and H_2, hence the highest achieved MF yield.
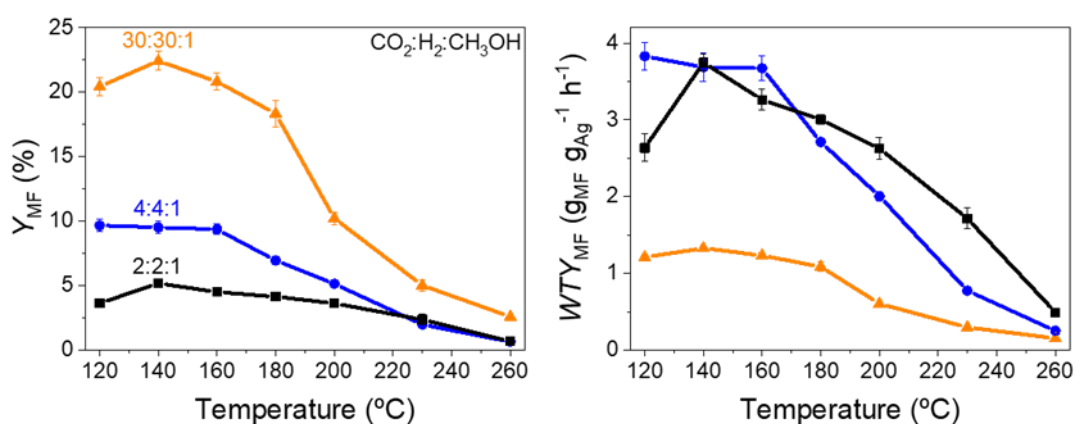
Figure 4.6. Effects of CO_2:H_2:CH_3OH molar ratio on (left) MF yield (Y_{MF}) and (right) weight time yield of MF (WTY_{MF}) over zirconia-supported Ag catalyst prepared via the impregnation method. Reaction conditions: GHSV = 4000 h^{-1} and 300 bar.

4.2.2 Surface species involved in CO_2 hydrogenation

Aside from the mechanistic hints provided by the catalytic data, *in situ* DRIFTS is performed to gain chemical insights into the surface chemical species formed over the different catalysts prepared via the impregnation method under reaction conditions, thus allowing molecular understanding of support effects observed when comparing the improved catalytic activity for ZrO_2 and Al_2O_3 vs. SiO_2.[15] The general challenge of such spectroscopic methodology lies in the complexity of spectra due to the presence of spectator species which are not directly involved in the reaction and to the overlapping signals arising from several chemical species that coexist on the catalyst surface. Transient response techniques together with multivariate spectral analysis allows a selective and sensitive monitoring of the dynamic behaviour of the active species involved in the complex catalytic system.[32] However, such approach cannot establish relationships among surface intermediates and catalytic performance. That is why *operando* methodology,[33-35] through simultaneous reactivity evaluation, is further employed in

UNIVERSITAT ROVIRA I VIRGILI
CONTINUOUS HYDROGENATION OF CARBON DIOXIDE TO FORMATES AND FORMIC ACID OVER HETEROGENEOUS CATALYSTS
Juan José Corral Pérez

Support effect and mechanistic insights

combination with transient techniques to elucidate surface species responsible for the target product formation.

As noted previously, MF is formed only when Ag is present on the metal oxide support materials. *In situ* DRIFTS measurements reveal that only carbonates are formed over pure ZrO_2 under the mixture of CO_2 and H_2 (1:1 molar ratio) at 230 °C and 5 bar (**Figure 4.7**).[36] The experimental condition is identical to that used in our previous study on Ag/SiO_2, hence the results can be directly compared.[15] The characteristic bands in the $v(C−H)$ region assigned to formate species are observed only when Ag is present on the support surface (**Figure 4.7**). To learn more about the nature of these surface species, a transient *in situ* DRIFTS study is performed by passing alternatingly the reactant gas (CO_2:H_2 at 1:1 molar ratio) and an inert gas (Ar) over Ag/ZrO_2 catalyst at 230 °C and 5 bar (**Figure 4.8a**). The IR spectra of "kinetically separable" surface species (**Figure 4.8b**) and their concentration profiles (**Figure 4.9**) are obtained by multivariate spectral analysis.
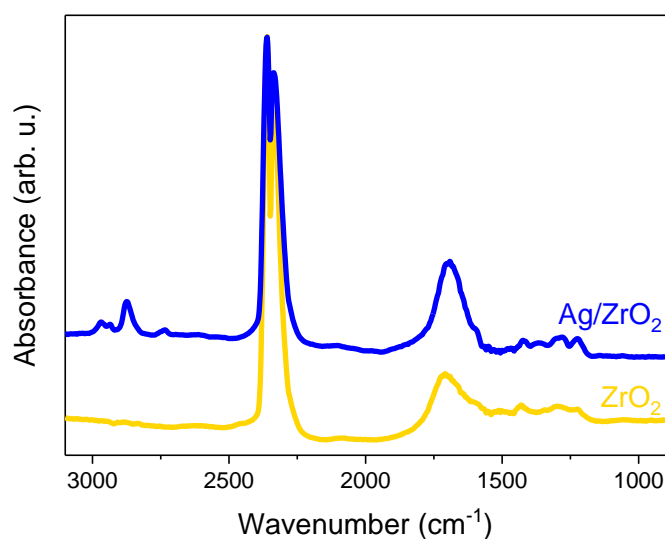

Figure 4.7. *In situ* DRIFTS spectra of ZrO_2 and Ag/ZrO_2 (prepared via the impregnation method) catalysts when exposed to CO_2 and H_2 at 230 °C and 5 bar.

In the $v(C−H)$ region (**Figure 4.8b**), the presence of two distinct surface species, whose concentrations respond to the partial pressure of CO_2 and H_2, is confirmed (**Figure 4.9**, solid line). In the $v(C−O)$ region, there are three distinguishable species and their concentration profiles are shown in **Figure 4.9** (dashed line). One of them show characteristic bands of carbonates over ZrO_2 (**Figure 4.8b**, black line).[23-24] The other two species behave kinetically identical to those observed in the $v(C−H)$ region (shown in the same line colour in **Figure 4.8b and 4.9**). These two species are assigned to formate species since their characteristic features are simultaneously observed in the $v(C−H)$ and $v(C−O)$ regions and are consistent with literature data.[17, 19, 36-37] Thus, two kinds of formate species are formed over the catalyst

Chapter 4

surface. The bands at 2940, 2838, 2723, 1648, 1394 and 1286 cm^{-1} (**Figure 4.8b**, orange line) are assigned to formates on Ag as previously proposed,[15] while these at 2969, 2923, 2877, 2815, 2753, 1733 and 1639 cm^{-1} (**Figure 4.8b**, green line) can be assigned to formates adsorbed over ZrO_2 support[19, 37] or possibly at the perimeter sites of Ag and ZrO_2.
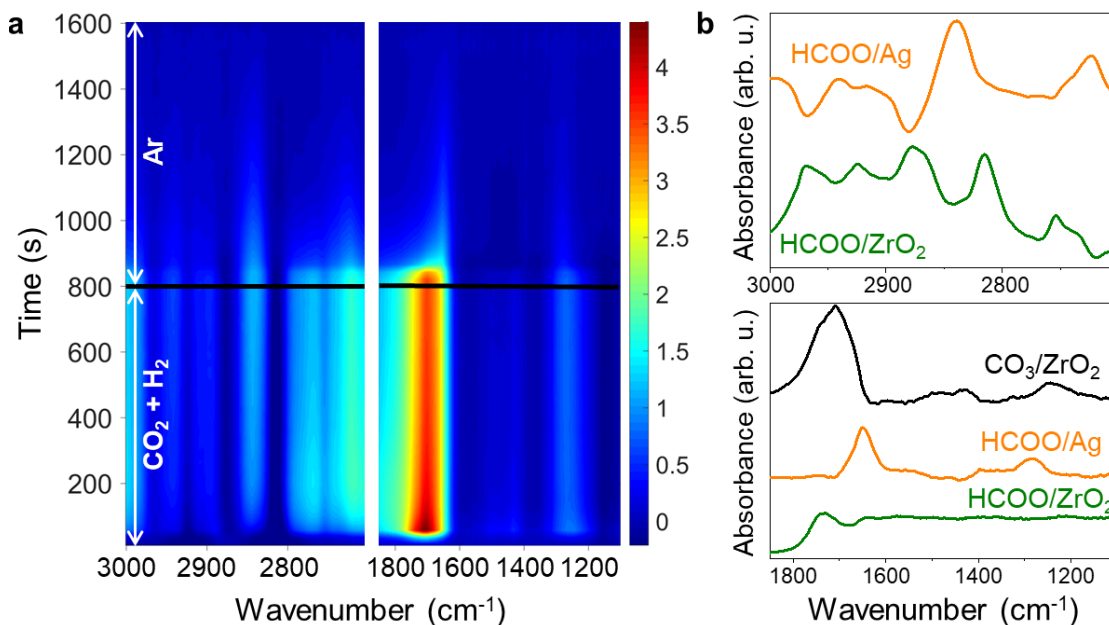
Figure 4.8. Transient DRIFTS study under a CO_2 hydrogenation condition over Ag/ZrO_2 catalyst prepared via the impregnation method. **a,**Time-resolved DRIFT spectra upon exposure to CO_2:H_2 = 1:1 molar ratio (the first half period) and then to Ar (the second half period) concentration perturbation experiment at 230 °C and 5 bar. The DRIFT spectra are shown in milli-absorbance unit taking the last spectrum in the Ar atmosphere as background. **b,** Components spectra obtained by multivariate spectral analysis applied on the time-resolved DRIFT spectra.

In order to further confirm the nature of the two kinds of formates discussed above, i.e. formates on Ag and formates on ZrO_2, the concentration profiles of these kinetically distinct species are more carefully examined. When the catalyst is exposed to CO_2 + H_2, carbonates (**Figure 4.9**, black line) and formates on Ag (**Figure 4.9**, orange line) are immediately formed reaching a stable concentration relatively quickly while formates on ZrO_2 slightly increase. After switching the reactant gas to argon, carbonates depletion is instantaneous while the decrease in the concentration of the formates on Ag (**Figure 4.9**, orange line) is accompanied by the compensating formation of formates on ZrO_2 (**Figure 4.9**, green line). The reversed concentration profiles of the two kinds of formates (**Figure 4.9**) indicates a spillover process of the formates formed on Ag under CO_2 + H_2 towards the support or possibly at the perimeter sites of Ag and ZrO_2. Such spillover process takes place more slowly under CO_2 + H_2 (**Figure 4.9a-b**) than argon (**Figure 4.9c-d**), most likely due to the presence of carbonates over the

UNIVERSITAT ROVIRA I VIRGILI
CONTINUOUS HYDROGENATION OF CARBON DIOXIDE TO FORMATES AND FORMIC ACID OVER HETEROGENEOUS CATALYSTS
Juan José Corral Pérez

Support effect and mechanistic insights

support (**Figure 4.9a-b**) that compete with formates for the same adsorption sites on ZrO_2, thus hindering the spillover process.
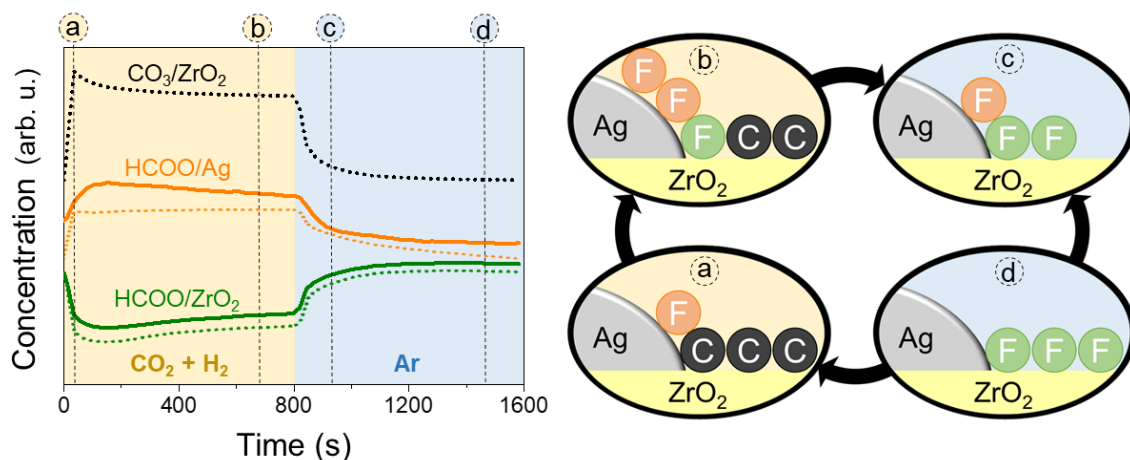
Figure 4.9. Concentration profiles of the corresponding components spectra in the v(C−O) (dashed line) and v(C−H) (solid line) regions obtained by the multivariate spectral analysis shown in **Figure 4.8**, and a scheme of the surface species, i.e. carbonates (C) and formates (F), involved in CO_2 hydrogenation over Ag/ZrO_2 catalyst under transient conditions (**a-d**).

It should be noted that in the case of Ag/SiO_2, formates on Ag are removed under argon while on SiO_2 they are not observed.[15] Hence, the stable formation of formates on support and the possibility of spillover from Ag are ascribed to the (Lewis acidic) properties of ZrO_2 support.[19] Importantly, this spillover phenomenon is also observed for Ag/Al_2O_3 (**Appendix B**, **Figure B.4**), confirming the stable formation/presence of formates on both support materials and explaining why acidic supports like ZrO_2 and Al_2O_3 exhibit better catalytic performance than SiO_2 in MF formation (**Figure 4.4**). However, it should be underlined that the acidity of these support materials also induces the formation of DME at high temperature and facilitates CO formation through the decomposition of MF (**Figure 4.5**).[30, 38]

4.2.3 Mechanistic insights into methyl formate formation

In order to understand how the formate species spillover from the Ag surface to the support affects the MF yield, transient DRIFTS measurements were performed under *operando* conditions (i.e., simultaneous reactivity measurements by mass spectrometry (MS)) over the catalysts prepared via the impregnation method. The MS signals of MF observed for Ag/ZrO_2 are depicted and compared to those of Ag/SiO_2 in **Figure 4.10**. In the first experiment, Ag/ZrO_2 is initially exposed to the gas flow of $CO_2 + H_2 + CH_3OH$ (vapor), followed by exposure to CH_3OH and then switched back to $CO_2 + H_2 + CH_3OH$ (**Figure 4.10a**). The two gas atmospheres are switched repeatedly and periodically. The IR spectra of "kinetically separable" species (**Appendix B**, **Figure B.5**), i.e. adsorbed CH_3OH (or methoxy), formates
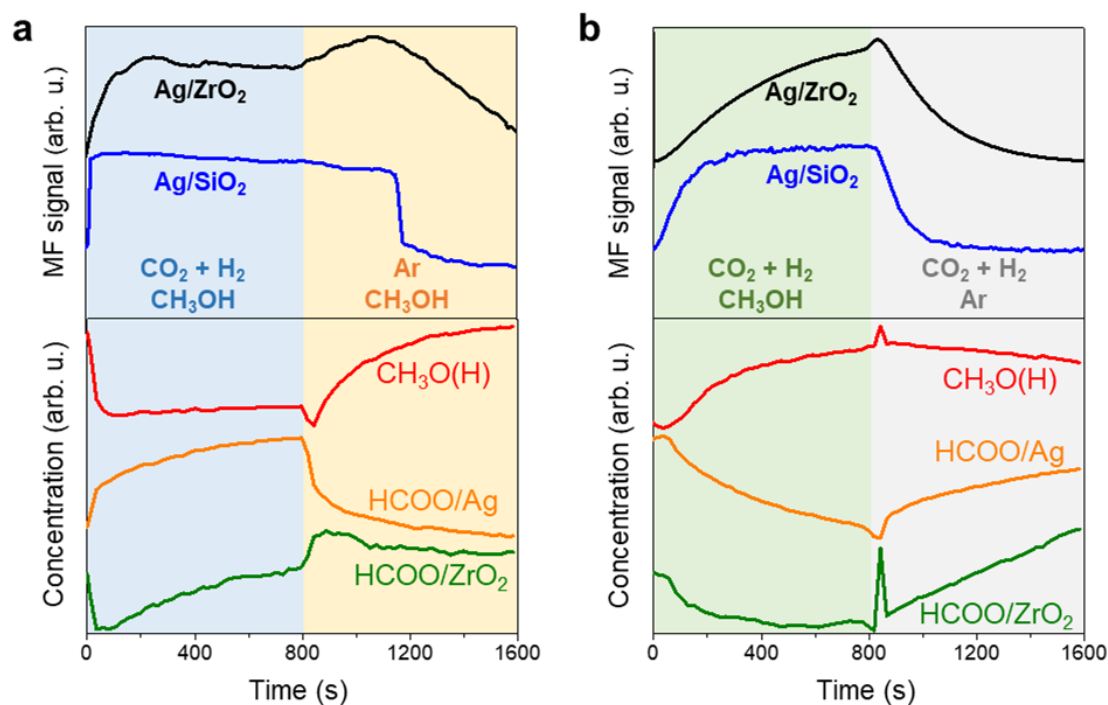
Chapter 4

on Ag and formates on ZrO_2, and their concentration profiles (**Figure 4.10a**) are obtained by the multivariate spectral analysis.

When the reactant gas is changed from CH_3OH (the second half period of **Figure 4.10a**) to $CO_2 + H_2 + CH_3OH$ (the first half period), MF is instantly produced, and its increasing formation profile is similar to that of formates over Ag but inversely correlated with that of adsorbed CH_3OH (**Figure 4.10a**). Upon switching the atmosphere to CH_3OH (the second half period), a slight enhancement in the production of MF is observed, which is apparently linked with the concentration change of formates on ZrO_2 (**Figure 4.10a**). After the initial increase in the concentration of formates on ZrO_2, their concentration decreases only slightly, indicating that they are not decomposed and can be stably present in the CH_3OH atmosphere. At the same time, the MF production rate decreases over time as methanol is increasingly adsorbed on the catalyst. Unlike for Ag/SiO_2, the initial increase in the concentrations of gaseous MF and surface formates on ZrO_2 upon switching to CH_3OH implies that the specific transient condition creates highly reactive environment between surface formates/formic acid with adsorbed methanol to enhance MF yield.

According to the concentration profiles of formates on Ag and ZrO_2 upon switching to the CH_3OH atmosphere (**Figure 4.10a**), the sudden increase in gaseous CH_3OH concentration induces an increase in the concentration of formates on ZrO_2 that promotes the formation of MF. This indicates a rapid migration of formates on Ag toward the perimeter sites and further over ZrO_2 (**Figure 4.11a**). Most likely this is due to the reaction of surface species with methanol to yield MF, thus creating vacant sites on ZrO_2 that accelerates the spillover process. This hypothesis is supported by the fact that the spillover of formates to ZrO_2 is slower under CO_2 and H_2 ($HCOO/ZrO_2$ in **Figure 4.9** vs **Figure 4.10a**), since the surface species cannot be consumed in the absence of methanol.

Another important observation is that the MF formation gradually decreases along the CH_3OH atmosphere (**Figure 4.10a**) despite the stable presence of formates on ZrO_2 and increasing amount of adsorbed CH_3OH. This indicates that the actual MF formation sites is highly location-sensitive; the formates that react with methanol to yield MF are likely those present close, i.e. at the interface between Ag and ZrO_2 (**Figure 4.11b**). In any case, formates on ZrO_2 could function as a sink to provide active formates reacting with CH_3OH at the perimeter sites through reverse-spillover (**Figure 4.11c**). However, if the distance from the formates on ZrO_2 to Ag is too large, the reverse-spillover and consequently the reaction toward MF formation seem prohibited by the blockage of near-perimeter sites on ZrO_2 by methanol (**Figure 4.11d**). This would explain the concentration profiles of the transient *operando* study, where both formates and adsorbed methanol coexist on ZrO_2 with reduced formation of MF.

UNIVERSITAT ROVIRA I VIRGILI
CONTINUOUS HYDROGENATION OF CARBON DIOXIDE TO FORMATES AND FORMIC ACID OVER HETEROGENEOUS CATALYSTS
Juan José Corral Pérez

Support effect and mechanistic insights

Figure 4.10. Transient *Operando* DRIFTS studies on the esterification of formates with CH_3OH to MF over Ag/ZrO_2. MS signal of MF (m/z = 60, top graphs) and concentration profiles of adsorbed CH_3OH and formates obtained by the multivariate spectral analysis (bottom graphs). MS signal of MF over Ag/SiO_2 as a reference.[15] The analysis was applied on the time-resolved DRIFT spectra of Ag/ZrO_2 upon exposure to **a**, CO_2 + H_2 + CH_3OH (the first half) vs Ar + CH_3OH (the second half period), and **b**, CO_2 + H_2 + CH_3OH (the first half) vs CO_2 + H_2 + Ar (the second half period) at 230 °C and 5 bar (total pressure).

To elucidate further how the reactive surface species interplay, methanol is discontinuously fed by alternatingly exposing the catalyst to the gas flows of CO_2 + H_2 + CH_3OH and CO_2 + H_2 and the reaction monitored under operando conditions (**Figure 4.10b**, **Appendix B**, **Figure B.6**). In this case, MF concentration follows a similar profile of gaseous and adsorbed CH_3OH but inversely with that of adsorbed formates on Ag. After switching from CO_2 + H_2 + CH_3OH (the first half period of **Figure 4.10b**) to CO_2 + H_2 (the second half period), adsorbed methanol is present on the catalyst at a high concentration whereas both formates on Ag and ZrO_2 gradually increase with time. Despite the presence of both adsorbed methanol and formates on the catalyst, MF formation drops progressively. This further supports the fact that the reaction between formates and CH_3OH only takes place at specific sites/location (**Figure 4.11b-c**). Since MF formation apparently responds to the concentrations of gaseous methanol and the adsorbed methanol, the adsorption and diffusion of CH_3OH on the catalyst surface are likely rate-limiting. This may be due not only to the strong binding of CH_3OH on ZrO_2[39-40] but also to the surface interaction of pre-adsorbed formates, competing with the adsorption and diffusion of CH_3OH over ZrO_2.

Chapter 4
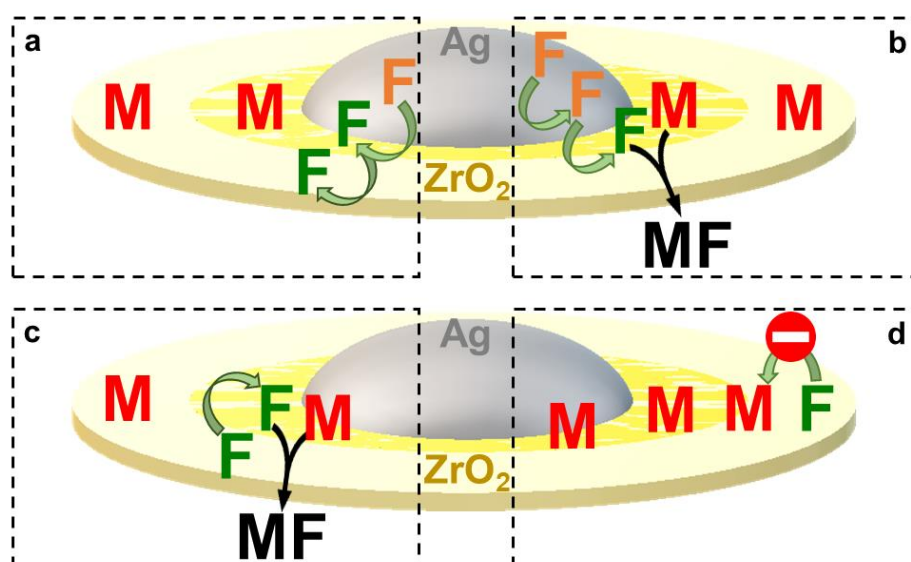
Figure 4.11. Suggested mechanisms for the formation of MF from CO_2, H_2 and CH_3OH over Ag/ZrO_2 catalyst by the *operando* studies shown in **Figure 4.10**. Surface species: methanol (M) and formates (F).

The abrupt and then gradual formation of formates on ZrO_2 in the absence of CH_3OH (**Figure 4.10b**, the second half period) evidences the initially enhanced spillover of formates from Ag to ZrO_2, leading to enhanced MF formation, followed by a gradual spillover competing for the adsorption site with surface $CH_3O(H)$. In contrast to the Ag/SiO_2 case, the MF formation rate decreases more gradually, most likely due to the presence of stable formates over support which were not observed over SiO_2.[15] The adsorbed CH_3OH can therefore be depleted in the vicinity of Ag through MF formation (**Figure 4.11b-c**) or through formates spillover (**Figure 4.11a**), which is why the access of CH_3OH to the perimeter sites affects more critically the MF formation rate. Another interesting observation is that the MF yield is not much influenced by the particle size of Ag according to the catalytic results (**Figure 4.4**). This implies that the rate-determining step under the steady-state condition is not the reaction at the perimeter sites. Rather it could be adsorption of reactants and/or diffusion of methanol/formates on the support surface thus determining the catalytic activity.

4.3 Conclusion

It is shown that silver nanoparticles supported on ZrO_2 and Al_2O_3 are highly active for the continuous and catalytic formation of methyl formate from CO_2, H_2 and CH_3OH. MF yield can reach a value of up to 16.2 g_{MF} g_{Ag} h^{-1} over Ag/ZrO_2 at 180 ºC without the detection of side-products. Transient *operando* vibrational spectroscopy studies together with multivariate spectral analysis show that Al_2O_3 and ZrO_2, two Lewis acidic supports, promote the spillover of formates from Ag to the support in contrast to SiO_2; these formates can then react with

UNIVERSITAT ROVIRA I VIRGILI
CONTINUOUS HYDROGENATION OF CARBON DIOXIDE TO FORMATES AND FORMIC ACID OVER HETEROGENEOUS CATALYSTS
Juan José Corral Pérez

Support effect and mechanistic insights

adsorbed CH_3OH at the perimeter sites to yield MF. The rate-determining step under steady-state condition is likely the adsorption of reactants and/or diffusion of methanol/formates on the support surface rather than reaction at the perimeter sites. The current catalytic system presents a great step forward from the conventional homogeneous CO_2 reduction catalysts since MF can be formed in the gas phase without the addition of basic additives, thus avoiding post-synthetic work-up of the formate salts generated in the homogeneously catalysed processes.

Chapter 4

Bibliography

1. Lee, J. S.; Kim, J. C.; Kim, Y. G., *Appl. Catal.* **1990,** *57* (1), 1-30.
2. Reymond, H.; Corral-Pérez, J. J.; Urakawa, A.; Rudolf von Rohr, P., *React. Chem. Eng.* **2018**.
3. Modesti, M.; Adriani, V.; Simioni, F., *Polym. Eng. Sci.* **2000,** *40* (9), 2046-2057.
4. Song, C.; Scharf, M. E., *Pestic. Biochem. Phys.* **2008,** *92* (2), 77-82.
5. Rong, L.; Xu, Z.; Sun, J.; Guo, G., *J. Energy Chem.* **2018,** *27* (1), 238-242.
6. Sodesawa, T., *React. Kinet. Catal. L.* **1986,** *32* (1), 63-69.
7. Tonner, S. P.; Trimm, D. L.; Wainwright, M. S.; Cant, N. W., *Ind. Eng. Chem. Prod. RD* **1984,** *23* (3), 384-388.
8. Wittstock, A.; Zielasek, V.; Biener, J.; Friend, C. M.; Bäumer, M., *Science* **2010,** *327* (5963), 319-322.
9. Zhang, Q.; Li, Y.; Zhang, L.; Chen, L.; Liu, Y.; Lu, Y., *Green Chem.* **2014,** *16* (6), 2992-2996.
10. Wu, C. Y.; Zhang, Z. F.; Zhu, Q. G.; Han, H. L.; Yang, Y. Y.; Han, B. X., *Green Chem.* **2015,** *17* (3), 1467-1472.
11. Yu, K. M. K.; Yeung, C. M. Y.; Tsang, S. C., *J. Am. Chem. Soc.* **2007,** *129* (20), 6360–6361.
12. Yu, K. M. K.; Tsang, S. C., *Catal. Lett.* **2011,** *141* (2), 259-265.
13. Álvarez, A.; Bansode, A.; Urakawa, A.; Bavykina, A. V.; Wezendonk, T. A.; Makkee, M.; Gascon, J.; Kapteijn, F., *Chem. Rev.* **2017,** *117* (14), 9804-9838.
14. Alvarez, A.; Borges, M.; Jose Corral-Perez, J.; Giner Olcina, J.; Hu, L.; Cornu, D.; Huang, R.; Stoian, D.; Urakawa, A., *Chemphyschem* **2017,** *18* (22), 3135-3141.
15. Corral-Pérez, J. J.; Bansode, A.; Praveen, C. S.; Kokalj, A.; Reymond, H.; Comas-Vives, A.; VandeVondele, J.; Copéret, C.; von Rohr, P. R.; Urakawa, A., *J. Am. Chem. Soc.* **2018,** *140* (42), 13884-13891.
16. Moroz, I. B.; Larmier, K.; Liao, W.-C.; Copéret, C., *J. Phys. Chem. C* **2018,** *122* (20), 10871-10882.
17. Pokrovski, K.; Jung, K. T.; Bell, A. T., *Langmuir* **2001,** *17* (14), 4297-4303.
18. Lam, E.; Larmier, K.; Wolf, P.; Tada, S.; Safonova, O. V.; Copéret, C., *J. Am. Chem. Soc.* **2018,** *140* (33), 10530-10535.
19. Larmier, K.; Liao, W.-C.; Tada, S.; Lam, E.; Verel, R.; Bansode, A.; Urakawa, A.; Comas-Vives, A.; Copéret, C., *Angew. Chem. Int. Edit.* **2017,** *56* (9), 2318-2323.
20. Filonenko, G. A.; Vrijburg, W. L.; Hensen, E. J. M.; Pidko, E. A., *J. Catal.* **2016,** *343*, 97-105.
21. Copéret, C.; Comas-Vives, A.; Conley, M. P.; Estes, D. P.; Fedorov, A.; Mougel, V.; Nagae, H.; Núñez-Zarur, F.; Zhizhko, P. A., *Chem. Rev.* **2016,** *116* (2), 323-421.
22. Roso, S.; Degler, D.; Llobet, E.; Barsan, N.; Urakawa, A., *ACS Sensors* **2017,** *2* (9), 1272-1277.
23. Borges Ordoño, M.; Urakawa, A., *J. Phys. Chem. C* **2019**.
24. Meyer, E. M.; Gambarotta, S.; Floriani, C.; Chiesi-Villa, A.; Guastini, C., *Organometallics* **1989,** *8* (4), 1067-1079.
25. Vilé, G.; Baudouin, D.; Remediakis, I. N.; Copéret, C.; López, N.; Pérez-Ramírez, J., *ChemCatChem* **2013,** *5* (12), 3750-3759.
26. Oakton, E.; Vilé, G.; S. Levine, D.; Zocher, E.; Baudouin, D.; Pérez-Ramírez, J.; Copéret, C., *Dalton T.* **2014,** *43* (40), 15138-15142.
27. Fedorov, A.; Liu, H.-J.; Lo, H.-K.; Copéret, C., *J. Am. Chem. Soc.* **2016,** *138* (50), 16502-16507.
28. Siddiqi, G.; Mougel, V.; Copéret, C., *Inorg. Chem.* **2016,** *55* (8), 4026-4033.
29. Ma, F.-Q.; Lu, D.-S.; Guo, Z.-Y., *J. Mol. Catal.* **1993,** *78* (3), 309-325.
30. Lam, E.; Corral-Pérez, J. J.; Larmier, K.; Noh, G.; Wolf, P.; Comas-Vives, A.; Urakawa, A.; Copéret, C., *Angew. Chem. Int. Edit. submitted*.

UNIVERSITAT ROVIRA I VIRGILI
CONTINUOUS HYDROGENATION OF CARBON DIOXIDE TO FORMATES AND FORMIC ACID OVER HETEROGENEOUS CATALYSTS
Juan José Corral Pérez

Support effect and mechanistic insights

31. Gokhale, A. A.; Dumesic, J. A.; Mavrikakis, M., *J. Am. Chem. Soc.* **2008,** *130* (4), 1402-1414.

32. Voronov, A.; Urakawa, A.; Beek, W. v.; Tsakoumis, N. E.; Emerich, H.; Rønning, M., *Anal. Chim. Acta* **2014,** *840*, 20-27.

33. Bañares, M. A., *Catal. Today* **2005,** *100* (1), 71-77.

34. Weckhuysen, B. M., *Phys. Chem. Chem. Phys.* **2003,** *5* (20), 4351-4360.

35. Urakawa, A., *Curr. Opin. Chem. Eng.* **2016,** *12*, 31-36.

36. Korhonen, S. T.; Calatayud, M.; Krause, A. O. I., *J. Phys. Chem. C* **2008,** *112* (41), 16096-16102.

37. Kouva, S.; Andersin, J.; Honkala, K.; Lehtonen, J.; Lefferts, L.; Kanervo, J., *Phys. Chem. Chem. Phys.* **2014,** *16* (38), 20650-20664.

38. Noh, G.; Lam, E.; Alfke, J. L.; Larmier, K.; Searles, K.; Wolf, P.; Copéret, C., *ChemSusChem* **2019,** *12* (5), 968-972.

39. Korhonen, S. T.; Bañares, M. A.; Fierro, J. L. G.; Krause, A. O. I., *Catal. Today* **2007,** *126* (1), 235-247.

40. Lam, E.; Larmier, K.; Tada, S.; Wolf, P.; Safonova, O. V.; Copéret, C., *Chin. J. Catal.* **2019,** (in press).

Chapter 4

UNIVERSITAT ROVIRA I VIRGILI
CONTINUOUS HYDROGENATION OF CARBON DIOXIDE TO FORMATES AND FORMIC ACID OVER HETEROGENEOUS CATALYSTS
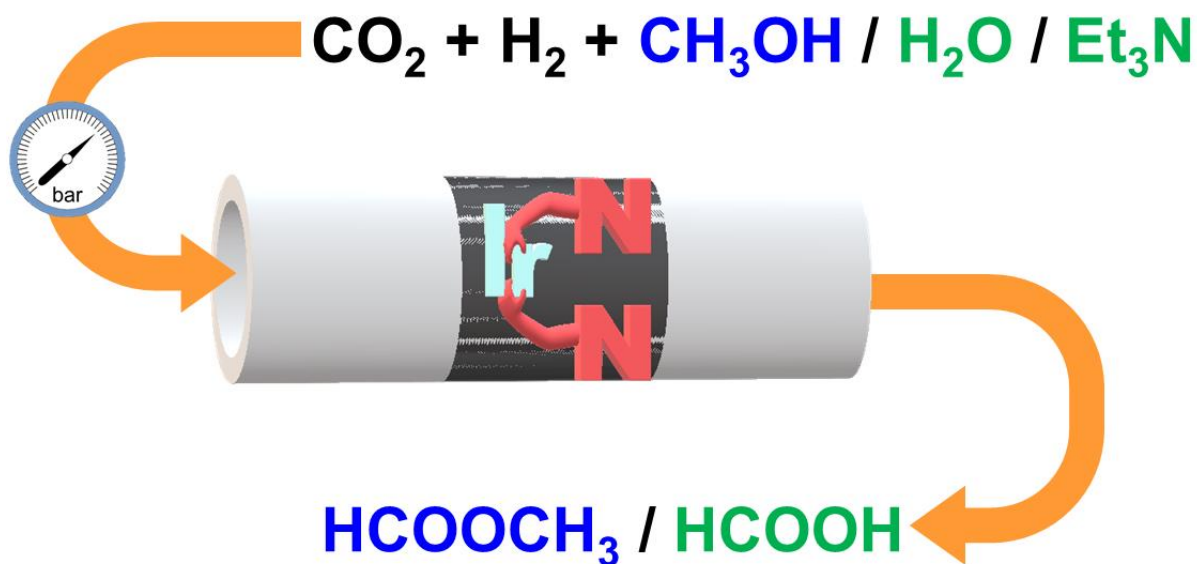Juan José Corral Pérez

82

5

Exploring the potential of Covalent Triazine Frameworks

Continuous hydrogenation of carbon dioxide to methyl formate and formic acid by a molecular iridium complex stably heterogenized on a covalent triazine framework

Chapter 5

5.1 Introduction

Immobilizing molecular metal complexes on solid supports is gaining increasing interest in the field of catalysis. This is because such strategy allows to benefit from the advantages of both homogeneous and heterogeneous catalysts. In other words, the well-defined active sites provided by the molecular complexes can enable high activity and selectivity to desired product, while solid support facilitates catalyst handling and separation from reactant/product fluids, thus making it feasible to operate the reaction under continuous flow. In addition to these benefits, the additional difficulty in establishing relationships between structure and activity in heterogeneous catalysis can be overcome.[1-2]

The material and structure of support are of critical importance because it must provide moieties where the molecular species can be stably coordinated, while resisting reaction conditions which are often harsh due to high temperature and/or pressure. The use of nanoporous polymers as support has attracted increasing attention since they meet all the above-mentioned requirements. In addition, these polymeric materials exhibit a tuneable porosity, high specific surface areas up to several thousand $m^2 g^{-1}$ and adjustable skeletons.[3-5] Among such polymers, covalent triazine frameworks (CTFs) are increasingly employed to successfully immobilize molecular complexes due to the numerous nitrogen moieties available in their structure.[5] Furthermore, a wide range of highly stable CTFs can be synthesised by varying the starting monomer, i.e. nitrile,[6-7] thus providing greater versatility in catalysis applications.

Currently, there is an increasing number of studies that prove the catalytic activity of iridium molecular complexes immobilised on different CTFs in CO_2 hydrogenation to formate/formic acid.[8-10] This reaction over heterogeneous catalysts supposes one of the remaining challenges in CO_2 valorisation.[11] The greatest hindrance to the development of heterogeneous catalysts arises from serious thermodynamic limitations of this reaction. It must not be forgotten that the conversion of gaseous carbon dioxide and hydrogen into liquid formic acid is strongly endergonic due to the unfavourable entropic contribution. Although a lot of effort has been deployed to catalyse homogeneously this reaction employing mainly Ir- and Ru-based complexes,[12-14] the recovery and recycling of expensive and soluble catalysts increase the operating costs and hamper its commercial viability.[15]

Hence, heterogenized molecular catalysts may open new avenues in the CO_2 hydrogenation to formate/formic acid. However, significant challenges regarding stability, elucidation of intermediate species and accessibility of the active sites remain to be addressed before the solid molecular catalysts can be a viable alternative in industry.[5] In literature, after reaction, metal leaching is not always studied and the coordination environment around Ir is

UNIVERSITAT ROVIRA I VIRGILI
CONTINUOUS HYDROGENATION OF CARBON DIOXIDE TO FORMATES AND FORMIC ACID OVER HETEROGENEOUS CATALYSTS
Juan José Corral Pérez

Exploring the potential of Covalent Triazine Frameworks

not deeply investigated. Some iridium leaching has been reported while its coordination environment remains the same after reaction.[9, 16] Despite the successful heterogenization of these materials, the catalytic tests are performed under batch conditions, thus failing to discern if the catalytic activity is due to either the leached or heterogenized complex. The use of solvents and basic additives to shift the thermodynamic equilibrium towards formate/formic acid[11] may have hindered its continuous operation.

In this work, a CTF based on 2,6-dicyanopyridine is used to immobilise [IrCp*Cl$_2$]$_2$ (Cp* = η^5-pentamethylcyclopentadienyl). This CTF offers more bipyridine moieties per CTF ring than the reported ones (based on 2-bromo-5-cyanopyridine or 5,5′-dicyano-2,2′-bipyridine) to coordinate the Ir complex.[9-10] This may help to prevent Ir leaching under continuous operation due to the highly available coordination sites throughout the framework. The catalyst is characterised before and after reaction by means of ATR-IR, N$_2$ adsorption and desorption, XRD, ICP-OES and XAS measurements. The catalytic activity of Ir-CTF is tested in the CO$_2$ hydrogenation to methyl formate under continuous operation not only to obtain an increased space-time-yield but also to avoid equilibrium limitations. The detection of CO as side product at low temperatures led to cofeed water or triethylamine rather than methanol to check if formic acid could be continuously yielded. Furthermore, transient *in situ* diffuse reflectance infrared Fourier transform spectroscopy (DRIFTS) studies in combination with multivariate spectral analysis are performed to elucidate the surface species formed over the CTF and Ir-CTF materials.

5.2 Experimental

5.2.1 Materials

2,6-dicyanopyridine (97%, Sigma Aldrich), pentamethylcyclopentadienyl iridium dichloride dimer (Alfa Aesar) and anhydrous ZnCl$_2$ (99.95, Alfa Aesar) were kept in a glovebox and used as received. Methanol (>99%, Sigma Aldrich) and triethylamine (>99%, Sigma Aldrich) were used as received. Liquid CO$_2$ (>99.9993%) and 10% Ar in H$_2$ (>99.999% for Ar or H$_2$, prior to mixing) were purchased from Abelló Linde.

5.2.2 Materials characterisation

Fourier transform infrared (FTIR) measurements of the samples before and after the reaction were performed on a Bruker Alpha spectrometer equipped with a DTGS detector at 4 cm^{-1} resolution in an attenuated total reflection (ATR) sampling configuration with a diamond internal reflection element.

The metal content was quantified by inductively coupled plasma optical emission spectrometry (ICP-OES). 10 mg of sample were digested in 2 mL of nitric acid (70 wt% acid)

Chapter 5

at 60 ºC for 2 days. Then, 1 mL of the resulting solution was diluted with Milli-Q water (1 L total volume) and analysed by using a PerkinElmer ICP 400 spectrometer.

Brunauer-Emmett-Teller (BET) surface area and pore size distribution of the materials were determined by N_2 physisorption experiments using Quantachrome Instruments, AUTOSORB iQ. Prior to the measurements, the material (50 mg) was outgassed at 150 °C and 4 mbar to clean the sample surface and pores.

Powder X-ray diffraction (PXRD) measurements were performed in a Bruker D8 Advance power diffractometer with a vertical 2theta-theta goniometer in transmission configuration with Cu Kα radiation (λ = 1.5406 Å).

Raman measurements were carried out on a BWTEK dispersive i-Raman portable spectrometer equipped with a 785 nm excitation laser and an external back-thinned CCD array detector (Exemplar Plus, BWTEK).

X-ray absorption spectroscopy (XAS) experiments were performed at the Swiss-Norwegian Beamlines (SNBL, BM31) of the European Synchrotron Radiation Facility (ESRF), in Grenoble, France. *Ex situ* measurements were carried out on samples placed in a capillary tube in transmission mode. All data were collected using Si (111) monochromator system and ionization chambers for normalization of the beam, sample data collection, and energy calibration by using a silver foil (fillings for ionization chambers at 20% absorption for I_0 and 80% absorption for I_t and I_{ref}). Scans were collected from 11.1 to 12.4 keV and the measurement duration of one XAS spectrum was about 9 min. 2 scans were acquired and merged for every sample to improve signal to noise ratio. The XAS data were processed using the IFEFFIT software package (Athena and Artemis)[17] to perform background subtraction, normalization, energy alignment, and extraction of χ(k) oscillatory functions. EXAFS oscillations were extracted by fitting a cubic spline function through the post-edge region. The k^2-weighted EXAFS oscillation was Fourier transformed without phase shift correction.

5.2.3 DRIFTS measurements

A custom-made high-pressure reaction cell, with a cylindrical cavity (3 mm in diameter and 3 mm vertical length) to place the catalyst powder, mounted in a Praying Mantis (Harrick) diffuse reflectance infrared Fourier transform spectroscopy (DRIFTS) optical system was used. The spectra were collected using a Bruker Vertex70v FT-IR spectrometer equipped with a liquid-nitrogen-cooled MCT detector at 4 cm^{-1} resolution. Details of the setup and method of *in situ* transient measurements are provided in **Chapter 2, Section 2.4.**

UNIVERSITAT ROVIRA I VIRGILI
CONTINUOUS HYDROGENATION OF CARBON DIOXIDE TO FORMATES AND FORMIC ACID OVER HETEROGENEOUS CATALYSTS
Juan José Corral Pérez

Exploring the potential of Covalent Triazine Frameworks

5.2.4 Multivariate spectral analysis

Multivariate spectral analysis was performed by means of multivariate curve resolution (MCR). MCR is a chemometric method used for better data processing and deconvolution of the complex spectra down to individual components based on kinetic resolution. It delivers the pure response profiles of the chemical species of an unresolved mixture when no previous information is available about the nature and composition of these mixtures. More details of the method and software used are specified in **Chapter 2, Section 2.5**

5.2.5 Reactor setup

Catalytic tests were performed in a continuous flow fixed-bed microreaction system. Details of the setup and the method of product analysis are described in **Chapter 2, Section 2.3.** In a typical experiment, 100 mg of catalyst (pelletized, crushed and sieved to 100-300 μm particle size) was loaded in a tubular reactor (ID: 2.95 mm, OD: 6.35 mm). Then, the reaction mixture (CO_2:H_2:CH_3OH = 4:4:1 molar ratio) was introduced into the reactor at a flow rate of 24 mL min^{-1} at 300 bar. The pressure in the reactor was regulated by an automatic back-pressure regulator. Before performing the quantitative analysis, the catalyst was under continuous flow conditions for 48h at 80 ºC. In this way, the possible catalyst leaching or even unreacted precursor that was not removed by the washing procedure would not have any effect on the catalytic performance. Product quantification was performed by an online gas chromatograph during the steady state operation of the reaction at specified temperature (100-180 °C) and pressure (300 bar). Ar was used as an internal standard for gas chromatography analysis and product selectivity was calculated taking only carbon-containing products into account.

When water and triethylamine were cofeed into the reactor, the outlet stream of the back-pressure regulator was passed to a U-shaped glass condenser placed in an ice bath. The gaseous products that were not condensed in the cold trap were continuously analysed by an online gas chromatograph. The condensed liquid was collected after 3 hours of reaction at a specified temperature and stored in the freezer until its analysis. The liquid products were analysed by using a high performance liquid chromatography (HPLC) system (Agilent 1200 series) equipped with a G1315D diode-array detector (DAD) and a Rezex™ ROA-Organic Acid H+ (8%) column (Phenomenex, 300 x 7.8 mm). An aqueous solution of H_2SO_4 (5mM, 0.5 mL min^{-1}) served as the eluent. The amounts of formic acid were quantified by using a calibration curve obtained by measuring standard samples of known concentration.

Chapter 5

5.3 Results and Discussion

5.3.1 Synthesis and characterization of CTF and Ir-CTF

A CTF based on 2,6-dicyanopyridine (DCP) was synthesised under ionothermal conditions as reported in literature (**Figure 5.1a**).[18,19] As depicted in **Figure 5.1b**, the dinitrile-monomer DCP (1.00 g, 7.74 mmol) and an excess of zinc chloride (5.28 g, 38.7 mmol) were ground to a fine powder and added to a glass ampoule (2 cm in diameter and ca. 4 cm in length) within a glovebox. $ZnCl_2$ served as catalyst and reaction medium in the trimerization reaction and subsequent oligomerization. A ball valve was connected to the ampoule to avoid the presence of air when removing from the glovebox. The ampoule was evacuated, flame-sealed and heated to 450 °C at a rate of 1 °C min^{-1} for 48 h in a furnace. Once cooled to room temperature, the black solid was ground and stirred in water (250 mL) for 24 h, followed by filtration and washing with water (3 × 30 mL). The solid was subsequently stirred in 1 M hydrochloric acid (250 mL) and heated to reflux at 100 °C for 24 h. Afterwards, the product was isolated by filtration, washed with water (3 × 30 mL) and acetone (3 × 30 mL) successively and dried under vacuum at 150 °C for 24 h, affording a fine black powder.
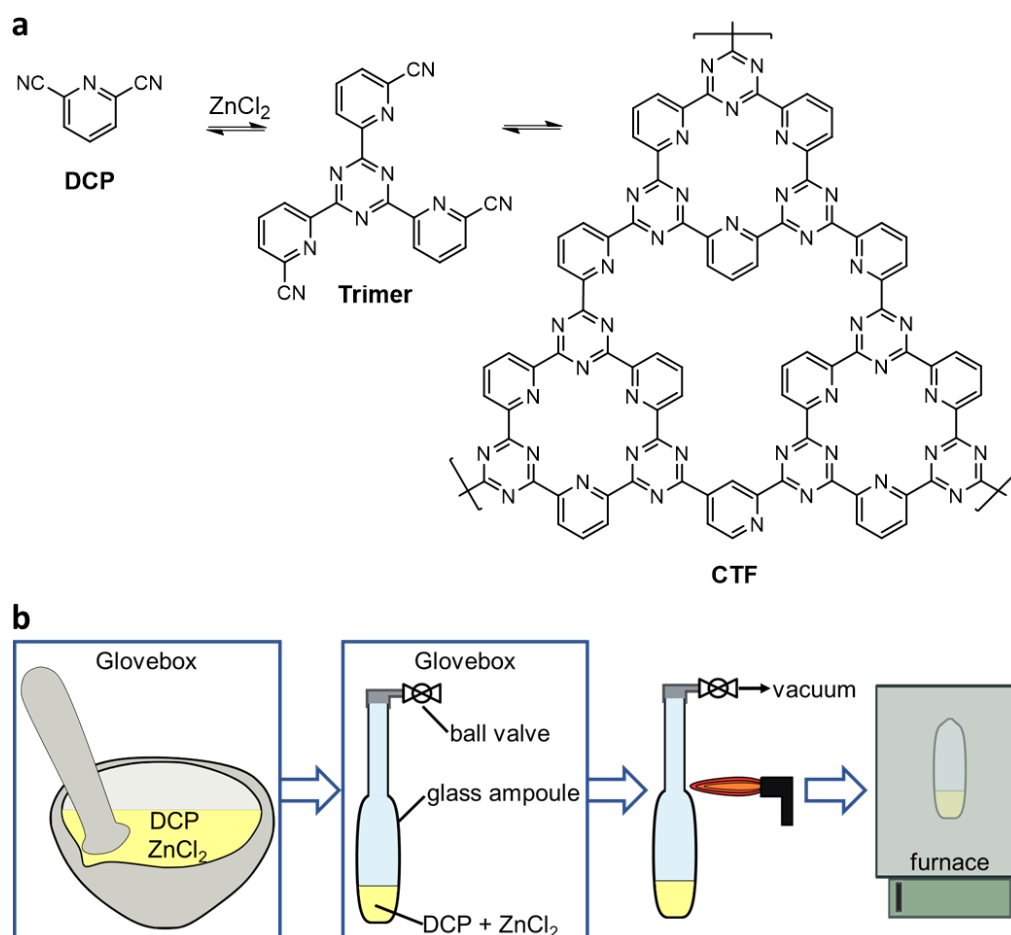

Figure 5.1. a, Idealised schematic formation of a CTF based on 2,6-dicyanopyridine (DCP). **b**, Schematic representation of the synthesis of a CTF in a glass ampoule.

The immobilization of the iridium complex on the solid CTF was performed as follows.[10] CTF (300 mg) was added to a two-necked round-bottomed flask equipped with a condenser and a stirrer bar, and the system was purged with nitrogen three times. $[IrCp^*Cl_2]_2$ (100 mg) was dissolved in degassed dichloromethane (40 mL) and added by a purged needle and syringe to the CTF. In case all the iridium is coordinated with the solid framework, a loading of 16 wt% Ir is expected. The reaction mixture was stirred under N_2 atmosphere and heated to reflux at 45 °C for 24 h. The solid was isolated by filtration, washed with methanol (3 × 30 mL) and acetone (3 × 30 mL) successively, and dried under vacuum at 120 °C for 24 h to ideally yield the solid molecular catalyst depicted in **Figure 5.2**. ICP-OES analysis revealed that the Ir loading of the material was 16.3 wt%.
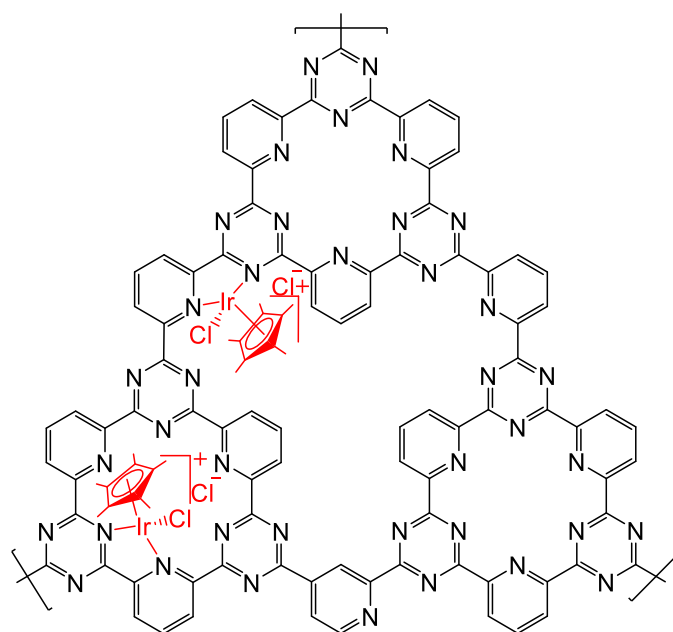

Figure 5.2. Structural representation of Ir-CTF.

The successful trimerization reaction of DCP to yield the desired CTF (**Figure 5.1a**) is confirmed by ATR-IR measurements (**Figure 5.3a**). In the ATR-IR spectrum of CTF, the absence of the nitrile stretching band at 2242 cm^{-1} indicates the complete conversion of the nitrile groups present in the starting monomer. Furthermore, the presence of bands at 1556 and 1224 cm^{-1} confirms the existence of C=N and C-N bonds in CTF.[9, 20] The IR features of CTF and Ir-CTF are virtually identical. Therefore, the functionalization of CTF with Ir does not induce significant changes in the structure of the framework. This is also observed in Raman spectroscopy (**Figure 5.3b**). The Raman G and D bands observed at 1580 and 1356 cm^{-1}, respectively, demonstrates that both CTF and Ir-CTF possess two-dimensional-honeycomb structure constructed from triazine and pyridine rings.[21] This is further confirmed by powder X-ray diffraction (XRD) analysis (**Figure 5.3c**). The broad peak at ca. 25° is characteristic of the graphitic layers with interlayer distance of ~3.4 Å.[7, 20-23] Regarding to the crystallinity of CTF,

Chapter 5

the XRD pattern indicates a predominantly amorphous structure. After the immobilization of the Ir complex, a diffraction peak at ca. 12° appears most likely due to the presence of chlorides in the framework.
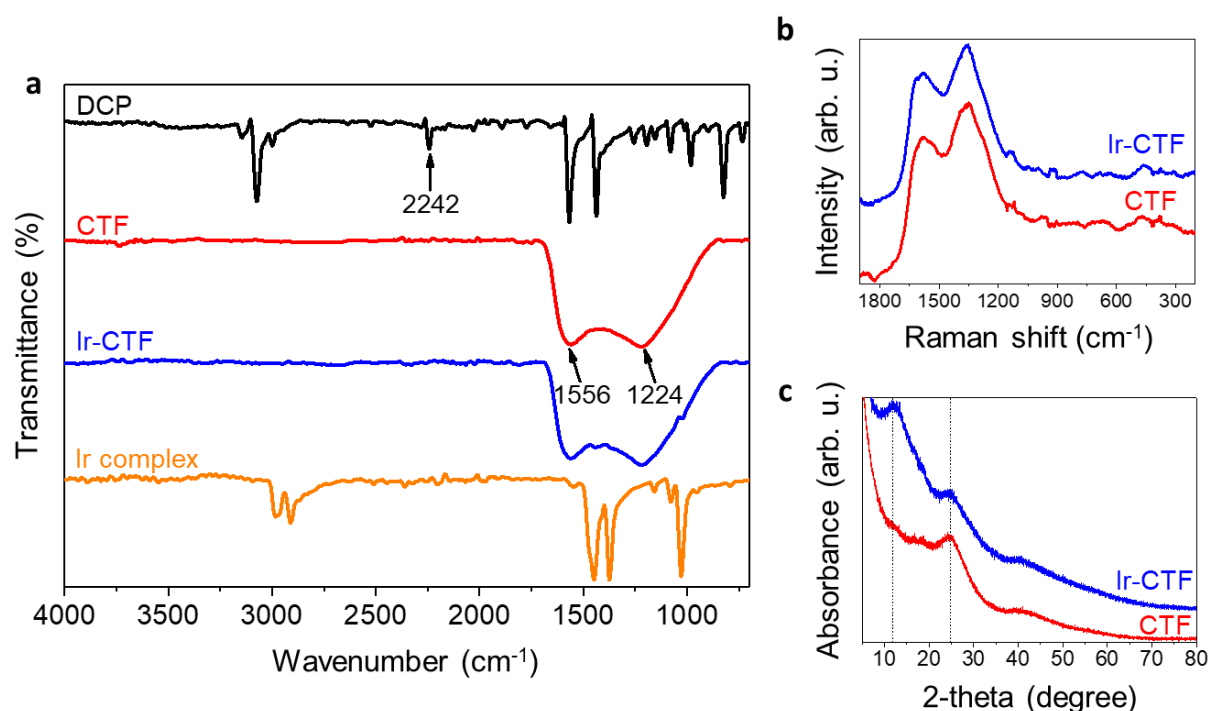

Figure 5.3. a, ATR-IR spectra of DCP (2,6-dicyanopyridine), CTF, Ir-CTF and iridium complex ([IrCp*Cl$_2$]$_2$). **b**, Raman spectra of CTF and Ir-CTF. **c**, PXRD patterns of CTF and Ir-CTF.

After having studied the structure of CTF and Ir-CTF materials, the porosity of these frameworks is investigated by means of nitrogen adsorption and desorption isotherms. As shown in **Figure 5.4a**, N$_2$ adsorption on CTF results in a type I isotherm, thus indicating microporosity and a limited mesoporosity. Another information provided by the adsorption measurements is the BET surface area (S_{BET}), CTF has a S_{BET} of 734 m^2 g^{-1}. This value is consistent with the ones reported in literature for this kind of CTF based on DCP.[5] The t-plot analysis indicates that the area attributed to micropores accounts for 97% of the total surface area. HK (Horvath-Kawazoe) pore size distribution derived from the adsorption branch of the isotherm of CTF shows that a large fraction of micropores has diameters around 0.9 nm (**Figure 5.4b**). Interestingly, the S_{BET} of CTF drastically decreases to 10 m^2 g^{-1} when functionalised with the Ir complex. Such decrease was also reported for a CTF based on 5,5′-dicyano-2,2′-bipyridine when the Ir loading is increased up to 10.6 wt%.[16] Furthermore, the N$_2$ adsorption and desorption isotherms of Ir-CTF are characteristic of a mesoporous material. Therefore, this change indicates that the Ir molecular complex and/or chlorides are largely occupying the pores of the CTF. This is further confirmed by the decrease in the total pore volume from 0.33 (CTF) to 0.016 (Ir-CTF) cm^3 g^{-1}. Consequently, the pore diameter of Ir-CTF

Exploring the potential of Covalent Triazine Frameworks

is mainly between 3 and 7.5 nm (mesoporous range), as estimated by the BJH (Barrett-Joyner-Halenda) pore size distribution derived from the desorption branch of the isotherm of Ir-CTF (**Figure 5.4c**).
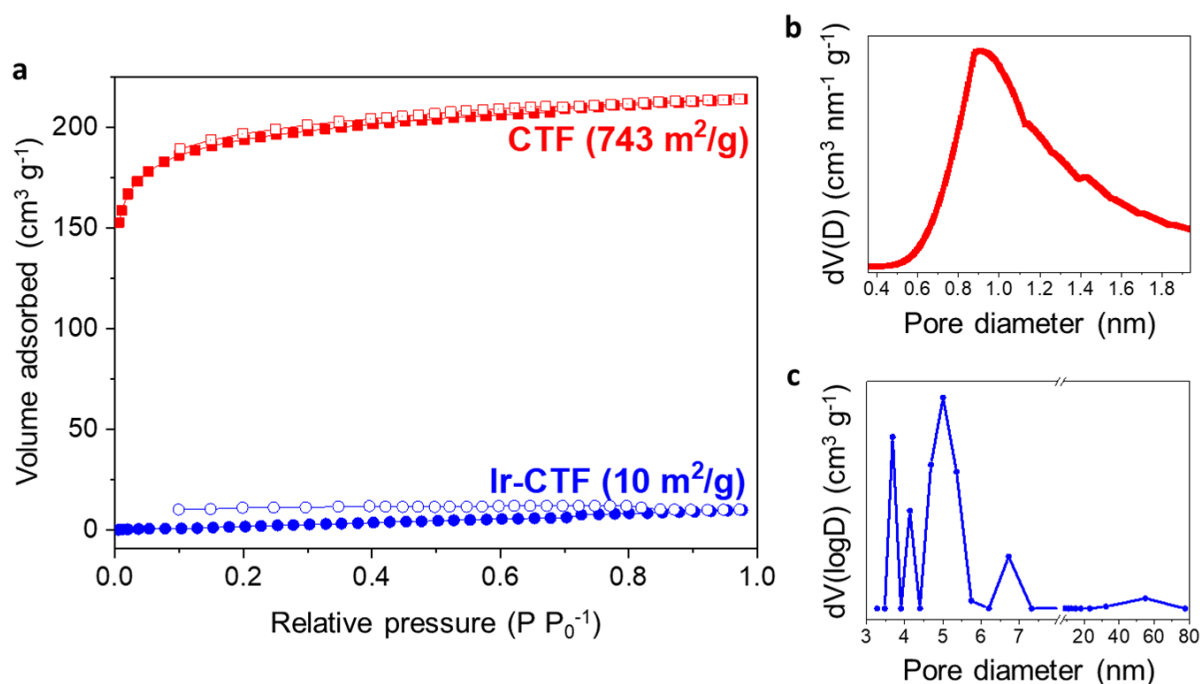
Figure 5.4. a, N_2 adsorption (open symbols) and desorption (filled symbols) isotherms at 77 K of CTF and Ir-CTF. BET surface area is shown in parenthesis. **b**, HK (Horvath-Kawazoe) pore size distribution derived from the adsorption branch of the isotherm of CTF. **c**, BJH (Barrett, Joyner, and Halenda) pore size distribution derived from the desorption branch of the isotherm of Ir-CTF.

Proving that Ir complex is coordinated with the numerous bipyridine moieties available in the solid CTF is required to confirm its heterogenization. Techniques such as infrared[23] and EDX[24] have been used to detect the presence of the metal complex on the CTF, thus suggesting its coordination. In literature, X-ray photoelectron spectroscopy (XPS) has been widely employed to study the chemical state of the metal centre, carbon and/or nitrogen. [9-10, 22, 25] However, deconvolution of XPS spectra might add significant uncertainty to the data.[26] In order to unambiguously determine the molecular structure of Ir-CTF, extended X-ray absorption fine structure (EXAFS) analysis of the Ir L_3 edge is performed in this study (**Figure 5.5**). According to the Fourier transforms (FT) of k^2-weighted EXAFS of the references $IrCl_3$ and Ir foil, peaks at 1.90 and 2.55 Å can be assigned to Ir-Cl and Ir-Ir bonds, respectively.[27-28] This suggests that the peak observed at 1.76 Å is attributed to Ir-N bonds. It is worth highlighting that the absence of the peak attributed to metallic Ir further corroborates the successful heterogenization of the Ir complex.

Chapter 5
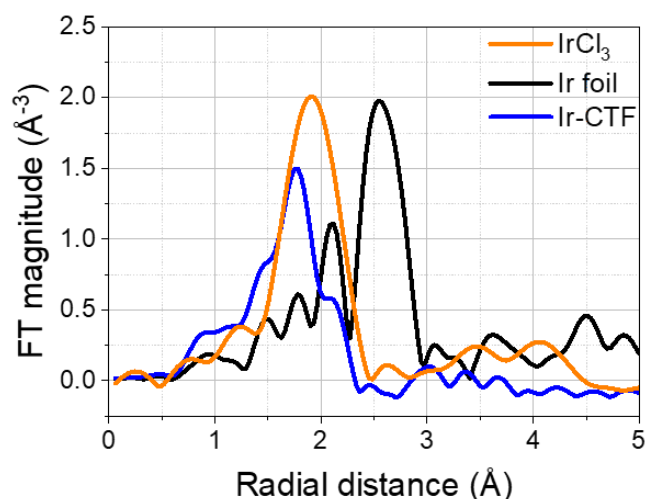
Figure 5.5. Fourier transforms (FT) of k^2-weighted EXAFS of $IrCl_3$, Ir foil and Ir-CTF.

5.3.2 Catalytic activity and characterization of the spent catalyst

The reactivity of both CTF and Ir-CTF is studied in the hydrogenation of CO_2 in the presence of methanol to yield MF at 300 bar. Temperatures above 180 ºC are not investigated to avoid the formation of Ir nanoparticles. As depicted in **Figure 5.6**, CTF is slightly active in the formation of MF and the temperature has virtually no effect on its yield. A blank test without methanol was performed (not shown) and no products were observed at all temperatures examined. Hence, methanol plays a role; it may be activated, i.e. through formation of methyl and methoxy species, over CTF to yield MF. The activation of methanol over CTF is confirmed by *in situ* DRIFTS measurements, that shows methoxy species stably adsorbed over bare CTF after methanol adsorption and subsequent desorption thorough removal of methanol from the cell (**Appendix C, Figure C.1**). As shown in **Figure 5.6**, Ir boosts the formation of MF, specially at 160 and 180 ºC. At these temperatures, carbon monoxide was observed as side-product without hindering the formation of MF.
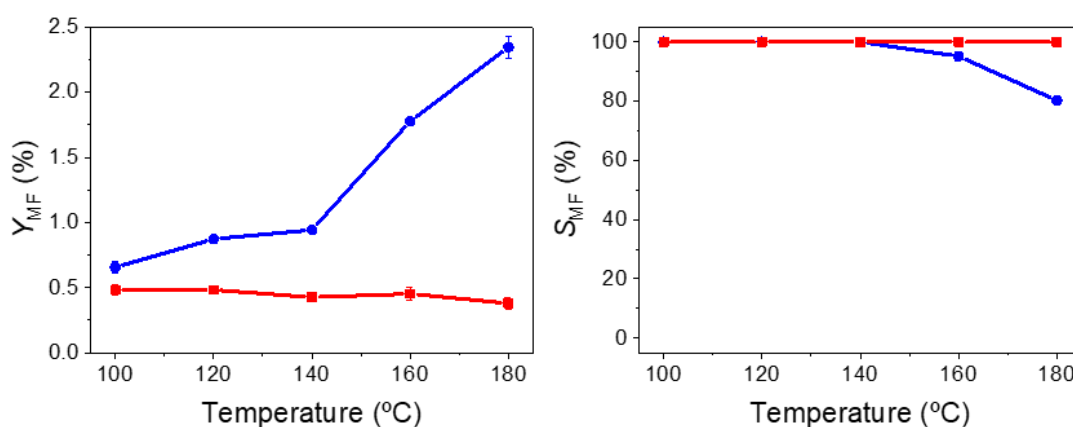
Figure 5.6. Effect of temperature on methyl formate yield (Y_{MF}) and selectivity to MF (S_{MF}) over CTF (red) and Ir-CTF (blue). Reaction conditions: $CO_2:H_2:CH_3OH = 4:4:1$ (molar ratio), 300 bar, GHSV = 14000 h^{-1}.

Exploring the potential of Covalent Triazine Frameworks

CO may come from reverse water–gas shift reaction (Reaction 5.1). However, it is unlikely that this endothermic reaction occurs at these relatively low temperatures to a great extent since according to Le Châtelier's principle, it is thermodynamically favoured at higher temperatures.[29] Furthermore, CO was not formed in the CO_2 hydrogenation in the absence of methanol (data not shown). Hence, CO formation is due to the presence of methanol in the reaction mixture. A possible explanation would be the decomposition of methyl formate to CO (Reaction 5.2), it seems quite feasible because the formation of MF and CO increased simultaneously. Another plausible explanation would be the formation of formic acid via CO_2 hydrogenation (Reaction 5.3) and its further decomposition at high temperature via dehydration reaction (Reaction 5.4).

$$CO_2 + H_2 \rightleftarrows CO + H_2O \tag{5.1}$$

$$HCOOCH_3 \rightleftarrows CO + CH_3OH \tag{5.2}$$

$$CO_2 + H_2 \rightleftarrows HCOOH \tag{5.3}$$

$$HCOOH \rightleftarrows CO + H_2O \tag{5.4}$$

Furthermore, in order to demonstrate continuous formic acid synthesis over the Ir-CTF catalyst, water[26, 30] or triethylamine[11] is co-fed into the reactor instead of methanol to create thermodynamically favourable environment for formic acid formation (**Table 5.1**). At 100 ºC, formic acid is selectively formed and its weight time yield (WTY) is much higher in triethylamine than in water, as expected from the stronger molecular interaction between the base and formic acid. In contrast, at 180 ºC the WTY of formic acid is greater in water, likely because the dissociation of the adduct formed with the amine to formic acid occurs at such temperature.[15] Generally, the overall turnover frequency (TOF) is higher at 180 ºC (TOF_{total} of 7.33 and 8.94 in water and triethylamine, respectively) than at 100 ºC (TOF_{total} of 0.23 and 1.61, respectively), although undesired CO formation is prominent. On the other hand, when the reaction is performed in methanol, the WTY of MF is greatly enhanced at 180 ºC compared to at 100 ºC, while retaining high selectivity to MF (TOF_{MF} of 3.03). In this sense, MF is an interesting intermediate product to achieve fast reaction kinetics, which is favoured at higher temperature, to selectivity synthesise formic acid through hydrolysis of methyl formate.[31]

Chapter 5

Table 5.1. Effects of water and triethylamine cofeeding and temperature on the weight time yield (*WTY*) of FA, MF, and CO over Ir-CTF catalyst. In brackets, TOF values are shown. For these calculations, the amount of Ir stably present during the reaction was used. Reaction conditions: 300 bar, GHSV = 14000 h^{-1}.

Reactant mixture	Temperature (ºC)	*WTY*$_{FA}$ (mg FA g$_{Ir}^{-1}$ h^{-1})	*WTY*$_{MF}$ (mg MF g$_{Ir}^{-1}$ h^{-1})	*WTY*$_{CO}$ (mg CO g$_{Ir}^{-1}$ h^{-1})
CO_2 + H_2 + CH_3OH (4:4:1 molar ratio)	100	-	264.5 (0.85)	-
	180	-	944.4 (3.03)	199.8 (1.37)
CO_2 + H_2 + H_2O (4:4:1 molar ratio)	100	53.9 (0.23)	-	-
	180	44.7 (0.19)	-	1039.5 (7.14)
CO_2 + H_2 + Et_3N (4:4:1 molar ratio)	100	385.5 (1.61)	-	-
	180	5.3 (0.02)	-	1300.0 (8.92)

After the reaction, the Ir-CTF catalyst is fully characterised to gain information about its stability. Structural changes of the spent catalyst are not observed in the ATR-IR spectrum (**Appendix C, Figure C.2**). Looking at the PXRD pattern, the diffraction peak at ca. 12° disappears and this indicates some leaching of the complex during the reaction (**Appendix C, Figure C.3**). The BET surface area of the spent catalyst increases to 61 m^2 g^{-1} by releasing the pore of the CTF blocked by an excess of the Ir complex. Indeed, the Ir content of the catalyst after the reaction determined by ICP-OES decreases to 7.6 wt%, confirming a certain loss of Ir during the reaction. It is important to note that despite the metal leaching, almost half of the initially loaded Ir remains in the solid framework during the reaction under the flow conditions for ca. 96 h at 300 bar. The presented catalytic results are obtained when the catalytic activity is stabilised after more than 48 h of stabilisation under the flow of the reaction mixture. Therefore, we can safely conclude that the activity originates from the stably immobilized active Ir sites.

In order to study the changes in the electronic state and coordination environment of the Ir during the reaction, XAS measurements are performed at room temperature at Ir L$_3$ edge (**Figure 5.7 and 5.8**). Based on the absorption edge shifting towards higher energy and on the increasing white line intensity (**Figure 5.7**), the Ir in the spent catalysts has a more oxidic character compared to the fresh catalyst. This may be due to the presence of coordinating species on Ir during the reaction, or possible oxidation of the Ir-hydride active centre upon exposure to air. Both would serve as an indirect proof of the presence of a single-site Ir active center during the reaction. The EXAFS results also show that Ir is isolated within the CTF

UNIVERSITAT ROVIRA I VIRGILI
CONTINUOUS HYDROGENATION OF CARBON DIOXIDE TO FORMATES AND FORMIC ACID OVER HETEROGENEOUS CATALYSTS
Juan José Corral Pérez

Exploring the potential of Covalent Triazine Frameworks

matrix after the reaction based on the absence of the peak at 2.55 Å characteristic of Ir-Ir bonds (*vide supra*) (**Figure 5.8**). STEM and EDX analyses further confirm the homogeneous dispersion of Ir before and after the reaction (**Appendix C, Figure C.4**).
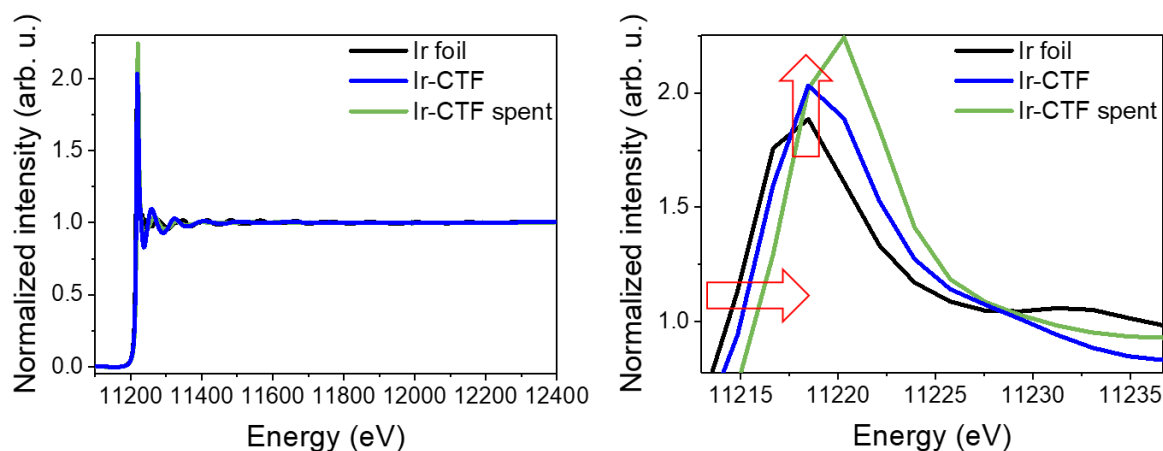
Figure 5.7. EXAFS spectra of the standard Ir foil and Ir-CTF before and after the reaction. X-ray absorption near edge structure (XANES) region is enlarged for clarity.
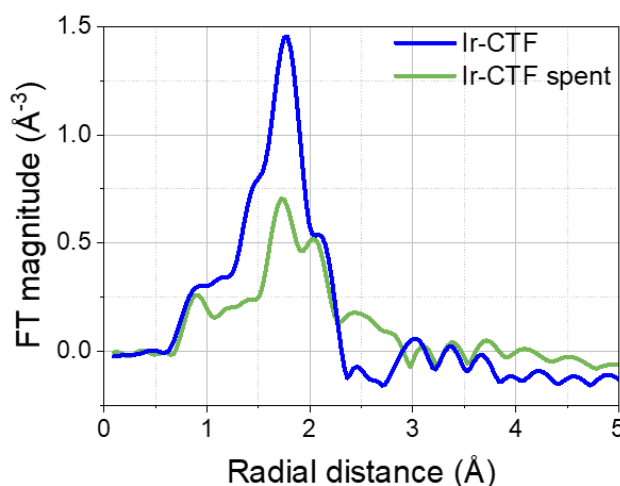

Figure 5.8. Fourier transforms (FT) of k^2-weighted EXAFS of Ir-CTF before and after the reaction.

5.3.3 Insights into the surface species formed over CTF and Ir-CTF

The catalytic activity of Ir-CTF towards methyl formate and formic acid confirms the formation of formates over the catalyst surface. However, to the best of our knowledge, there is no literature regarding the nature of the surface species formed over CTFs during CO_2 hydrogenation. In order to unravel the interaction of these frameworks with CO_2 and H_2, *in situ* DRIFTS measurements are performed with CTF and Ir-CTF in the mixture of CO_2 and H_2 at 140 ºC and 5 bar. As depicted in **Figure 5.9**, no notable spectroscopic features are observed for CTF. On the other hand, the presence of Ir induces the formation of surface species, as indicated by the bands in the region between 1750 and 2200 cm^{-1}. The absence of bands in

Chapter 5

the v(C–H) region (2600 – 3100 cm^{-1}) implies that bidentate formates are not present over Ir-CTF. The concentration of the surfaces species is drastically increased at higher pressures (**Figure 5.9**), as reported for bidentate formates over silica-supported silver nanoparticles.[32] Interestingly, for both CTF and Ir-CTF, the spectral region between 2250 and 2400 cm^{-1} shows the presence of distinct spectral features which overlap with but are obviously different from the bands of gaseous CO_2. This is attributed to the excellent CO_2 adsorption capabilities of the CTF through its numerous nitrogen sites present in the framework serving as Lewis basic sites.[20] However, very little is known about the interaction between CO_2 with these nitrogen-rich materials.
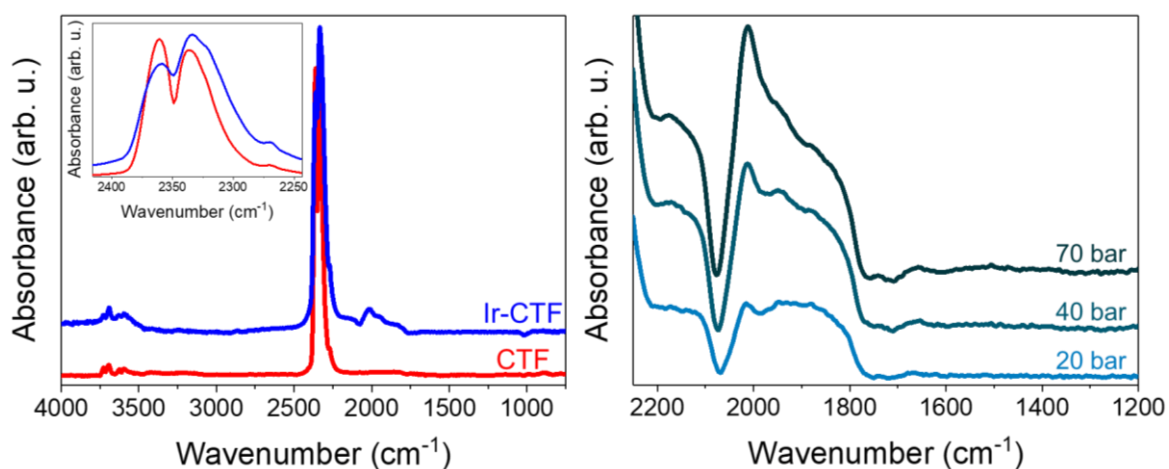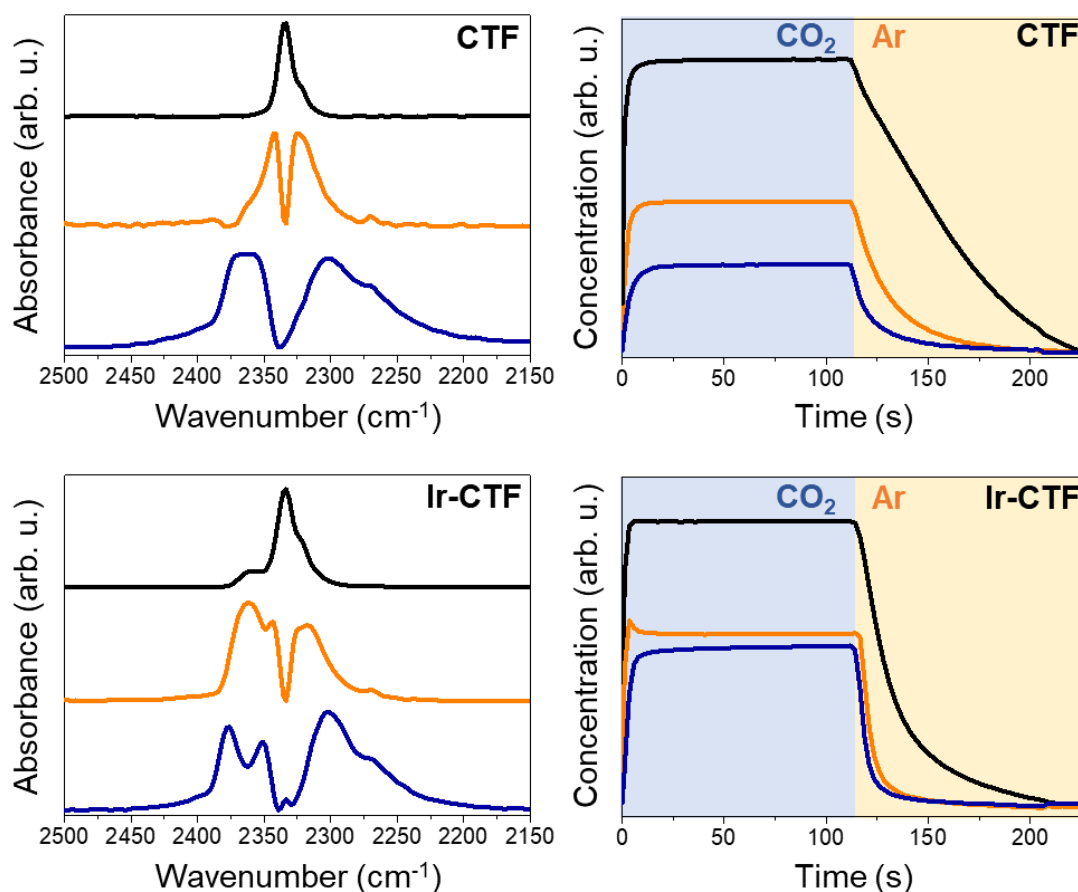

Figure 5.9. (left) *In situ* DRIFT spectra of CTF and Ir-CTF upon exposure to CO_2:H_2 = 1:1 (molar ratio) at 140 °C and 5 bar. Gaseous CO_2 region is enlarged for clarity. (right) *In situ* DRIFT of Ir-CTF upon exposure to CO_2:H_2 = 1:1 (molar ratio) at 140 °C and 20, 40 and 70 bar.

To gain more precise information about the nature of CO_2 interaction with the CTF and Ir-CTF, a transient *in situ* DRIFTS study was performed by alternatingly passing pure CO_2 and Ar over CTF and Ir-CTF at 140 ºC and 5 bar (**Appendix C, Figure C.5**). The results show that there are three kinetically separable species (**Figure 5.10**) over the CTF. The band at 2334 cm^{-1} (**Figure 5.10**, black) is assigned to asymmetric stretching of CO_2 adsorbed on CTF due to a clear restriction of molecular rotation. Its concentration profile indicates that the CO_2 is strongly adsorbed since it is slowly removed by Ar at the relatively high temperature. Although the spectral features of the other two species (**Figure 5.10**, orange and blue lines) somewhat resemble that of gaseous CO_2, their bands are highly distorted. In fact, the concentration profile of one species (**Figure 5.10**, blue line) follows the expected profile of CO_2 gas in the DRIFTS cell. The distortion of the spectral features may be caused by the strong electrostatic interactions between the nitrogen sites and the carbon atoms of the CO_2 molecules.[33] In case of Ir-CTF, the band of CO_2 adsorbed on CTF is also observed, but its removal is faster under Ar. This weaker interaction of CO_2 with the framework is likely caused by the decrease in the

surface area when Ir is present (**Figure 5.4**). For Ir-CTF, the two kinetically distinguishable spectra due to weakly interacting CO_2 with the material (**Figure 5.10**, orange and blue lines) show new features in comparison to the case of CTF. Hence, the Ir complex induces different interactions with CO_2,[34] but not very strongly as suggested by the concentration profiles of these species. Furthermore, a direct interaction of CO_2 with the Ir sites is implied by the emergence of a band at 2008 cm^{-1} under CO_2 over Ir-CTF (**Appendix C, Figure C.5**), which may be attributed to η^2-C,O mode of CO_2 on the metal.[35]


Figure 5.10. Components spectra and the corresponding concentration profiles obtained by multivariate spectral analysis applied on the time-resolved DRIFT spectra of CTF and Ir-CTF upon exposure to CO_2 (the first half period) and then to Ar (the second half period) at 140 ºC and 5 bar.

The activation of CO_2 over Ir may promote the formation of formates or formic acid, provided that hydride or atomic hydrogen is present on the metal. In order to prove the presence of hydride, a transient *in situ* DRIFTS study was performed by alternatingly passing pure H_2 and Ar over Ir-CTF at 140 ºC and 5 bar (**Figure 5.11**). Under H_2, bands at 1950, 2141 and 2264 cm^{-1} appear together and gradually. After switching to Ar, these bands progressively decrease, thus indicating a strong interaction and a relatively high stability in Ar. These bands are not observed over bare CTF (**Figure 5.11**). Hence, the spectroscopic features observed point to the existence of an interaction between Ir and H_2. According to literature, these bands can be

Chapter 5

assigned to Ir-H stretching vibrations.[36] The interaction between Ir and hydrogen is further confirmed by the slight shifts of these bands in a transient study using deuterium instead of hydrogen (**Figure 5.11**). This small shift may indicate dominant presence of a molecular H_2 complex (Ir-H_2 or Ir-D_2 – precursor of hydride) instead of hydride species. After having proved that CO_2 can be activated over Ir and CTF separately, while H_2 is exclusively activated on Ir to yield hydride/H_2 species, the formation of formate or formic acid over Ir-CTF via CO_2 hydrogenation is naturally explained. The strong interaction of CO_2 with CTF would be particularly beneficial to enhance the local concentration of CO_2 near Ir. In the *in situ* DRIFT spectra of Ir-CTF upon exposure to CO_2 and H_2 (**Figure 5.9**), the bands attributed to the activation of CO_2 and H_2 respectively can be unambiguously elucidated. Still, the bands at 1741, 1888 and 2175 cm^{-1} are not observed in the transient studies using either CO_2 or H_2 as a probe molecule. As mentioned above, the absence of bands in the v(C–H) region excludes the presence of bidentate formates (κ^2-HCOO). Hence, these features indicate that monodenate formate species (κ^1-HCOO) is formed at the Ir site as well accepted for Ru-catalysed CO_2 hydrogenation.[37-38]
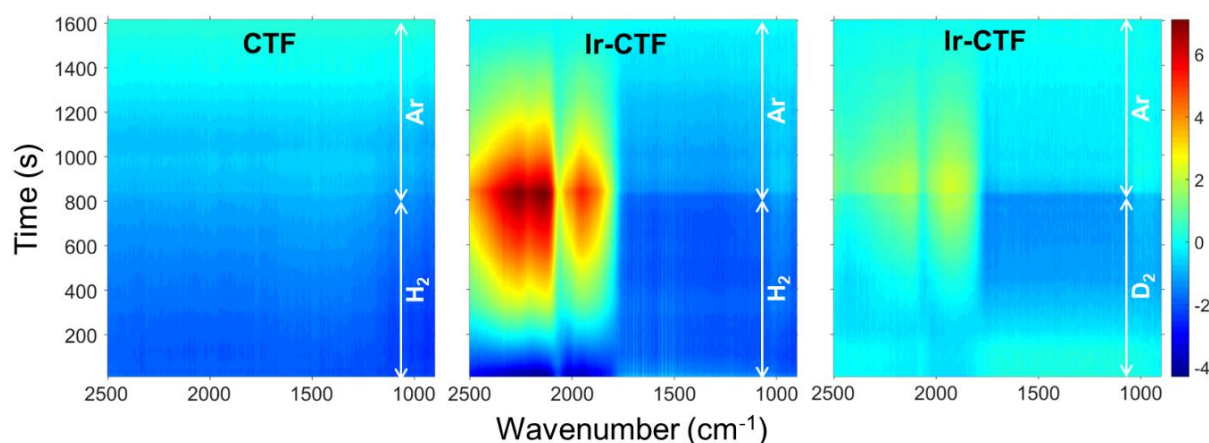
Figure 5.11. Transient DRIFTS study over CTF and Ir-CTF. Time-resolved DRIFT spectra upon exposure to H_2 or D_2 (the first half period) and then to Ar (the second half period) at 140 °C and 5 bar. The DRIFT spectra are shown in milli-absorbance unit taking the last spectrum in the Ar atmosphere as background.

5.4 Conclusion

This study proves the successful immobilisation of an iridium molecular complex ([IrCp*Cl$_2$]$_2$) on a solid covalent triazine framework. For the first time, this heterogenized catalyst has been tested under flow conditions in the presence of a solvent while taking advantage of high pressure conditions. Despite the continuous flow and harsh conditions of reaction pressure, almost half of the initial iridium loading (the rest is leached) is still coordinated with the bipyridine moieties of CTF after reaction. When methanol is cofed into the reactor together with CO_2 and H_2, methyl formate is yielded with full selectivity up to 140

UNIVERSITAT ROVIRA I VIRGILI
CONTINUOUS HYDROGENATION OF CARBON DIOXIDE TO FORMATES AND FORMIC ACID OVER HETEROGENEOUS CATALYSTS
Juan José Corral Pérez

Exploring the potential of Covalent Triazine Frameworks

ºC. At higher temperatures (140-180 ºC), MF formation is boosted while CO is also present. The presence of CO at such relatively low temperatures implies that its origin is the decomposition of formic acid. This is confirmed by employing water and triethylamine instead of methanol since they can stabilize formic acid and promote its yield. Besides demonstrating that formic acid is formed over Ir-CTF catalyst and is the origin of the observed CO, these studies are the first examples of a continuous synthesis of formic via CO_2 hydrogenation over a heterogeneous catalyst. According to spectroscopic studies, CTF is a promising support since it can strongly interact with CO_2 and methanol. When Ir compex is present, it seems that CO_2 and H_2 are respectively activated over the metallic centre, thus forming monodentate formate species. Such species are suggested to be involved in the formation of formic acid, which can either react with methanol to yield MF or be stabilized in water or with a base such as triethylamine. The present study opens new avenues for continuous formic acid synthesis over heterogenized catalysts, which may be inching closer to commercial viability.

Chapter 5

Bibliography

1. Copéret, C.; Chabanas, M.; Petroff Saint-Arroman, R.; Basset, J.-M., *Angew. Chem. Int. Edit.* **2003,** *42* (2), 156-181.
2. Copéret, C.; Allouche, F.; Chan, K. W.; Conley, M. P.; Delley, M. F.; Fedorov, A.; Moroz, I. B.; Mougel, V.; Pucino, M.; Searles, K.; Yamamoto, K.; Zhizhko, P. A., *Angew. Chem. Int. Edit.* **2018,** *57* (22), 6398-6440.
3. Das, S.; Heasman, P.; Ben, T.; Qiu, S., *Chem. Rev.* **2017,** *117* (3), 1515-1563.
4. Kaur, P.; Hupp, J. T.; Nguyen, S. T., *ACS Catal.* **2011,** *1* (7), 819-835.
5. Artz, J., *ChemCatChem* **2018,** *10* (8), 1753-1771.
6. Kuhn, P.; Thomas, A.; Antonietti, M., *Macromolecules* **2009,** *42* (1), 319-326.
7. Kuhn, P.; Antonietti, M.; Thomas, A., *Angew. Chem. Int. Edit.* **2008,** *47* (18), 3450-3453.
8. Bavykina, A. V.; Rozhko, E.; Goesten, M. G.; Wezendonk, T.; Seoane, B.; Kapteijn, F.; Makkee, M.; Gascon, J., *ChemCatChem* **2016,** *8* (13), 2217-2221.
9. Gunasekar, G. H.; Park, K.; Ganesan, V.; Lee, K.; Kim, N.-K.; Jung, K.-D.; Yoon, S., *Chem. Mater.* **2017,** *29* (16), 6740-6748.
10. Park, K.; Gunasekar , G. H.; Prakash, N.; Jung, K.-D.; Yoon, S., *ChemSusChem* **2015,** *8* (20), 3410-3413.
11. Álvarez, A.; Bansode, A.; Urakawa, A.; Bavykina, A. V.; Wezendonk, T. A.; Makkee, M.; Gascon, J.; Kapteijn, F., *Chem. Rev.* **2017,** *117* (14), 9804-9838.
12. Onishi, N.; Kanega, R.; Fujita, E.; Himeda, Y., *Adv. Synth. Catal.* **2019,** *361* (2), 289-296.
13. Moret, S.; Dyson, P. J.; Laurenczy, G., *Nat. Commun.* **2014,** *5*, 4017.
14. Jessop, P. G.; Joó, F.; Tai, C.-C., *Coordin. Chem. Rev.* **2004,** *248* (21), 2425-2442.
15. Pérez-Fortes, M.; Schöneberger, J. C.; Boulamanti, A.; Harrison, G.; Tzimas, E., *Int. J. Hydrogen Energ.* **2016,** *41* (37), 16444-16462.
16. Gunasekar, G. H.; Park, K.; Jeong, H.; Jung, K.-D.; Park, K.; Yoon, S., *Catalysts* **2018,** *8* (7), 295.
17. Ravel, B.; Newville, M., *J. Synchrotron Radiat.* **2005,** *12* (4), 537-541.
18. Katekomol, P.; Roeser, J.; Bojdys, M.; Weber, J.; Thomas, A., *Chemistry of Materials* **2013,** *25* (9), 1542-1548.
19. Hug, S.; Tauchert, M. E.; Li, S.; Pachmayr, U. E.; Lotsch, B. V., *Journal of Materials Chemistry* **2012,** *22* (28), 13956-13964.
20. Wang, G.; Leus, K.; Zhao, S.; Van Der Voort, P., *ACS Appl. Mater. Inter.* **2018,** *10* (1), 1244-1249.
21. Buyukcakir, O.; Je, S. H.; Talapaneni, S. N.; Kim, D.; Coskun, A., *ACS Appl. Mater. Inter.* **2017,** *9* (8), 7209-7216.
22. Palkovits, R.; Antonietti, M.; Kuhn, P.; Thomas, A.; Schüth, F., *Angew. Chem. Int. Edit.* **2009,** *48* (37), 6909-6912.
23. Xu, R.; Wang, X.-S.; Zhao, H.; Lin, H.; Huang, Y.-B.; Cao, R., *Catal. Sci. Technol.* **2018,** *8* (8), 2224-2230.
24. Bavykina, A. V.; Olivos-Suarez, A. I.; Osadchii, D.; Valecha, R.; Franz, R.; Makkee, M.; Kapteijn, F.; Gascon, J., *ACS Appl. Mater. Inter.* **2017,** *9* (31), 26060-26065.
25. Bavykina, A. V.; Goesten, M. G.; Kapteijn, F.; Makkee, M.; Gascon, J., *ChemSusChem* **2015,** *8* (5), 809-812.
26. Mondelli, C.; Puértolas, B.; Ackermann, M.; Chen, Z.; Pérez-Ramírez, J., *ChemSusChem* **2018,** *11* (17), 2859-2869.
27. Arikawa, T.; Takasu, Y.; Murakami, Y.; Asakura, K.; Iwasawa, Y., *J. Phys. Chem. B* **1998,** *102* (19), 3736-3741.
28. Du, W.; Wang, Q.; Saxner, D.; Deskins, N. A.; Su, D.; Krzanowski, J. E.; Frenkel, A. I.; Teng, X., *J. Am. Chem. Soc.* **2011,** *133* (38), 15172-15183.
29. Daza, Y. A.; Kuhn, J. N., *RSC Adv.* **2016,** *6* (55), 49675-49691.

UNIVERSITAT ROVIRA I VIRGILI
CONTINUOUS HYDROGENATION OF CARBON DIOXIDE TO FORMATES AND FORMIC ACID OVER HETEROGENEOUS CATALYSTS
Juan José Corral Pérez

Exploring the potential of Covalent Triazine Frameworks
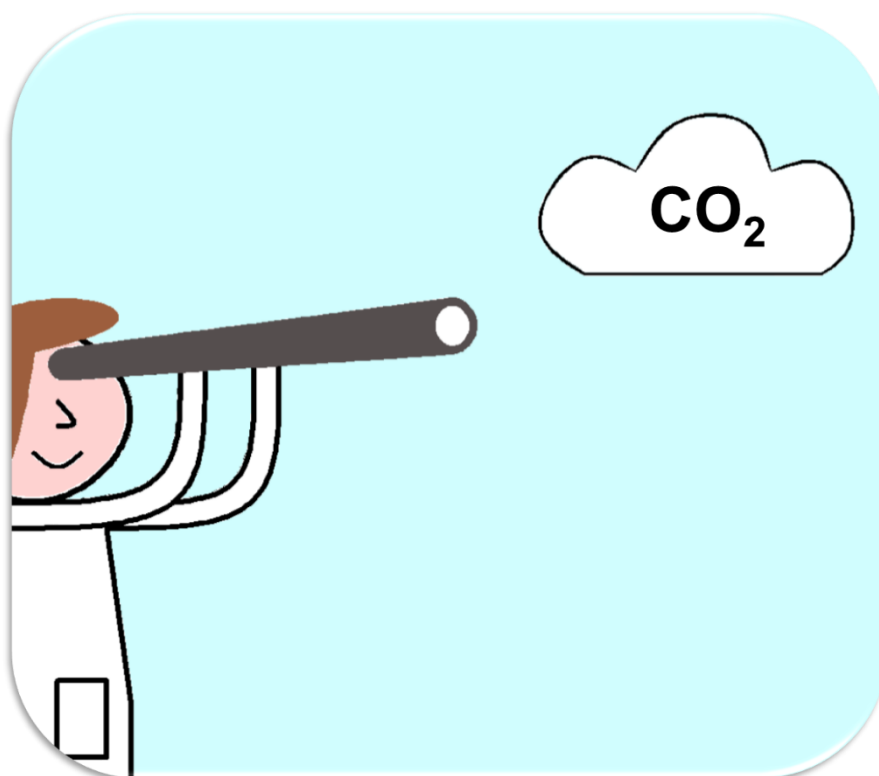
30.   Park, H.; Lee, J. H.; Kim, E. H.; Kim, K. Y.; Choi, Y. H.; Youn, D. H.; Lee, J. S., *Chem. Commun.* **2016,** *52* (99), 14302-14305.

31.   Reymond, H.; Corral-Pérez, J. J.; Urakawa, A.; Rudolf von Rohr, P., *React. Chem. Eng.* **2018,** *3* (6), 912-919.

32.   Corral-Pérez, J. J.; Bansode, A.; Praveen, C. S.; Kokalj, A.; Reymond, H.; Comas-Vives, A.; VandeVondele, J.; Copéret, C.; von Rohr, P. R.; Urakawa, A., *J. Am. Chem. Soc.* **2018,** *140* (42), 13884-13891.

33.   Vogiatzis, K. D.; Mavrandonakis, A.; Klopper, W.; Froudakis, G. E., *ChemPhysChem* **2009,** *10* (2), 374-383.

34.   Iskra, A.; Gentleman, A. S.; Kartouzian, A.; Kent, M. J.; Sharp, A. P.; Mackenzie, S. R., *J. Phys. Chem. A* **2017,** *121* (1), 133-140.

35.   Gibson, D. H., *Coordin. Chem. Rev.* **1999,** *185-186*, 335-355.

36.   Preti, C.; Tosi, G., *Z. Anorg. Allg. Chem.* **1977,** *432* (1), 259-263.

37.   Urakawa, A.; Jutz, F.; Laurenczy, G.; Baiker, A., *Chem. Eur. J.* **2007,** *13* (14), 3886-3899.

38.   Urakawa, A.; Iannuzzi, M.; Hutter, J.; Baiker, A., *Chem. Eur. J.* **2007,** *13* (24), 6828-6840.

UNIVERSITAT ROVIRA I VIRGILI
CONTINUOUS HYDROGENATION OF CARBON DIOXIDE TO FORMATES AND FORMIC ACID OVER HETEROGENEOUS CATALYSTS
Juan José Corral Pérez

Chapter 5

UNIVERSITAT ROVIRA I VIRGILI
CONTINUOUS HYDROGENATION OF CARBON DIOXIDE TO FORMATES AND FORMIC ACID OVER HETEROGENEOUS CATALYSTS
Juan José Corral Pérez

Chapter 5

6

Conclusions and outlook

Chapter 6

6.1 Summary of the thesis

Within the context of methyl formate (MF) as a transient intermediate to circumvent the thermodynamic constraints that hamper the direct formic acid synthesis from CO_2 and H_2 over heterogeneous catalysts, the subject of this thesis was the continuous MF synthesis via carbon dioxide (CO_2) hydrogenation in the presence of methanol (CH_3OH) at high pressure conditions.

Firstly, a high-pressure laboratory scale microreactor setup for the continuous catalytic hydrogenation of CO_2 to MF at pressures up to 300 bar was successfully designed and implemented, accomplishing one of the major tasks of the present thesis (**Chapter 2**). This system was very versatile since it allowed to cofeed liquid solvents such as methanol without causing oscillations in the reactant composition. The reaction product analysis was carried out by an online GC system equipped with two parallel detection channels. Furthermore, the reactor system could be controlled and automatized safely by an in-house designed LabVIEW program. Besides such technical progress to evaluate the catalytic performance, another achievement was the design and construction of a high-pressure reaction cell to study the reaction mechanism. This cell allowed to place the catalyst under reaction conditions, including high temperature (up to 260 ºC) and pressure (up to 90 bar), so that the surface species formed over the powder catalyst could be characterised by *in situ* and *operando* diffuse reflectance infrared Fourier transform spectroscopy (DRIFTS). Protocols and methods were established to tackle the complexity of the obtained spectra due to the presence of spectator species, which are not directly involved in the reaction, and to the overlapping signals arising from several chemical species that coexist on the catalyst surface. Transient response techniques together with multivariate spectral analysis allowed a selective and sensitive monitoring of the dynamic behaviour of the active species involved in the complex catalytic system.

Methyl formate synthesis by hydrogenation of carbon dioxide in the presence of methanol was studied in the abovementioned high-pressure microreactor setup and DRIFTS cell. Silica-supported silver nanoparticles were shown to be a significantly more active catalyst for the continuous methyl formate synthesis than the known gold and copper counterparts, and the origin of the unique reactivity of Ag was clarified (**Chapter 3**). Ag displays the lowest activation barrier for the formation of formates because it binds atomic hydrogen weakly and formates strong enough, whereas Au binds formates too weakly and Cu binds H too strongly. Transient *in situ* and *operando* vibrational spectroscopy and DFT calculations shed light on the reactive intermediates and reaction mechanisms: a key feature is the rapid formation of surface chemical species in equilibrium with adsorbed carbon dioxide. Such species is assigned to

Conclusions and outlook

carbonic acid interacting with water/hydroxyls on silica and promoting the esterification of formic acid with adsorbed methanol at the perimeter sites of Ag on SiO_2 to yield methyl formate. This study highlighted the importance of employing combined methodologies to verify the location and nature of active sites and to uncover fundamental catalytic reaction steps taking place at metal-support interfaces.

After having proved that adsorbed methanol reacts with formate species or formic acid at the perimeter sites of Ag on SiO_2 to yield MF, it was anticipated that the reaction performance and mechanism could be strongly influenced by the nature of the support material. That was why the effect of the support on MF yield for silver nanoparticles was investigated in **Chapter 4**. Silver nanoparticles supported on different materials were evaluated in the CO_2 hydrogenation in the presence of methanol to MF. Supports such as ZrO_2 and Al_2O_3 provided more active catalysts at lower temperatures than on the previously reported SiO_2. Process parameters such as temperature, gas hourly space velocity (GHSV) and molar ratio of reactants were studied to achieve the highest MF yield reported to date and to gather implications on the reaction mechanisms. Under optimized and continuous operation, the methyl formate yield increases up to 22% without detectable side-products. Transient *in situ* and *operando* DRIFTS were performed to elucidate the surface reaction mechanism. Formate species formed over Ag can spill over ZrO_2 and Al_2O_3 depending on the reactant atmosphere and coverage of support surface. The formates are stably present on these supports, thus providing formates or formic acid which can further react with adsorbed methanol near the perimeter sites of Ag and support to yield MF. The adsorption and diffusion of CH_3OH on the catalyst surface seems to be rate-limiting in the reaction.

These studies provided catalytic and mechanistic insights into the continuous MF synthesis using traditional heterogeneous catalysts, i.e. supported metal oxide catalysts. A new approach using an heterogenized molecular catalyst was also explored in **Chapter 5**. A covalent triazine framework (CTF) based on 2,6-dicyanopyridine was used to immobilise an iridium complex, $[IrCp^*Cl_2]_2$ ($Cp^* = \eta^5$-pentamethylcyclopentadienyl). The successful immobilisation of the iridium molecular complex on a solid CTF was proven by means of X-ray absorption spectroscopy (XAS) measurements. For the first time, this heterogenized catalyst has been tested under flow conditions in the presence of a solvent while taking advantage of high pressure conditions. Despite the continuous flow and harsh conditions of pressure, almost half of the initial iridium loading (the rest is leached) was still coordinated with the bipyridine moieties of CTF after reaction. Furthermore, significant changes in the structure of the spent catalyst were not observed. Methyl formate was yielded with full selectivity up to 140 ºC when methanol was cofeed into the reactor together with CO_2 and H_2. At higher

Chapter 6

temperatures, MF formation was boosted while CO was also present. The origin of CO formation was found in the decomposition of formic acid. This was confirmed by employing water and triethylamine instead of methanol since they could stabilize formic acid and promote its yield. These studies are the first examples of a continuous synthesis of formic via CO_2 hydrogenation over such a heterogeneous catalyst. According to *in situ* spectroscopic studies, CTF is a promising support since it can activate CO_2 and methanol. The immobilised iridium complex played a key role in the activation of CO_2 and H_2 over the metallic centre, thus forming monodentate formate species. Such species must be involved in the formation of formic acid, which can either react with methanol to yield MF or be stabilized in water or with a base such as triethylamine. This last chapter opens up new avenues in the feasibility of a continuous formic acid synthesis over heterogenized catalysts, which may be inching closer to commercial viability.

UNIVERSITAT ROVIRA I VIRGILI
CONTINUOUS HYDROGENATION OF CARBON DIOXIDE TO FORMATES AND FORMIC ACID OVER HETEROGENEOUS CATALYSTS
Juan José Corral Pérez

Conclusions and outlook

6.2 Open challenges and outlook

Based on the present thesis, methyl formate can be continuously synthesized via CO_2 hydrogenation in the presence of methanol using not only traditional heterogeneous catalysts (supported metal oxide catalysts) but also heterogenized molecular ones. The next steps should be aimed at exploring the industrial feasibility of a continuous formic synthesis from CO_2 and H_2.

A preliminary study showed the feasibility of continuously producing formic acid in a two-step process by exploiting methyl formate as a thermodynamically stable intermediate (**Figure 6.1**).[1] This concept was proven by the evaluation of several reactor configurations. Operating the $Cu/ZnO/Al_2O_3$ reactor at 260 °C granted methanol excess for an efficient methyl formate synthesis via the subsequent esterification reaction in the second reactor over a silver-based catalyst at 140 °C. The acidic resin Amberlyst 15 was placed in the second reactor together with the silver-based catalyst or separately in a third one. The position of the acidic resin determined the composition of the effluent stream. The significant loss of carbon balance in the studied configurations, reaching as low as 71.34%, indicated a substantial production of formic acid. Although formic acid could not be quantified, its presence was evidenced by pH measurement after the reaction combined to NMR analysis of the liquid products. Although identification of formic acid remains arduous, the proposed reactive pathway exceeds the thermodynamic limits of the direct synthesis path over supported metal oxide catalysts.[1]
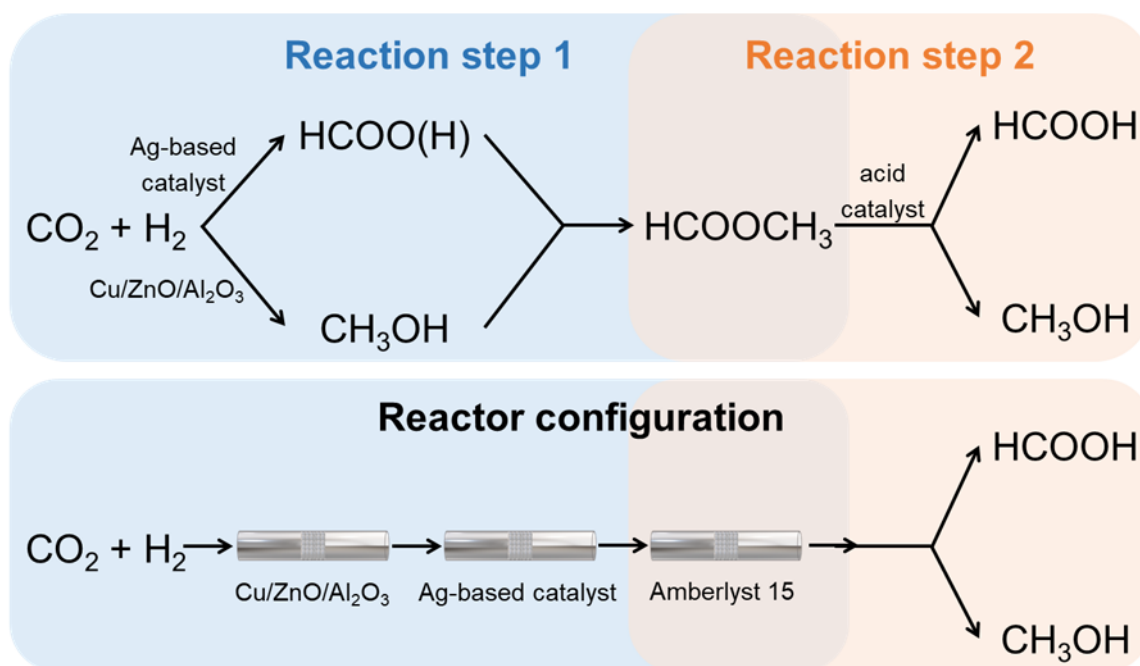
Figure 6.1. The new synthetic approach of formic acid and methanol using sequential connected reactors packed with heterogeneous catalysts (water is not shown for brevity).

Chapter 6

Although the continuous multi-step approach offers a promising strategy for an efficient CO_2 valorisation into formic acid, the use of heterogenized catalysts can lead to a direct CO_2 hydrogenation to formic acid in only one step. The study of an iridium immobilised complex presented in this thesis leaves ample room for improvement. The first aspect for consideration is the catalyst design. It has been demonstrated by *in situ* spectroscopic studies that the porous covalent framework can strongly interact with CO_2 and methanol, which can have a positive impact in the catalytic performance. However, the high content of iridium complex resulted in a decrease of the surface area of the material, thus not taking full advantage of the properties of the porous support. Hence, the loading of metal complex should be further studied to find an ideal synergistic effect between the complex and support. Another important point is to optimize the reaction conditions, such as temperature, pressure, gas hourly space velocity and reactant composition. For instance, increasing the concentration of water or base in the composition feeding would increase the formic acid yield significantly. It is worth highlighting that the base-free process using water would be very convenient to fulfil the principles of green chemistry, thus avoiding the use of basic additives and the post-synthetic steps required to convert the formate salt into formic acid in free form.[2]

Once the design of the immobilised iridium catalyst and reaction conditions were optimised, the implementation of a membrane reactor would be of great value. Membrane reactors are attracting increasing attention because reaction and separation takes place simultaneously in the same physical device.[3] Hence, capital costs can be reduced (no need of a external separation unit) while reactor performance is enhanced in equilibrium-limited reversible reactions (the product(s) or by-product(s) can be selectively removed from the reactants).[4-5] Given the unfavourable thermodynamics of the direct synthesis of formic acid from CO_2 and H_2, the selective removal of formic acid dissolved in water may have a huge impact in shifting the equilibrium towards products. Among the possible configurations, a catalytic packed-bed membrane reactor is proposed for the continuous synthesis of formic acid (**Figure 6.2**). As depicted in **Figure 6.2**, the heterogenized iridium catalyst would be placed in the reaction channel, between the membrane and shell of the membrane reactor. This membrane would allow the selective removal of the formic acid that is formed via CO_2 hydrogenation and subsequent dissolved in water. This strategy would increase the yield of formic acid. Furthermore, the unreacted CO_2 and H_2 could be easily recirculated into the reactor to enhance the catalytic performance. Another interesting configuration would be the coating of the covalent triazine framework on the membrane. In literature, a covalent triazine framework has been successfully coated on cordierite monoliths.[6] If the membrane was successfully coated, the iridium complex would be directly immobilised on the membrane. Although this strategy is much more complex, it may have a more positive impact on the formic acid

UNIVERSITAT ROVIRA I VIRGILI
CONTINUOUS HYDROGENATION OF CARBON DIOXIDE TO FORMATES AND FORMIC ACID OVER HETEROGENEOUS CATALYSTS
Juan José Corral Pérez

Conclusions and outlook

formation since its diffusion path from the metal centre to the membrane would be shorter, thus avoiding its decomposition back to CO_2 and H_2.
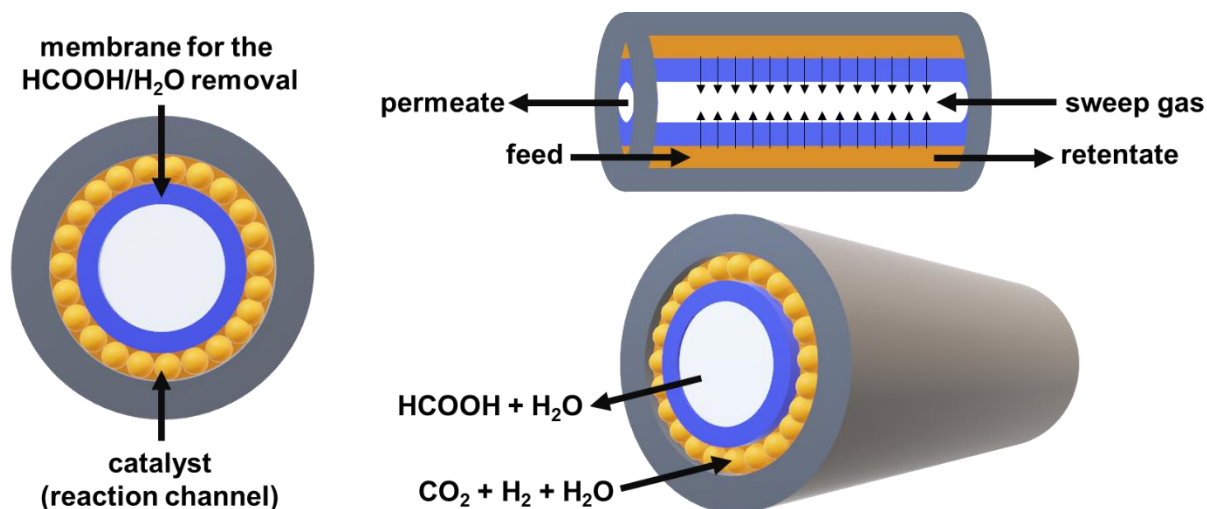
Figure 6.2. Different views of the catalytic packed-bed membrane reactor proposed for the continuous formic acid synthesis via CO_2 hydrogenation. The permeate is the fraction that flows through the membrane. The retentate is the fraction containing the components that have not been transported through the membrane. The sweep gas is a gas present in the permeate side of a membrane reactor to lower the partial pressure of the permeating species and increase the driving force.

Chapter 6

Bibliography

1. Reymond, H.; Corral-Pérez, J. J.; Urakawa, A.; Rudolf von Rohr, P., *React. Chem. Eng.* **2018,** *3* (6), 912-919.
2. Mondelli, C.; Puértolas, B.; Ackermann, M.; Chen, Z.; Pérez-Ramírez, J., *ChemSusChem* **2018,** *11* (17), 2859-2869.
3. Gallucci, F.; Basile, A.; Hai, F. I., Introduction – A Review of Membrane Reactors. In *Membranes for Membrane Reactors*.
4. Diban, N.; Aguayo, A. T.; Bilbao, J.; Urtiaga, A.; Ortiz, I., *Ind. Eng. Chem. Res.* **2013,** *52* (31), 10342-10354.
5. Sun, Y. M.; Khang, S. J., *Ind. Eng. Chem. Res.* **1990,** *29* (2), 232-238.
6. Bavykina, A. V.; Olivos-Suarez, A. I.; Osadchii, D.; Valecha, R.; Franz, R.; Makkee, M.; Kapteijn, F.; Gascon, J., *ACS Applied Materials & Interfaces* **2017,** *9* (31), 26060-26065.

UNIVERSITAT ROVIRA I VIRGILI
CONTINUOUS HYDROGENATION OF CARBON DIOXIDE TO FORMATES AND FORMIC ACID OVER HETEROGENEOUS CATALYSTS
Juan José Corral Pérez

Conclusions and outlook

Chapter 6

Appendices

Appendix A

Appendix A – Supplementary information of chapter 3

A.1 Analysis of DFT results

A.1.1 Formation of formates on Cu(111), Ag(111), and Au(111)

DFT calculations support the superior reactivity of the Ag catalyst towards formate formation; activation barrier for formates formation is lower for Ag (0.61 eV) compared to Cu (0.71 eV) and Au (0.97 eV) (**Figure A.1**). Based on a detailed analysis of the DFT results (see **Figure A.1.1.2**), we find that the activation energy for the formation of surface formate (HCOO) is simply given by the interplay between weak and strong adsorption of H and HCOO, respectively. The lowest energy barrier for bidentate κ^2-formate formation over Ag can be attributed to its weak binding to H and sufficiently strong binding to HCOO. In contrast, Au binds HCOO too weakly, whereas Cu binds H too strongly.
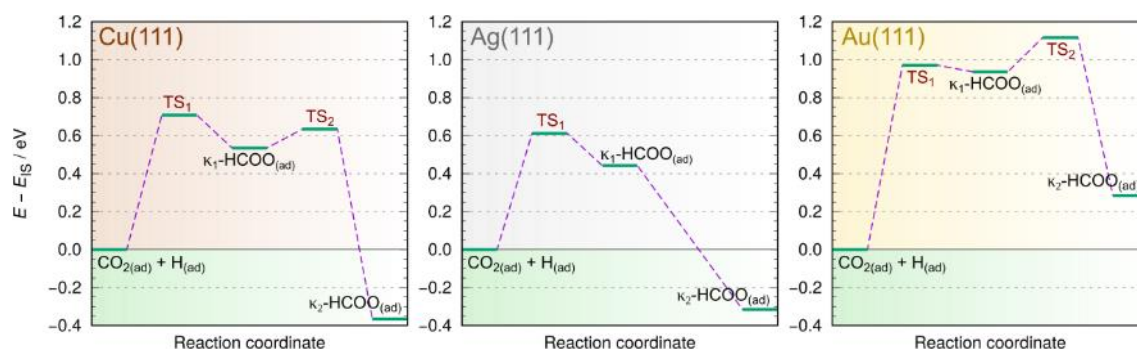
Figure A.1. PBE-D''/plane-wave calculated reaction profiles for formate formation reaction. $H_{(ad)}$ + $CO_{2(ad)} \rightarrow \kappa^1$-$HCOO_{(ad)} \rightarrow \kappa^2$-$HCOO_{(ad)}$ on Cu(111), Ag(111), and Au(111). κ^1-HCOO and κ^2-HCOO are monodentate and bidentate formates, respectively.

A.1.2 Silver displays the lowest barrier for the formation of formates

We present below an analysis of DFT results, calculated with the PBE-D''/plane-wave method (for the description of respective computational method, see the end of **Section 7.1.1.3**), to rationalize why Ag displays the lowest barrier among coinage metals for the formation of formate, $H_{(ad)}$ + $CO_{2(ad)} \rightarrow HCOO_{(ad)}$. To this end, we modeled the reaction on Cu(111), Ag(111) and Au(111) surfaces and on each of them several different reaction channels were considered, which either followed a direct path to bidentate κ^2-formates (κ^2-$HCOO_{(ad)}$) or an indirect one that proceeds through the formation of monodentate κ^1-formates, $H_{(ad)}$ + $CO_{2(ad)} \rightarrow \kappa^1$-$HCOO_{(ad)} \rightarrow \kappa^2$-$HCOO_{(ad)}$. We find that activation barriers are lower for the latter, even though the κ^1-formates are by about 0.6 eV less stable than κ^2-$HCOO_{(ad)}$ (on Ag(111) the κ^1-$HCOO_{(ad)}$ is not even a local minimum but rather a wide plateau). The lowest identified activation energies (E^*) and respective transition states (TS) for reaction paths that

UNIVERSITAT ROVIRA I VIRGILI
CONTINUOUS HYDROGENATION OF CARBON DIOXIDE TO FORMATES AND FORMIC ACID OVER HETEROGENEOUS CATALYSTS
Juan José Corral Pérez

Supplementary information of chapter 3

proceed through κ^1-HCOO$_{(ad)}$ are presented in **Figure A.2**, while those for the direct path to κ^2-HCOO$_{(ad)}$ are presented in **Figure A.3**.

To help disentangling the factors that determine the height of the activation barrier for CO_2 hydrogenation, we first analyze the reverse reaction—i.e., the formate decomposition, HCOO$_{(ad)}$ → H$_{(ad)}$ + CO$_{2(ad)}$—for a very simple reason. Namely, it is known that dissociation reactions obey linear energy relationships to a much better extent than association reactions.[1] For the sake of definiteness, the analysis presented below corresponds to transition states TS$_1$ (cf. **Figure A.2**), but it should be noted that the analysis leads to the same conclusion even if other sets of transition states are considered (i.e., either (i) TS$_1$ for Cu and Ag and TS$_2$ for Au (cf. **Figure A.2**) or (ii) TS of the direct path to κ^2-HCOO$_{(ad)}$, **Figure A.3**). We find that the reverse activation energy, $E^*_{reverse}$ (i.e., the barrier for formate decomposition, calculated with respect to TS$_1$ and κ^2-HCOO$_{(ad)}$), is proportional to adsorption binding energy of κ^2-HCOO, E_b^{HCOO}, and can be to a very good approximation written as (in eV units):

$$E^*_{reverse} \approx -0.14 - 0.41 E_b^{HCOO} \tag{A.1}$$

The corresponding correlation between the PBE-D''/plane-wave calculated $E^*_{reverse}$ and $|E_b^{HCOO}|$ is shown in **Figure A.4a**. This equation has a very simple physical meaning and it tells that the stronger the formate bonds to the surface, the more difficult is to break it to CO$_{2(ad)}$ and H$_{(ad)}$.

It is straightforward to pass from the reverse to the forward activation energy, E^*, and the relation is given by:

$$E^* = E^*_{reverse} + \Delta E \tag{A.2}$$

where ΔE is the reaction energy for the forward reaction, H$_{(ad)}$ + CO$_{2(ad)}$ → κ^2-HCOO$_{(ad)}$, which is given by:

$$\Delta E \approx E_b^{HCOO} - E_b^{H} - E_b^{CO2} \tag{A.3}$$

where E_b^{H} and E_b^{CO2} are adsorption binding energies of H and CO_2, respectively. PBE-D''/plane-wave calculated adsorption, activation, and reaction energies are tabulated in **Table A.1**. Equation A.3 is written with the "≈" instead of the "=" operator, because in **Table A.1** the respective E_b^{H} and E_b^{CO2} values correspond to standalone adsorbed species, whereas in NEB calculation the two reactant species are close to one another — this discrepancy is however

Appendix A

small, about 0.05 eV in all the cases (cf. **Table A.1**). Plugging equation A.3 into A.2 and using equation A.1 gives (in eV units):

$$E^* \approx -0.14 + 0.59 E_b^{HCOO} - E_b^H - E_b^{CO2} \qquad (A.4)$$

It can be realized from **Table A.1** that the adsorption binding energy of CO_2 is rather small in magnitude and similar on all the three considered metals, about –0.2 eV. Hence, equation A.4 can be simplified by incorporating the E_b^{CO2} into the constant term. The resulting equation is therefore (in eV units):

$$E^* \approx C + 0.59 E_b^{HCOO} - E_b^H \qquad (A.5)$$

where the value of the constant C was obtained by fitting equation A.5 to DFT data (cf. **Table A.1**) and the resulting value is –0.01. Due to its small magnitude the C was neglected and the slope adjusted from 0.59 to 0.60, hence:

$$E^* \approx 0.60 E_b^{HCOO} - E_b^H \qquad (A.6)$$

The correlation between the so estimated and the DFT calculated activation energies is very good (see **Figure A.4b**) and correspondingly the activation energy estimator of equation A.6 should be usable. This estimator demonstrates that the height of the activation barrier for the formate formation is mainly given by adsorption binding energies of H and HCOO with the binding energy of H being almost twice as important as that of HCOO.

In the above analysis, the activation energies corresponding to TS_1 of **Figure A.2** were considered, but the same conclusion—concerning the role of H and HCOO binding energies—is reached if the activation energies for direct formation of κ^2-$HCOO_{(ad)}$ (cf. **Figure A.3**) are considered instead.

The estimator of equation A.6 therefore reveals that for the activation energy to be small, the catalyst should bind H weakly and HCOO strongly, but only in relative sense, because $HCOO_{(ad)}$ is a reaction intermediate in the formation of MF. Hence, HCOO should not bind too strongly to catalyst or else its further reaction with methyl will be difficult. This is a classical example of Sabatier principle.

On the basis of the above analysis, we can clearly explain why Ag displays the smallest formate formation activation energy among the three metals. Namely, it binds H the weakest, but HCOO strong enough. In contrast, Au bonds HCOO too weakly, whereas Cu binds H too strongly (cf. **Table A.1** and equation A.6). The usefulness of our devised activation energy

UNIVERSITAT ROVIRA I VIRGILI
CONTINUOUS HYDROGENATION OF CARBON DIOXIDE TO FORMATES AND FORMIC ACID OVER HETEROGENEOUS CATALYSTS
Juan José Corral Pérez

Supplementary information of chapter 3

estimator of equation A.6 is not only that it allows us to understand in a physically simple way the two principle factors that determine the height of the activation barrier for formate formation, but moreover to facilitate the rapid screening of new potentially superior catalyst materials, because the estimator only needs the adsorption binding energies of H and HCOO as inputs. Note that calculating activation energies is rather difficult and computationally intensive, whereas calculating adsorption energies is rather straightforward and by one to two orders of magnitude computationally cheaper.
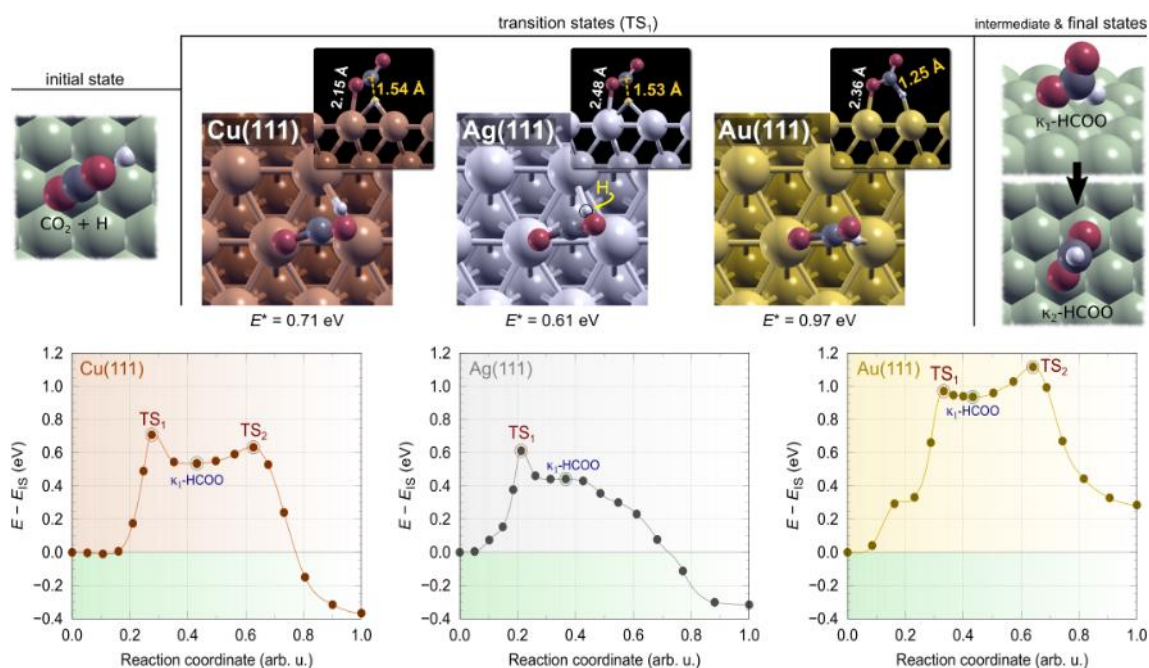
Figure A.2. PBE-D''/plane-wave calculated transition states (TS, top-row) and minimum-energy paths (MEP, bottom-row) for formate formation on Cu(111), Ag(111), and Au(111) that proceeds through monodentate κ^1-HCOO as the intermediate state. Each MEP was constructed from two separate NEB calculations, i.e., (1) $H_{(ad)} + CO_{2(ad)} \rightarrow \kappa^1$-HCOO$_{(ad)}$. and (2) κ^1-HCOO$_{(ad)} \rightarrow \kappa^2$-HCOO$_{(ad)}$, and the respective transition states are labeled as TS$_1$ and TS$_2$. The TS structures, shown in the top-row, are the TS$_1$ structures; the corresponding activation energies are also stated. Exemplar initial ($H_{(ad)} + CO_{2(ad)}$), intermediate (κ^1-HCOO$_{(ad)}$) and final state (κ^2-HCOO$_{(ad)}$) structures are shown on the left and right side (top-row), respectively.

Appendix A
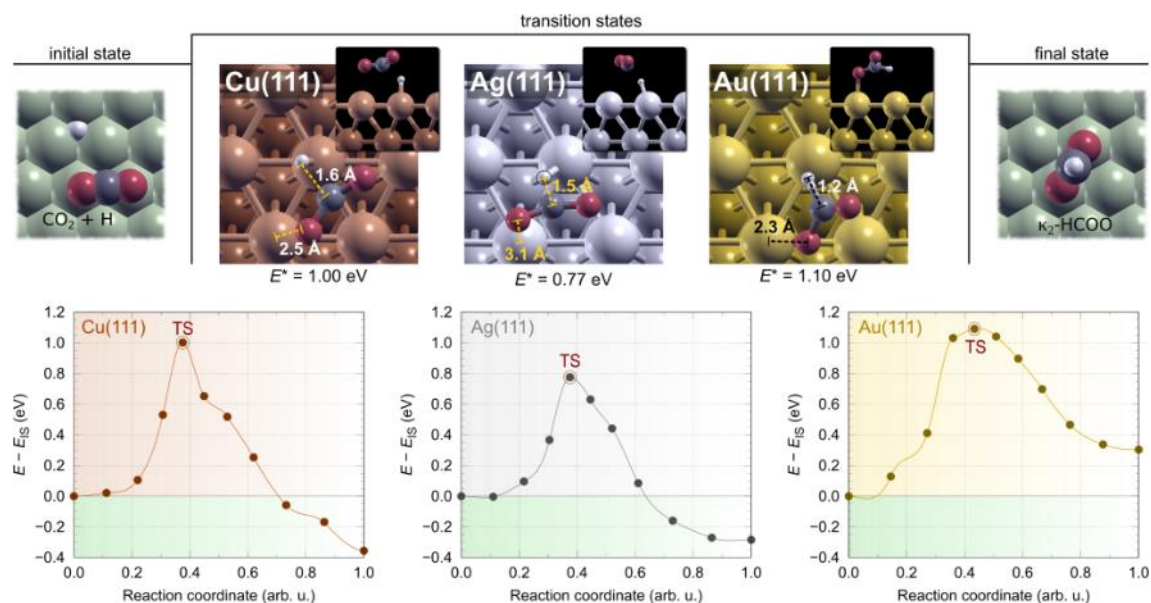
Figure A.3. As in **Figure A.2** but for the direct path from $H_{(ad)}$ + $CO_{2(ad)}$ to κ^2-$HCOO_{(ad)}$.
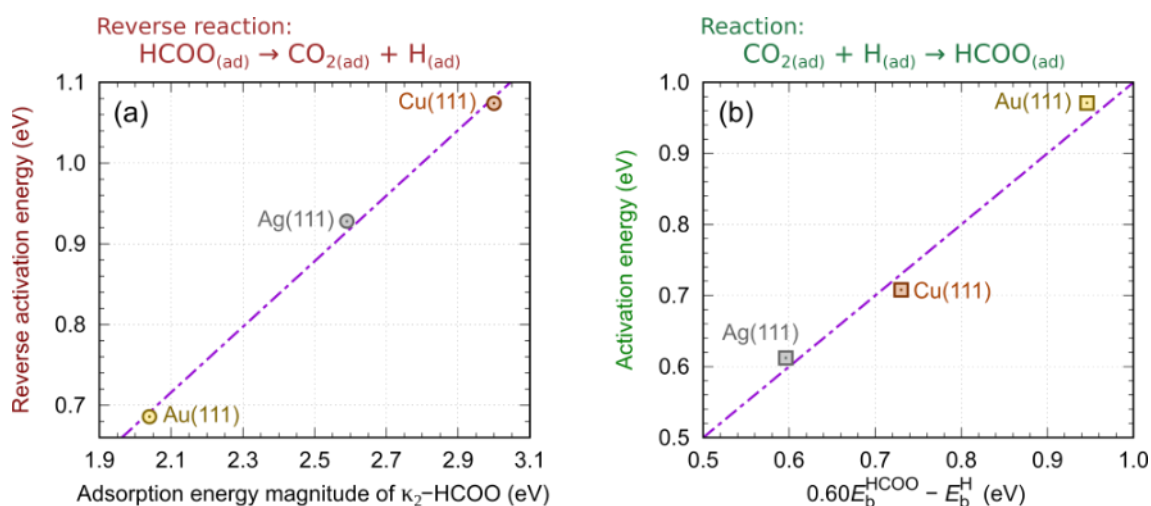
Figure A.4. **a**, Correlation between the PBE-D''/plane-wave calculated activation energy (calculated with respect to TS_1 of **Figure A.2**) for the reverse reaction, $HCOO_{(ad)} \rightarrow H_{(ad)} + CO_{2(ad)}$, and adsorption binding energy magnitude of the formate; the root-mean-squared (RMS) error is 0.02 eV and the maximum error is 0.02 eV. **b**, Correlation between the PBE-D'' calculated activation energy for the forward reaction, $H_{(ad)} + CO_{2(ad)} \rightarrow HCOO_{(ad)}$, and the activation energy estimator of equation A.6; the RMS error is 0.03 eV and the largest error is 0.03 eV. The RMS errors are calculated as $\sqrt{(\sum_i (y_i - f_i)^2/(N-m))}$, where y_i is the activation energy and f_i its estimate via equation A.1 or A.6, whilst N and m are the number of data points and number of fitting parameters, respectively.

Supplementary information of chapter 3

Table A.1. PBE-D''/plane-wave calculated adsorption binding energies (E_b) of H, CO_2, and κ^2-HCOO as well as activation (E^*) and reaction (ΔE) energies for formate formation reaction, $H_{(ad)} + CO_{2(ad)} \rightarrow$ $HCOO_{(ad)}$. Beware that E_b^H and E_b^{HCOO} are calculated with respect to atomic H and HCOO radical, respectively.

	E_b^H (eV)	E_b^{CO2} (eV)	E_b^{HCOO} (eV)	E^* (eV)	ΔE (eV)
Cu(111)	−2.53	−0.16	−3.00	0.71	−0.37[a] (−0.31)[b]
Ag(111)	−2.15	−0.17	−2.59	0.61	−0.32[a] (−0.27)[b]
Au(111)	−2.17	−0.20	−2.04	0.97[c]	+0.29[a] (+0.33)[b]

[a] Obtained from NEB calculation, where $H_{(ad)}$ and $CO_{2(ad)}$ reactants are coadsorbed close to one another.

[b] Obtained from standalone adsorption energies via equation A.3.

[c] Corresponds to TS_1 (see **Figure A.2**).

A.1.3 Formation of formic acid on Cu(111), Ag(111), and Au(111)

On Cu(111), Ag(111), and Au(111) we also modeled the formation of formic acid that proceeds from co-adsorbed formate and atomic hydrogen, κ^2-$HCOO_{(ad)} + H_{(ad)} \rightarrow HCOOH_{(ad)}$. The identified transition states (TS) and activation energies (E^*) are presented in **Figure A.5**, while formic acid adsorption binding energies (E_b), reaction energies (ΔE), and activation energies are reported in **Table A.2**. Formation of HCOOH is endothermic on Cu(111) and exothermic on Ag(111) and Au(111); the ΔE follows the Cu > Ag > Au trend. Activation energies follow the same trend and numerical analysis reveals that the reaction obeys the Brønsted–Evans–Polanyi linear relationship, $E^* = a + b\Delta E$, to a moderate extent. However, by scrutinizing the structural details of the TS structures in **Figure A.5**, the argument can be made more quantitative. Note that the TS structure on all three surfaces appear analogous and its most relevant characteristic is that it involves significantly perturbed HCOO reactant, while $H_{(ad)}$ is affected to a much smaller extent. Namely, HCOO rotates helicopter-like with one O atom toward the coadsorbed $H_{(ad)}$ and by doing so the respective O−surface bond is completely broken. In contrast, $H_{(ad)}$ only diffuses from the fcc to the bridge site (in the TS structure the H−surface bond length is similar to its equilibrium value), but it is known that $H_{(ad)}$ is not very sensitive to specifics of the surface site;[2-3] for example, on Cu(111) the difference in E_b between fcc and bridge site is 0.14 eV. Also the variation of H−surface bond strength on the three surfaces is way smaller than that of HCOO (cf. **Table A.1**). This reasoning suggests that the stronger the formate binds to the surface, the more difficult is to break its O−surface bond and correspondingly the larger should be the activation barrier. Hence (in eV units):
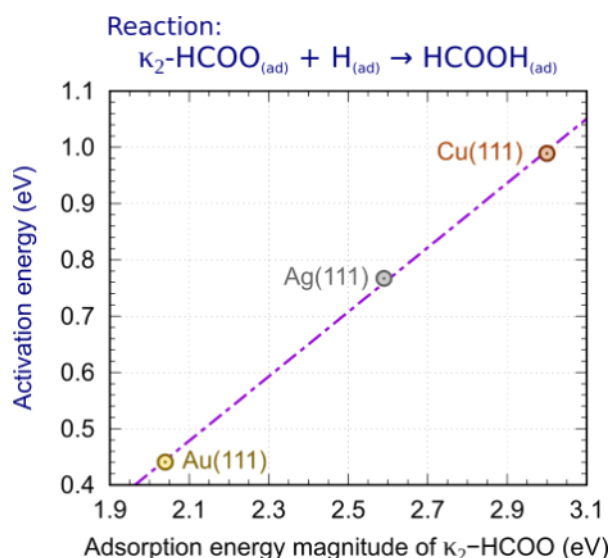
Appendix A

$$E^* \approx a + bE_b^{HCOO} = -0.72 + 0.57E_b^{HCOO} \qquad (A.7)$$

where the values of a and b were obtained by fitting the data; the corresponding correlation between the PBE-D'' calculated E^* and $|E_b^{HCOO}|$ is shown in **Figure A.6** and it can be seen that equation A.7 predicts E^* remarkably well. Notice from equation A.7 that the value of b is close to one-half, which has a simple physical meaning: namely, the HCOO in the TS structure has one of the two O−surface bonds broken, hence the activation energy roughly scales as half the formate−surface bond strength.
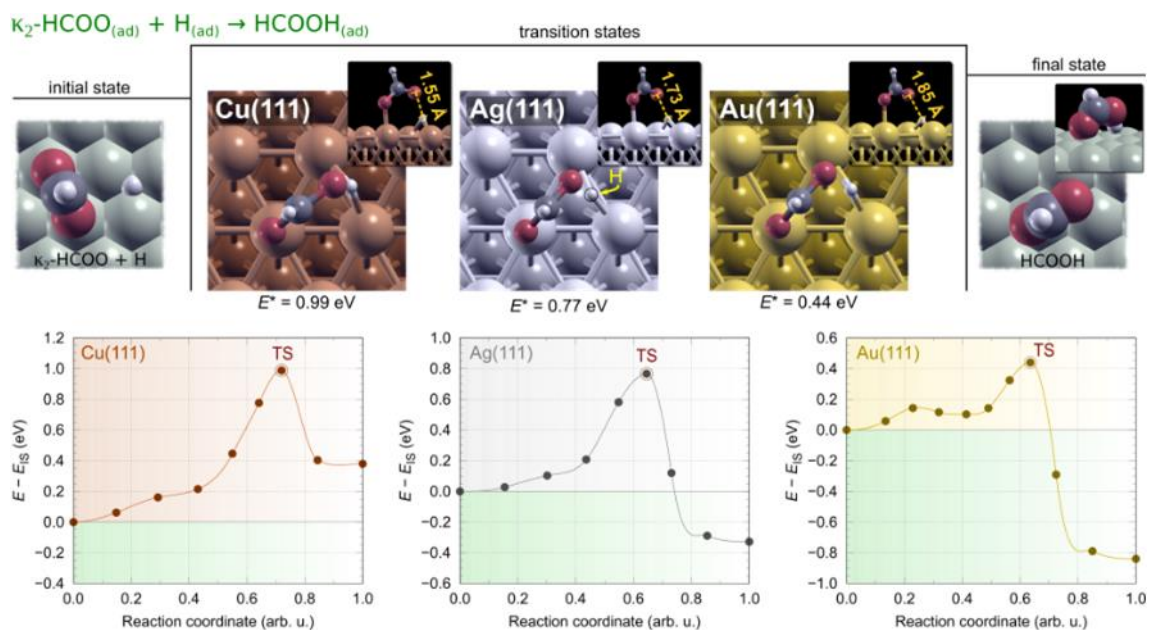
Figure A.5. PBE-D''/plane-wave calculated transition states (TS, top-row) and minimum-energy paths (bottom-row) for formation of formic acid on Cu(111), Ag(111), and Au(111) from κ^2-formate and atomic hydrogen, κ^2-HCOO$_{(ad)}$ + H$_{(ad)}$ → HCOOH$_{(ad)}$. The corresponding activation energies are also stated. Exemplar initial (κ^2-HCOO$_{(ad)}$ + H$_{(ad)}$) and final state (HCOOH$_{(ad)}$) structures are shown on the left and right side (top-row), respectively.

UNIVERSITAT ROVIRA I VIRGILI
CONTINUOUS HYDROGENATION OF CARBON DIOXIDE TO FORMATES AND FORMIC ACID OVER HETEROGENEOUS CATALYSTS
Juan José Corral Pérez

Supplementary information of chapter 3

Figure A.6. Correlation between the PBE-D''/plane-wave calculated activation energy for formation of formic acid, κ^2-HCOO$_{(ad)}$ + H$_{(ad)}$ → HCOOH$_{(ad)}$, and adsorption binding energy magnitude of the κ^2-formate. The RMS error is 0.01 eV.

Table A.2. PBE-D''/plane-wave calculated adsorption binding energies (E_b) of HCOOH as well as activation (E^*) and reaction (ΔE) energies for its formation, κ^2-HCOO$_{(ad)}$ + H$_{(ad)}$ → HCOOH$_{(ad)}$.

	E_b^{HCOOH} (eV)	E^* (eV)	ΔE (eV)
Cu(111)	−0.53	0.99	+0.38
Ag(111)	−0.45	0.77	−0.33
Au(111)	−0.43	0.44	−0.84

Computational Details and Models. We used the pseudopotential method with ultrasoft pseudopotentials[4,5] and the PWscf code from the Quantum ESPRESSO distribution.[6-7] The Kohn–Sham orbitals were expanded in a plane-wave basis set up to a kinetic energy cutoff of 30 Ry (240 Ry for the charge density cutoff). Brillouin zone (BZ) integrations were performed with the special-point technique[8] and a Methfessel-Paxton smearing[9] of 0.03 Ry. Surfaces were modeled by periodic slabs consisting of four (111) layers. The bottom layer was constrained to the bulk positions and the in-plane lattice spacing was fixed to the PBE-D'' calculated lattice parameters of 3.64, 4.16, and 4.14 Å for Cu, Ag, and Au, respectively, whereas all other degrees of freedom were relaxed. The thickness of the vacuum region was set to about 13 Å and molecules were adsorbed on one side of the slab. Molecular adsorption

<u>Appendix A</u>

and surface reactions were modeled with (3 × 3) supercell and the 4 × 4 × 1 uniformly shifted k-point mesh.

Surface reactions were modeled as the minimum energy paths (MEPs) using the climbing-image nudged elastic band (CI-NEB) method.[10-11] Vibrational frequencies were calculated using the PHONON package[12] from the QUANTUM ESPRESSO distribution.[6-7]

Reparametrization of PBE-D to PBE-D". For a description of physisorption dispersion interactions, we employed a reparametrized empirical dispersion correction of Grimme,[13-14] that consists of a damped C_6R^{-6} like energy term on top of the PBE. However, the original PBE-D (also known as PBE-D2) overestimates the molecular bonding to metal surfaces. To remedy the overbonding we reparametrized the C_6 coefficients of Cu, Ag, and Au. The resulting method is denoted by the PBE-D" label, where the double prime indicates the reparametrization of the original method. For the PBE-D" the C_6 values are reparametrized[15] so as to reproduce the experimental physisorption energy of a flat lying benzene on Cu(111), Ag(111), and Au(111). The resulting C_6 values are 225.5, 547, and 776 Ry Bohr^{-6} for Cu(111), Ag(111), and Au(111), respectively. For the estimated experimental physisorption energies of benzene on Cu(111), Ag(111), and Au(111) we used 0.77, 0.75, and 0.82 eV, respectively. These values were obtained from experimental TPD data[16] with Redhead equation by using the TPD peak temperatures of 225, 220, and 239 K, respectively, heating rate of 4 K s^{-1} and a preexponential factor of $v = 10^{17}$ s^{-1}, which corresponds to experimentally determined prefactor for flat lying benzene on Pd(111).[17]

Energy equations. Adsorption binding energies are calculated as

$$E_b^X = E_{X/surf} - E_X - E_{surf} \tag{A.8}$$

where X stands for adsorbate (X ≡ CO_2, H, and HCOO). E_X, E_{surf}, and $E_{X/surf}$ are total energies of isolated adsorbate, metal slab, and adsorbate/slab systems, respectively. Note that in the case of H and HCOO, the adsorption binding energy is calculated with respect to atomic H and HCOO radical in the initial state (and not with respect to H_2 and HCOOH). The E_b^X is therefore a measure of the adsorbate–surface binding energy, which is why we use the naming "adsorption binding energy".

Surface reactions were modelled as the minimum energy paths (MEPs). The configuration of the maximum energy along the MEP is the transition state (TS). The activation energy is calculated as $E^* = E_{TS} - E_{IS}$ and the corresponding reaction energy is given by $\Delta E = E_{FS} - E_{IS}$, where E_{IS}, E_{TS}, and E_{FS} are total energies of initial- (IS), transition-, and final-state (FS) of a

UNIVERSITAT ROVIRA I VIRGILI
CONTINUOUS HYDROGENATION OF CARBON DIOXIDE TO FORMATES AND FORMIC ACID OVER HETEROGENEOUS CATALYSTS
Juan José Corral Pérez

Supplementary information of chapter 3

given elementary reaction step, respectively. The threshold for the magnitude of atomic forces along the MEP was set to 50 meV Å^{-1}.

**Molecular graphics.** Molecular graphics were produced by the XCRYSDEN graphical package.[18]

A.1.4 Evaluation of the adsorption of CO_2 and the formation of carbonic acid on silica

We evaluated several configurations of carbonic acid (H_2CO_3) adsorbed on the hydroxylated SiO_2 surface. The reaction energies ΔE_1 and reaction Gibbs free energies ΔG_1 reported in **Table A.3** refer to the formation of adsorbed carbonic acid on SiO_2 from $CO_{2(g)}$ and $H_2O_{(g)}$, whereas the energies ΔE_2 and ΔG_2 refer to the formation of adsorbed carbonic acid on SiO_2 from $CO_{2(g)}$ and preadsorbed water molecule, $H_2O_{(ad)}$. The optimized structures of the SiO_2 surface and water molecule adsorbed thereon are shown in **Figure A.7**. These results were obtained with the PBE-D3/DZVP method (the description of respective computational method is provided at the end of **Section 7.1.1.3**).

Table A.3. PBE-D3/DZVP formation energies (ΔE_1 and ΔE_2) of carbonic acid on SiO_2 calculated with respect to $CO_2(g)$ and $H_2O(g)$ in the gas phase, and to $CO_2(g)$ and H_2O adsorbed on the SiO_2 surface, respectively. The corresponding Gibbs energies (ΔG_1 and ΔG_2) are calculated at 230 °C and 5 bar.

Evaluated structure	ΔE_1 energy (eV) From $CO_2(g)$ + $H_2O(g)$	ΔG_1 energy (eV) From $CO_2(g)$ + $H_2O(g)$	ΔE_2 energy (eV) From $CO_2(g)$ + $H_2O(ad)$	ΔG_2 energy (eV) From $CO_2(g)$ + $H_2O(ad)$
Si-OH --- OH-C(O)-OH (1)	-0.31	1.74	0.30	1.21
Si-OH --- OH-C(O)-OH (2)	-0.42	1.57	0.19	1.04
Si-OH --- OH-C(O)-OH (3)	-0.65	1.44	-0.04	0.91
Si-OH --- OH-C(O)-OH (4)	-0.74	1.37	-0.13	0.84
Si-OH --- OH-C(O)-OH (5)	-0.84	1.23	-0.23	0.69
Si-OH --- OH-C(O)-OH (6)	-1.05	1.02	-0.44	0.49

Appendix A
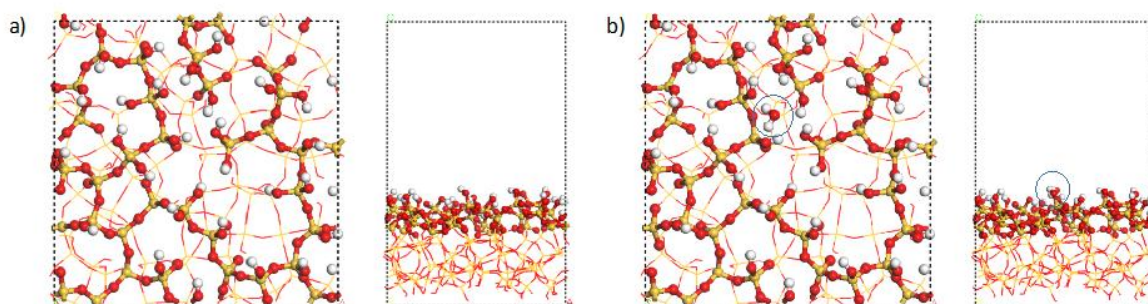
Figure A.7. Top and side views of the PBE-D3/DZVP optimized structures of the **a**, initial SiO_2 surface (7.2 OH nm^{-2}) and **b**, the silica surface with one water molecule adsorbed on it. A blue circle shows the position of the water molecule in the latter structure.

The structures of carbonic acid adsorbed on the SiO_2 surface are shown in **Figure A.8**. The most stable structure (**Figure A.8f**) has ΔE_1 and ΔG_1 energies equal to −1.05 and +1.02 eV, respectively. The reason that ΔG_1 is so much more endergonic than ΔE_1 is mainly due to the loss of roto-translational degrees of freedom upon adsorption of CO_2 and H_2O. At 230 °C and 5 bar the calculated roto-translational TS contributions are 1.11 and 1.01 eV for CO_2 and H_2O, respectively. However, if carbonic acid forms in reaction of CO_2 with adsorbed water, which is covering the surface under these conditions, the resulting Gibbs formation energies (ΔG_2) are significantly more favourable than with respect to CO_2 and H_2O in the gas phase. The most favourable structure has ΔG_2 values equal to +0.49 eV. Note that the values of ΔE_2 and ΔG_2 will vary depending on the site considered for the adsorption of the initial water molecule. The resulting structure of the most favourable structure of carbonic acid adsorbed on the SiO_2 surface has multiple hydrogen bonds with the surface (Figure 5b).

UNIVERSITAT ROVIRA I VIRGILI
CONTINUOUS HYDROGENATION OF CARBON DIOXIDE TO FORMATES AND FORMIC ACID OVER HETEROGENEOUS CATALYSTS
Juan José Corral Pérez

Supplementary information of chapter 3
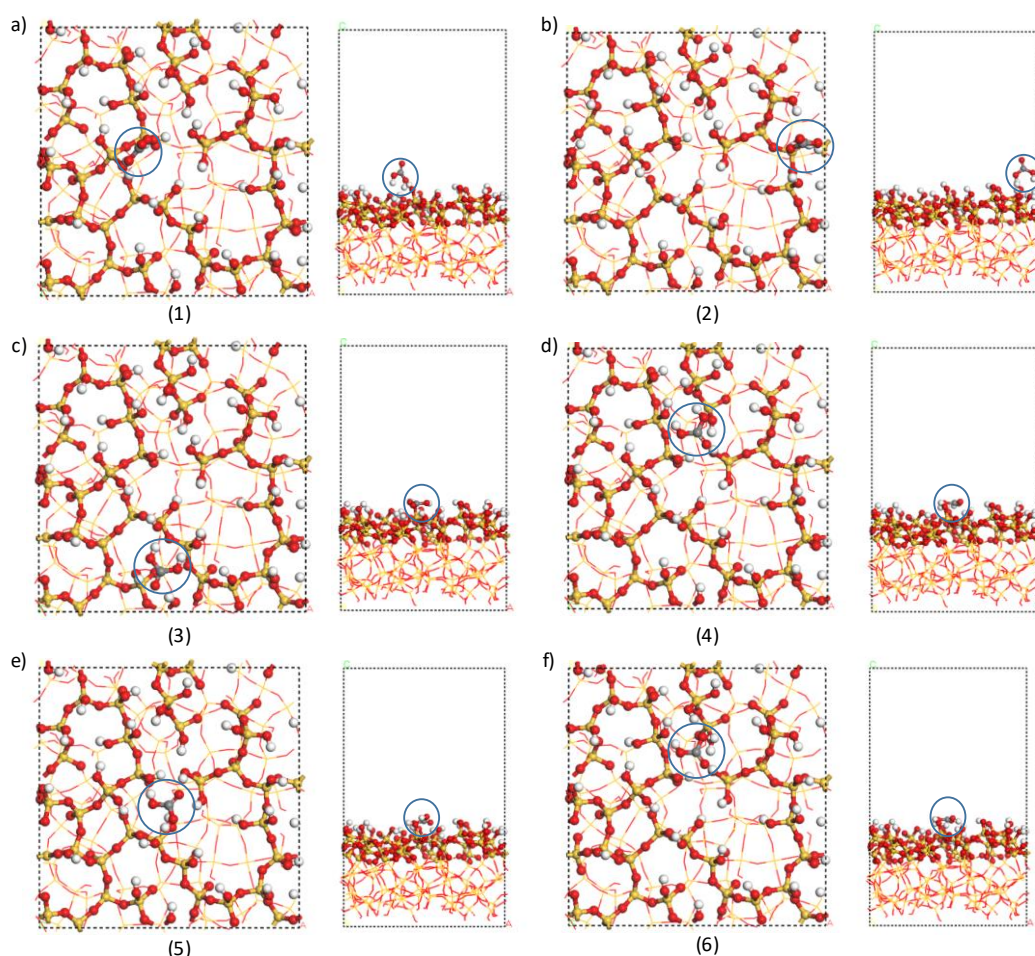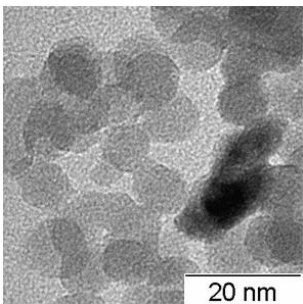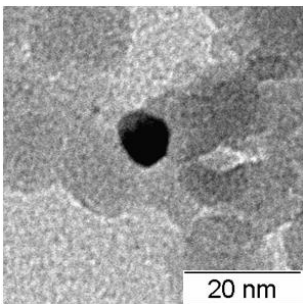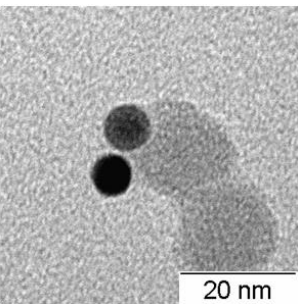
Figure A.8. a-f, Top and side views of the six structures of carbonic acid adsorbed on the SiO_2 surface as obtained from PBE-D3/DZVP calculations. The labels correspond to the numbering of **Table A.3**. A blue circle shows the position of carbonic acid for each structure.

Computational Details and Models. All the calculations on the evaluation of the adsorption of CO_2 and the formation of H_2CO_3 on SiO_2 were performed using the CP2K code.[19-20] The PBE density functional was used[21] in combination with D3 dispersion corrections as proposed by Grimme and co-workers.[22] The DFT calculations were performed using GTH pseudo potentials,[23-24] plane-waves and Gaussian basis sets.[25] The DZVP basis set was used for all the atoms.[26] The energy cutoff selected for the auxiliary plane wave basis set was equal to 300 Ry. The total energy was converged to 5×10^{-7} Hartree. The convergence criteria equal to 2×10^{-4} Hartree/bohr and 3×10^{-3} bohr were used for the gradient and the displacement respectively. We selected one of the models of amorphous SiO_2 developed by A. Comas-Vives.[27] In particular we considered the one with the highest degree of hydroxylation, with an OH coverage equal to 7.2 OH per nm^2, since it is the one that represents best the experimental system. The model has dimensions equal to 21.4 Å $\times$ 21.4 Å $\times$ 34.2 Å The Gibbs energies have been calculated at 230 °C and 5 bar. The entropy of adsorbed species at 230 °C was calculated using the harmonic approximation, with all the degrees of freedom treated as vibrational.

Appendix A

A.2 Additional data

Table A.4. TEM images and EDX analysis of silica-supported 1wt% metal catalysts with 5 randomly selected areas.

	Cu/SiO$_2$	Ag/SiO$_2$	Au/SiO$_2$
Metal (wt%)	1.2	1.5	1.2

UNIVERSITAT ROVIRA I VIRGILI
CONTINUOUS HYDROGENATION OF CARBON DIOXIDE TO FORMATES AND FORMIC ACID OVER HETEROGENEOUS CATALYSTS
Juan José Corral Pérez

Supplementary information of chapter 3

Table A.5. PBE-D''/plane-wave calculated vibrational frequencies of identified formates (κ^2-HCOO and κ^1-HCOO), formic acid (HCOOH), carbonic acid (H_2CO_3), and carbonates (CO_3) on Cu(111), Ag(111), and Au(111) as well as of isolated CO_2 and H_2CO_3. Vibrations of HCOO are labelled as: $v_1 \equiv$ O–C–O symmetric deformation, $v_2 \equiv$ out of plane bend, $v_3 \equiv$ O–C–O symmetric stretch, $v_4 \equiv$ C–H in plane bend, $v_5 \equiv$ O–C–O asymmetric stretch, $v_6 \equiv$ C–H stretch. Vibrational frequencies of CO_3 and CO_2 are written in table's columns according to frequency similarity to HCOO vibrations, whereas for HCOOH and H_2CO_3 the seven highest frequencies are stated, where v_7 & $v'_7 \equiv$ O–H stretch, $v_6 \equiv$ C–H stretch (HCOOH only), $v_5 \equiv$ C=O stretch. The most stable adsorption mode of each species is highlighted with coloured stripe (cf. refer to **Table A.8**, **Table A.9** and **Table A.10**).

	v_1	v_2	v_3	v_4	v_5	v_6	v_7	v'_7
Cu(111)								
κ_2–HCOO$_{top-top}$	738	981	1299	1306	1502	2927		
κ_2–HCOO$_{top-bridge}$	738	978	1272	1299	1494	2943		
κ_1–HCOO$_{O-hollow}$	707	979	1092	1307	1673	2894		
κ_1–HCOO$_{O-bridge}$	684	961	1066	1299	1711	2627		
κ_1–HCOO$_{O-top\,(0°)}$	717	904	1141	1303	1709	2172		
κ_1–HCOO$_{O-top\,(30°)}$	714	924	1132	1258	1711	2145		
HCOOH O$_{top}$+H$_{bridge}$	989	1129	1285	1344	1630	2988	3103	
HCOOH O$_{top}$+H$_{top}$	990	1130	1291	1342	1633	2986	3095	
CO$_3$ top–top	664	752	927	1101	1533			
CO$_3$ bridge–top	646	726	745	1088	1685			
CO$_3$ bridge–bridge	639	764	900	949	1694			
CO$_3$ hollow–hollow	628	752	887	916	1708			
Ag(111)								
κ_2–HCOO$_{top-top}$	724	983	1290	1303	1519	2872		
κ_2–HCOO$_{top-bridge}$	731	987	1281	1300	1507	2881		
κ_1–HCOO$_{O-hollow}$	/							
κ_1–HCOO$_{O-bridge}$	678	962	1128	1294	1688	2514		
κ_1–HCOO$_{O-top\,(0°)}$	701	916	1169	1269	1690	2174		
κ_1–HCOO$_{O-top\,(30°)}$	695	919	1164	1248	1690	2146		
HCOOH O$_{top}$+H$_{bridge}$	997	1114	1279	1344	1666	2973	3257	
HCOOH O$_{top}$+H$_{top}$	999	1112	1279	1344	1665	2963	3234	
H$_2$CO$_3$ O$_{top}$+H$_{bridge}$	969	1113	1228	1425	1669		3331	3737
CO$_3$ top–top	/							
CO$_3$ bridge–top	641	770	851	1127	1535			
CO$_3$ bridge–bridge	612	775	881	1006	1574			
CO$_3$ hollow–hollow	/							
Au(111)								
κ_2–HCOO$_{top-top}$	736	968	1277	1285	1509	2891		
κ_2–HCOO$_{top-bridge}$	728	968	1270	1285	1506	2886		
κ_1–HCOO$_{O-hollow}$	/							
κ_1–HCOO$_{O-bridge}$	654	955	1101	1277	1680	2392		
κ_1–HCOO$_{O-top\,(0°)}$	680	917	1132	1256	1687	2063		
κ_1–HCOO$_{O-top\,(30°)}$	689	963	1162	1293	1651	2548		
HCOOH O$_{top}$+H$_{bridge}$	1000	1108	1273	1343	1667	2966	3348	
HCOOH O$_{top}$+H$_{top}$	999	1109	1275	1341	1664	2969	3266	
CO$_3$ top–top	613	739	953	1198	1486			
CO$_3$ bridge–top	635	759	866	1130	1538			
CO$_3$ bridge–bridge	/							
CO$_3$ hollow–hollow	/							
vacuum								
CO$_2$	651			1301		2344		
H$_2$CO$_3$	941	1072	1228	1406	1748		3752	3753

Appendix A

Table A.6. Estimated lifetime of κ^1-HCOO (before it transforms to κ^2-HCOO) at $T = 230$ °C. The lifetime was calculated as $\tau = v^{-1} \exp(E^*/kT)$, where the value of 10^{12} s^{-1} was taken for the frequency prefactor v; E^* is the κ^1-HCOO $\rightarrow \kappa^2$-HCOO energy barrier (see **Figure A.2**) and k is the Boltzmann constant.
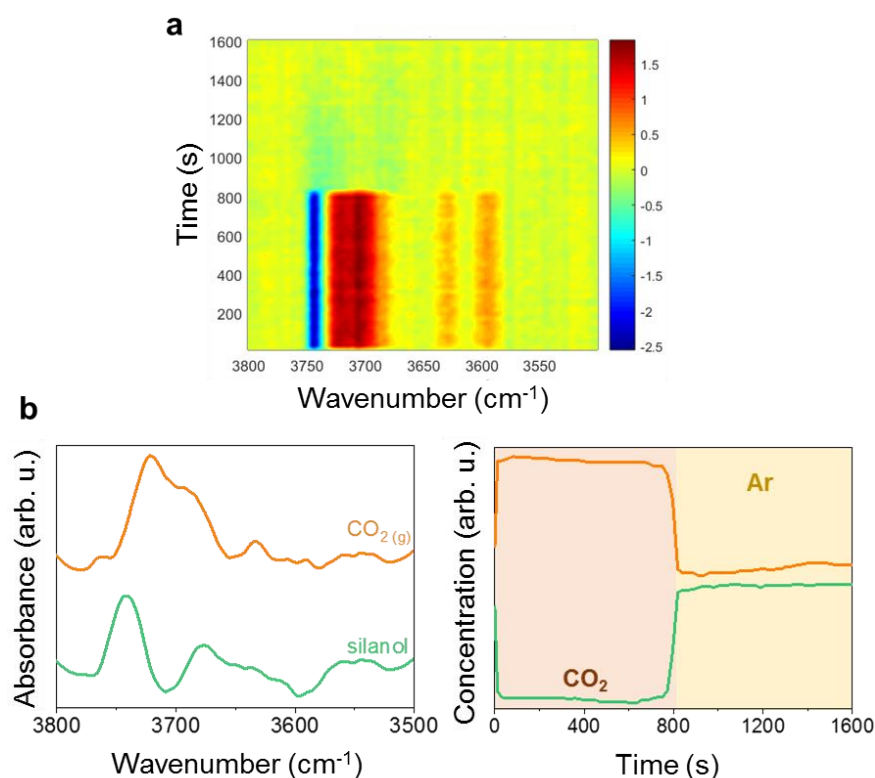
	E^* (eV)	τ (s)
Cu(111)	0.10	10^{-11}
Ag(111)	0.00[a]	on the order of molecular vibration
Au(111)	0.18	10^{-10}

[a]not a local minimum but rather a wide plateau; "instability" confirmed by vibrational calculations
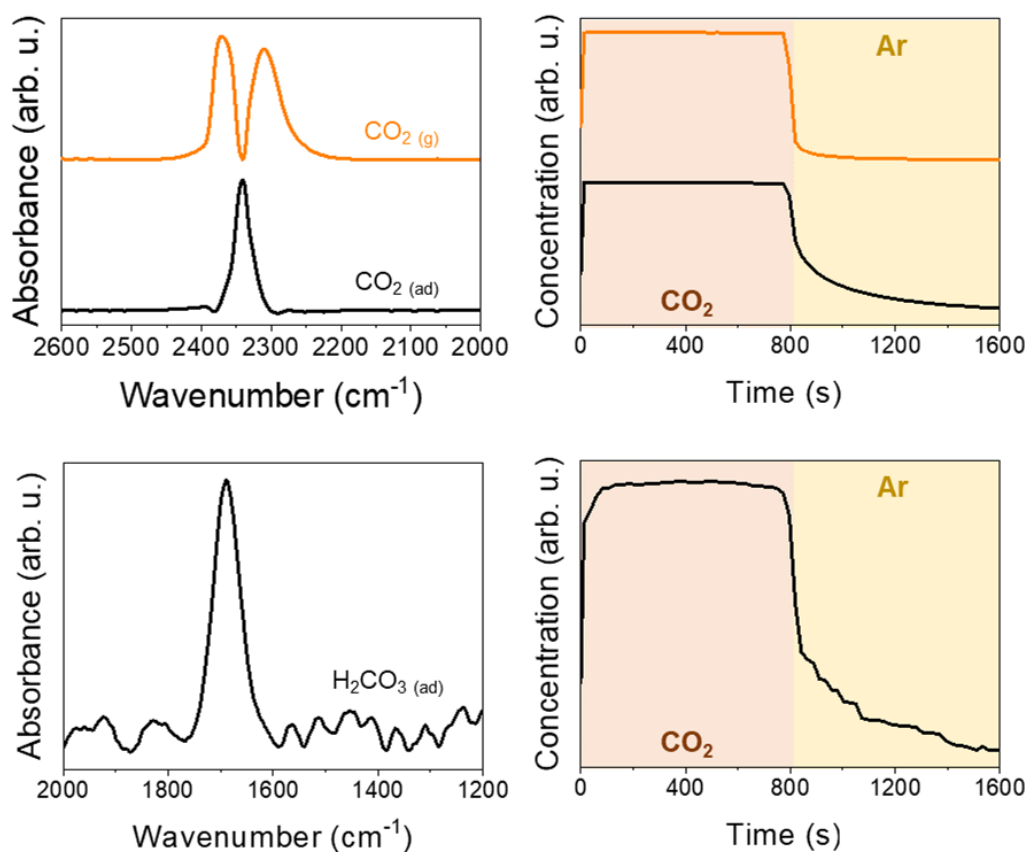
Figure A.9. DRIFT spectra of gaseous and adsorbed CO_2, and H_2CO_3 (left) and the corresponding concentration profiles (right). Spectra and concentration profile obtained by MCR analysis applied on the time-resolved DRIFT spectra of pure SiO_2 upon exposure to CO_2 (the first half period) vs. Ar (the second half period) concentration perturbation experiment at 230 °C and 5 bar.

UNIVERSITAT ROVIRA I VIRGILI
CONTINUOUS HYDROGENATION OF CARBON DIOXIDE TO FORMATES AND FORMIC ACID OVER HETEROGENEOUS CATALYSTS
Juan José Corral Pérez

Supplementary information of chapter 3

Figure A.10. a, Time-resolved DRIFT spectra of SiO_2 upon exposure to CO_2 (the first half period) vs. Ar (the second half period) concentration perturbation experiment at 230 °C and 5 bar. The DRIFT spectra were calculated taking the last spectrum in the Ar atmosphere as background. **b**, (left) Two components spectra, i.e. gaseous CO_2 and silanol groups, and (right) the corresponding concentration profiles obtained by MCR analysis applied on the depicted DRIFT spectra.
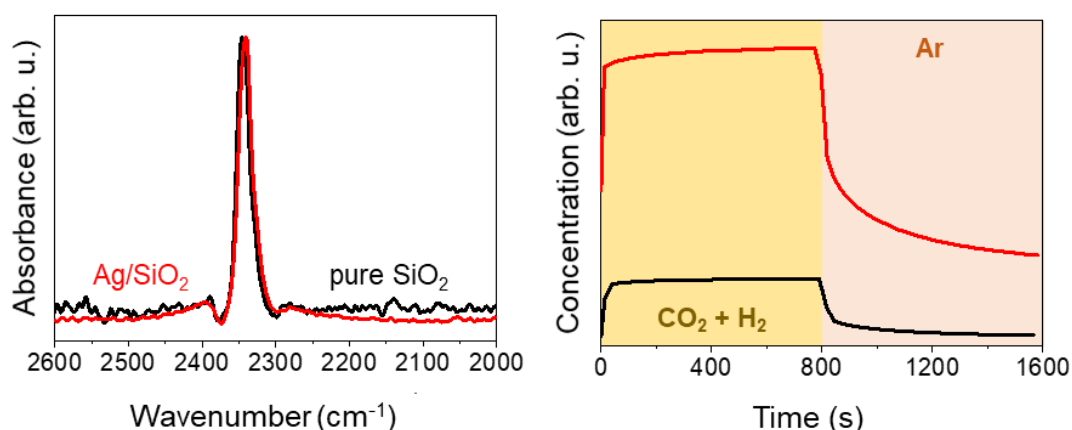
Figure A.11. Comparison between the (left) spectra of adsorbed CO_2, and (right) the corresponding concentration profile (normalized by the spectral intensity). Spectra and concentration profile obtained by MCR analysis applied on the time-resolved DRIFT spectra of 1 wt% Ag/SiO_2 and pure silica, respectively, upon exposure to CO_2 (the first half period) vs. Ar (the second half period) concentration perturbation experiment at 230 °C and 5 bar.

Appendix A
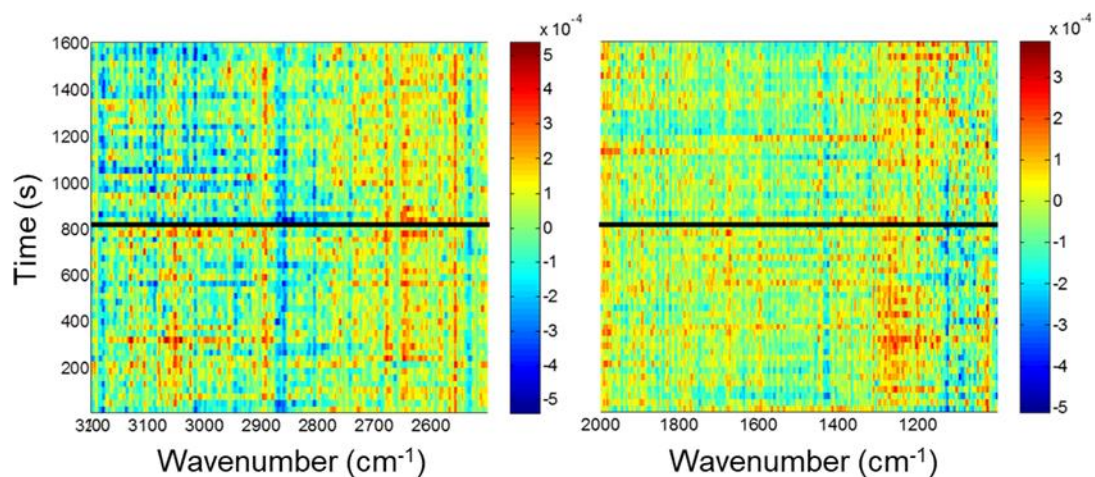
Figure A.12. Time-resolved DRIFT spectra of silica upon exposure to $CO_2:H_2$ = 1:1 molar ratio (the first half period) vs. Ar (the second half period) concentration perturbation experiment at 230 °C and 5 bar. The DRIFT spectra were calculated taking the last spectrum in the Ar atmosphere as background.

Table A.7. Calculated areas (A) of the bands at 1600 and 1688 cm^{-1} shown in *in situ* DRIFT spectra of supported 1 wt% metal catalysts upon exposure to $CO_2:H_2$ = 1:1 (molar ratio) at 230 °C (Figure 2).
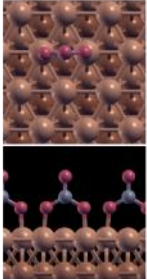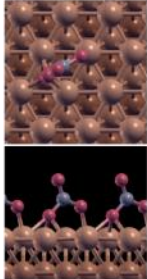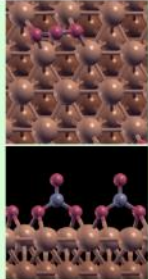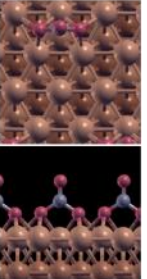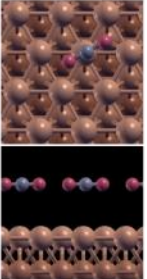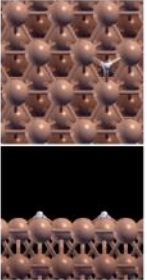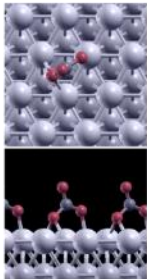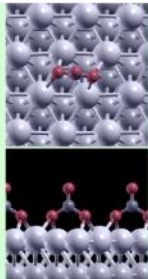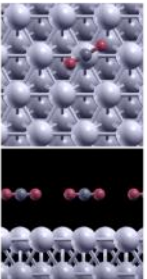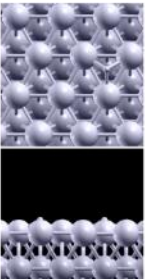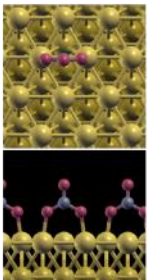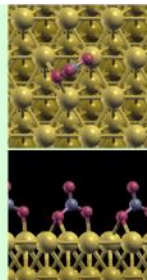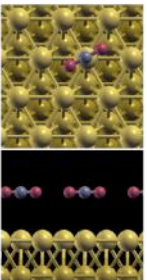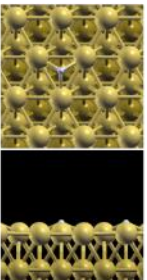
	Pressure (bar)	$A_{band\ at\ 1600\ cm^{-1}}$	$A_{band\ at\ 1688\ cm^{-1}}$	$A_{band\ at\ 1600\ cm^{-1}}/A_{band\ at\ 1688\ cm^{-1}}$
Ag	1	0.22	0.11	1.9
	40	1.00	0.17	5.7
Au	1	0.29	0.17	1.7
	40	0.62	0.18	3.5
Cu	1	0.27	0.15	1.8
	40	0.88	0.26	3.4

UNIVERSITAT ROVIRA I VIRGILI
CONTINUOUS HYDROGENATION OF CARBON DIOXIDE TO FORMATES AND FORMIC ACID OVER HETEROGENEOUS CATALYSTS
Juan José Corral Pérez

Supplementary information of chapter 3

Table A.8. Identified adsorption structures and respective PBE-D"/plane-wave calculated adsorption energies of formates (bidentate κ^2-HCOO and monodentate κ^1-HCOO). The most stable adsorption modes of κ^2- and κ^1-HCOO at each surface are emphasized. Adsorption energies (E_{ads}) are calculated with respect to $CO_{2(g)}$ + ½ $H_{2(g)}$ as $E_{ads} = E_{HCOO/slab} - (E_{slab} + E_{CO2} + ½E_{H2})$, where E_X are the total energies of respective species and slab stands for metal slab (X ≡ HCOO/slab, slab, CO_2, or H_2). For the most stable κ^2-HCOO also the reaction energies (ΔE) for the $CO_{2(ad)}$ + $H_{(ad)}$ → $HCOO_{(ad)}$ reaction are reported.

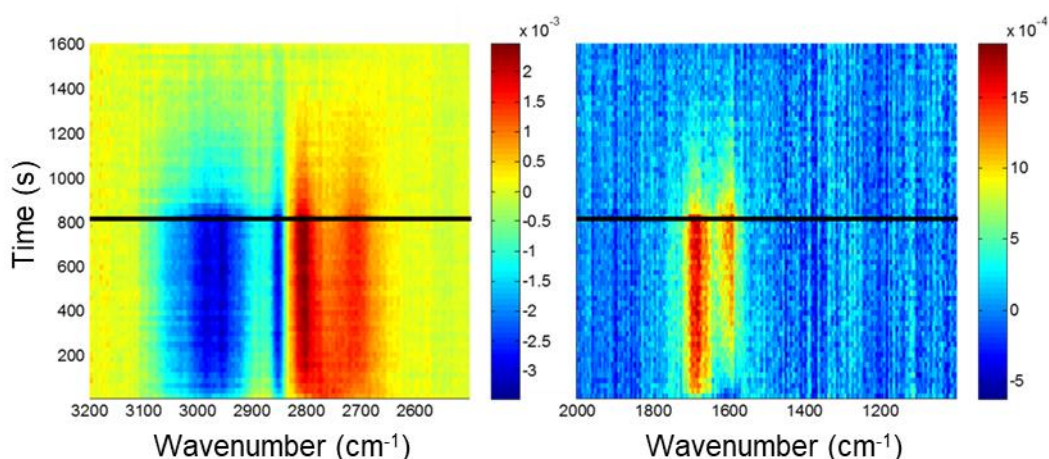|	bidentate κ_2–HCOO		monodentate κ_1–HCOO			
	κ_2 top–top	κ_2 top–bridge	κ_1 O–hollow	κ_1 O–bridge	κ_1 O–top (0°)	κ_1 O–top (30°)
	E_{ads}, ΔE (eV)	E_{ads} (eV)	E_{ads} (eV)	E_{ads} (eV)	E_{ads} (eV)	E_{ads} (eV)
Cu(111)	**−0.79**, −0.37	−0.67	**−0.25**	−0.03	+0.11	+0.14
Ag(111)	**−0.39**, −0.32	−0.38	/	**+0.24**	+0.37	+0.38
Au(111)	**+0.17**, +0.29	/	/	+0.92	**+0.82**	+0.84

Appendix A

Table A.9. Identified adsorption structure and respective PBE-D"/plane-wave calculated binding energies of carbonates (CO_3) on Cu(111), Ag(111), and Au(111). The most stable identified CO_3 adsorption mode on each surface is emphasized. Adsorption modes of CO_2 and H are also presented. Binding energies of species X are calculated as $E_b^X = E_{X/slab} - (E_{slab} + E_X)$. For CO_2 the binding energy equals the adsorption energy. Label "wrt" stands for "with respect to".

*on Cu(111) it looks more like hollow–top

	CO_3 top-top	CO_3 bridge–top*	CO_3 bridge–bridge	CO_3 hollow–hollow	CO_2	H_{fcc}
	E_b wrt $CO_{3(g)}$ (eV)	E_b wrt $CO_{3(g)}$ (eV)	E_b wrt $CO_{3(g)}$ (eV)	E_b wrt $CO_{3(g)}$ (eV)	E_{ads} wrt $CO_{2(g)}$ (eV)	E_b wrt $H_{(g)}$ (eV)
Cu(111)	−3.91	−4.23	**−4.33**	−4.25	−0.16	−2.53
Ag(111)	/	−3.51	**−3.59**	/	−0.17	−2.15
Au(111)	−2.57	**−2.59**	/	/	−0.20	−2.17

UNIVERSITAT ROVIRA I VIRGILI
CONTINUOUS HYDROGENATION OF CARBON DIOXIDE TO FORMATES AND FORMIC ACID OVER HETEROGENEOUS CATALYSTS
Juan José Corral Pérez

Supplementary information of chapter 3

Table A.10. Adsorption structures and respective PBE-D"/plane-wave calculated adsorption energies of formic acid (HCOOH) on Cu(111), Ag(111), and Au(111) and carbonic acid (H_2CO_3) on Ag(111). The most stable identified adsorption mode on each surface is emphasized. In the $O_{top}+H_{bridge}$ adsorption mode the HCOOH can orient across either the hcp or the fcc site: calculations indicate that both orientations are degenerate (the difference is 2 meV, which is below computational accuracy).
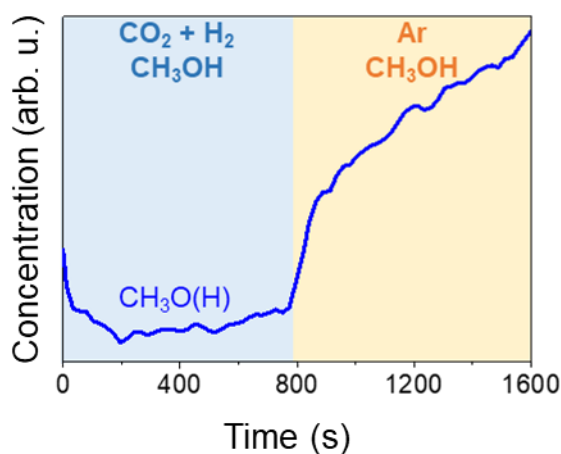

Figure A.13. Time-resolved DRIFT spectra of 1 wt% Ag/SiO_2 upon exposure to CH_3OH during $CO_2:H_2$ = 1:1 molar ratio (the first half period) vs. Ar (the second half period) concentration perturbation experiment at 230 °C and 5 bar. The DRIFT spectra were calculated taking the last spectrum in the Ar and CH_3OH atmosphere as background.

Appendix A
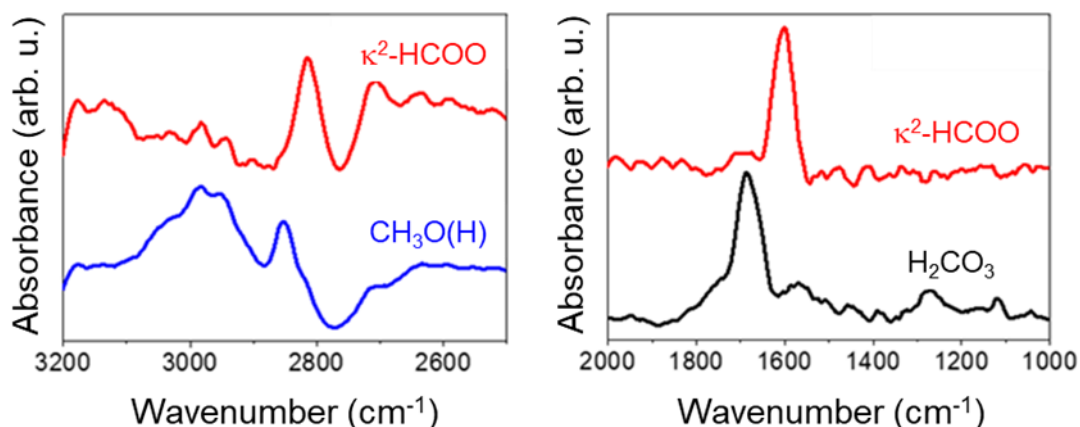
Figure A.14. Components spectra obtained by MCR analysis applied on the DRIFT spectra shown in **Figure A.13**.

Figure A.15. Concentration profile of $CH_3O(H)$ obtained by MCR analysis applied on the DRIFT spectra shown in **Figure A.13**.

Figure A.16. Time-resolved DRIFT spectra of silica upon exposure to CH_3OH during $CO_2:H_2 = 1:1$ molar ratio (the first half period) vs. Ar (the second half period) concentration perturbation experiment at 230 °C and 5 bar. The DRIFT spectra were calculated taking the last spectrum in the Ar and CH_3OH atmosphere as background.
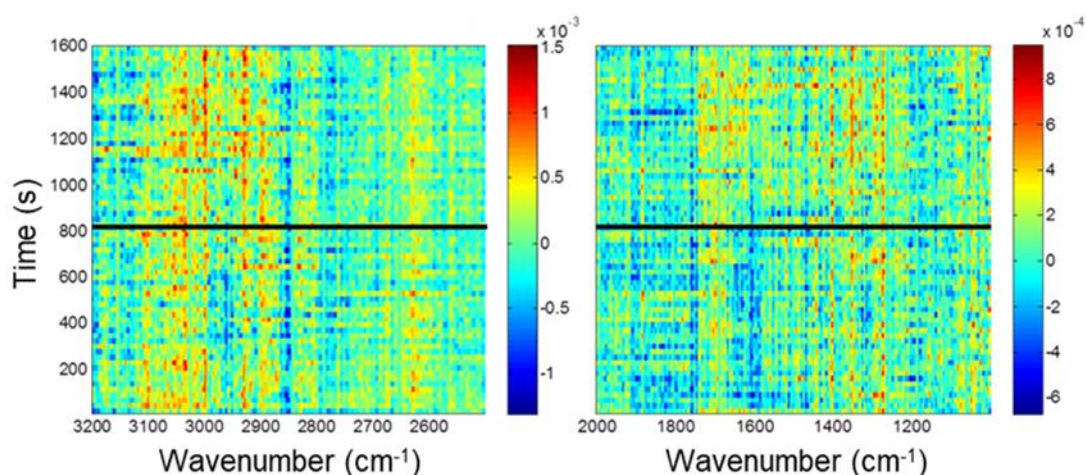
UNIVERSITAT ROVIRA I VIRGILI
CONTINUOUS HYDROGENATION OF CARBON DIOXIDE TO FORMATES AND FORMIC ACID OVER HETEROGENEOUS CATALYSTS
Juan José Corral Pérez

Supplementary information of chapter 3

Adsorption and evacuation measurements. CH_3OH (500 mbar) was introduced into the DRIFTS cell by passing helium through a saturator and physically adsorbed molecules were removed by evacuation at 0 mbar using a HiCube Eco turbo pumping station (Pfeiffer Vacuum) for 10 min. Afterwards, the continuous flow of the reactant mixture (CO_2:H_2 = 1:1 molar ratio) was introduced to the reaction cell at 1 and 40 bar respectively. The background spectra were recorded before flowing the CH_3OH and reactant mixture, respectively.
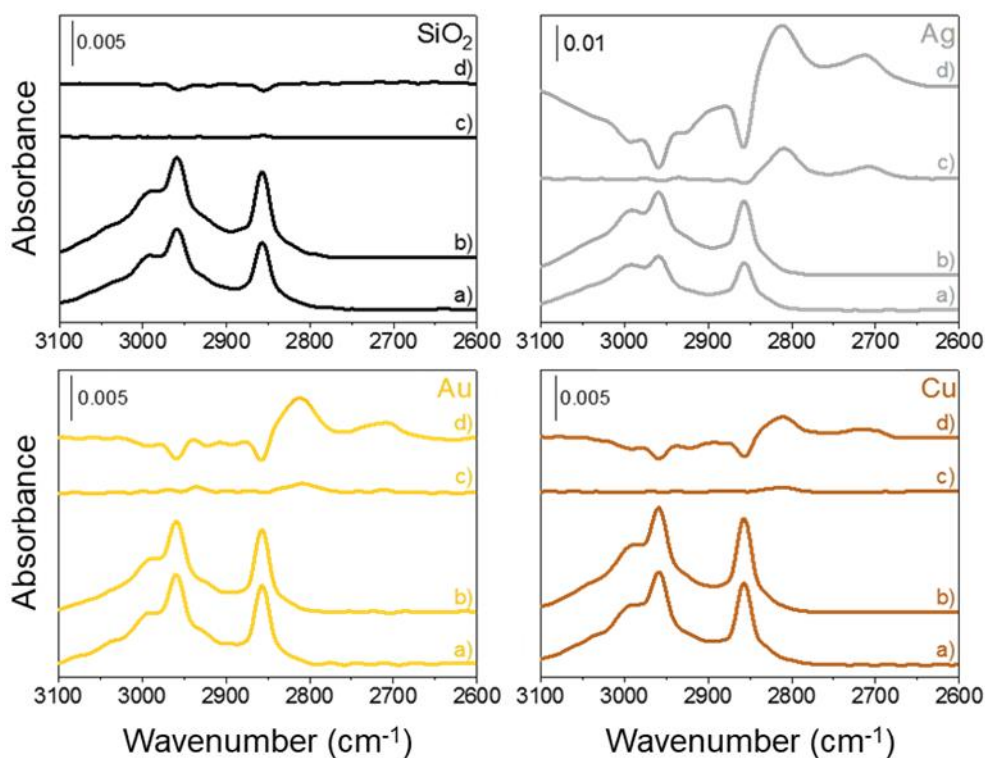

Figure A.17. *In situ* DRIFT spectra of silica and silica-supported 1 wt% metal catalysts at 230 °C. **a**, In presence of CH_3OH (500 mbar). **b**, After evacuation (0 mbar) and upon exposure to CO_2:H_2 (1:1 molar ratio) at **c**, 1 bar and **d**, 40 bar. The background spectra were recorded under H_2 before exposure to CH_3OH and CO_2+H_2, respectively.

Appendix A
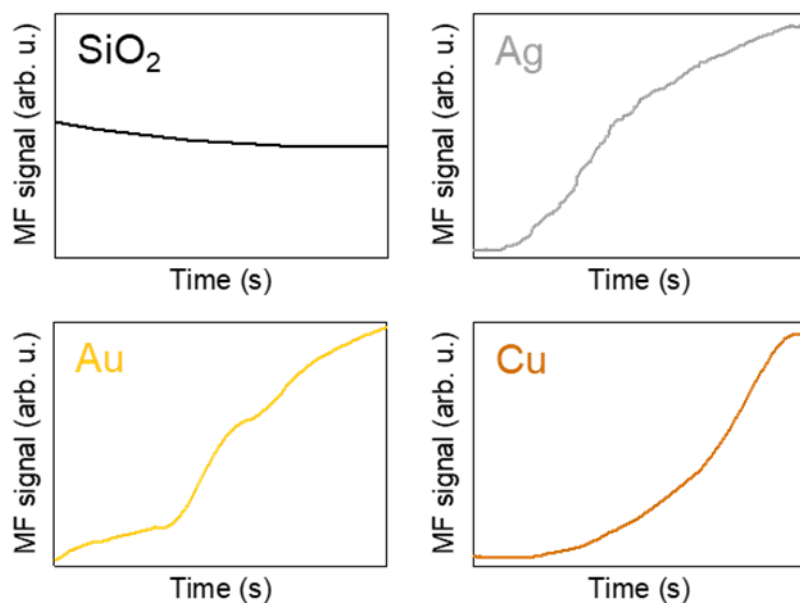
Figure A.18. MS signal of MF (m/z = 60) during *in situ* DRIFTS measurements of silica and silica-supported 1wt% metal catalysts at 230 °C upon exposure to CO_2:H_2 (1:1 molar ratio) at 40 bar when CH_3OH is desorbed and formate species are formed (**Figure A.17d**).
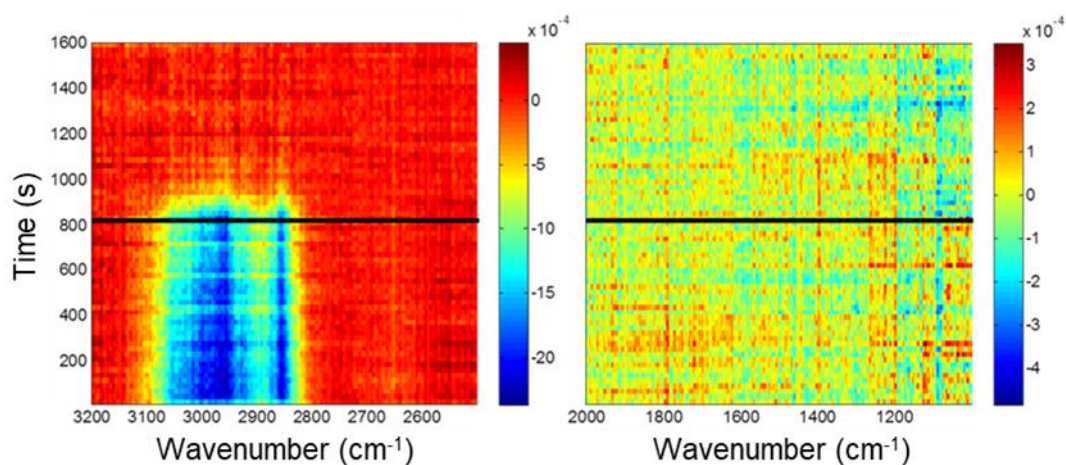
Figure A.19. Time-resolved DRIFT spectra of silica upon exposure to CO_2:H_2 = 1:1 molar ratio during CH_3OH (the first half period) vs. Ar (the second half period) concentration perturbation experiment at 230 °C and 5 bar. The DRIFT spectra were calculated taking the last spectrum in the Ar and CO_2+H_2 atmosphere as background.

UNIVERSITAT ROVIRA I VIRGILI
CONTINUOUS HYDROGENATION OF CARBON DIOXIDE TO FORMATES AND FORMIC ACID OVER HETEROGENEOUS CATALYSTS
Juan José Corral Pérez

Supplementary information of chapter 3
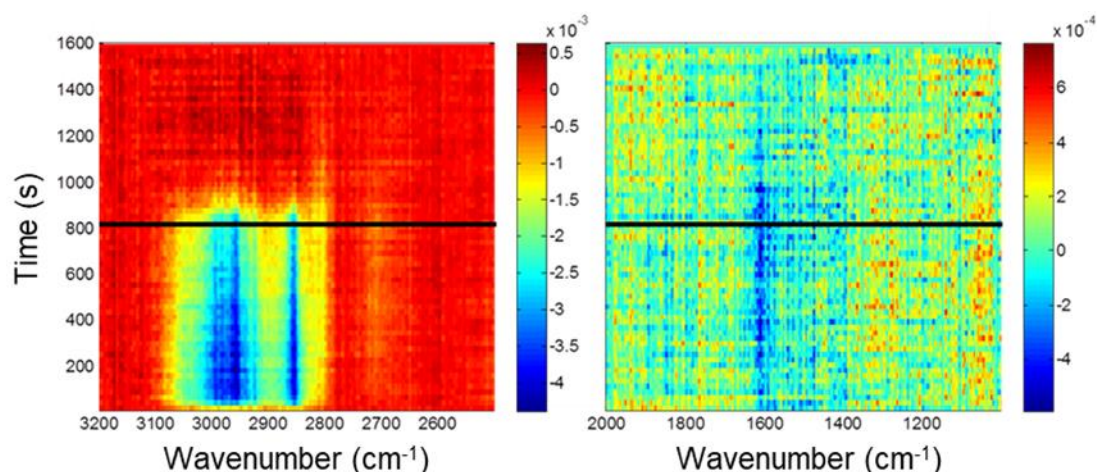
Figure A.20. Time-resolved DRIFT spectra of 1 wt% Ag/SiO_2 upon exposure to CO_2:H_2 = 1:1 molar ratio during CH_3OH (the first half period) vs. Ar (the second half period) concentration perturbation experiment at 230 °C and 5 bar. The DRIFT spectra were calculated taking the last spectrum in the Ar and CO_2+H_2 atmosphere as background.
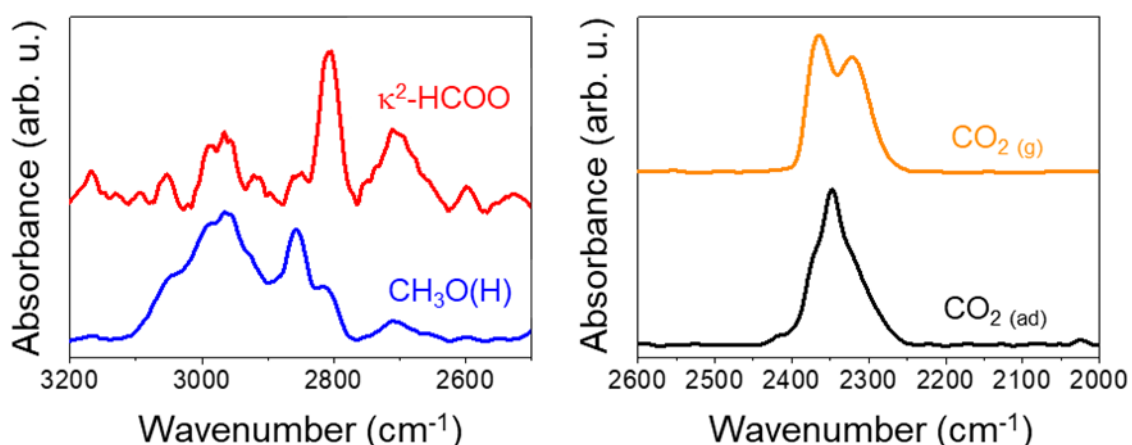
Figure A.21. Components spectra obtained by MCR analysis applied on the DRIFT spectra shown in **Figure A.20**.

Figure A.22. Concentration profile of $CH_3O(H)$ obtained by MCR analysis applied on the DRIFT spectra shown in **Figure A.20**.

<u>Appendix A</u>

Bibliography

1.   Michaelides, A.; Liu, Z. P.; Zhang, C. J.; Alavi, A.; King, D. A.; Hu, P., *J. Am. Chem. Soc.* **2003,** *125* (13), 3704-3705.
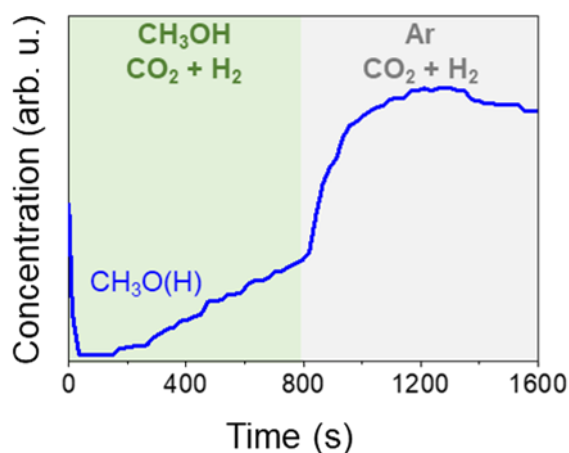2.   Kokalj, A.; Bonini, N.; Sbraccia, C.; de Gironcoli, S.; Baroni, S., *J. Am. Chem. Soc.* **2004,** *126* (51), 16732-16733.
3.   Peljhan, S.; Koller, J.; Kokalj, A., *J. Phys. Chem. C* **2014,** *118* (2), 933-943.
4.   Vanderbilt, D., *Phys. Rev. B* **1990,** *41* (11), 7892-7895.
5.   Ultrasoft pseudopotentials for H, C, O, Cu, Ag, and Au atoms were taken from the Quantum Espresso PseudoPotential Download Page: <u>http://www.quantum-espresso.org/pseudopotentials</u> (files: H.pbe-rrkjus.UPF, C.pbe-rrkjus.UPF, O.pbe-rrkjus.UPF, Cu.pbe-d-rrkjus.UPF, Ag.pbe-d-rrkjus.UPF, Au.pbe-nd-rrkjus.UPF), 2015.
6.   Giannozzi, P.; Baroni, S.; Bonini, N.; Calandra, M.; Car, R.; Cavazzoni, C.; Ceresoli, D.; Chiarotti, G. L.; Cococcioni, M.; Dabo, I.; Dal Corso, A.; de Gironcoli, S.; Fabris, S.; Fratesi, G.; Gebauer, R.; Gerstmann, U.; Gougoussis, C.; Kokalj, A.; Lazzeri, M.; Martin-Samos, L.; Marzari, N.; Mauri, F.; Mazzarello, R.; Paolini, S.; Pasquarello, A.; Paulatto, L.; Sbraccia, C.; Scandolo, S.; Sclauzero, G.; Seitsonen, A. P.; Smogunov, A.; Umari, P.; Wentzcovitch, R. M., *J. Phys.-Condes. Matter* **2009,** *21* (39), 395502.
7.   Giannozzi, P.; Oliviero, A.; Thomas, B.; Oana, B.; Marco Buongiorno, N.; Matteo, C.; Roberto, C.; Carlo, C.; Davide, C.; Matteo, C.; Nicola, C.; Ivan, C.; Andrea Dal, C.; Stefano de, G.; Pietro, D.; Robert, D.; Andrea, F.; Andrea, F.; Guido, F.; Giorgia, F.; Ralph, G.; Uwe, G.; Feliciano, G.; Tommaso, G.; Junteng, J.; Mitsuaki, K.; Hsin-Yu, K.; Anton, K.; Emine, K.; Michele, L.; Margherita, M.; Nicola, M.; Francesco, M.; Ngoc Linh, N.; Huy-Viet, N.; Alberto, O.-d.-l.-R.; Lorenzo, P.; Samuel, P.; Dario, R.; Riccardo, S.; Biswajit, S.; Martin, S.; Ari Paavo, S.; Alexander, S.; Iurii, T.; Timo, T.; Paolo, U.; Nathalie, V.; Xifan, W.; Stefano, B., *J. Phys-Conds. Mat.* **2017,** *29* (46), 465901.
8.   Monkhorst, H. J.; Pack, J. D., *Phys. Rev. B* **1976,** *13* (12), 5188-5192.
9.   Methfessel, M.; Paxton, A. T., *Phys. Rev. B* **1989,** *40* (6), 3616-3621.
10. Henkelman, G.; Jonsson, H., *J. Chem. Phys.* **2000,** *113* (22), 9978-9985.
11. Henkelman, G.; Uberuaga, B. P.; Jonsson, H., *J. Chem. Phys.* **2000,** *113* (22), 9901-9904.
12. Baroni, S.; de Gironcoli, S.; Dal Corso, A.; Giannozzi, P., *Rev. Mod. Phys.* **2001,** *73* (2), 515-562.
13. Grimme, S., *J. Comput. Chem.* **2006,** *27* (15), 1787-1799.
14. Barone, V.; Casarin, M.; Forrer, D.; Pavone, M.; Sambi, M.; Vittadini, A., *J. Comput. Chem.* **2009,** *30* (6), 934-939.
15. Gustincic, D.; Kokalj, A., *Phys. Chem. Chem. Phys.* **2015,** *17* (43), 28602-28615.
16. Syomin, D.; Kim, J.; Koel, B. E.; Ellison, G. B., *J. Phys. Chem. A* **2001,** *105* (35), 8387-8394.
17. Rocklein, M. N.; Arnold, T. V.; Gerth, C. M.; Land, D. P., *J. Phys. Chem. A* **2004,** *108* (3), 1009-1013.
18. Kokalj, A., *J. Mol. Graph.* **1999,** *17* (3-4), 176-179.
19. Mueller, L. L.; Griffin, G. L., *J. Catal.* **1987,** *105* (2), 352-358.
20. Hutter, J.; Iannuzzi, M.; Schiffmann, F.; VandeVondele, J., *Wires. Comput. Mol. Sci.* **2013,** *4* (1), 15-25.
21. Perdew, J. P.; Burke, K.; Ernzerhof, M., *Physical Review Letters* **1996,** *77* (18), 3865-3868.
22. Grimme, S.; Antony, J.; Ehrlich, S.; Krieg, H., *J. Chem. Phys.* **2010,** *132* (15), 154104.
23. Goedecker, S.; Teter, M.; Hutter, J., *Phys. Rev. B* **1996,** *54* (3), 1703-1710.
24. Krack, M., *Theor. Chem. Acc.* **2005,** *114* (1), 145-152.
25. Lippert, B. G.; Parrinello, J. H.; Michele, *Mol. Phys,* **1997,** *92* (3), 477-488.
26. VandeVondele, J.; Hutter, J., *J. Chem. Phys.* **2007,** *127* (11), 114105.
27. Comas-Vives, A., *Phys. Chem. Chem. Phys.* **2016,** *18* (10), 7475-7482.

UNIVERSITAT ROVIRA I VIRGILI
CONTINUOUS HYDROGENATION OF CARBON DIOXIDE TO FORMATES AND FORMIC ACID OVER HETEROGENEOUS CATALYSTS
Juan José Corral Pérez

Supplementary information of chapter 3

Appendix A

Appendix A

UNIVERSITAT ROVIRA I VIRGILI
CONTINUOUS HYDROGENATION OF CARBON DIOXIDE TO FORMATES AND FORMIC ACID OVER HETEROGENEOUS CATALYSTS
Juan José Corral Pérez
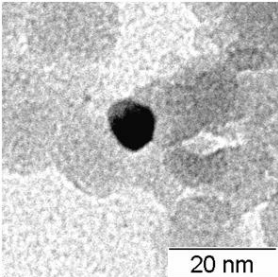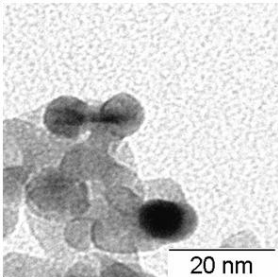
Supplementary information of chapter 4

Appendix B – Supplementary information of chapter 4

Table B.1. The amounts of adsorbed-desorbed CO_2 and NH_3 to measure the basicity and acidity of the different supports

Support	µmol CO_2 g_{cat}^{-1}	µmol NH_3 g_{cat}^{-1}
ZrO_2	144	362
γ-Al_2O_3	88	575
CeO_2	117	89
SiO_2	-	-
pumice	-	-

-The detected signals of CO_2 and NH_3 were too small to be quantified

Table B.2. TEM images, metal loading (determined by EDX analysis with 5 randomly selected areas) and BET surface area of silica-, zirconia- and γ-alumina-supported silver catalysts prepared via the impregnation method

	SiO_2	ZrO_2	γ-Al_2O_3
	20 nm	20 nm	20 nm
Ag (wt%)	1.5	1.7	1.8
Ag size (nm)	≤8	≤9	≤8
S_{BET} (m^2 g^{-1})	146	95	155

Appendix B
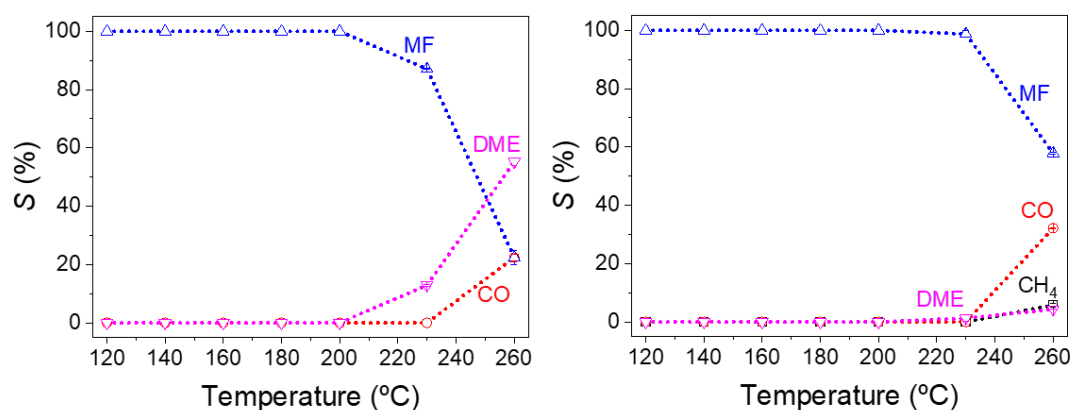
Figure B.1. Selectivity (S) to MF, DME, CO and CH_4 over Ag supported on (left) γ-alumina and (right) zirconia prepared via the SOMC approach. Reaction conditions: CO_2:H_2:CH_3OH = 4:4:1 (molar ratio), 300 bar, GHSV = 9,000 h^{-1}
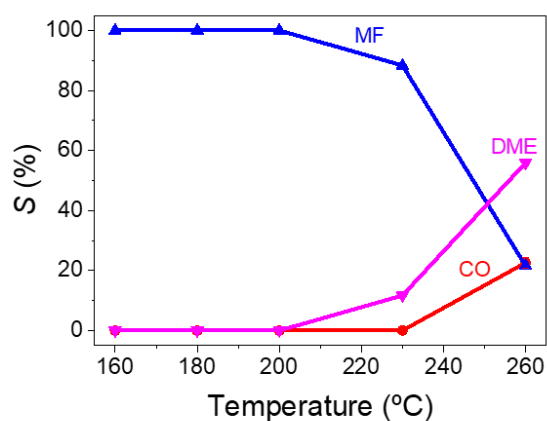
Figure B.2. Selectivity (S) to MF, DME, CO and CH_4 over Ag supported on γ-alumina prepared via the impregnation method. Reaction conditions: CO_2:H_2:CH_3OH = 4:4:1 (molar ratio), 300 bar, GHSV = 9,000 h^{-1}

UNIVERSITAT ROVIRA I VIRGILI
CONTINUOUS HYDROGENATION OF CARBON DIOXIDE TO FORMATES AND FORMIC ACID OVER HETEROGENEOUS CATALYSTS
Juan José Corral Pérez

Supplementary information of chapter 4
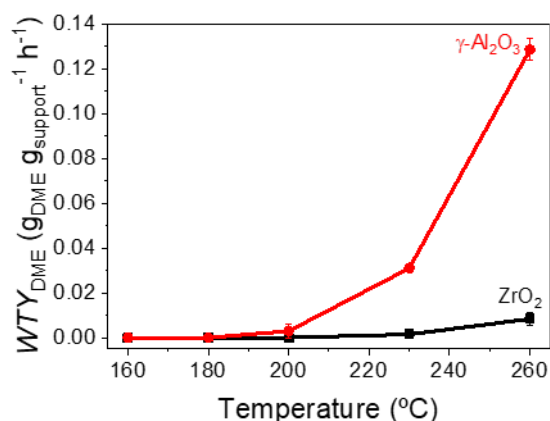
Figure B.3. Effects of reaction temperature on weight time yield of DME (WTY_{DME}) over γ-alumina and zirconia. Reaction conditions: 300 bar, GHSV = 9000 h^{-1}, CO_2:H_2:CH_3OH = 4:4:1 (molar ratio)
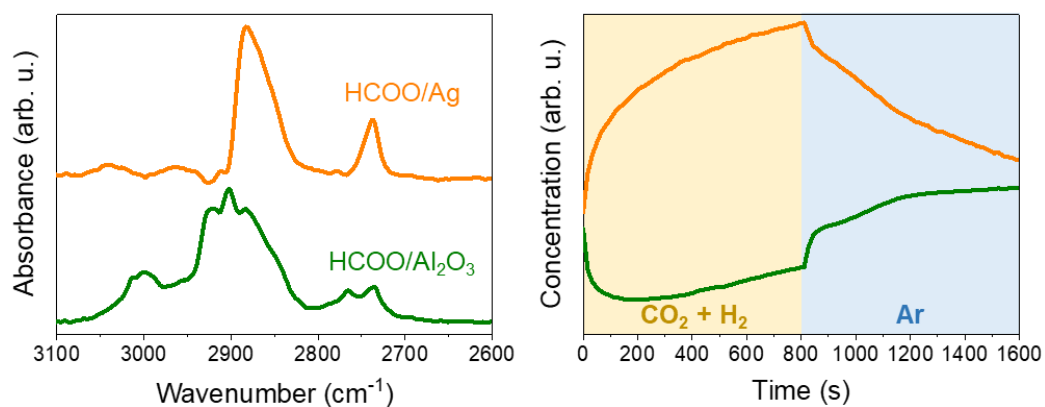
Figure B.4. (left) Two components spectra, i.e. formates over Ag and Al_2O_3 respectively, and (right) the corresponding concentration profiles obtained by MCR analysis applied on the time-resolved DRIFT spectra of Ag/Al_2O_3 upon exposure to CO_2:H_2 = 1:1 molar ratio (the first half period) vs. Ar (the second half period) concentration perturbation experiment at 230 °C and 5 bar. The DRIFT spectra were calculated taking the last spectrum in the Ar atmosphere as background

Appendix B
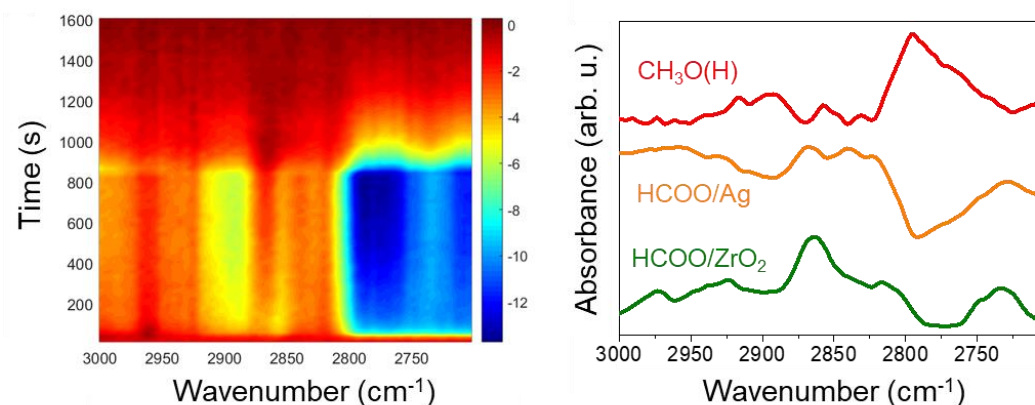
Figure B.5. (left) Time-resolved DRIFT spectra of Ag/ZrO$_2$ upon exposure to CH$_3$OH during CO$_2$:H$_2$ = 1:1 molar ratio (the first half period) vs. Ar (the second half period) concentration perturbation experiment at 230 °C and 5 bar. The DRIFT spectra were calculated taking the last spectrum in the Ar and CH$_3$OH atmosphere as background. No baseline correction was applied. (right) Three components spectra, i.e. adsorbed CH$_3$OH and formates over Ag and ZrO$_2$ respectively obtained by MCR analysis applied on the depicted DRIFT spectra
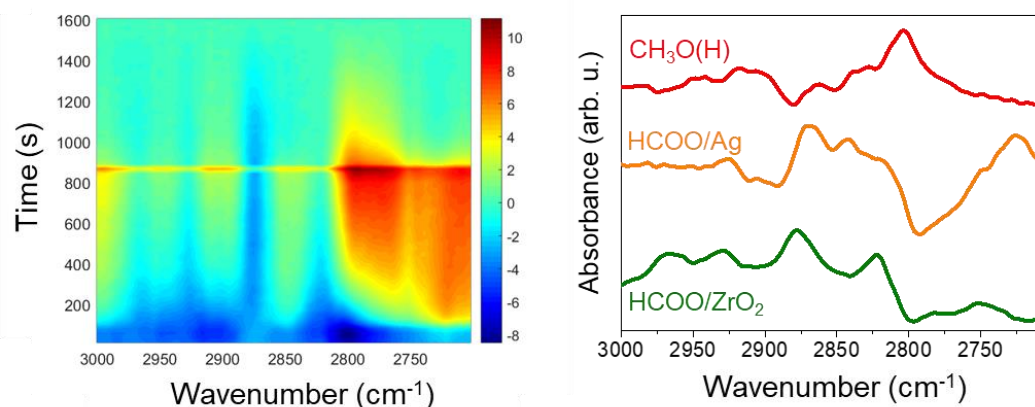
Figure B.6. (left) Time-resolved DRIFT spectra of Ag/ZrO$_2$ upon exposure to CO$_2$:H$_2$ = 1:1 molar ratio during CH$_3$OH (the first half period) vs. Ar (the second half period) concentration perturbation experiment at 230 °C and 5 bar. The DRIFT spectra were calculated taking the last spectrum in the Ar and CO$_2$+H$_2$ atmosphere as background. No baseline correction was applied. (right) Three components spectra, i.e. adsorbed CH$_3$OH and formates over Ag and ZrO$_2$ respectively obtained by MCR analysis applied on the depicted DRIFT spectra

UNIVERSITAT ROVIRA I VIRGILI
CONTINUOUS HYDROGENATION OF CARBON DIOXIDE TO FORMATES AND FORMIC ACID OVER HETEROGENEOUS CATALYSTS
Juan José Corral Pérez

Supplementary information of chapter 4

UNIVERSITAT ROVIRA I VIRGILI
CONTINUOUS HYDROGENATION OF CARBON DIOXIDE TO FORMATES AND FORMIC ACID OVER HETEROGENEOUS CATALYSTS
Juan José Corral Pérez

145

Appendix B

Appendix B

UNIVERSITAT ROVIRA I VIRGILI
CONTINUOUS HYDROGENATION OF CARBON DIOXIDE TO FORMATES AND FORMIC ACID OVER HETEROGENEOUS CATALYSTS
Juan José Corral Pérez

Supplementary information of chapter 5

Appendix C – Supplementary information of chapter 5
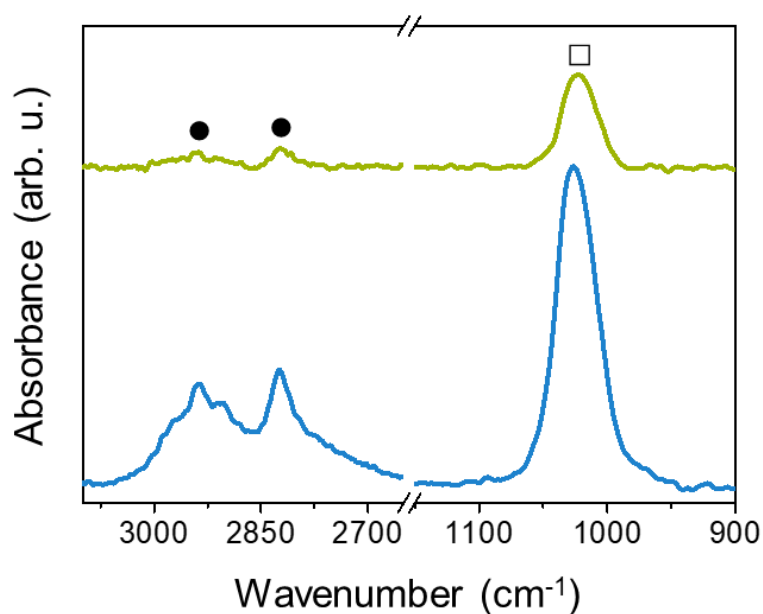
Figure C.1. *In situ* DRIFT spectra of CTF upon exposure to CH₃OH vapor (blue) for 30 min and followed by evacuation under Ar (green) after 2 hours at 140 °C and 5 bar. The background spectrum was recorded under Ar before exposure to CH₃OH. Characteristic bands of methyl and methoxy species are shown respectively with symbols: CH₃ (●) and OCH₃ (□).
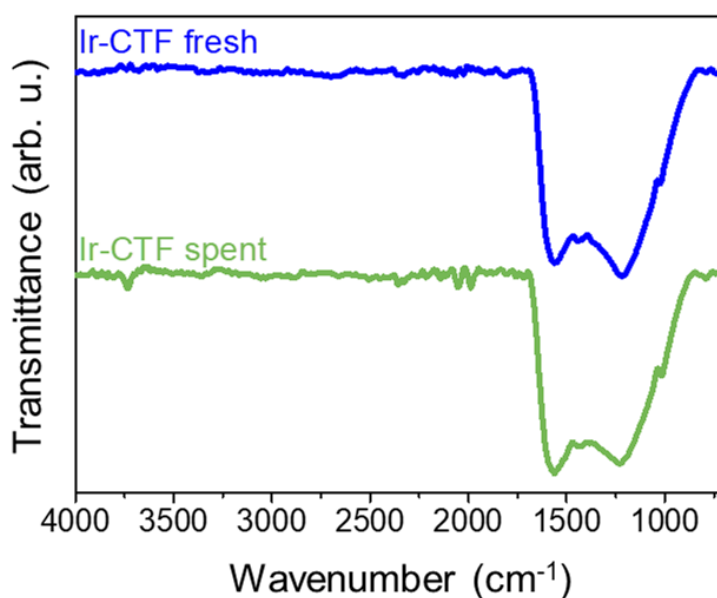
Figure C.2. ATR-IR spectra of Ir-CTF before and after the reaction.

Appendix C
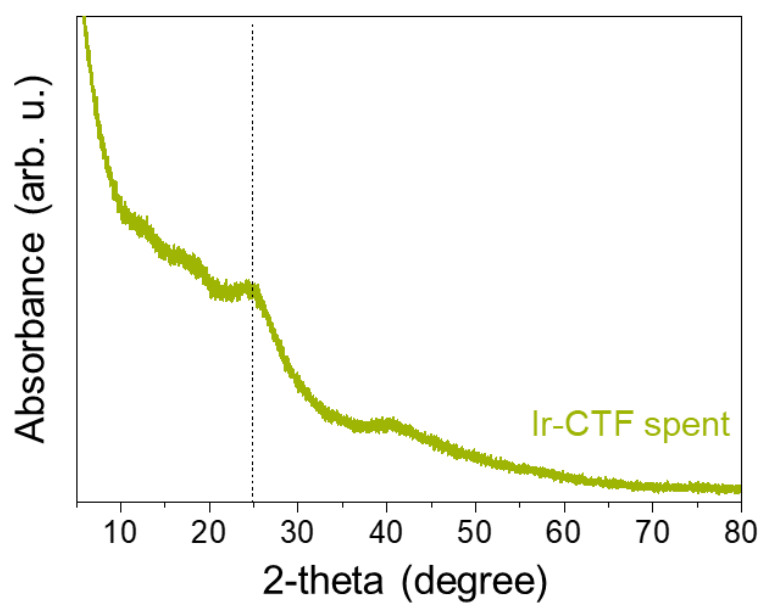
Figure C.3. Powder X-ray diffraction (XRD) pattern of Ir-CTF after the reaction.
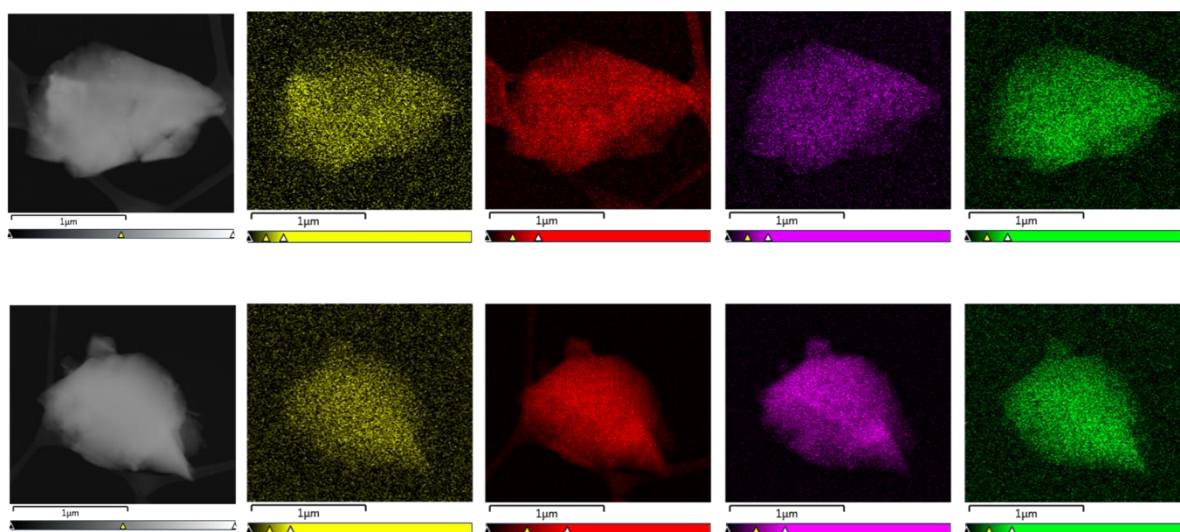
Figure C.4. STEM and EDX mapping images of iridium (yellow), carbon (red), nitrogen (purple), and chlorine (green) for Ir-CTF before (top) and after (bottom) the reaction.

UNIVERSITAT ROVIRA I VIRGILI
CONTINUOUS HYDROGENATION OF CARBON DIOXIDE TO FORMATES AND FORMIC ACID OVER HETEROGENEOUS CATALYSTS
Juan José Corral Pérez

Supplementary information of chapter 5
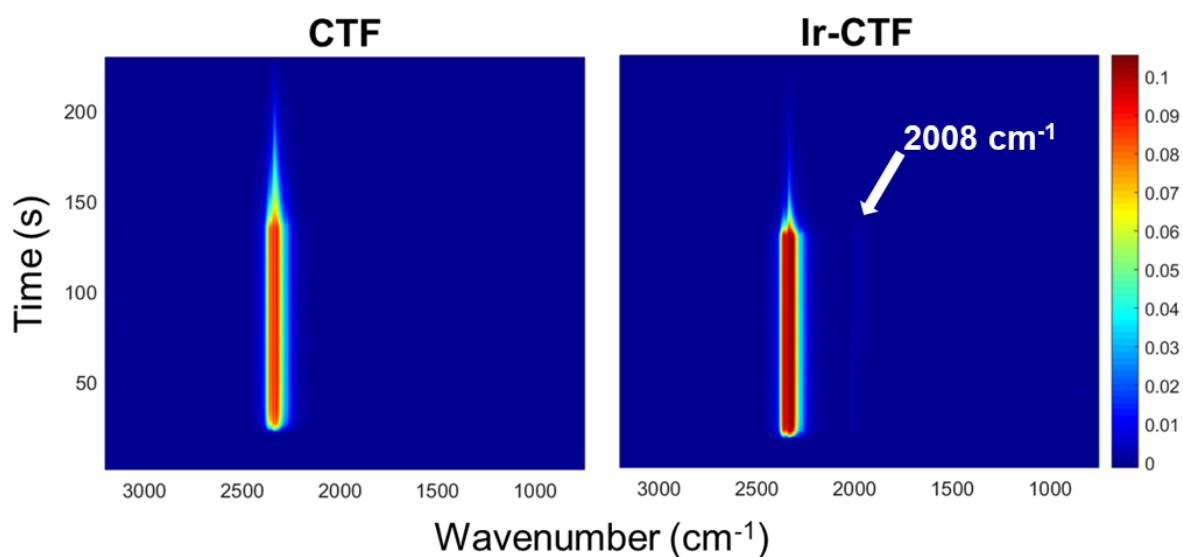
Figure C.5. Time-resolved DRIFT spectra upon exposure to CO_2 (the first half period) and then to Ar (the second half period) concentration perturbation experiment at 140 °C and 5 bar. The DRIFT spectra are shown in milli-absorbance unit taking the last spectrum in the Ar atmosphere as background.

Appendix C

UNIVERSITAT ROVIRA I VIRGILI
CONTINUOUS HYDROGENATION OF CARBON DIOXIDE TO FORMATES AND FORMIC ACID OVER HETEROGENEOUS CATALYSTS
Juan José Corral Pérez

Appendix C

150

SHORTHAND AND GLOSSARY

ΔG^0_{298K}	Gibbs free energy
ALS	Alternating Least Square
ATR	Attenuated Total Reflection
BET	Brunauer-Emmett-Teller
BJH	Barrett-Joyner-Halenda
BPR	Back pressure regulator
BV	Ball valve
Cp*	η^5-pentamethylcyclopentadienyl
CTF	Covalent Triazine Framework
DAD	Diode-array detector
DCP	2,6-dicyanopyridine
DFT	Density Functional Theory
DME	Dimethyl ether
DRIFTS	Diffuse Reflectance Infrared Fourier Transform Spectroscopy
E*	Activation energy
E_b	Adsorption binding energy
EDX	Energy-Dispersive X-ray Spectroscopy
ESRF	European Synchrotron Radiation Facility
ESRL	Earth System Research Laboratory
EXAFS	Extended X-ray Absorption Fine Structure
F	Filter
FID	Flame Ionization Detector
FT	Fourier transform
FTIR	Fourier transform infrared

Shorthand and glossary

GC	Gas chromatography
GHG	Greenhouse gas
GHSV	Gas Hourly Space Velocity
GISS	Goddard Institute for Space Studies
HAADF	High Angle Annular Dark Field
HK	Horvath-Kawazoe
HPLC	High Performance Liquid Chromatography
ICP-OES	Inductively Coupled Plasma Optical Emission Spectrometry
ID	Inner diameter
IEA	International Energy Agency
IR	Infrared
MCR	Multivariate Curve Resolution
MES	Modulation Excitation Spectroscopy
MF	Methyl formate
MFC	Mass flow controller
MS	Mass spectrometry
NASA	National Aeronautics and Space Administration
NOAA	National Oceanic and Atmospheric Administration
NRV	Non-return valve
NV	Needle valve
OD	Outside diameter
PBE	Perdew–Burke–Ernzerhof
PI	Pressure indicator
POF	Porous Organic Framework
PRV	Pressure relief valve
PXRD	Powder X-ray diffraction

UNIVERSITAT ROVIRA I VIRGILI
CONTINUOUS HYDROGENATION OF CARBON DIOXIDE TO FORMATES AND FORMIC ACID OVER HETEROGENEOUS CATALYSTS
Juan José Corral Pérez

Shorthand and glossary

RD	Rupture disc
S	Selectivity
SOMC	Surface organometallic chemistry
SS	Stainless Steel
STEM	Scanning Transmission Electron Microscopy
TCD	Thermal Conductivity Detector
TEM	Transmission Electron Microscopy
TFC	World total final consumption)
TI	Temperature indicator
TOF	Turnover frequency
TPES	World total primary energy supply
WTY	Weight Time Yield
X	Conversion
XANES	X-ray Absorption Near Edge Structure
XAS	X-ray Absorption Spectroscopy
XPS	X-ray Photoelectron Spectroscopy
Y	Yield

Shorthand and glossary

LIST OF PUBLICATIONS

Journal publications

1   Continuous hydrogenation of carbon dioxide to formic acid and methyl formate by a molecular iridium complex stably heterogenized on a covalent triazine.

   Juan José Corral-Pérez, Amelia Billings, Dragos Stoian, and Atsushi Urakawa. *Submitted manuscript*

2   Lewis acidic supports promote the selective hydrogenation of carbon dioxide to methyl formate in the presence of methanol over Ag catalysts.

   Juan José Corral-Pérez, Christophe Copéret, and Atsushi Urakawa. *Submitted manuscript*

3   CO_2 hydrogenation on Cu/Al_2O_3: role of metal/support interface in driving the activity and the selectivity of a bifunctional catalyst.

   Erwin Lam, **Juan José Corral-Pérez**, Kim Larmier, Gina Noh, Patrick Wolf, Aleix Comas-Vives, Atsushi Urakawa, and Christophe Copéret. *Submitted manuscript*

4   Plasmonic effect on nanoparticles and pseudo single atoms of silver based catalysts.

   Mahak Dhimana, Ravishankar Kadamb, Dragos Stoian, **Juan José Corral-Pérez**, Atsushi Urakawa, Radha V. Jayaram, and Vivek Polshettiwar. *Submitted manuscript*

5   Decisive role of perimeter sites in silica-supported Ag nanoparticles in selective hydrogenation of CO_2 to methyl formate in the presence of methanol.

   Juan José Corral-Pérez, Atul Bansode, C. S. Praveen, Anton Kokalj, Helena Reymond, Aleix Comas-Vives, Joost VandeVondele, Christophe Copéret, Philipp Rudolf von Rohr, and Atsushi Urakawa. Journal of the American Chemical Society. **2018**, 140 (42), 13884-13891

6   Towards a continuous formic acid synthesis: a two-step carbon dioxide hydrogenation in flow.

   Helena Reymond, **Juan José Corral-Pérez**, Atsushi Urakawa, and Philipp Rudolf von Rohr. Reaction Chemistry & Engineering. **2018**, 3, 912-919

Journal publications

7 CO_2 activation over catalytic surfaces.

Andrea Álvarez, Marta Borges, **Juan José Corral-Pérez**, Joan Giner Olcina, Lingjun Hu, Damien Cornu, Rui Huang, Dragos Stoian, and Atsushi Urakawa. ChemPhysChem. **2017**, 18, 3135

8   Silica-poly(styrenesulphonic acid) nanocomposites as promising acid catalysts.

María José Campos-Molina, **Juan José Corral-Pérez**, Rafael Mariscal, Manuel López Granados. Catalysis Today. **2017**, 279 (2), 155-163

9   Sub-micron spheres of an imine-based covalent organic framework: supramolecular functionalization and water-dispersibility.

David Rodríguez-San-Miguel, **Juan José Corral-Pérez**, Eva Gil-González, David Cuellas, Jesús Arauzo, Victor M. Monsalvo, Verónica Carcelén, and Félix Zamora. CrystEngComm. **2017**, 19, 4872-4876

10   Avocado seed: modeling extraction of bioactive compounds.

Francisco Javier Segovia, **Juan José Corral-Pérez**, and María Pilar Almajano. Industrial Crops and Products. **2016**, 85, 213-220

11   Improvements in the aqueous extraction of polyphenols from borage (*Borago officinalis L.*) leaves by pulsed electric fields. Pulsed electric fields (PEF) applications.

Francisco Javier Segovia, Elisa Luengo, **Juan José Corral-Pérez**, Javier Raso, and María Pilar Almajano. Industrial Crops and Products. **2015**, 65, 390-396

UNIVERSITAT ROVIRA I VIRGILI
CONTINUOUS HYDROGENATION OF CARBON DIOXIDE TO FORMATES AND FORMIC ACID OVER HETEROGENEOUS CATALYSTS
Juan José Corral Pérez

List of publications

Conference contributions

1 Unique reactivity of silver in CO_2 hydrogenation to formates and subsequent esterification with methanol to methyl formate.

April **2018**, 6th International Congress on Operando Spectroscopy, Estepona (Spain) – **poster presentation**.

2 Unique reactivity of Ag and mechanistic insights into selective CO_2 hydrogenation to methyl formate.

January **2018**, Materials, Characterization, and Catalysis workshop, Zürich (Switzerland) – **oral presentation**.

3 Unravelling the role of catalytically active metals in continuous production of methyl formate by hydrogenation of carbon dioxide.

August **2017**, 13th European Congress on Catalysis - A bridge to the future, Florence (Italy) – **oral (flash) presentation**.

4 New insights into the CO_2 hydrogenation towards methyl formate using silver as a catalytically active metal.

June **2017**, SECAT'17: Catálisis para un mundo más sostenible, Oviedo (Spain) – **oral presentation.**

5 Continuous production of methyl formate by hydrogenation of carbon dioxide.

April **2016**, Conference on Carbon Dioxide Catalysis, Algarve (Portugal) – **poster presentation.**

Journal publications

Journal publications

CURRICULUM VITAE

PERSONAL INFORMATION

Name   Juan José Corral Pérez

Date of birth   May 12th, 1991

Nationality   Spanish

Email   jjcorralperez@gmail.com

EDUCATION

Master's Degree in Business Management   04/2019 – Present

EOI Business School, Madrid (Spain)

- Within the Challenging U program of CEPSA

PhD in Chemical Science and Technology   09/2015 – Present

Universitat Rovira i Virgili, Tarragona (Spain)

- Severo Ochoa PhD fellowship in the framework of the Mobility Programme with ETH Zürich

Master's Degree in Energy and Fuels for the Future   09/2013 – 07/2014

Universidad Autónoma de Madrid, Madrid (Spain)

GPA: 9.03/10

- Beneficiary of the Iberdrola Foundation Scholarships, through its Call for Energy and Environment Postgraduate Studies in Spain

Bachelor's Degree in Chemical Engineering   09/2009 – 07/2013

Universitat Politècnica de Catalunya, Barcelona (Spain)

GPA: 8.89/10

- Award for the best academic record (class of 2013)
- Award for being among the students with the highest university entrance grades (Caixa Manresa)

Curriculum Vitae

WORK EXPERIENCE

Challenging U Graduate   04/2019 – Present

CEPSA, Madrid (Spain)

- Training program at the sales and marketing department of solvents and sulphur business unit

PhD Student   09/2015 – 04/2019

Institut Català d'Investigació Química, Tarragona (Spain)

- Development of catalytic materials and processes for the synthesis of chemical energy carriers from carbon dioxide

Visiting PhD Student   06/2017 – 11/2017

ETH Zürich, Zürich (Switzerland)

- Synthesis and characterization of monodispersed supported metal nanoparticles via the surface organometallic approach

Research Assistant   09/2014 – 07/2015

Abengoa Research, Madrid (Spain)

- Synthesis and characterization of nanomaterials for water applications

Graduate Research Assistant   01/2014 – 07/2014

Institute of Catalysis and Petrochemistry (ICP-CSIC), Madrid (Spain)

- Study of heterogeneous acid catalysts for biodiesel production from oils with high content of free fatty acids

Undergraduate Research Assistant   09/2012 – 07/2013

Universitat Politècnica de Catalunya, Barcelona (Spain)

- Extraction of polyphenolic compounds from plants and agro-industrial by-products

UNIVERSITAT ROVIRA I VIRGILI
CONTINUOUS HYDROGENATION OF CARBON DIOXIDE TO FORMATES AND FORMIC ACID OVER HETEROGENEOUS CATALYSTS
Juan José Corral Pérez

Curriculum Vitae

SKILLS

Languages   Spanish (native), Catalan (native), English (Certificate in Advanced English), French (B1)

Programming   Visual Basic, MATLAB, GAMS, CPLEX, R

Software   Aspen HYSYS, SolidWorks, Origin, Minitab, Microsoft Office

Research   High-pressure fixed-bed microreactors, *in situ/operando* spectroscopic studies, heterogeneous catalysis, Multivariate Curve Resolution analysis, catalyst synthesis and characterization, gas and HPLC chromatography, nanotechnology, food science

SKILLS